



Cite this: DOI: 10.1039/d1cs00450f

High-voltage liquid electrolytes for Li batteries: progress and perspectives

 Xiulin Fan *^a and Chunsheng Wang *^b

Since the advent of the Li ion batteries (LIBs), the energy density has been tripled, mainly attributed to the increase of the electrode capacities. Now, the capacity of transition metal oxide cathodes is approaching the limit due to the stability limitation of the electrolytes. To further promote the energy density of LIBs, the most promising strategies are to enhance the cut-off voltage of the prevailing cathodes or explore novel high-capacity and high-voltage cathode materials, and also replacing the graphite anode with Si/Si-C or Li metal. However, the commercial ethylene carbonate (EC)-based electrolytes with relatively low anodic stability of ~ 4.3 V vs. Li^+/Li cannot sustain high-voltage cathodes. The bottleneck restricting the electrochemical performance in Li batteries has veered towards new electrolyte compositions catering for aggressive next-generation cathodes and Si/Si-C or Li metal anodes, since the oxidation-resistance of the electrolytes and the *in situ* formed cathode electrolyte interphase (CEI) layers at the high-voltage cathodes and solid electrolyte interphase (SEI) layers on anodes critically control the electrochemical performance of these high-voltage Li batteries. In this review, we present a comprehensive and in-depth overview on the recent advances, fundamental mechanisms, scientific challenges, and design strategies for the novel high-voltage electrolyte systems, especially focused on stability issues of the electrolytes, the compatibility and interactions between the electrolytes and the electrodes, and reaction mechanisms. Finally, novel insights, promising directions and potential solutions for high voltage electrolytes associated with effective SEI/CEI layers are proposed to motivate revolutionary next-generation high-voltage Li battery chemistries.

Received 10th May 2021

DOI: 10.1039/d1cs00450f

rsc.li/chem-soc-rev
^a State Key Laboratory of Silicon Materials and School of Materials Science and Engineering, Zhejiang University, Hangzhou 310027, China. E-mail: xlfan@zju.edu.cn

^b Department of Chemical and Biomolecular Engineering, University of Maryland, College Park, MD 20742, USA. E-mail: cswang@umd.edu

Xiulin Fan

His research interest is electrolytes and interphases in high-energy batteries. He has been recognized as a highly cited researcher by Clarivate since 2020.

Dr Fan received his bachelor's and PhD degrees from Zhejiang University in 2007 and 2012, respectively. From 2013 to 2017, he worked as a Postdoctoral Research Associate at the University of Maryland College Park (UMD), and then was promoted to an Assistant Research Scientist in 2017 at UMD. Since August 2019, Dr Xiulin Fan has been a professor at School of Materials Science and Engineering, Zhejiang University. His


Chunsheng Wang

His work has been cited more than 35 000 times, with an H-index of 101 (Google Scholar). He has been recognized as a highly cited researcher by Clarivate since 2018. He received the UMD Invention of the Year for 2015 and 2021.

Prof. Chunsheng Wang is a Robert Franklin and Frances Riggs Wright Distinguished Chair Professor in the Department of Chemical & Biomolecular Engineering at UMD and a co-founder and UMD Director of the Centre for Research in Extreme Batteries (CREB), a joint battery research center between UMD and US Army Research Lab, and currently serves as an Associate Editor of ACS Applied Energy Materials. He obtained his PhD degree in

1. Introduction

Li ion batteries (LIBs) have revolutionized the energy storage area since their advent in the market in 1991.¹ Currently, LIBs based on LiCoO_2 (LCO)/ $\text{LiNi}_x\text{Mn}_y\text{Co}_{1-x-y}\text{O}_2$ (NMC)/ $\text{LiNi}_{0.8}\text{Co}_{0.15}\text{Al}_{0.05}\text{O}_2$ (NCA) as a cathode and graphite as an anode not only monopolize the small battery market for portable electronic devices, but have also been successfully utilized in electric vehicles, as well as for stationary energy storage, in which NCA and NMC can be considered as the second-generation cathode materials for LIBs.² With the fast advancement of the cathode materials, a key issue that needs to be tackled is the anodic stability of the electrolytes, which not only determines the highest potential that can be charged for the cathodes and hence the reversible capacities, but also determines the cycling performance of the cell.³

The conventional EC-based carbonate electrolytes possess inferior anodic stability of >4.3 V vs. Li^+/Li ,^{4,5} which renders them highly unstable against high-voltage cathodes. Solvent molecules such as EC could undergo oxidation and polymerization on the highly catalytic surface of the NMC/NCA layered cathode materials, thus forming a protective polycarbonate species.² However, these polycarbonate species are still not stable enough at high voltage. Even Li_2CO_3 , a relatively stable component in the solid electrolyte interphase (SEI) layer, could be oxidized over 3.5 V, releasing O_2/CO_2 gases.⁶ The low anodic stability of the commercialized EC-based electrolytes has highly restricted the commercialization of these high voltage cathode materials. Even within the voltage limits of the electrolytes, the overcharge and the increase of the resistance during cycling

could also easily raise the potential of the cathode into the unstable zone of the electrolyte and induce safety concerns. In addition, conventional EC-based electrolytes cannot build a robust SEI on Li anodes either, as evidenced by a low cycling Coulombic efficiency of $<95\%$.⁷

The energy density (E) is a critical parameter for rechargeable batteries and directly related to the electrode specific capacity (Q) and cell voltage (V). It can be calculated based on eqn (1) and (2),⁸ where the thermodynamic cell voltage is defined by the electrochemical potential difference between the cathodes and the anodes ($V_c - V_a$).

$$\frac{1}{Q} = \frac{1}{Q_a} + \frac{1}{Q_c} \quad (1)$$

$$E = (V_c - V_a)Q \quad (2)$$

Q_a and Q_c are the anode and cathode specific capacity, respectively. To achieve a high voltage cell, the potential window of the electrolyte should be as wide as possible, because this stable window defines the selection of the cathodes and anodes, and thereby determines the voltages of the paired cells. Fig. 1a presents a timeline of groundbreaking discoveries for the secondary battery technologies since the 1800s.⁹ Placing the LIB technology in the reversible battery historical context could bring us in-depth inspiration and insight into the quest for next generation batteries with higher energy densities. Before Li batteries, all of the reversible batteries are based on aqueous electrolyte systems, restricting the reversible voltage to <2 V and energy density to <100 Wh kg^{-1} . The breakthrough and

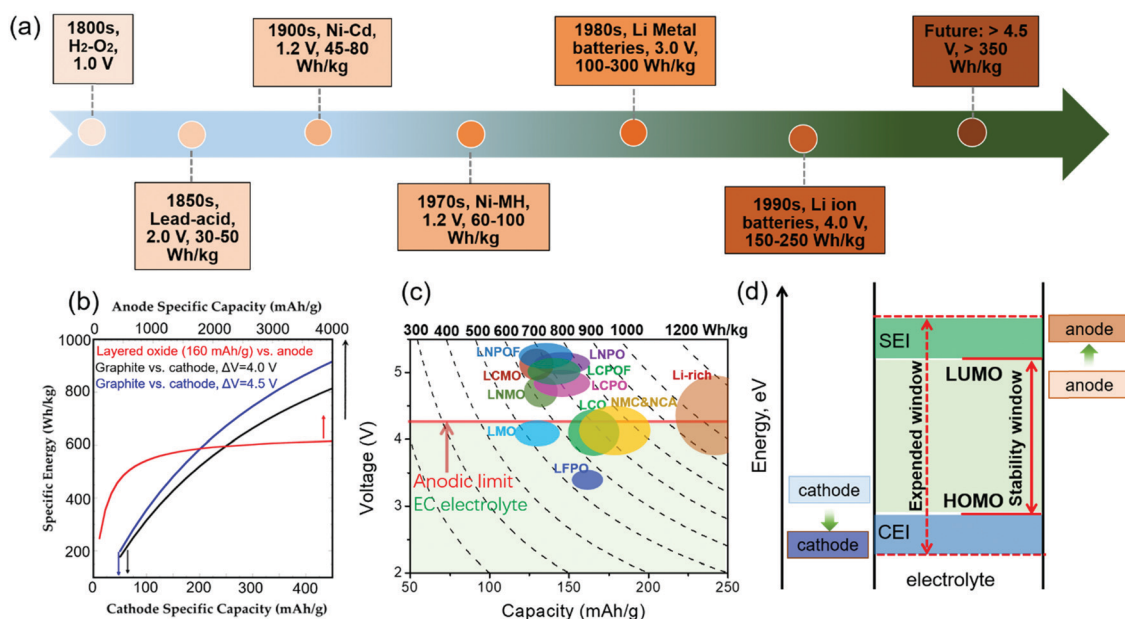


Fig. 1 (a) Milestones of reversible battery chemistries developed since 1800s until today. (b) Energy density variation of a battery by varying the capacity of cathode (dark and blue curve) and anode (red curve). The effect of voltage increase on the energy density is highlighted by the blue (4.5 V) and dark (4.0 V) curves. (c) The approximate reversible capacities and the working voltage windows of the commercialized and intensively investigated intercalation cathode materials. The gravimetric energy density is calculated merely based on cathode materials. (d) Schematic illustration of electrolyte working mechanisms in LIBs. (b) Reprinted with permission from ref. 89. Copyright 2018 American Chemical Society.

commercialization of non-aqueous liquid electrolytes successfully hoisted the electrolyte working potential range over 4.0 V and realized reversible LIBs with a voltage of >3.0 V and energy density of >200 W h kg⁻¹. In recent decades, LIBs with graphite as the anode and layered NMC as cathode have further enhanced the energy density of LIBs. Because of the lowest potential of Li⁺/Li among all of the redox couples and high capacity of Li metal, Li batteries will still hold the highest voltage and highest energy density among the batteries in the forthcoming future.

Besides the energy density, another important parameter for the cell is the power density. The energy quality released at higher potential V is superior to that released at lower V because of the square relationship between the electrical power P and the potential V (eqn (3)).¹⁰

$$P = (V_c - V_a)^2/R \quad (3)$$

Therefore, increasing the cutoff voltage of the commercial cathodes or developing novel high-voltage and high-capacity cathodes and meanwhile selecting low potential anodes could essentially improve the energy and power densities of the battery. Among the cathodes with moderate operation voltage, Ni-rich layered cathodes stand out, because of the optimal electrochemical performance with a high specific capacity of >200 mA h g⁻¹, high average discharge voltage of 3.8 V, and high electrode density of >3.2 g cm⁻³.^{11–14} Other high energy layered cathodes are Li-rich cathodes,^{15–18} which can be defined as $x\text{Li}_2\text{MnO}_3 \cdot (1-x)\text{LiMO}_2$ (Ni, Mn, Co) composites,^{19,20} employ oxide anion redox for Li storage in addition to transition metal redox and need to be charged to over 4.6 V to trigger the anion redox, and therefore call for highly anti-oxidized electrolytes.^{21,22} The anion redox in the Li-rich cathodes will induce the formation of highly oxidative species such as peroxide O₂²⁻ ions, superoxide O₂⁻, and molecular O₂, which can significantly react with the electrolytes chemically.^{18,20} On the high voltage cathodes, a number of good reviews/perspectives have been published recently and the operation principles of these cathodes have been described in detail.^{12,13,21,23–30} Although the layered cathodes possess these merits, the capacity and energy density are largely restrained by the commercial electrolytes due to the serious side reactions between the conventional EC-based electrolytes and the catalytic surfaces of the delithiated NMC,^{31–34} which could accelerate the transition metal dissolution into the electrolytes and the pulverization of the cathode structures.³⁵ The most effective strategy for achieving high energy density of LIB is to increase the capacity and potential of the cathode rather than increasing the anode capacity as shown in Fig. 1b, which can also be deduced by eqn (1) and (2). In addition to layered cathodes, 5 V high voltage cathodes such as spinel LiNi_{0.5}Mn_{1.5}O₄ (LNMO),^{36–41} inverse spinel LiNiVO₄,^{42–44} olivine LiCoPO₄ (LCPO),^{45–53} and post-5 V ultra-high voltage cathodes such as olivine LiNiPO₄ (LNPO),^{54–58} spinel LiCoMnO₄ (LCMO),^{59–62} and orthorhombic Li₂CoPO₄F (LCPOF)^{63–67} have also been extensively investigated in the past decade (Fig. 1c).

Until now, the origins for the degradation of the high-voltage cells could be mainly attributed to four reasons:^{68–70} (1) progressive oxidation of the electrolytes on the high voltage cathodes,^{71,72} (2) surface reconstruction of the cathodes;^{72–75} (3) transition metal dissolution at the cathode–electrolyte interface;^{76–86} (4) cracks and pulverizations of cathode materials due to the large volume change during lithiation/delithiation processes.⁸⁷ These four degradation mechanisms are fundamentally correlated. Surface reconstruction of the cathodes substantially occurs simultaneously as the parasitic reactions between the delithiated cathodes and the electrolytes with a cutoff voltage of >4.2 V,^{88–91} which have been extensively documented for almost all of the high voltage cathode materials. The reconstruction of the surface layer principally reduces the transition metal valences, induces dissolution of some transition metal species, increases the charge transfer resistance of the cathode, and eventually results in the degradation of the electrochemical performance of the cell upon cycling.^{89,92,93} On the dissolved TM ions, they will not only lead to the capacity decay of the cathodes, but also diffuse to the anode sides due to the concentration and electric gradient, and are *in situ* reduced, resulting in the malfunction of the SEI and avalanche degradation of the cells.^{77,79–82,85,94–99} The cracks and pulverization induce the continuous parasitic reactions between the cathode and electrolytes due to the exposed fresh surfaces. The oxidizable electrolyte could readily seize the oxygen from the delithiated cathode, and therefore accelerate the surface reconstruction and side reactions at high voltages. In contrast, the oxidization-resistance electrolytes, such as fluorinated electrolytes, effectively suppress the surface reconstruction and the TM dissolution.^{71,100} Therefore, exploring high voltage electrolytes to block the parasitic reactions between the highly reactive delithiated cathodes and the electrolytes is one of the most effective methods to further enhance the electrochemical performance of the high energy cells.¹⁰¹

The oxidation process is complicated, during which the electrolyte salts will be involved,^{102–104} however the solvents are believed to be the major component in the commercial electrolytes responsible for the catalytic decompositions on the highly oxidized delithiated cathode surfaces. For the SEI on the anode, the reduction of both salts and solvents contributes to the SEI. The compact and electron-insulating SEI/CEI could effectively passivate the electrodes and block the possible side reactions between the electrodes and the electrolyte. Therefore, two fundamental strategies could be utilized to widen the electrochemical windows (Fig. 1d): (i) expand the intrinsic electrolyte stability window thermodynamically by replacing the conventional EC-based electrolyte with more stable solvent electrolytes; (ii) by forming more compact and effective SEI/CEI layers to widen the working stability window kinetically. More often than not, it is difficult to distinguish these two strategies intentionally, because some related passivation layers are always formed in the battery operations because of the wide working voltage and the catalytic effect for the delithiated cathode.³

In this review, we focus on the recent progress on the liquid electrolytes with wide-potential windows. The design principles

were discussed and highlighted. Since the SEI/CEI layers, which are *in situ* formed from the electrochemical/chemical reactions between the electrodes and the electrolytes, play a critical role in the electrochemical performance of the cell, a significant part of this review will be devoted to their chemistry, the reaction mechanisms, as well as the correlations between the electrochemical performance and the interphases. We minimally discuss the Li metal anodes with the electrolytes, as several good reviews have summarized the Li metal anodes and electrolytes in the past few years.^{105–108} Solid state electrolytes (ceramic/glassy) will not be covered in this review either, since a number of related reviews/perspectives on the solid-state electrolytes are available recently.^{109–111} Besides, it is believed that the LIBs based on the high voltage cathodes (NMC, NCA, LCO, and 5 V LNMO *etc.*) and graphite/Si-C anodes using liquid electrolytes will still dominate the commercial Li batteries in the near future. Even plenty of the so-called “solid-state electrolytes” contains some indispensable liquid electrolytes to ensure their proper functionality.¹¹² Therefore, differing from the solid-state electrolyte reviews, herein we mainly focused on the voltage widening principles of the liquid electrolytes, placing the emphasis on the compatibility and reaction mechanisms between the electrolyte and electrodes, which should be of extensive interest to a broad audience working on rechargeable batteries to maximize the electrochemical performance.

2. Degradation of carbonate electrolytes on high voltage cathodes

Thanks to the pioneering work conducted by Dahn¹¹³ and Tarascon *et al.*,^{114,115} who unveiled the fundamental difference between EC and PC solvents on the Li ion interaction into the graphitic anodes, EC has become an indispensable component in the commercialized Li electrolytes since the 1990s.^{3,116,117} Recent investigations indicate that EC solvent is a double-edged sword in LIBs, which exhibits an excellent protecting effect toward the graphite anodes due to the good SEI-formation capability at the graphite/electrolyte interface,^{3,117} however, meanwhile as one of the least oxidation-resistant carbonate solvents,^{118–121} EC also exerts an actually adverse effect on the electrochemical properties for high voltage cathodes by forming a less robust CEI layer.^{118–120,122–127} Almost all of the electrolyte decomposition species including inorganic and oxygenated organic compounds on the cathode surfaces are related to EC or solvated EC decomposition.^{128–130} Several mechanisms were proposed to explain these adverse effects, such as nucleophilic attack,^{32,131–133} electrophilic attack,^{134,135} dehydrogenation reactions,^{123,130,136} and ring opening reactions,^{128,137} which lead to the cathode reconstruction and transition-metal dissolution^{92,138,139} at the high-voltage delithiated cathodes.

Understanding the parasitic reactions between the delithiated cathodes and the carbonate electrolytes is critically important to further improve the high voltage and high-energy

Li batteries. The passivation film on the cathodes was first reported by Goodenough *et al.* in the LCO systems.¹⁴⁰ Then, intensive investigations were devoted to unveiling the origin and its formation mechanism using XPS, XAS, MS, FTIR, Raman spectra *etc.*^{33,141,142} As the pioneer who focused on the surface phenomena between the electrode and the carbonate electrolytes, Aurbach *et al.*^{32,143–145} thoroughly investigated different cathode systems in the non-aqueous electrolytes, including LCO, LNO, LMO and LNMO cathodes, and pointed out that the active cathodes are always covered by the passivation films once aged in the carbonate electrolytes. Similar to the Li⁺ intercalation processes into the graphite anodes, the Li ions have to migrate through this surface films before intercalating into the Li_xMO_y cathodes.¹⁴³ Therefore, a number of researchers utilized the same term of “SEI” to also depict this passivation layer on the cathode surfaces,^{146,147} while others adopted the “CEI” (cathode electrolyte interphase),^{148–150} “EEI” (electrode electrolyte interphase)^{88,138,151} or “SPI” (solid permeable interface)¹⁵² to describe these passivation layers. To distinguish the “SEI” formed on the cathode surface from that formed on the anode, we will use “CEI” to denote the passivation layers on the cathodes in this review. Surprisingly, the compositions of the CEI formed on the cathode surface are generally similar to the SEI layers on the anodes,^{142,148,153–155} although the CEI layers mainly result from oxidation reactions between the delithiated cathode and the organic electrolytes and are apparently much thinner.^{154–160} Compared with ten to hundred nanometers of the SEI layer on the anodes,^{161–163} the thicknesses of most CEI layers are generally less than 5 nm.^{158,159,164}

The oxidation behaviors of the carbonate electrolyte are highly related to the cathode surfaces. The carbonate electrolytes can withstand a high voltage of ~5.0 V without obvious oxidations on the inert metal surfaces, which have been proved by theoretical calculations and electrochemical tests such as linear-sweep voltammetry (LSV) techniques,^{92,165} yet it could be easily oxidized at a much lower voltage catalyzed by the delithiated cathodes.^{166–169} A consensus exists in the community on the compositions and some protective natures of the CEI on the high voltage cathodes, however, the underlying CEI formation mechanisms are still in debate, and even in contrast. In this section, we summarized the prevailing CEI formation mechanisms on cathode surfaces in the carbonate electrolytes, which can shed light on the exploration of the novel high voltage electrolytes.

Nucleophilic reaction mechanism

As the solvents in the commercial electrolytes, the alkyl carbonate molecules generally possess electrophilic characteristics.¹⁷⁰ Aurbach *et al.*^{32,33,142} compared the oxidation phenomenon of three different electrolytes, LiPF₆, LiC(SO₂CF₃)₃ (LiTFSI) and LiAsF₆ in a mixture of the conventional EC/DMC solvents on layered LNO, layered LCO, and spinel LiMn₂O₄ (LMO) cathodes. The impedance increase and oxidizing reactivity of these three cathodes are in the following trend LNO > LCO > LMO, which is probably due to the strongest nucleophilic nature of oxygen

on the delithiated LNO surface. Besides the periodic influence on the reactivity, the crystal structure of cathodes also highly impacts the reactivity of the cathode surface even through with the same central transition metal atoms. The nucleophilicity or basicity of the O atoms in the delithiated layered Li_xMO_2 is higher than that in the spinel $\text{Li}_x\text{M}_2\text{O}_4$ and olivine Li_xMPO_4 compounds,¹⁷¹ therefore, the Li_xMO_2 exhibits a more aggressive reactivity to the carbonate electrolytes than $\text{Li}_x\text{M}_2\text{O}_4$ and Li_xMPO_4 compounds. In the olivine compounds, the P atoms with the +5 valence could partially shield the nucleophilic nature of the O atoms.¹⁷¹ Hence, to maximize the ion transport kinetics, nanosized olivine and spinel materials can be utilized as cathodes without serious side reactions at the surfaces,^{172–175} while for the layered NMC cathodes the assembled spherical particles with a size of microns to minimize the surface areas monopolized the market.^{30,176} Micro-sized single-crystal NMC cathodes are also intensively developed to further lower the surface reactivity.^{83,177–181} The basicity or the nucleophilicity of the O in the layered Li_xMO_2 cathodes enhances with higher covalency and higher electronegativity of O–M bonds, which is related to the feasibility of the electron donations from the O atoms to the electrolyte solvents. Shao-Horn *et al.*⁹² suggested that the capability of the electron donation in the layered Li_xMO_2 from the O p band to nucleophilically attack the electrolyte solvent is increased from early to later metal ions in the first transition metal row as the O p band energy increases. Based on this hypothesis, the Lewis basicity or the nucleophilicity of O in Li_xNiO_2 should be higher than in Li_xCoO_2 , which is partially supported by the higher reactivity of the delithiated LNO in the carbonate electrolytes.^{182,183} and higher impedance resistance of the cycled LNO.¹⁸⁴ The nucleophilic reactions between the O on the surface of the delithiated cathodes and electrolytes leads to the decomposition of the electrolyte solvents and the formation of Li alkoxides and semicarbonates.

Dehydrogenation reaction mechanism

The most widely utilized descriptors for the electrolyte stability are the lowest unoccupied molecular orbital (LUMO) and highest occupied molecular orbital (HOMO) of the free solvent molecules.^{92,185–191} However, the presence of the salts, solvation structures, impurities, and interactions between the cathode surface and the electrolyte critically affect the redox potentials of the solvents, leading to offset as high as 4 eV from the HOMO energies.^{186,192,193} For example, Zhang *et al.*¹⁹⁴ calculated the oxidation potentials of eleven solvent molecules including 1,2-dimethoxyethane (DME), 1,3-dioxolane (DOL), tetrahydrofuran (THF), EC, propylene carbonate (PC), dimethyl carbonate (DMC), diethyl carbonate (DEC), ethyl methyl carbonate (EMC), vinylene carbonate (VC), butylene carbonate (BC) and catechol carbonate (CC) *via* DFT assuming a one-electron transfer oxidation process from the solvent molecule to an inert electrode to form a radical cation. The absolute values of the calculated thermodynamic potentials for the solvent oxidation show relatively large uncertainty and significantly higher (> 1.0 V) than the experimental values, which should be due to the simplified solvation model, the neglect of the specific

solvent-ion and solvent-ion-cathode surface interactions, and the different reaction pathways.¹⁹⁴ Recent computations showed that the EC-based electrolytes could be chemically dehydrogenated and oxidized on delithiated high-voltage cathode surface, especially with increasing Ni content.^{195,196} Borodin *et al.*^{132,193,195,196} screened almost all of the polar solvents in Li electrolytes such as carbonates, ethers, sulfones and phosphates by quantum chemistry (QC) calculations and molecule dynamic (MD) simulations. The results showed that the intrinsic oxidation potentials of these solvents are much higher than the experimental values for the electrolytes if the dehydrogenation reactions (H-transfers) are not considered. Shao-Horn *et al.*¹⁹⁷ compared the energetics of four different chemical reactions between EC molecules and Li_xMO_2 layered and MO rocksalt cathode surfaces using DFT calculations. EC dehydrogenation was energetically more favorable on the layered cathodes than electrophilic attack, nucleophilic attack, and EC dissociation with oxygen extraction from the cathode surface. As shown in Fig. 2a, the delithiation reaction of Li_xCoO_2 exerts negligible effects on the electrophilic reaction. In contrast, EC dehydrogenation becomes energetically favorable upon decreasing lithium content in Li_xCoO_2 , reaching a lowest reaction energy < -2.5 eV for the fully delithiated state. The increased reactivity of the delithiated cathode surface with higher degree of delithiation promotes the accumulation of decomposition products such as the polymeric and salt-derived (PF_3O , $\text{Li}_x\text{NiO}_y\text{F}_z$, $\text{Li}_x\text{PF}_y\text{O}_z$) species in the CEI layer, which was validated by online electrochemical mass spectrometry,¹⁹⁸ Raman,¹⁹⁹ FTIR spectroscopies,¹³⁶ nuclear magnetic resonance (NMR),^{199,200} and XPS on the layered delithiated cathode surface upon charging.^{142,148,199,201–205}

Similar to the effect of the delithiation state on the electrophilic reaction, the M^{3+} in LiMO_2 possesses a similar electrophilic reactivity to EC with weak exothermic energies in the range of -0.5 to 0 eV (Fig. 2b). By contrast, the tendency of EC dehydrogenation is highly material dependent and increases from early to late transition metal in the periodic table, which can ideally explain the formation of interfacial reduced phases and the higher reactivity of NMC cathodes with increased Ni content.^{14,73,183,206–214} The more O–M covalency or more O p states pinned Fermi level in the Ni-rich cathodes induces higher driving force for the surface O to oxidatively dehydrogenate or dissociate more carbonate solvents such as EC to generate surface proton species and concurrently reduce transition metal ions.^{134,136}

Resorting to *in situ* FT-IR measurements, Shao-Horn *et al.*¹³⁶ detected the EC dehydrogenation on a Ni-rich cathode at relatively low voltage of ~3.8 V, even though EC could be stable against oxidation on a Pt surface up to 4.8 V.²¹⁵ The reactions were also confirmed by DFT calculations, and the degradation species include De-H EC, VC and dehydrogenated oligomers. As shown in Fig. 2b, upon charging NMC811 from open circuit voltage (OCV) to 4.4 V *vs* Li^+/Li , significant VC signals at ~1830 cm^{-1} were detected with two hydrogen atoms removed from EC to form a C=C bond in the ring, which were in good agreement with the attenuated total reflection (ATR)

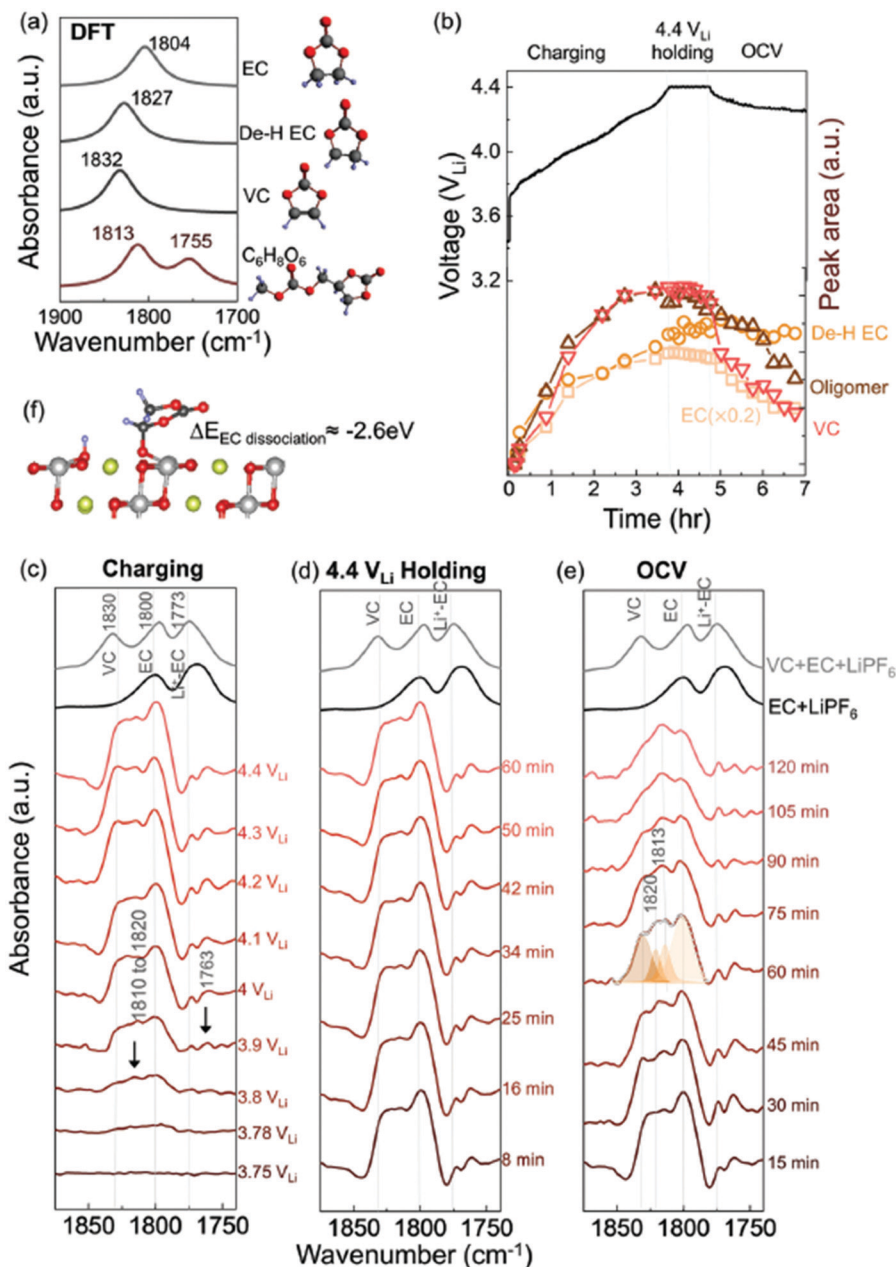


Fig. 2 *In situ* FTIR spectra on NMC811 surface in 1.5 M LiPF₆ EC electrolyte. (a) DFT calculated IR spectra of EC, de-H EC, VC (formed by removing two hydrogens in EC), and oligomer C₆H₈O₆; (b) relationship between the voltage profiles of the NMC811 and deconvoluted peak areas of EC and its decomposed products at ~1813 cm⁻¹ (de-H EC), 1830 cm⁻¹ (VC), ~1820 cm⁻¹ (oligomers with EC-like rings) during delithiated, potentiostatic holding and OCV rest. (c) *In situ* FTIR spectra (C=O stretching region, in red) on NMC811 surface during delithiation to 4.4 V, and (d) potentiostatic holding at 4.4 V, and (e) resting at OCV in a 1.5 M LiPF₆ EC electrolyte, and ATR (attenuated total reflection) spectra for 1.5 M LiPF₆ EC and 1.5 M LiPF₆ EC/VC (5 : 1) electrolyte (in black). (f) Diagram of EC dehydrogenation on the LiNiO₂ surface and its energetics. Reprinted with permission from ref. 136. Copyright 2020 The Royal Society of Chemistry.

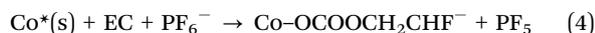
spectrum of VC + EC + LiPF₆ electrolyte (Fig. 2c) and the calculated VC spectra (Fig. 2a). The increased intensity ratio of the VC to EC (~1800 and 1773 cm⁻¹) from 3.8 V to 4.4 V demonstrates the significant oxidation of the EC by a dehydrogenation reaction mechanism on the surface of the Ni-rich cathode. Meanwhile, the broad peaks centered at ~1815 cm⁻¹ and ~1763 cm⁻¹ (black arrow in Fig. 2c) can be assigned to the oligomers with EC-like rings.^{216,217} Besides, the feature around

1813 cm⁻¹, which starts showing up at ~3.8 V vs Li/Li⁺, also contain C=O stretching of de-H EC with one hydrogen atom removed from EC, whose formation was energetically favorable with driving force of about -2.6 eV (Fig. 2f). In contrast, the dehydrogenation reactions were not observed on the Al₂O₃ coated NMC or in highly concentrated electrolytes, indicating that the *ex situ* formed protecting layers or the *in situ* formed salt-derived CEI layers could effectively block the parasitic

reactions of the electrolytes and the delithiated cathodes, which theoretically explained the highly improved electrochemical performance for the coated NMC^{218–235} and the merits of the concentrated electrolytes.^{122,236–240} It should be pointed out that the coupling of the H-transfer during carbonate oxidation was also confirmed by electron paramagnetic resonance,²⁴¹ Raman spectroscopy and *ex situ* diffuse reflectance infrared Fourier transform spectroscopy (DRIFTS).¹⁹⁷

Ring opening reaction mechanism

Resorting to the DFT calculations, Musgrave *et al.*¹²⁸ revealed that the Lewis acid–base complexation between the EC molecule and either delithiated LCO or PF₅ weakens the C–O bonds of the EC ring and accordingly reduces the barrier of EC ring-opening reactions. This ring opening reaction catalyzed by the delithiated cathode surface and PF₅ Lewis acid leads to the formation of CEI layers composed of an organic and organo-fluorine film. In the reaction, the EC molecules first adsorb onto two neighboring surface Co sites, as shown in Fig. 3a, which is thermodynamically favored by about 1.07 eV. Then, the adsorbed EC (EC_{ads}) molecules donate 0.12e[−] to the LCO surface, eventually resulting in the ring opening reaction of EC_{ads} molecules *via* the following equation (eqn (4)):



In addition to reacting with the traces of H₂O to form HF and POF₃, the *in situ* formed PF₅ Lewis acid further reacts with the free EC molecules in the electrolytes, forming a Lewis acid–base complex as shown in Fig. 3b, in which the reaction equation (eqn (5)) could be:



This proposed mechanism was partially echoed by Lucht *et al.*,²⁴² who analyzed the surface of LNMO polarized at different voltage ranges (4.0–4.3 V, and 4.7–5.3 V) in 1 M LiPF₆ EC/DMC/DEC electrolyte by XPS and FTIR spectra. They found that at the voltage of <4.3 V *vs.* Li, the leakage current is relatively low and the electrolyte decomposition products are limited (Fig. 3c and d). As the voltage increases to >4.7 V, the leakage current dramatically surges with a poly(ethylene-carbonate) passivation film formed on the LNMO surface, indicating that the organic-based CEI cannot effectively block the continuously parasitic reactions between the delithiated cathode and the electrolytes at high voltages. Based on first principles calculations, Kumar *et al.*¹³⁰ proposed a two-step reaction mechanism for the EC decomposition on the predominant surface (111) of the charged LiMn₂O₄ (LMO) cathode despite its relatively mild operating potential. The first step is the proton transfer from EC to the LMO(111) cathode surface (dehydrogenation) with higher energy barrier, followed by the ring opening of the dehydrogenated EC molecules. A highly charged cathode with low Li content prompts EC ring opening degradation *via* a dehydrogenation reaction. Interestingly, these authors also found that different lattice planes can alter the reaction route, for example, on the LMO (100) surface the

reaction is initiated with EC's ring opening process and then the dehydrogenation starts.

Resorting to DFT simulations, Leung¹³⁴ proposed an EC decomposition mechanism on the (100) surface of LiMn₂O₄ under vacuum conditions, which consists of essential multi-steps as shown in Fig. 3e–j. An intact EC molecule first physically absorbs on the (100) surface with carbonyl oxygen strongly coordinated to the surface Mn⁴⁺ ions (Fig. 3e). Then, the carbonyl carbon (C_C) nucleophilically attacked by the oxygen atom on the LMO surface, transforms into a 4-coordinated configuration (Fig. 3f). Immediately, the C_C–O_E bond is broken (Fig. 3g). Both of the C_C and O_E on the broken bond are coordinated to the LMO surface, while the carbonyl oxygen (O_C) is detached (Fig. 3g). Then the proton on the CE atom migrates to the LMO surface oxygen (Fig. 3h). Without further electron transfer, configuration Fig. 3h will self-regulate into Fig. 3i during simulation. Among these steps, it is believed that the rate-determining step of the C_C–O_E bond breaking process is the bonding formation between the cathode surface oxygen atoms O_{surface} with the C_C atoms. To resolve the EC decomposition enigma, not only the surface structure of the cathode but also the adsorbed species on the surface termination should be seriously considered. Following Leung's work,¹³⁴ Xu *et al.*¹³⁵ analyzed the EC reaction pathways on different NMC surface terminations using DFT-based *ab initio* calculations. The EC ring-opening process under ultrahigh vacuum (UHV) conditions can be divided into two steps (Fig. 4a). The first step is the formation of O_{surface} and C_C bonds with a relatively high energy barrier of 290 meV (from intermediate #0 to #2). Then, the C_C–O_E bond breaks with a low energy barrier (from intermediate #2 to #4). This reaction mechanism is in good agreement with Leung's work and possesses the same rate-limiting step. Compared to Tebbe's reaction pathway,¹²⁸ in which all of the reaction energy barriers are higher than 1 eV, the reaction route proposed by Xu *et al.*¹³⁵ is kinetically feasible with a lower reaction energy barrier of 290 meV. If the real electrolyte condition, *i.e.* EC molecules solvated with Li⁺, is considered, this rate-determining reaction barrier is further lowered to only ~17 meV (Fig. 4b). Once EC molecules coordinate with Li⁺, the electron charge of the C_C will be reduced by 0.2e, making the C_C atom more electron deficient and reactive. Therefore, the EC molecule ring-opening process is a fundamentally fast chemical reaction independent of the potential. The surface passivated by the hydroxyl –OH and fluorine –F species (Fig. 4c) can critically raise the energy barrier of the EC ring-opening reactions; for example, the TM–F bond can raise the energy barrier from 17 to 490 meV, which poses a positive effect on the electrochemical performance of the NMC in the EC-based electrolyte. This mechanism can well explain the superior electrochemical performance of fluoride-coated high voltage cathodes^{35,115,243–246}

It should be pointed out that these proposed EC degradation mechanisms are not isolated but intertwined to some extent, each of which highlights some aspects of decomposition reactions. For example, the spontaneous C_C–O_{surface} bond formation between EC molecule and cathode surface before

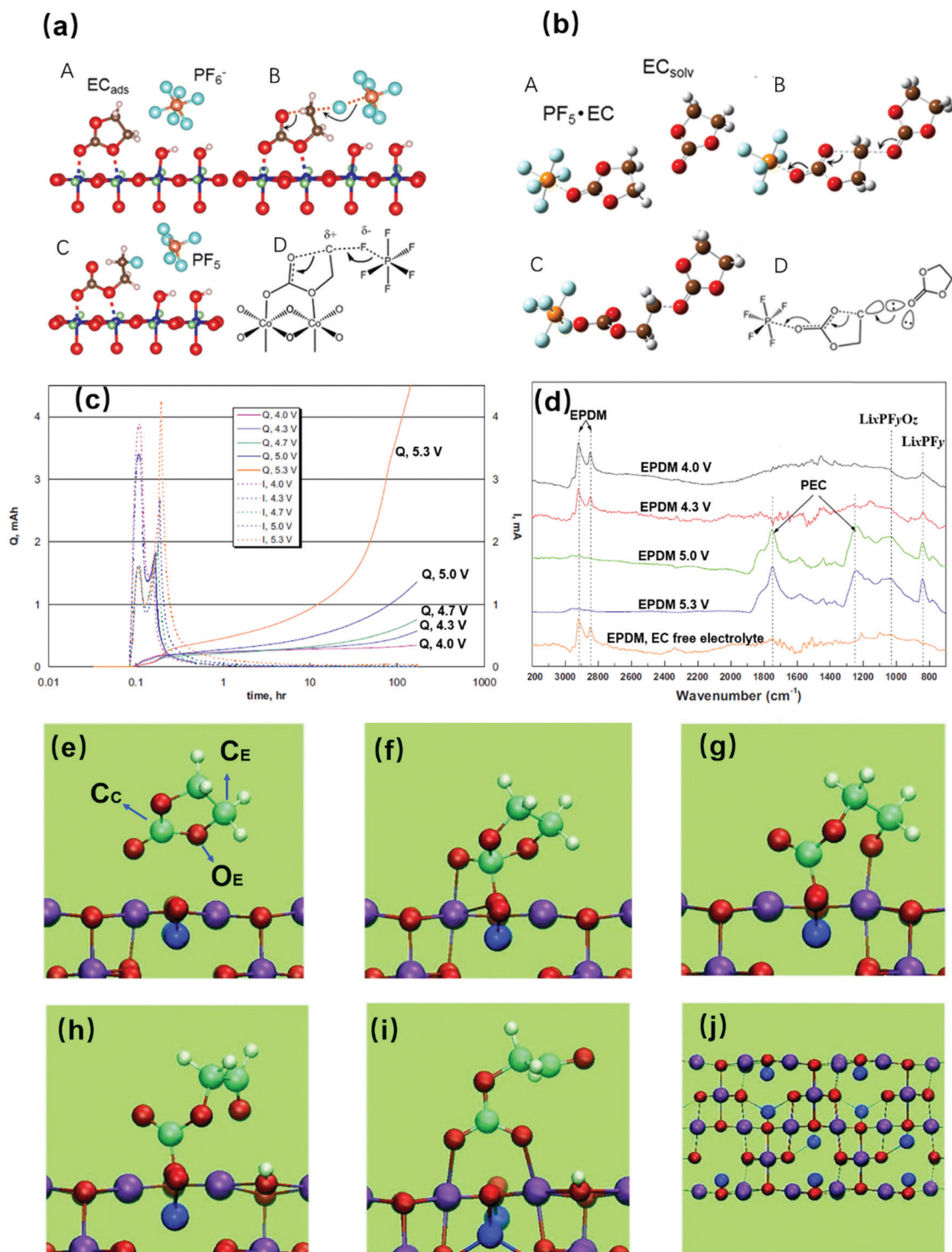


Fig. 3 (a) Ring-opening reaction of EC_{ads} molecules activated by the LCO surface. (b) Ring-opening reaction of EC molecules activated by PF_5 Lewis acid. The atoms shown in different colors are C (brown), O (red), H (white), Co (blue), F (light blue), P (orange) and Li (green). Variation of charge (Q, solid line) and current (I, dash line) vs time for the Li-free $Ni_{0.5}Mn_{1.5}O_3$ electrode (c) and FTIR-ATR spectra of the LNMO cathodes (d) polarized at different voltages in the 1 M $LiPF_6$ EC/DMC/DEC electrolyte. The EPDM represents ethylene propylene diene monomer binder. (e) An EC molecule physisorbs on the $Li_{0.6}Mn_2O_4$ surface (100); (f) intermediate B; (g) intermediate C; (h) intermediate D; without further electron migration, configuration (h) will reorganize to (i). (j) $Li_6Mn_{20}O_{40}$ (100) surface slab with most stable Li distribution structure viewed along the (011) direction. (a and b) Reprinted with permission from ref. 128 Copyright 2016 American Chemical Society. (c and d) Reprinted with permission from ref. 242 Copyright 2010 IOP Publishing, Ltd. (e–j) Reprinted with permission from ref. 134 Copyright 2012 American Chemical Society.

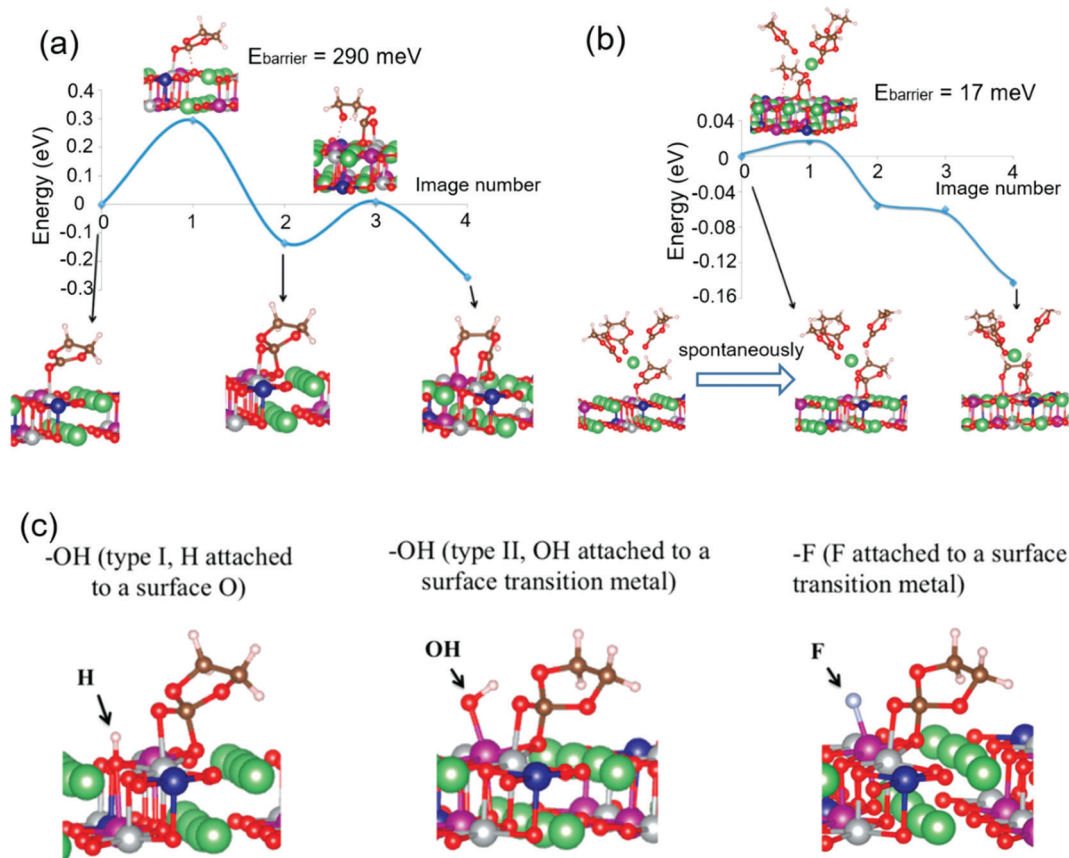


Fig. 4 Reaction energy profiles for the single EC molecule bond breaking process for (a) free EC with NMC surface under ultrahigh vacuum conditions; (b) Li-ion solvated EC with NMC surface. (c) Atomic structures of the NMC surface bonded with hydroxyl -OH and fluorine -F radicals. Reprinted with permission from ref. 135 Copyright 2017 American Chemical Society.

the EC ring-open reaction is probably related to the electrophilic Li^+ binding with EC, which prompts the nucleophilic attack by the exposed oxygen atoms on the NMC surface.¹³⁵ Apart from these discussed reactions between the delithiated cathodes and electrolytes, some side reactions between the carbon black, impurities in the electrolytes or on the cathode surface, and the electrolyte solvents at high voltages are also possible and even dominate the oxidation reactions in the formation process and first several cycles in the cells.¹³³ Besides, considering the inevitable H_2O generation during the anodic decomposition of the EC electrolyte,²⁴⁷ H_2O -driven degradation of the high voltage cells cannot be excluded either.

Further strict experimental characterization and rigorous calculations are needed on the model cathodes to bridge the understanding of the formation of the CEI layers (Li_2CO_3 , LiF, $\text{Li}_x\text{PF}_y\text{O}_z$, RCOF, RCO_2Li , RCOOR, polymeric species *etc.*) on the cathode surface and released gases (CO , CO_2 *etc.*), and evaluate the proposed reaction mechanisms. For example, resorting to *in situ* surface-enhanced Raman spectroscopy (SERS) Liu *et al.*²⁴⁸ investigated the compositions of CEIs on the NMC111 in the conventional EC/DMC electrolyte and quasi-quantitatively assessed the CEI evolutions during a delithiation/lithiation process. Yu *et al.*²⁴⁹ correlated the electrochemical performance of NMC622 with the composition and

properties of CEI using XPS and synchrotron soft XAS. Yet, one conclusion can be drawn that the conventional EC-based electrolytes, which have been commercialized for about 30 years,¹¹⁷ cannot satisfy the higher voltage cathode developments, and the ongoing push on the higher voltage and higher energy Li batteries call for exploration of the novel electrolyte systems.

As one of the most important species in SEI/CEI, LiF significantly changed the stability of SEI/CEI.³ Tremendous efforts have been conducted in recent years to investigate the formation mechanisms,^{250–254} distributions in the interphases,^{250,252,255–261} mechanical properties,^{262,263} Li ion conduction,^{264–268} and electrochemical effects.^{250,256,261} With the explosive investigations on the Li metal anodes recently, more and more researchers believe that LiF could at least play a significant role in the elimination of the Li dendrites and in the enhancement of the Coulombic efficiencies of Li plating/stripping,^{7,122,261,269–275} thanks to the high interfacial energy between the LiF and the Li metal anodes.^{122,271,276} LiF weakly bonds to Li surface due to the high interface energy, which promotes the Li diffusion along Li/LiF SEI interface, while the high interface energy at Li/LiF suppresses the Li penetration into LiF SEI as dendrites. One concern for LiF-rich SEIs is the low ionic conductivity of crystalline LiF,^{142,277–279} which could critically increase the interfacial resistance. It should be

emphasized that LiF also has the widest band gap, which could sufficiently block the electron transport within only two or three atomic layers,^{276,280} and expand the electrochemical stability window.²⁸¹ Therefore, the area specific resistance (ASR) of LiF SEIs is still smaller than other types of SEI due to the extremely thin thickness of LiF. In addition, a recent study demonstrated that the ionic conductivity of LiF could exponentially enhance by the reduction of the crystalline size and doping with other insulator species, such as Li₂CO₃ and Al₂O₃,^{282–285} In addition, LiF in the CEI enhances the robustness of the CEI on the cathode side.²⁸⁶

3. EC-free electrolytes

3.1. EC-free carbonate electrolyte

As the most intensively explored solvents, alkyl carbonates have dominated the electrolyte solvents since the birth of the Li battery because of the excellent overall physicochemical properties, such as high dielectric constants, low viscosities, favorable ionic conductivities, relatively wide liquid-range temperature windows *etc.* Therefore, elimination of less-stable EC from the carbonate solvents and meanwhile maintaining the linear carbonates as the skeleton solvents seems a most viable and practical solution for the established high-voltage Li battery infrastructures.¹¹⁸

In retrospect, profound efforts were devoted to exploring film-forming additives to enable the functionality of the PC-based electrolyte at the nascent era of Li-ion chemistry.^{287,288} With the success of EC-based electrolytes, effects gradually veered to reinforcing the SEI/CEI on the electrodes hoping to extend the cell life.^{3,33} In 2012, Amatuucci *et al.*²⁸⁹ re-opened the door for the EC-free carbonate electrolytes by mixing selected linear alkyl carbonate solvents such as EMC with some film-forming enablers like fluoroethylene carbonate (FEC) and vinylene carbonate (VC) for the 4 V LIBs. Immediately, Dahn *et al.*^{118,119,125–127,290–295} systematically investigated different linear carbonate solvent combinations with various film-forming enablers and compared the electrochemical performance of graphite||NMC pouch cells for higher cut-off voltage of >4.4 V, which are summarized in Table 1. With the optimized enablers such as FEC, VC, (4*R*,5*S*)-4,5-difluoro-1,3-dioxolan-2-one (DFEC), methylene-ethylene carbonate (MEC), prop-1-ene-1,3-sultone (PES), succinic anhydride (SA) and pyridine phosphorus pentafluoride (PPF), low rates of parasitic reactions, low impedance, favorable ion conductivity and high Coulombic efficiency were achieved.^{118,119,295} The elimination of EC effectively improved the high voltage performance of graphite||NMC cells at both room temperature and high temperatures.^{119,125} As shown in Fig. 5, the cells in the EC-free electrolytes with enablers demonstrate much better cycling performance, higher capacity retention and smaller polarization for long-term cycling. Among the tested film enablers, FEC (Fig. 5g) and DFEC (Fig. 5h) possess a better suppressing effect on the polarization growth. With the enablers optimization, an extremely high capacity retention of 85% was achieved for graphite||NMC532 pouch cell even after 3000 cycles with a high 4.4 V cut-off voltage,¹²⁷ representing a

Table 1 Additives and their capability to passivate the graphite anode in 1 M LiPF₆ EMC without EC

Additives	Abbreviation	Ability to passivate the graphite	Ref.
Ethylene carbonate	EC	Yes	113 and 296
Vinylene carbonate	VC	Yes	118 and 293
Prop-1-ene,1,3-sultone	PES	Yes	118
Fluoroethylene carbonate	FEC	Yes	118 and 294
(4 <i>R</i> ,5 <i>S</i>)-4,5-Difluoro-1,3-dioxolan-2-one	DFEC	Yes	118
Methylene-ethylene carbonate	MEC	Yes	118
Succinic anhydride	SA	Yes	118 and 292
Maleic anhydride	MA	No	118
Diphenyl carbonate	DPC	No	118
Vinyl ethylene carbonate	VEC	No	118

breakthrough of the EC-free carbonate electrolyte for NMC full cells.

EC-free electrolytes exert an even better compatibility with the ultrahigh-Ni layered cathodes such as LiNi_{0.94}Co_{0.06}O₂.¹²⁴ Using LiPF₆/LiFSI-EMC electrolytes with VC as an additive, a high capacity retention of 81% was achieved after 1000 cycles at 25 °C, while the capacity retention is only 56% for the conventional EC electrolyte. To unveil the surface reaction mechanism and the CEI compositions on the cathodes, Manthiram *et al.*¹²⁴ visualized the CEI layer *via* ⁶Li labeling with a TOF-SIMS technique. The aged cathode is covered by decomposed species of the ⁷Li abundant electrolyte in the baseline EC-based electrolyte (Fig. 5i and j), which could benefit the electrochemical performance of the cathode to some extent. However, the high concentration of ⁶Li₂F⁺ species indicates that the delithiated cathode also suffers from severe interaction with the electrolytes, leading to the transition-metal dissolution and capacity decay in the cycling. While in the EMC acyclic carbonate electrolyte, transition-metal dissolution is highly depressed (Fig. 5k). Based on these results and previous studies,^{138,139} the authors¹²⁴ proposed the possible reaction mechanism: EC chemically decomposes in the presence of singlet oxygen released from the delithiated layered cathode and generates hydrogen peroxide, which further reacts with LiPF₆, and prompts the transition-metal dissolution. In contrast, the acyclic carbonate solvents such as EMC are more stable against these side reactions. Moreover, thermal abuse tests show that the delithiated cathode could react with an EC-based electrolyte at a much lower temperature, while the exothermal reactions were sufficiently subsided in an EMC-based electrolyte. The transition-metal dissolution associated with non-reversible phase transition catalyzed by EC at the delithiated layered cathode surface promotes thick resistance surface layers, leading to larger cell impedance and fast capacity decay in EC-based electrolytes. With the elimination of EC, the electrolyte possesses high stability on the aggressive cathodes, and therefore gives a considerable boost on the electrochemical performance of the high-energy Li cells.^{124,297} Further advances on the diversified SEI enablers and their combinations could further promote the

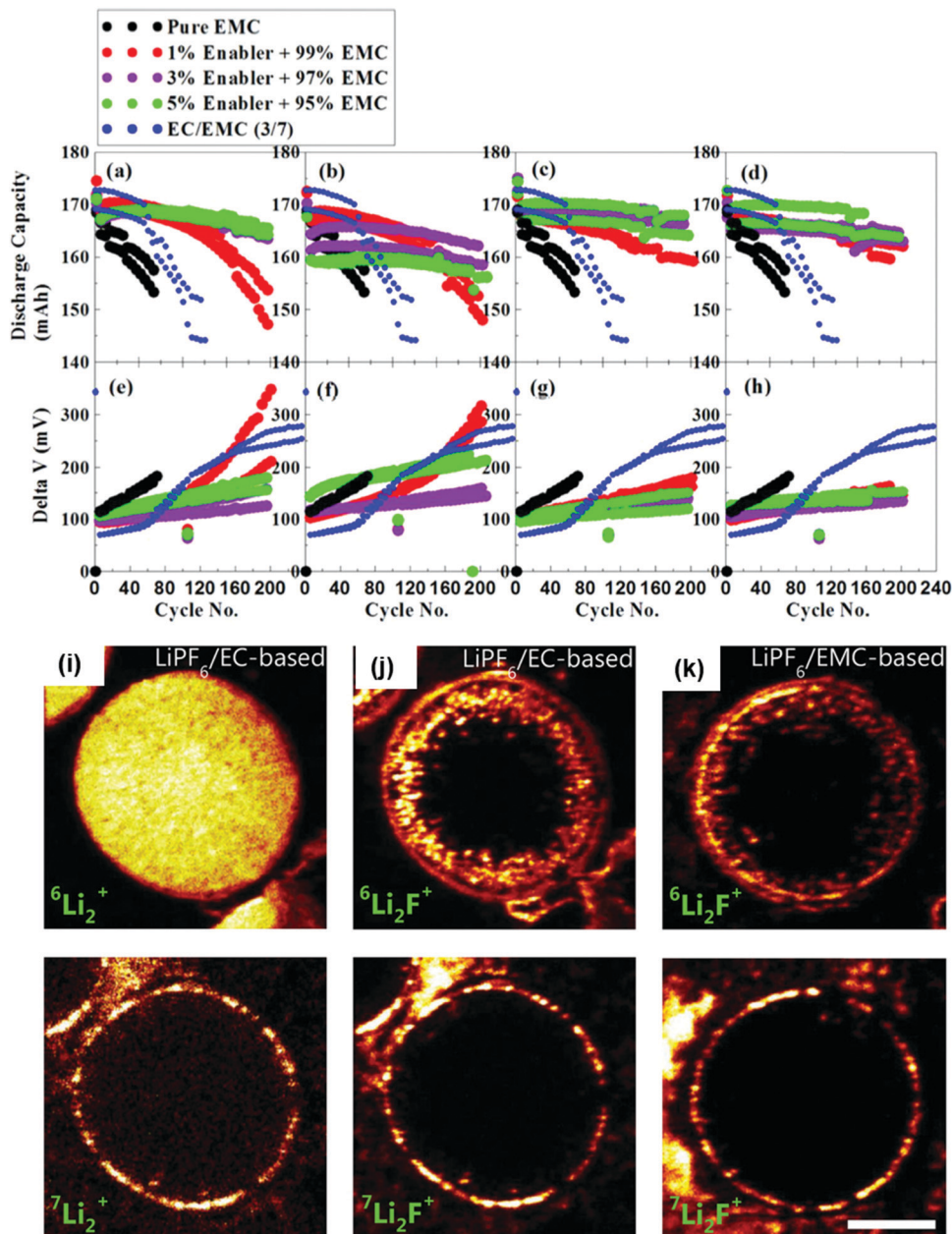


Fig. 5 Discharge capacities (a–d) and cell polarizations (e–h) vs. cycling number for graphite||NMC442 pouch cells with EC-free EMC based electrolytes with different electrolyte enablers and different enabler concentrations during CCCV cycling at 40 °C between 2.8 V and 4.4 V. The charge/discharge current density is 0.4C. A constant voltage was applied until the current density dropped below C/20 after the charge voltage increased to 4.4 V. (a and e) The enabler is VC; (b and f) the enabler is MEC; (c and g) the enabler is FEC; (d and h) the enabler is DiFEC. For comparison, the electrochemical performances for the conventional EC/EMC electrolyte are also compiled. Time-of-flight secondary ion mass spectrometry (TOF-SIMS) mapping on the delithiated $\text{LiNi}_{0.94}\text{Co}_{0.06}\text{O}_2$ in an EC-based electrolyte (1.0 M LiPF_6 EC/EMC(3:7) + 2% VC) (i, j) and EMC-based electrolyte 1.5 M LiPF_6 EMC + 3% VC (k). Before TOF-SIMS analysis, the $\text{LiNi}_{0.94}\text{Co}_{0.06}\text{O}_2$ cathode was first charged to 4.2 V vs. graphite anode and then kept for one week at 45 °C. Scale bar, 10 μm . (a–h) Reprinted with permission from ref. 119 Copyright 2017 The Electrochemical Society. (i–k) Reprinted with permission from ref. 124 Copyright 2019 John Wiley & Sons, Inc.

high-energy Li ion batteries and possible commercialization of EC-free carbonate electrolytes.

3.2. Fluorinated electrolytes

The C–F bonds in organic molecules have significant effects on the HOMO and LUMO level of the solvents and positively affect the interfacial chemistry for the Li ion and Li metal batteries. In

addition, these fluorinated solvents are flame-retardant and even non-flammable,^{117,123,298–303} which can enhance the electrode passivation, as well as the thermal stability.^{298,300–302,304,305} Some fluorinated solvents have been utilized as the additives or co-solvents for the electrolyte for over ten years, and typical examples are the FEC,^{303,306–308} and 3,3,3-trifluoropropylene carbonate (TFPC).³⁰⁹

Fluorinated molecules possess several interesting features compared to the nonfluorinated counterparts, including highly reduced melting points, increased surface tension, and high stability at high temperatures, therefore the fluorinated electrolytes are excellent candidates for the extreme batteries with wide-temperature window and high-voltage window. A highly fluorinated phosphate ester (tris(hexafluoro-iso-propyl)phosphate, HFiP) was synthesized by Xu *et al.*,³¹⁰ and was identified as being effective to stabilize the spinel LNMO 5V cathodes even with only 1 wt% in the carbonate electrolytes. Arai *et al.*^{303,311,312} and Naoi *et al.*^{313,314} demonstrated that introducing the highly fluorinated ether into the electrolyte could effectively suppress the flammability of the carbonates, therefore critically improve the safety of the batteries. Fig. 6 compiles the molecular structures of some reported fluorinated solvents for non-aqueous electrolytes, which can be classified into three groups, fluorinated carbonates, fluorinated carbamates, and fluorinated ethers. Among these three fluorinated solvents, the fluorinated ethers possess lowest dielectric constant, but have a good wettability to both the separators and the electrodes.^{123,315} Therefore, the fluorinated ethers cannot be utilized as the solo electrolyte solvents, and are always coupled with other high-dielectric solvents to ensure an acceptable ion conductivity.^{315,316} Taking advantage of this unique feature, novel electrolyte systems “localized high-concentration electrolytes” or “pseudo-concentrated electrolytes” were developed by Zhang *et al.*^{317–319} and He *et al.*,³²⁰ which possess the merits of high-concentrated electrolytes and the dilute electrolytes simultaneously.³²¹ These features of novel electrolytes will be discussed in the concentrated electrolyte section.

Zhang and co-workers^{100,322–324} blended several fluorinated electrolytes, and tested the anodic stability in the 3-electrode electrochemical cells, and the electrochemical performance of the LTO||LNMO and graphite||LNMO full cells. All of the commercial Gen2 (1.2 M LiPF₆ in EC/EMC) and fluorinated electrolytes remain stable at 5.3 V with limited leakage current density (Fig. 7a). However, when the potential increases to 5.7 V, the commercial Gen2 exhibits a ten times higher leakage current density than the fluorinated electrolytes (Fig. 7b), indicating the much higher oxidation of the conventional carbonate solvents on the Pt electrode. The high initial Coulombic efficiency and the high capacity retention for LTO||LNMO cell at high-temperature test confirmed the excellent anodic stability of the fluorinated electrolytes.³²² Besides, the fluorinated electrolytes endow the cells with high rate capability although their ion conductivities are lower than that of the carbonate electrolytes,^{123,322} indicating that the passivation layers formed in the fluorinated electrolyte are thin and compact with good Li ion conductivity. Fan *et al.*,^{123,257} designed a fully fluorinated electrolytes using LiPF₆ as salt, and FEC, fluorinated linear carbonate (FEMC) and fluorinated ether 2,2,2-trifluoroethyl-3',3',3',2',2'-pentafluoropropyl ether (HFE) as the solvents with a weight ratio of 2:6:2. In the electrolyte solvents, HFE with the highest fluorine content produces the most LiF in SEI/CEI per solvent molecule during reduction, while FEC has the highest dielectric constant and highest affinity to Li ions, which

is responsible for salt dissolution. The FEMC has a compromised salt solubility and high anodic stability on the delithiated cathodes.^{325,326} This all-fluorinated electrolyte not only significantly enhances the cycling Li plating/stripping Coulombic efficiency to ~99.2%, but also dramatically improves the anodic stability on the aggressive cathodes including 4.4 V NMC811 and 5 V LCPO cathodes. The all-fluorinated electrolyte leads to a highly stable Li||LCPO cell with a capacity retention of ~93% for over 1000 cycles, and the record-high CE of 99.81%, surpassing the conventional carbonate and FEC-added electrolytes (Fig. 7c). Calculations indicate that the fluorinated solvents are more stable at the delithiated Li_xCoPO₄ surface (Fig. 7d–h). Combined with the XPS results, the authors speculate that the *in situ* formed thin fluorine-rich CEI deactivated the catalytic activity of the aggressive cathode surfaces, leading to the high electrochemical performance. Soon afterwards, Zhao *et al.*³²⁷ prepared a 1.2 M LiPF₆ FEC/DMC/HFE electrolyte with 0.15 M LiDFOB as additive and applied it to high-voltage Li||LCO cells, entailing a high capacity retention of ~84% after 300 cycles even with a high cutoff voltage of 4.5 V. In contrast, the Li||LCO cell in conventional 1.2 M LiPF₆ EC/DMC electrolyte only exhibits less than 150 cycles in the same cycling protocols. It should be pointed out that these fluorinated electrolyte concepts also work in the Na ion batteries.^{328–330}

Because of the high SEI formation capability for the fluorinated electrolytes, the fluorinated electrolyte shows a good compatibility to the graphite and Li metal anodes.^{7,123,272,276,331} Dahn *et al.*^{331,332} tested the graphite||NMC442 pouch cells with a high cutoff voltage of 4.5 V using the fluorinated electrolyte (1 M LiPF₆ FEC/TFEC + *x*% prop-1-ene-1,3-sultone (PES)). Compared to the cells with the commercial carbonate or sulfolane-based electrolytes with additive blends, the cells with FEC/TFEC-based electrolytes exhibit much better capacity retentions (Fig. 8a and c), smaller polarizations (Fig. 8b and d) in the prolonged cycling and smaller voltage drop (Fig. 8e), indicating that the fluorinated electrolytes generate a dense and compact SEI/CEI layer on the electrodes. Plenty of additives have been explored in the past decade to enhance the anodic stability of the carbonate electrolytes, in which VC, PES, methylene methanedisulfonate (MMDS), 1,3,2-dioxathiolane-2,2-dioxide (DTD), and tris(trimethylsilyl) phosphite (TTSPi) stand out.³³³ Surprisingly, the FEC/TFEC electrolyte entails a much better electrochemical performance for the graphite||NMC442 pouch cell (Fig. 8c and d) even than the optimized carbonate electrolytes with combined additives such as EC/EMC + PES/MMDS/TTSPi (PES-211) or EC/EMC + 2%PES + 2%TAP electrolytes.^{333,334} At high cutoff-voltage 4.5 V and 40 °C, the graphite||NMC442 pouch cell in FEC/TFEC electrolyte maintains a capacity retention of over 80% for 800 cycles, which represents one of the best electrochemical performance for the graphite||NMC cells in such harsh conditions. The relatively large resistance for the cells in the fluorinated electrolytes could be mitigated by adding some promising additives such as ES, MMDS, or TTSPi (Fig. 8f).

Smart *et al.*³³⁵ synthesized a series of fluorinated carbonate solvents and revealed that these fluorinated carbonates could effectively improve the low-temperature electrochemical

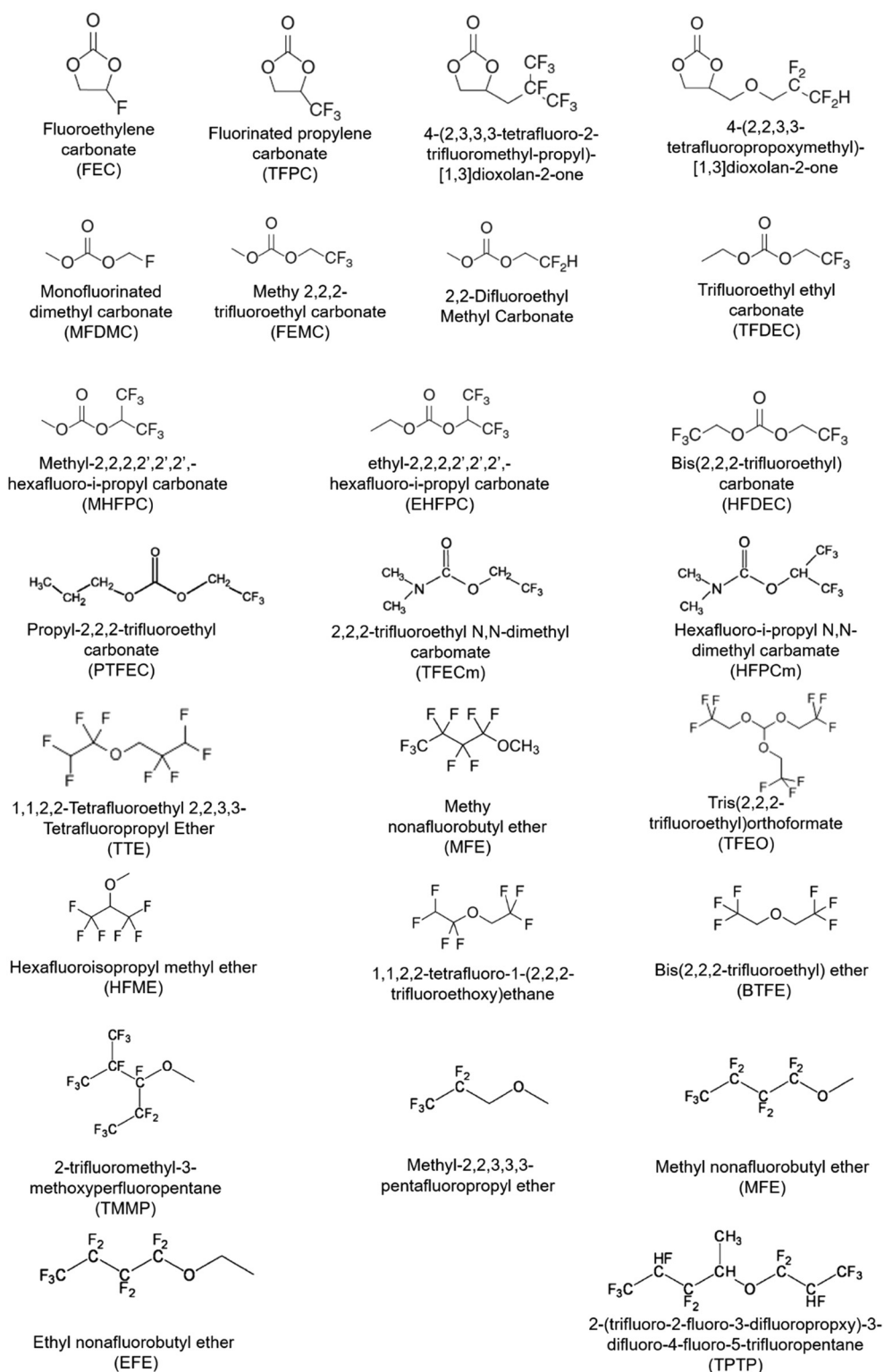


Fig. 6 Chemical structures of some representative fluorinated carbonates, carbamates and ethers for high-voltage Li ion battery electrolytes.

performance of the full cells. Recently, all-temperature batteries that could operate at any place on earth were developed by Fan *et al.*³¹⁵ based on the fluorinated electrolytes with non-polar fluorinated ether solvents, representing an encourage

path towards creating safe Li batteries with a sufficiently wide operational temperature window. For the fluorinated ether solvents, exceptions were recently achieved by Bao and co-workers,³³⁶ who covalently grafted an ether to the

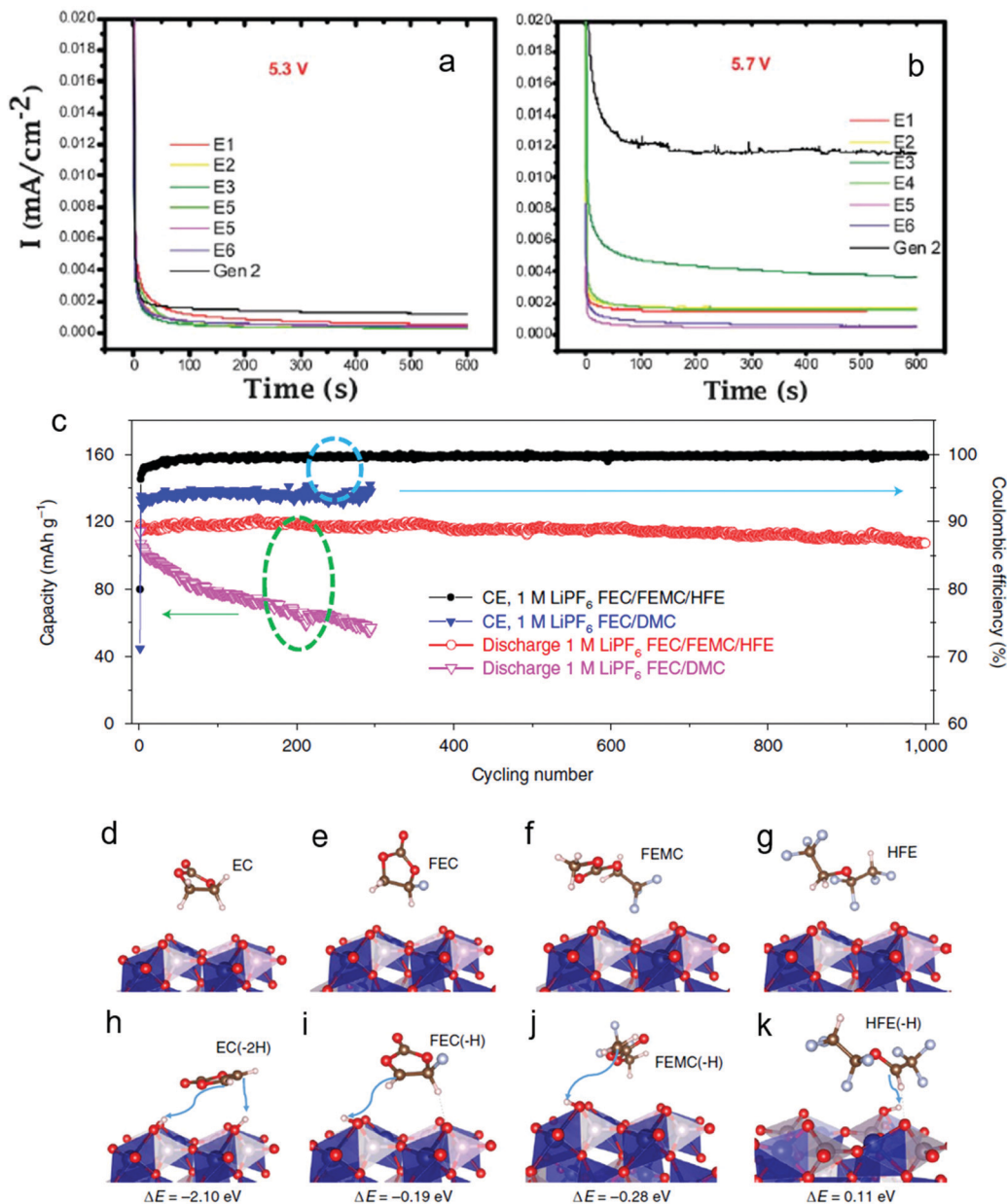


Fig. 7 Electrochemical stability and electrochemical performance of different electrolytes in high voltage cells. Current variation polarized at 5.3 V (a) and 5.7 V (b) for the different electrolytes using a 3-electrode electrochemical cell with Pt as the working electrode. Gen2, 1.2 M LiPF₆ in EC/EMC (3 : 7); E1, 1.2 M LiPF₆ in EC/EMC/FEPE (2 : 6 : 2); E2, 1.2 M LiPF₆ in EC/EMC/FEPE (2 : 5 : 3); E3, 1.2 M LiPF₆ in FAEC/EMC/FEPE (2 : 6 : 2); E4, 1.2 M LiPF₆ in FAEC/EC/EMC/FEPE (1 : 1 : 6 : 2); E5, 1.2 M LiPF₆ in FAEC/FEMC/FEPE (2 : 6 : 2); E6, 1.2 M LiPF₆ in EC/FEMC/FEPE (2 : 6 : 2). (c) Cycling performance of the LCPO in different electrolytes at 1C. (d–g) initial configurations; (h–k) final configurations and the reaction energies ΔE of EC, FEC, FEMC, and HFE solvents at the fully delithiated LiCoPO₄ (CoPO₄)(010) surface obtained from PBE+U DFT calculations. Brown spheres, C; Red spheres, O; White spheres, H; Light-blue spheres, F. Reaction energy ΔE is the energy difference between the physisorbed solvent molecules on the CoPO₄(101) surface and the reacted solvents. (a and b) Reprinted with permission from ref. 322 Copyright 2013 The Royal Society of Chemistry. (c–k) Reprinted with permission from ref. 123 Copyright 2018 Springer Nature.

hydrofluoroethers and realized a balance between ionic conductivity ($\sim 2.7 \times 10^{-4} \text{ S cm}^{-1}$ at room temperature) and oxidation stability ($\sim 5.6 \text{ V vs. Li}^+/\text{Li}$) for the fluorinated ether as the single solvent electrolytes. The new class of fluorinated ether electrolytes can support the NMC811 cathode for >100 cycles with a current density of 0.2C.³³⁶ To broaden the voltage window, some skeleton polymer solvents in polymer or

gel electrolytes are grafted with fluorinated branches to increase the anodic stability,³³⁷ which follow similar mechanisms to the liquid electrolytes.

3.3. Sulfone electrolytes

Sulfone is an economical byproduct by many chemical manufacturers, produced by tons and commonly utilized in high

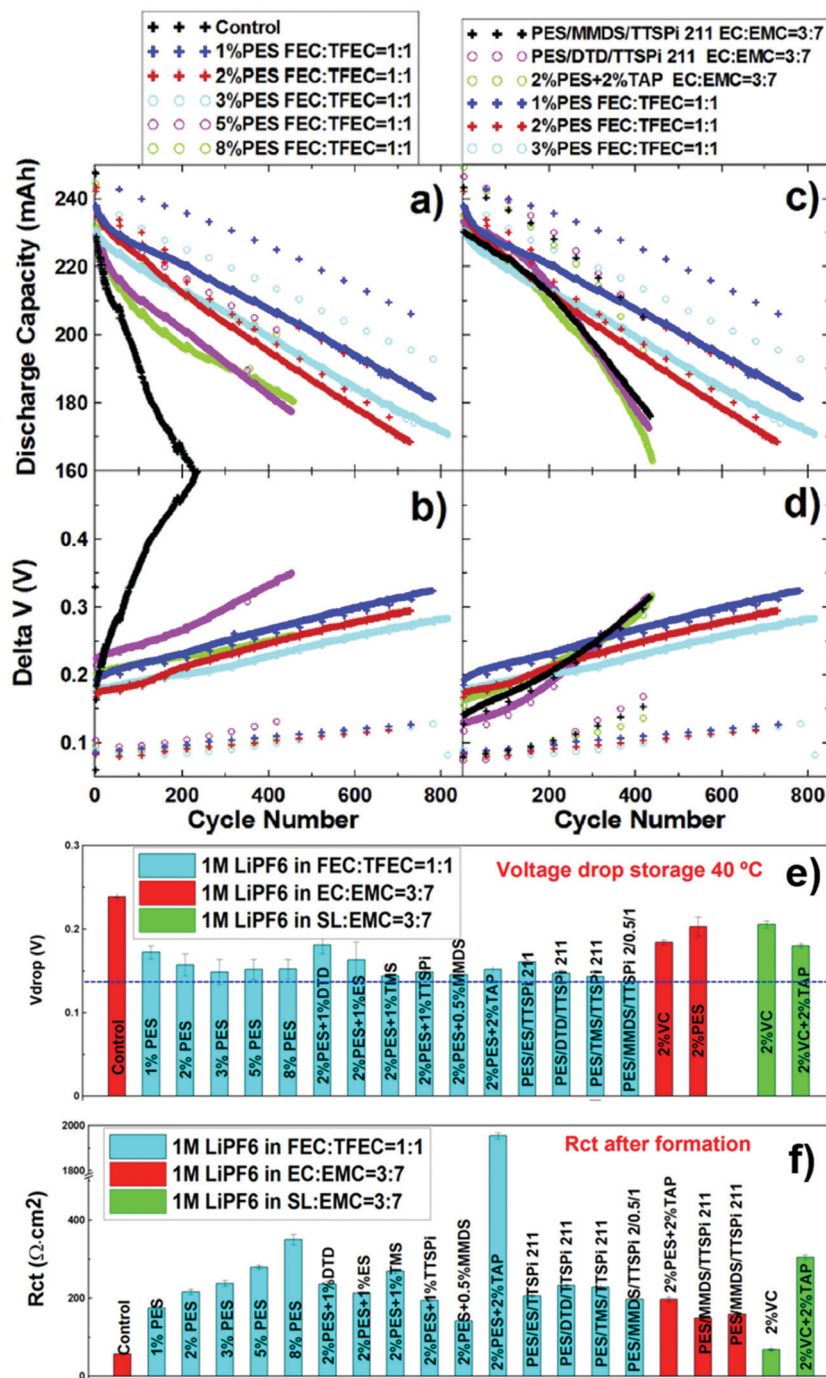


Fig. 8 Electrochemical performance of the graphite||NMC442 pouch cells cycling in different electrolytes between 2.8 V and 4.5 V at 40 °C. (a and c) Capacity vs. cycling number, the current density is 100 mA; (b and d) are the corresponding ΔV between the average charged and discharged potentials. (e) The V_{drop} of the cell in different electrolytes during 500 h storage at 40 °C and 4.5 V. (f) Charge transfer resistance (R_{ct}) measured after formation. The control electrolyte is 1 M LiPF₆ EC/EMC (EC:EMC = 3:7 wt% ratio). (a–d) Reprinted with permission from ref. 331 Copyright 2016 Elsevier. (e and f) Reprinted with permission from ref. 332 Copyright 2016 Elsevier.

temperature industry for organic and inorganic preparation as an extraction and reaction solvent, and metal and fungicide treatments.^{338,339} Compared to carbonyl in carbonate molecules and ether-groups in oligoethers, the stronger electron-withdrawing sulfonyl group serves to lower the energy level of the HOMO, leading to higher oxidation stability.³ Angell and

co-workers^{340–345} were the pioneers to introduce the sulfones (SL) into the solvent repertoire for the Li electrolytes, which show an remarkable electrochemical stability of >5.5 V vs. Li/Li⁺ even on the high surface activated charcoal, representing a leap towards the maximization of the anodic stability for the non-aqueous electrolytes.

Xu *et al.*³⁴¹ and Sun *et al.*^{342,343} synthesized a series of cyclic and acyclic sulfones and compared their physical and electrochemical properties. No oxidation reactions were detected before 5.5 V vs. Li⁺/Li for any sulfone electrolytes, while the compatibility between the sulfones and graphite could be altered by changing the functional groups of the sulfones. The impressive anodic stability of the sulfone electrolytes has been verified by various scenarios.^{345–349} For example, Dahn *et al.*³⁴⁶ realized the reversible intercalation/deintercalation of PF₆[−] into the graphite layers with a high-cutoff voltage of 5.6 V, while for the EC-based electrolyte, high solvent-oxidation reactions were detected at voltage of >4.8 V. It should be pointed out that batteries based on the anion intercalation into graphite were initiated by McCulloch and Carlin in 1994,³⁵⁰ and are flourishing in recent years benefiting from rapid progress of the innovative electrolytes.^{351–356} Amine *et al.*³⁴⁷ paired the 5 V LNMO cathode with an LTO anode, which exhibits a stable cycling performance for over 1000 cycles under 2C rate. The high anodic stability of the SL electrolytes and good compatibility with the LTO are the main reasons behind the outstanding electrochemical performance for the high-voltage LNMO spinel cathode.^{347,357} In virtue of high

anodic stability, ethyl methyl sulfone (EMS) electrolytes were adopted to unveil the delithiation reaction mechanisms of layered cathodes in the wide potential range up to 5.4 V vs. Li⁺/Li.³⁵⁸

To unveil the mechanism of high anodic stability for the SL electrolytes, Jiang *et al.*^{359,360} computed the electrochemical oxidation potentials for experimental tested SL electrolytes at HF (Hartree–Fock), B3LYP, PBE, and MP2 (Moller–Plesset perturbation theory to the second order) levels of theory for three solvation models (PCM, SMD and IPCM). It showed that the calculated oxidation potential of the four linear SL molecules using the MP2/PCM method are generally in good agreement with the experimental results. Orbital analysis revealed that the sulfone group dominantly contributes to the HOMO orbitals for the nonfunctionalized sulfone molecules. Fig. 9a depicts the electronic static potential map on the isosurface (0.001 a.u.) of electronic density for an ethylmethoxyethyl sulfone (EMES) molecule, which is a representative ether-functionalized sulfone. The large negative electrostatic potential on the sulfone oxygen (−43.5 kcal mol^{−1}) and strong positive potential (31.2 kcal mol^{−1}) along the branches for the EMES molecule lead to the large polarity and high anodic stability. Xing *et al.*^{361–363} calculated

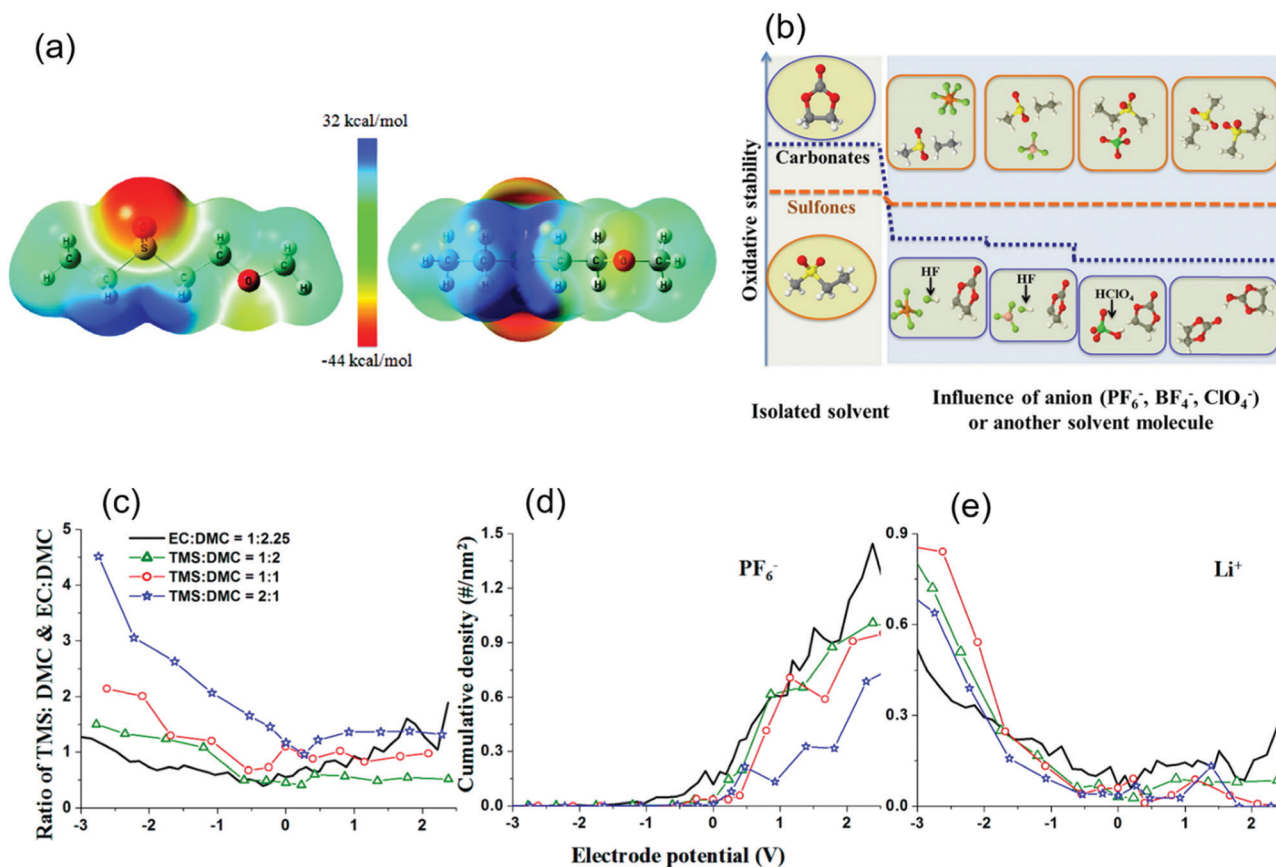


Fig. 9 (a) Side view (left) and top view (right) of electrostatic potentials for ethylmethoxyethyl sulfone (EMES). (b) Oxidation comparison between the SL and carbonate electrolytes with or without Li salts. Ratio of cumulative densities of TMS:DMC and EC:DMC in the interfacial layer (c), and the cumulative density in the interfacial layer of PF₆[−] (d) and Li⁺ (e) ions as a function of electrode potential. (a) Reprinted with permission from ref. 359 Copyright 2011 American Chemical Society. (b) Reprinted with permission from ref. 362 Copyright 2013 American Chemical Society. (c–e) Reprinted with permission from ref. 363 Copyright 2012 American Chemical Society.

and compared the oxidation pathways of three carbonates and eleven sulfones in the presence of anions and other solvent molecules by DFT calculations with a polarized continuum model. Surprisingly, the oxidation potential of isolated SL molecules is lower than that of carbonates. However, at the presence of anions and other solvents, the sulfones exhibit a higher stability, which is the key reason of higher anodic stability of SL-based electrolytes compared to carbonates (Fig. 9b). This result was echoed by the Borodin *et al.*,³⁶⁴ who demonstrated that the presence of most anions (BF_4^- , PF_6^- , FSI^- and $\text{B}(\text{CN})_4^-$) near the solvents could significantly decrease the anodic stability of most solvents such as carbonates (EC, DMC) and alkyl phosphates (TMP) due to the spontaneous H- and F-abstraction reaction that follows the initial electron removal step. As for SLs, the barrier of H-transfer is higher than other solvents, although the oxidation stability is also lower than the isolated unsolvated SL molecules.

Sulfones as the electrolyte solvent candidates possess several merits such as high dielectric permittivity, high anodic stability and low flammability. However, three annoying issues, *i.e.* high melting point, high viscosity and poor stability to the Li and graphite anodes, also persist and should be carefully tackled if utilized as the electrolyte solvents. Grafting functional groups in the sulfone molecules^{342,343,359,360,365,366} and mixing with other solvents/additives^{345,347–349,357,367–376} are two most effective methods to resolve these issues. Table 2 lists over 30 bifunctional SL solvents containing ether, ester, and carbonate moieties with diversified physical properties. Sun and Angell³⁴³ grafted different oligo ethylene glycol segments onto EMS ($T_m = 35^\circ\text{C}$). These new sulfones have a lower melting point than EMS and possess a wider electrochemical stability window than carbonate electrolytes but narrower than the non-functionalized SL. The ether groups in the functionalized SL molecules are easy to oxidize, resulting in a decreased anodic potential. This oxidation reaction can be largely mitigated by the neighbor sulfone group compared to the pure ether electrolytes,³⁵⁹ and fluorination of these side branches could hoist the anodic potential to almost the level of the non-functionalized SL.³⁶⁰ However, incorporation of the oligoether segments increases the viscosity and lowers the electrolyte conductivities.

Demeaux *et al.*³⁷⁷ pointed out that SL-based electrolytes could produce a nonstable and resistive layer on the Li metal surface, and meanwhile generate RSO_2^- and RSO_3^- species, which can diffuse to the cathode interface, and induce a drastic increase of charge transfer resistance. These drastic side-reactions between the SL-based electrolytes and the Li metal anode were also confirmed by the serious color change in the cycled Li metal.³⁷⁷ Meanwhile, the sulfones are also incompatible with the graphite anodes. Zhang *et al.*³⁷² investigated the effects of the different Li salts (LiBF_4 , LiPF_6 , LiFSI , LiTFSI , LiDFOB , and LiTDI) on the electrochemical properties of the EC-free SL electrolytes, and on the performance of the graphite anodes with carboxymethyl cellulose (CMC) as binders. Out of these salts, LiDFOB exhibits the best graphite anode cycling, even better than the commercial 1 M LiPF_6 EC/DEC (3:7, wt) electrolyte. It should be pointed out that the cycling

performance of the graphite anodes in the electrolyte are also highly influenced by the binders, and the CMC binders promote the SEI formations on the graphite anodes.³⁷⁸

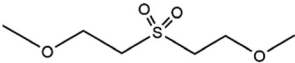
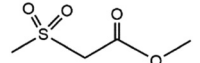
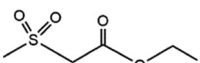
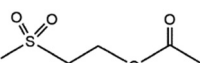
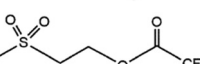
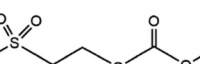
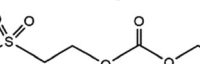
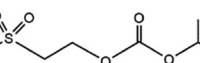
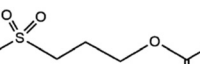
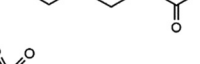
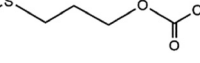
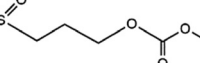
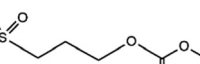
For the SL-based electrolyte, one important feature that should be pointed out is that once the SL solvents are mixed with carbonate solvents, the SL solvents rather than the carbonates dominate the anodic stability.^{349,357,363,370,376} Using $\text{LiPF}_6\text{-TMS/DMC}$ as a model electrolyte, Xing *et al.*³⁶³ demonstrated that the DMC molecules are located approximately 0.8 Å further away from the cathode surface than that in the $\text{LiPF}_6\text{-EC/DMC}$ carbonate electrolyte. The dominant SL molecules and the scarcity of the carbonates (Fig. 9c–e) adjacent to the cathode surface effectively increase the anti-oxidation stability of the SL mixed electrolytes, which is consistent with experimental results. A similar phenomenon was also observed in the SL–ethyl acetate (EA) system by Watanabe *et al.*³⁷⁰ The mixed-solvent electrolyte shows a high anodic stability, but slightly lower than that of pure SL, following the order of $\text{SL} > \text{SL-EA} > \text{EA} > \text{EC-EMC}$. The electrochemical performance of the 5 V $\text{Li}||\text{LNMO}$ cells in the SL–EA electrolyte was highly improved by addition of VC, which is one of the most effective additives as the enabler for the SL-electrolytes in the LIBs.^{344,348,367,368,370,379} Dahn *et al.*³⁷⁹ demonstrated that even 1% VC in the 1 M LiPF_6 SL/EMC 3:7 (w:w) could induce the LIBs to operate better than in the control-electrolyte (1 M LiPF_6 EC/EMC 3:7 (w:w)), while the cells using 1 M LiPF_6 SL/EMC without VC do not work at all because of the incompatibility between the SL and the graphite anodes. Fig. 10a shows the OCV vs. time of graphite||NMC442 pouch cells charged to 4.5 V with different amounts of VC stored at 40 and 60 °C. Compared to the cells with a control electrolyte, all VC-added SL/EMC cells show smaller voltage drop and the increased amount of VC leads to better storage performance at 40 °C. As the temperature increases to 60 °C, 3% VC exhibits a better storage performance than the control-electrolyte cells (Fig. 10b). Higher VC addition results in the higher resistance during cycling due to the continuous reactions of VC at the high-voltage surface of the delithiated cathode (Fig. 10c and d). Recently, Dahn and Xia³⁶⁷ demonstrated that the cycling and storage performance of the graphite||NMC could be further enhanced by adding other electrolyte additives, especially 2% triallyl phosphate (TAP), which exhibits smaller voltage drop during storage, higher CE and lower gas evolution during storage at 60 °C and 4.5 V as well as better capacity retention during long-term cycling (Fig. 10e and f).

Apart from these mentioned additives, other additives tested effective for the carbonate electrolytes also function well in SL-based electrolytes. Chen *et al.*³⁷¹ added the *p*-toluene-sulfonyl isocyanate (PTSI) as a film-forming additive in TMS-based electrolytes, which can form an effective SEI layer on the anode, supporting a good Li^+ ion intercalation/deintercalation cycle. Moreover, compared to the pure TMS electrolyte the electrolyte with PTSI shows lower melting points and better wettability. Using LiDFOB and TMPSi combinations in the SL electrolyte, Cui *et al.*³⁸⁰ increased the reversible capacity retention of graphite||LNMO from 64.1% to 80.5% for 300 cycles.

Table 2 Representative functionalized sulfones with distinct physical properties^{341,343,366}

Sulfone	Structure	mp (°C)	bp (°C)	ρ (g cm ⁻³)	η (cP)
TetraMS		27	285		
TriMS		75	95–97/0.5 mm (290) ^a		
MTS		< -20	150–153/20 mm (290) ^a		
MESL		< 0 ^b	94–96 (0.7 torr) 280–282		
EESL		24	308	1.21	19.1
IESL		< 0 ^b	105–107 (0.6 torr) 298–301	1.16	15.8
GLSL		< 0 ^b	310		
ACSL		65	248		
MCSL		92	232		
ECSL		56	272		
EMS		36.5	85–87/4.0 mm (~240) ^a		
MMMS			67/0.25 mm (~265) ^a		
MEMS		15	97 (2.0 torr) 261	1.21	11.5
EMES		2.0	103–105/1.0 mm (~286) ^a		
EMEES		< 0 ^b	170	1.15	12.0
EMEEES		< 0 ^b	> 290		

Table 2 (continued)

Sulfone	Structure	mp (°C)	bp (°C)	ρ (g cm ⁻³)	η (cP)
DMES		47	> 290		
MMSA		65	286		
EMSA		< 0 ^b	260	1.25	27.5
MSEA		48	102–104 (2.0 torr) 261	1.21	11.5
MSTFA		-1	98–100 (2.0 torr) 260–263	1.94	41.9
MSEMC		42	292	1.30 ^c	15.5 ^c
MSDEC		21	282	1.24 ^c	7.4 ^c
MSEiPC		57	244		
MSPA		< 0 ^b	250	1.23	49.2
MSPTFA		5	261	1.42	> 50
MSPMC		42	282	1.26 ^c	15.9 ^c
MSPEC		< 0 ^b	262	1.24	> 50
MSPiPC		21	281	1.19	> 50
MCPS		45	138–142 (0.6 torr) 343–347		

^a Reduced bp under atmospheric pressure by nomograph. ^b No crystallization and melting peaks observed by DSC even to -70 °C. ^c The values of density ρ and viscosity η are obtained at 60 °C.

3.4. Nitrile electrolytes

As demonstrated above, the high anodic stability of the sulfones can be ascribed to the high intrinsic stability of the sulfone group against oxidation at high voltage when used as the bulk electrolyte solvents. In contrast, more often than not, the anodic stability of the nitriles is believed to be due to the preferential chemisorption on the high-voltage cathode surfaces, which generates a layer of $-C\equiv N-TM$ complexes, and repels other species from the intimate contact with the catalytic surfaces of cathodes.^{381–389} In 1994, Ue *et al.*³⁹⁰ demonstrated that adiponitrile and glutaronitrile-based electrolytes can support an electrochemical double-layer capacitor (EDLC) for over 7.8 V *vs.* Li⁺/Li. Therefore, if adopting the nitriles as the electrolyte solvents, the commercialization of 5 V high-voltage

cathodes becomes possible, considering the similarity between the EDLC and batteries.^{382,391,392}

Similar to carbonate functional groups in alkyl carbonate solvents, which present high dipolar moment and dielectric constant, and dissociate types of salts, the terminal electron-rich nitrile (CN) groups are the high nucleophilic sites for coordinating Li ions.^{382,393} Smiatek and co-workers³⁹³ compared the dynamic and solvation structures of the adiponitrile with salts of LiBF₄ and LiTFSI by MD calculations and experimental characterization, which demonstrates that anion species could highly influence the molecular solvation, ion complex, and ionic conductivities. The ion complex formation is more evident for LiBF₄ compared to LiTFSI due to the smaller size of the BF₄⁻ anion. Similar phenomena

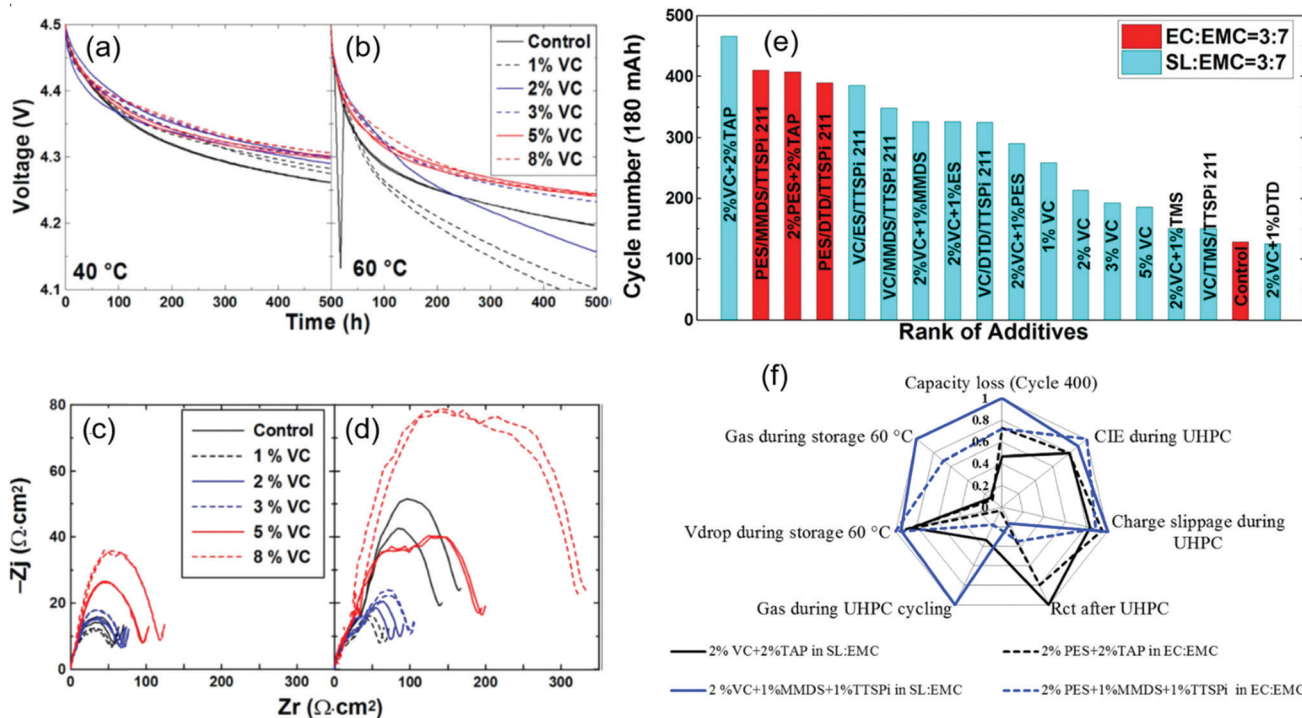


Fig. 10 Electrochemical performance of graphite||NMC442 pouch cells in 1 M LiPF₆ SL/EMC (3:7 wt% ratio) electrolytes containing different additives. OCV vs. time for graphite||NMC442 pouch cells charged to 4.5 V with different contents of VC stored at (a) 40 °C and (b) 60 °C; Impedance spectra of graphite||NMC442 pouch cells with different VC additive contents (c) before and (d) after UHPC test. (e) Cycling number when the cell capacity reaches 180 mA h for graphite||NMC442 pouch cells in the SL/EMC electrolyte with different additive combinations. (f) "Radar" plot for the additive combinations. The best additive combination should have the values close to the center of the radar plot. (a–d) Reprinted with permission from ref. 379 Copyright 2015 The Electrochemical Society. (e and f) Reprinted with permission from ref. 367 Copyright 2016 Elsevier.

were also reported in acetonitrile electrolytes.^{394–396} Thanks to the intrinsic high stability of the nitrile-based electrolyte, Okada *et al.*³⁹⁷ formulated a sebaconitrile-based electrolyte, 1 M LiBF₄ EC/DMC/SN (25:25:50 vol%), which exhibits excellent electrochemical stability above 6 V vs. Li⁺/Li and supports the reversibility of the 5.3 V Li₂NiPO₄F cathode. Abu-Lebdeh and co-workers³⁹⁸ examined a series of aliphatic dinitrile single solvent (N≡C-(CH₂)_n-C≡N, *n* = 3, 4, 5, 6, 7, 8) electrolytes, and compared binary (with EC) and ternary solvent (with EC/DMC) electrolytes. In the single aliphatic dinitrile electrolyte, the electrochemical window can be expanded to a record wide window of over 7 V. With addition of carbonate solvents, the window narrows, but still maintains 6–6.5 V.

As Aurbach *et al.*³⁹⁹ pointed out that the anodic and cathodic stabilities of the electrolytes are usually antagonistic. The poor cathodic stability and impoverished SEI formation capability of the nitriles crucially restricted their utilization in the graphite anodes. Therefore, other anodes rather than graphites are usually adopted to pair the cell in the pure nitrile electrolytes,^{400,401} or SEI enablers are necessary if utilizing graphite as an anode.^{285,382,397,402–404} For instance, Ghamouss *et al.*^{400,401} paired NCM111|LTO cells in the LiTFSI-adiponitrile electrolyte, which showed an extended cycling stability for over 200 cycles with a capacity retention of >98% and an extremely high CE close to 100%. Blending adiponitrile with DMC solvent and

LiDFOB and LiFSI as salts, Ehteshami and co-workers^{285,403,404} found that LiDFOB induced a more protective SEI layer than LiFSI, and the electrochemical performance of the cell could be further improved with the addition of FEC.

On the high anodic stability of the nitrile-based electrolytes, Xing *et al.*⁴⁰⁵ recently proposed a different mechanism using the succinonitrile (SN) as a representative solvent. Although the free SN molecules possess high anodic stability against oxidation, their interaction with salt anions critically lowers their oxidizable potential, leading to the formation of N-containing interphases on the cathode surface. To verify this mechanism, two different Co₃O₄ electrodes were utilized to test the stability in the baseline electrolyte (carbonate electrolyte without SN). One Co₃O₄ electrode was pre-soaked in the SN electrolyte (Fig. 11a), and the other was polarized in the SN-containing electrolyte at 4.5 V, then washed with DMC solvent (Fig. 11d). Serious color change of the baseline electrolyte after scanning test demonstrates the serious oxidation reactions between the pre-soaked Co₃O₄ and baseline electrolyte. In contrast, the oxidation of the baseline electrolyte is critically suppressed for the pre-scanned Co₃O₄ electrode, indicating that the formation of the CEI originated from the SN electrolyte, which effectively blocked the parasitic reactions. XPS results (Fig. 11c and 11f) further confirmed the formation of the N-rich interphase on the electrode surface. The compact and stable CEI layer derived from the nitrile decomposition was

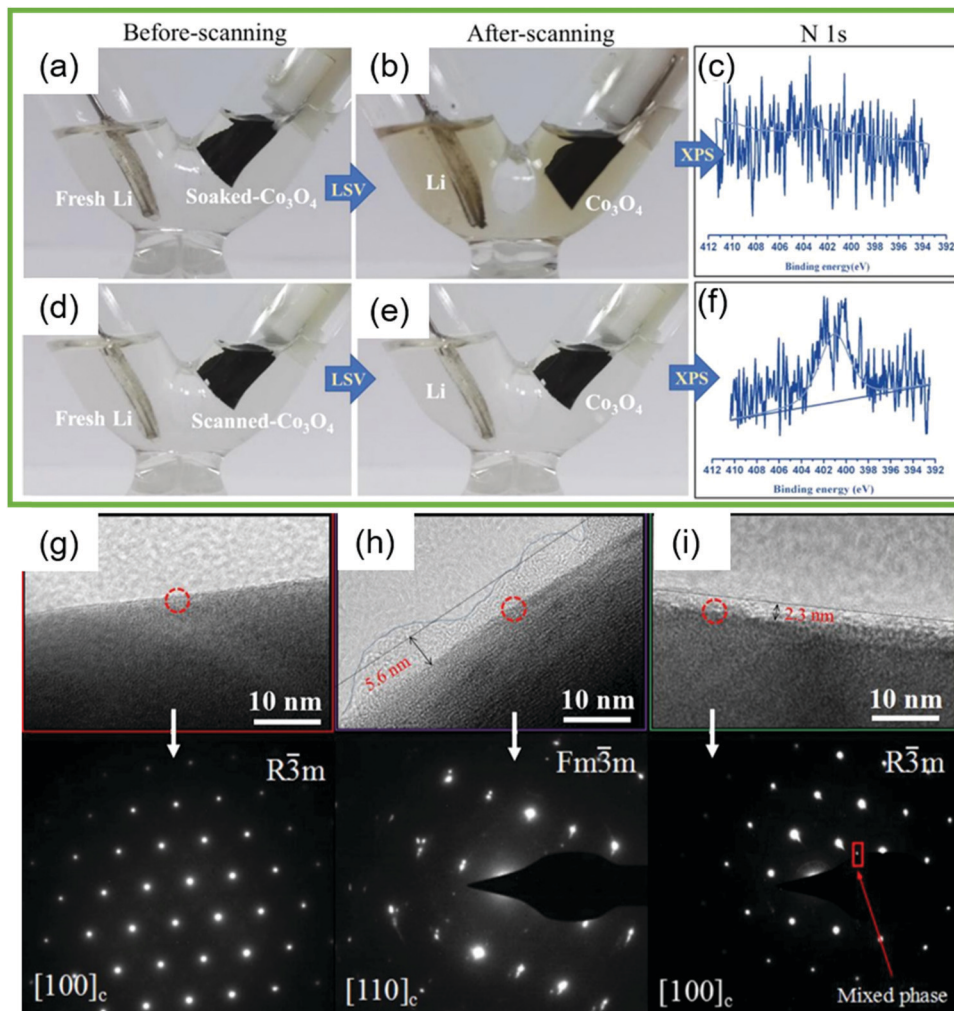


Fig. 11 Digital images of Li/soaked Co_3O_4 and Li/pre-scanned Co_3O_4 cells before (a and d) and after (b and e) linear sweep voltammetry (LSV) scanning. The N 1s XPS spectra of the soaked Co_3O_4 (c) and pre-scanned Co_3O_4 (d) after LSV scanning in the carbonate electrolyte without succinonitrile. TEM images of pristine NMC532 (g), cycled with a commercial carbonate electrolyte (h), cycled with the SN/FEC electrolyte (i) and corresponding electron diffraction images of the locations marked in (g–i). (a–f) Reprinted with permission from ref. 405 Copyright 2017 American Chemical Society. (g–i) Reprinted with permission from ref. 388 Copyright 2019 Elsevier.

also detected in NMC532 cell for a succinonitrile electrolyte (Fig. 11g–i),^{388,406} which minimized the parasitic reactions between the electrolytes and the cathodes.^{390,411,412}

The solvent variation fundamentally changes the electrolyte features, including the HOMO and LUMO energy, and interactions between Li^+ , anions and solvents, which critically influence the properties of the SEI/CEI layers on the electrodes. Among these promising EC-free systems, fluorinated electrolyte stands out in all-round properties such as the extremely high anodic stability, good passivation capability to most of the electrodes, favorable ion conductivity, good wettability to the electrodes and separators, and less-flammability. It is believed that the fluorinated electrolyte would create a niche market even through the cost is relatively higher than the commercial electrolytes. Moreover, the penetration of LIBs into multiple application areas would further promote the development of fluorinated electrolytes.

4. Concentrated electrolytes

The concentrated electrolyte concept could be traced back to as early as 1985, in which Dahn *et al.*⁴⁰⁷ revealed that the PC co-intercalation into ZrS_2 layered materials could be essentially suppressed if the LiAsF_6 concentration was increased to over a certain threshold (~ 3 M). In the past decade, this concept flourished with the expectation to further widen the electrochemical window and thereby increase the energy density of the cells,^{238,315,318,408–428} even though the ion conductivity is decimated because of the increased interactions of Li^+ and the anions.^{423,429} The concentrated electrolytes not only allow high reversible Li-ion intercalation into the graphite without participation of EC or other film-formation enablers,^{428,430–434} inhibit the Li dendrite formation in the Li-metal batteries,^{122,317,404,415,416,435} but also notably improve the anodic stability of the electrolytes on high-voltage cathodes.^{122,236,237,421,436,437}

In the conventional dilute electrolytes (*e.g.* 1 M), the molecular structures are predominantly solvent separated ion pair configurations, *i.e.* the majority of the solvent molecules are in a free state and the solvated Li ions and the anions are uniformly dispersed in these free solvents without formation of contact dimers (CDs) and contact ion pairs (CIPs, anion coordinating with one Li ion). As the salt concentration increases, the population of the free solvent molecules decreases with the simultaneous formation of CIPs and aggregate clusters (AGGs, anion coordinating with two or more Li ions).^{438,439} Inspiring is that these coordinated structures also effectively improve oxidation-resistance properties owing to their lower HOMO energies than the free solvent molecules and significantly improve the Li⁺ transference number to >0.5 along with the Li ion transport mechanism evolution from vehicular-type to Grotthuss-type.^{440–442} Representative calculated HOMO energies for different concentrated electrolytes are listed in Table 3. Although the absolute value of the HOMO energies varies for the same solvation structures calculated by different models, trend is the same, *i.e.* as the Li⁺ ions solvated with less solvent molecules, the HOMO energy substantially decreases, indicating the increase of the anodic stability. Besides the universal characteristics of the highly concentrated electrolytes, the anion species critically affect the structure and dynamics of concentrated systems.^{443–445} For example, the Li transference number in LiTFSI systems is higher than that in LiFSI systems because of the stronger TFSI–solvent interaction, even though the ions transport in LiFSI systems is always faster than that in LiTFSI systems.⁴⁴⁴ At high concentrations, the

solvent-shared dimers (SSDs), and CDs dominate in the LiPF₆-PC system, while CIPs, CDs, and AGGs prevail in the LiBF₄-PC electrolyte.⁴⁴³ Besides the well-established elimination of “free” solvent molecules at high concentrations,^{237,446–449} the CIP and AGG formation could entail the involvement of anions in the formation of the passivation layers,^{450–452} and thereby substantially increase the inorganic components in the SEI/CEI,^{122,236,412,413,453} and improve the electrolyte oxidation resistance.^{195,454} The unique electrolyte structure and the anion-derived interphases endow the electrolyte with encouraging features, such as a wide working potential window,^{122,421,436} high thermal stability,⁴¹⁰ low flammability,^{237,455} and good current collector corrosion-resistance.^{122,237,410,456} Therefore, the electrochemical performance of the high-voltage cells could be remarkably improved using the concentrated electrolytes. Table 4 compiles the electrochemical performance of representative cells with concentrated electrolytes or localized concentrated electrolytes.

Increasing the salt concentration can widen the potential window of the electrolytes, yet it seems that a threshold exists with the salt-to-solvent molar ratio of 1 : 2.²⁸⁶ Above this threshold, solvent decomposition was critically suppressed in all electrolyte systems. To distinguish from the conventional salt-in-solvent dilute electrolytes, in this section we utilized the term “solvent-in-salt”, which was firstly proposed by Suo *et al.*,^{431,464} to describe these kinds of highly concentrated electrolytes.^{425,457} Some researchers name the highly concentrated electrolytes with the specific composition of [Li(solvent)]X as “room-temperature ionic liquid” or the “quasi-ionic liquid” because of the electrochemical similarity between the ionic liquid and these types of super-concentrated electrolytes.^{3,458–462} The “quasi-ionic liquid” electrolytes will be discussed in the ionic liquid section.

Table 3 HOMO energy levels calculated for different solvents and the concentrated electrolytes

Composition	Atomic unit	HOMO energy level	Ref.
PC		−12.5	421
Li ⁺ (PC) ₄		−15.3	421
Li ⁺ (PC) ₃		−15.7	421
Li ⁺ (PC) ₂		−16.3	421
Li ⁺ (PC)		−16.9	421
PC		−8.0	463
Li ⁺ (PC) ₄		−11.0	463
Li ⁺ (PC) ₃		−11.5	463
Li ⁺ (PC) ₂		−12.1	463
Li ⁺ (PC)		−12.7	463
DMC		−7.8	463
Li ⁺ (DMC) ₄		−11.6	463
Li ⁺ (DMC) ₃		−12.0	463
Li ⁺ (DMC) ₂		−12.4	463
Li ⁺ (DMC) ₁		−12.8	463
G3 (all <i>trans</i>)	−0.42093	−11.45	459
[Li(G3) ₁] ⁺	−0.57001	−15.51	459
[Li(G3) ₁][TFSI]	−0.44483	−12.10	459
G4 (all <i>trans</i>)	−0.42116	−11.46	459
[Li(G4) ₁] ⁺	−0.54742	−14.90	459
[Li(G3) ₁][TFSI]	−0.43357	−11.80	459

Note: the HOMO energies of PC and Li⁺(PC)_{*n*} from ref. 421 are estimated by first-principle calculations using the Gaussian 09W (MP2 6-31G(d)). The HOMO energies of PC, DMC, Li⁺(PC)_{*n*} and Li⁺(DMC)_{*n*} from ref. 463 are calculated based on Gaussian 09W (B3LYP/6-31G(d)). The HOMO energies of G3, G4 and related solvated structures from ref. 459 are calculated based on Gaussian 03 (HF/6-311G**).

4.1. Carbonate-in-salt electrolytes

In 2003, Ogumi *et al.*⁴³⁰ realized the Li⁺ intercalation into graphite in a solo PC electrolyte by increasing the LiTFSI concentration, unveiling the essential distinctions between the diluted and concentrated electrolyte for the graphite anodes. After that, Matsumoto *et al.*⁴⁵⁶ demonstrated that the concentrated LiTFSI EC/DEC electrolyte could effectively suppress the Al corrosion at high voltage, which has been regarded as one of the annoying features for the low-concentrated LiTFSI/LiFSI electrolytes.^{492–494} Dahn *et al.*^{464,495} revealed that even in the conventional LiPF₆ EC-based electrolyte, higher concentration of LiPF₆ (>2 M) can effectively restrict the impedance growth of graphite||LCO in prolonged cycling if the cell is charged to over 4.3 V.⁴⁹⁵ In 2014, Henderson *et al.*⁴¹⁰ theoretically investigated the physical and electrochemical behaviors of EC–LiTFSI systems. Two crystalline solvates with the composition of (EC)₁–LiTFSI and (EC)₃–LiTFSI were identified in the phase diagram for EC–LiTFSI mixtures, and between these two solvates a crystallinity gap exists from 1.7–1 to 2.5–1 EC–LiTFSI.

Doi *et al.*^{421,436} compared the 5 V LNMO electrochemical performance in the LiBF₄/PC and LiPF₆/PC electrolytes with

Table 4 Selected cycling performances of high voltage Li cells in concentrated non-aqueous electrolytes or localized concentrated electrolytes

Electrolytes	Electrodes and cutoff voltage	Cycling performance	Ref.
7.25 mol kg ⁻¹ LiBF ₄ PC	Li LNMO, 5.0 V	92.5%@50th	436
4.27 mol kg ⁻¹ LiPF ₆ PC	Li LNMO, 5.0 V	92.3%@50th	421
2.0 M LiPF ₆ EC/EMC + 2% VC	Graphite LCO, 4.2 V, 40 °C	98%@50th	464
10 m LiFSI EC/DMC	Li NMC622, 4.6 V	86%@100th	122
5.49 M LiFSI DMC	Li LNMO, 5.2 V	95%@100th	237
8.67 mol kg ⁻¹ LiBF ₄ DMC	Li NMC811, 4.3 V	93.3%@50th	463
3.0 M LiPF ₆ EC/EMC/DMC (1 : 1 : 1 by vol)	Li Li _{1.2} Ni _{0.15} Fe _{0.1} Mn _{0.55} O ₂ , 4.8 V	94%@500th	465
6.5 M LiPF ₆ EC/DMC	Li NMC622, 4.6 V	78%@100th	466
4.0 M LiTFSI + 0.5 M LiDFOB FEC/DMC	Li LNMO, 4.9 V	88.5%@500th	467
5.4 M LiBF ₄ PC/FEC (1 : 1, <i>n/n</i>)	Graphite Li ₂ CoPO ₄ F, 5.2 V	70%@700th	468
7 m LiFSI FEC	Li LNMO, 5.0 V,	94.3%@150th	275
2.5 mol kg ⁻¹ LiBF ₄ PC/HFE (2 : 1 by vol)	Li LNMO, 5.0 V	96%@45th	316
0.96 mol kg ⁻¹ LiPF ₆ DMC/HFE (1 : 2 by vol)	Li NMC811, 4.3 V	92.4%@100th	469
5 M LiFSI DME	Li NMC111, 4.3 V	92%@500th	470
4.9 M LiFSI DME	Li NMC622, 4.3 V	80%@301th	471
4.6 m LiFSI + 2.3 m LiTFSI DME	Li NMC622, 4.4 V	88%@300th	472
2 M LiDFOB + 2 M LiTFSI DME	Li NMC111, 4.3 V	80%@500th	473
LiTFSI-triglyme (1 : 1 by mol)	Li LCO, 4.2 V	77%@200th	459
LiFSI-0.7DME-0.6PEO (1 : 0.7 : 0.6 in mol.)	Li NMC111, 4.3 V, 60 °C	86.7%@300th	474
3.0 m LiFSI sulfolane	MCMB LNMO, 4.85 V	69%@1000th	448
3.25 m LiTFSI + 0.1 m LiNO ₃ Sulfone	Li NMC811, 4.4 V	99.5%@200th	475
LiFSI-1.2DME-3TTE (1 : 1.2 : 3 by mol.)	Li NMC811, 4.4 V	87%@300th	476
1 M LiFSI DME/TFE (1.2 : 3 by mol.)	Li NMC811, 4.4 V	80%@300th	319
3.0 M LiFSI DME/TTE (8 : 2 by vol.) + 1wt% FEC	Li NMC811, 4.2 V	99.1%@100th	477
1.5 M LiFSI + 0.15 M LiCO ₂ CF ₃ DME/HFE (3 : 5 by vol.)	Li NMC532, 4.3 V	83%@250th	478
1.2 M LiFSI TEP/BTFE (1 : 3 by vol.)	Li NMC622, 4.4 V	97%@600th	479
1.4 M LiFSI DMC/TTE (2.2 : 3 by mol.)	Graphite NMC811, 4.4 V	100%@400th	480
1.4 M LiFSI DMC/TTE (2.2 : 3 by mol.)	Graphite Li _{1.2} Ni _{0.15} Co _{0.1} Mn _{0.55} O ₂ , 4.7 V	91.7%@100th	481
1.2 M LiFSI DMC/BTFE (1 : 2 by mol.)	Li NMC111, 4.3 V	80%@700th	317
LiFSI-3TMS-3TTE (1 : 3 : 3 by mol.)	Li NMC111, 4.3 V	80%@150th	482
2 M LiFSI DMC/1,2-dfBen (3 : 7 by vol.)	Li NMC532, 4.3 V	80%@140th	483
2.5 M LiTFSI DMC/HFME (1 : 1 by vol.)	Graphite NMC111, 4.35 V	89.2%@500th	320
3 M LiPF ₆ DMC/FEC/HFPM (6 : 1 : 3 by vol.)	Li LNMO, 5.0 V	94%@400th	484
LiFSI-1.5DMC-1.5TTE (1 : 1.5 : 1.5 by mol.)	Li NMC622, 4.6 V	93.5%@100th	485
2.5 M LiTFSI + 0.5 M LiDFOB succinonitrile	Li LCO, 4.5 V	77%@750th	486
5.3 M LiFSI TMP	Graphite LNMO, 4.8 V	96%@100th	487
LiFSI-2TEP (1 : 2 by mol.) + 5% FEC + 0.05 M LiBOB	Li LCO, 4.3 V	88%@350th	286
2.8 M LiFSI TEP + 10% FEC	Li NMC811, 4.3 V	95.7%@100th	488
1.2 M LiFSI TEP/FEC/BTFE (1.2 : 0.13 : 4 by mol.)	Si/graphite NMC111, 4.2 V	89.8%@600th	489
1.2 M LiFSI TEP/EC/BTFE (1 : 0.3 : 3 by mol.)	Graphite NMC811, 4.3 V	85.4%@300th	490
LiFSI-AN-VC (0.52 : 1 : 0.09 by mol.)	Li NMC111, 4.3 V	80%@400th	491

varied concentrations. As the salt concentration increases, the anodic stability of the electrolyte was enhanced, as indicated by the drops of HOMO energy for PC molecules with lowering the solvation number (-15.7, -16.3 and -16.9 eV for Li⁺(PC)₃, Li⁺(PC)₂, Li⁺(PC)), which was validated by LSV tests (Fig. 12a). The irreversible capacity, which is mainly due to the oxidative side reactions of electrolyte, was critically suppressed with the increase of the electrolyte concentration (Fig. 12b). After 50 cycles, a capacity retention of 92.3% was achieved for the concentrated electrolyte, while for the dilute electrolyte this value is less than 80% (Fig. 12b). Quite recently, Yamada *et al.*⁴⁶⁸ optimized the LiBF₄-PC electrolyte blends with FEC as an electrolyte additive, realized an extremely wide electrochemical stability window of > 5.5 V. Using 5.9 M LiBF₄ PC/FEC (7 : 3), the capacity retention for the graphite||Li₂CoPO₄F cell was as high as 70% after 700 cycles with an average CE of ~99.6%, representing a breakthrough for the post 5 V Li₂CoPO₄F-based batteries.

Compared to ether electrolytes, carbonate electrolytes were generally believed to be not compatible with the Li metal

anodes because of the facile reactions between the carbonyl groups and the Li metal.⁴⁹⁶ Recently, it was found that on increasing the LiFSI concentration in carbonate electrolyte to nearly saturation, the Li plating/stripping CE can reach >99%, and meanwhile the anodic stability can be further improved compared to the conventional carbonate and ether-in-salt electrolytes. The impact of the carbonate-in-salt electrolyte on the electrodes is schematically illustrated in Fig. 12c and d. Compared to the uneven and fragile CEI layers formed on the NMC in a conventional carbonate electrolyte, the fluorinated compact CEI layers derived from anion decomposition could effectively protect the cathodes from attack by acidic species.^{122,465,467} At 5.0 V vs. Li⁺/Li, the oxidation current density in the 10 m LiFSI-EC/DMC electrolyte is only 1/100 that of 4 m LiFSI-DME or 1/7 that of the 1 M LiFSI-EC/DMC electrolyte (Fig. 13a). Therefore, the carbonate-in-salt electrolyte endows Ni-rich Li||NMC batteries with a much better electrochemical performance, even though a harsher charge-discharge protocol with a 4.6 V cutoff voltage was employed (Fig. 13b-d). Such a high cutoff voltage

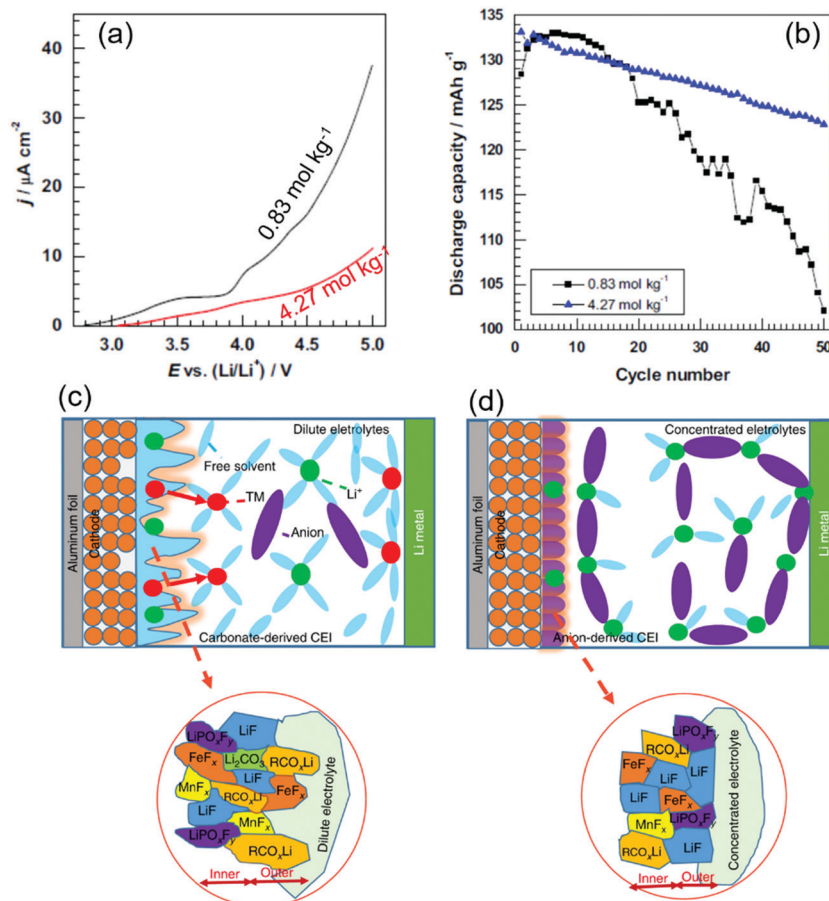


Fig. 12 Electrochemical performance of PC based electrolytes with different concentrated $\text{LiPF}_6/\text{LiBF}_4$ salts ($0.83 \text{ mol kg}^{-1} \text{ LiPF}_6$ PC and $4.27 \text{ mol kg}^{-1} \text{ LiPF}_6$ PC) on LNMO cathodes. Oxidation stabilities for different electrolytes of $0.83 \text{ mol kg}^{-1} \text{ LiPF}_6$ PC and $4.27 \text{ mol kg}^{-1} \text{ LiPF}_6$ PC as evaluated on Pt electrodes at a scanning rate of 1.0 mV s^{-1} . (b) Comparison of cycling performance for LNMO in the two electrolytes ($0.83 \text{ mol kg}^{-1} \text{ LiPF}_6$ PC and $4.27 \text{ mol kg}^{-1} \text{ LiPF}_6$ PC). Schematic comparison of diluted electrolyte (c) and concentrated electrolyte (d) on the cathode. (a and b) Reprinted with permission from 421 Copyright 2016 Elsevier. (e and f) Reprinted with permission from ref. 465 Copyright 2020 Springer Nature.

typifies a more rigorous test on the oxidation stability of the electrolytes on the catalytic delithiated cathode. After 100 cycles, the cell in a carbonate-in-salt electrolyte retained a capacity of $\sim 86\%$, possessing an improvement of almost 100% compared to the cell in the conventional salt-in-carbonate electrolyte.

However, solvent-in-salt electrolytes suffer poor wettability to the separators and the electrodes, increased viscosity, and decreased ion conductivity, all of which are adverse for the electrochemical devices. To conquer these intrinsic drawbacks for the highly concentrated electrolytes, Xu and Zhang *et al.*^{317,480} blended a “localized high-concentration electrolyte” (LHCE) with assistance of the highly fluorinated ether, in which the LiFSI salts are preferentially coordinated with polar carbonate molecules, independent of the content of the fluorinated ether bis(2,2,2-trifluoroethyl)ether (BTFE). BTFE serves as the diluent in the system. The extremely strong peak of $\text{Li}-\text{O}_{\text{DMC}}$ ($\text{DMC}-\text{LiFSI}$) located at 1.95 \AA together with the two tiny peaks of $\text{Li}-\text{OBTFE}$ at 5.63 and 4.65 \AA in the electrolytes imply that the Li^+ ion solvation occurs mainly by the DMC molecules (Fig. 13e), while the Raman spectra further proved this

phenomenon (Fig. 13f). The LHCE inherits the good anodic stability from the highly concentrated electrolytes, and meanwhile critically overcomes the drawbacks of the concentrated electrolytes, such as the viscosity and wettability issues.^{320,497,498} Therefore, the $\text{Li}||\text{NMC111}$ battery in the LHCE demonstrates a better electrochemical performance than the conventional 1 M and highly concentrated electrolytes. When cycled at a slow charge and fast discharge current protocol, the $\text{Li}||\text{NMC111}$ demonstrates a capacity retention of $> 80\%$ even after 700 cycles (Fig. 13g). Almost at the same time, He *et al.*³²⁰ demonstrated better electrochemical performance of the graphite $||\text{NMC111}$ pouch cell in the LiTFSI DMC/HFME LHCE electrolyte than in dilute and concentrated ($\text{LiTFSI}/\text{DMC} = 1:1.5$, $n:n$) electrolytes. Quite recently, several high-performance LHCEs were also reported including LiPF_6 FEC/FEMC/HFE,¹²³ LiPF_6 DMC/FEC/HFPM,⁴⁸⁴ LiBF_4 DMC/HFE⁴⁶⁹ and LiFSI DMC/TTE(HFE)⁴⁸⁵ electrolytes. In these three electrolyte systems, HFPM (1,1,1,3,3,3-hexafluoroisopropyl methyl ether) and HFE (1,1,2,2-tetrafluoroethyl 2,2,3,3-tetrafluoropropyl ether) are two highly fluorinated ethers and act as the diluent in the electrolytes.

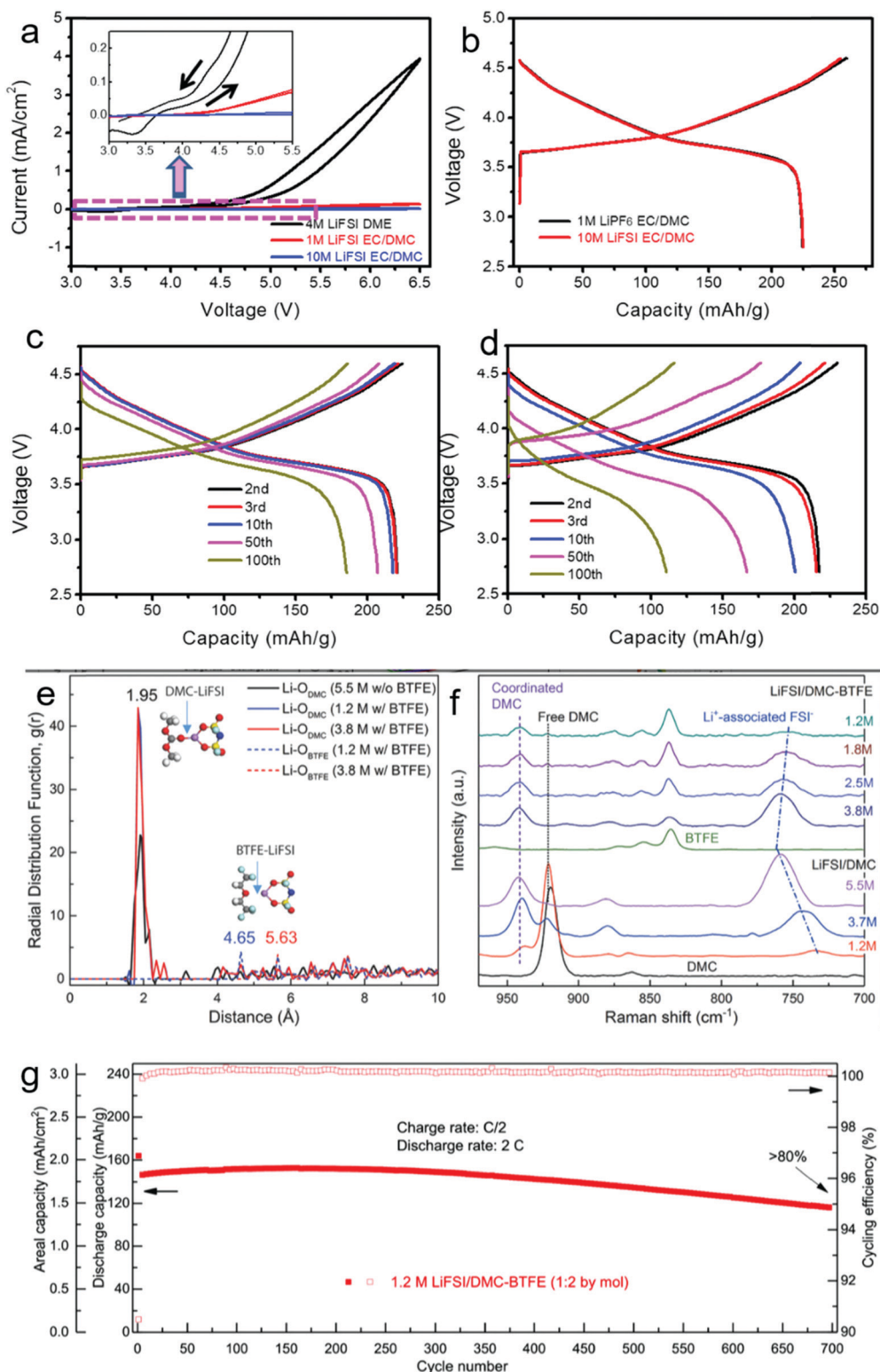


Fig. 13 Electrochemical performance of the Li||NMC batteries in a conventional dilute electrolyte (1 M LiPF₆ EC/DMC), carbonate-in-salt electrolyte (10 m LiFSI EC/DMC) and electrochemical performance of the Li||NMC cells in the “localized high-concentration electrolyte”. (a) Oxidation comparison between the 1 M LiPF₆ EC/DMC, 4 m LiFSI DME, and 10 m LiFSI EC/DMC electrolytes. The scanning rate is 10 mV s⁻¹. (b) The initial charge and discharge curves for the Li||NMC622 in the two electrolytes. (c) Charge and discharge curves of the Li||NMC622 cell in different cycles in carbonate-in-salt electrolyte (10 m LiFSI EC/DMC). (d) Charge and discharge curves of Li||NMC622 cell in different cycles in conventional dilute electrolyte (1 M LiPF₆ EC/DMC). The cutoff voltage is 4.6 V. (e) Radial distribution functions of Li–O_{DMC} and Li–O_{BTFE} pairs calculated from AIMD (*ab initio* molecular dynamics) simulation trajectories at 30 °C, with insets showing the structures of DMC–LiFSI and BTFE–LiFSI solvent–salt pairs. (f) Progression of Raman spectra with different salt concentrations in pure DMC and various DMC/BTFE mixtures. (g) Long cycling test of Li||NMC111 in 1.2 M LiFSI/DMC–BTFE (1:2 by mol) at C/2 charge and 2C discharge density. (a–d) Reprinted with permission from ref. 122 Copyright 2018 Elsevier. (e–f) Reprinted with permission from ref. 317 Copyright 2018 John Wiley & Sons, Inc.

4.2. Ether-in-salt electrolytes

The functionality of ether electrolytes is based on C–O–C ether groups, including ethereal solutions (*e.g.* dimethyl ether, DME; tetraethylene glycol dimethyl ether, TEGDME) or polyethers (*e.g.* polyethylene oxides, PEO) and its derivatives. The intrinsic low anodic stability of the ethereal group trammels the utilization of ether electrolytes generally in the low voltage battery systems (< 4 V) such as Li–S⁴⁹⁹ and Li–O₂ cells.⁵⁰⁰

The extremely high content salts fundamentally changed the physical and electrochemical performance of the ether electrolytes.^{501–503} Pappenfus *et al.*⁵⁰⁴ tested the anodic stability of the [Li(G4)]TFSI and [Li(G4)]BETI complex, which exhibits a high anodic stability of > 4.5 V vs. Li⁺/Li on the stainless steel electrode. Shortly afterwards, Watanabe *et al.*^{458,459} focused on this phenomenon and thoroughly investigated the anodic stability and the related mechanism of different concentrated ether electrolytes. Compared with the oxidation limit of 4 V for the LiTFSI-in-glyme, the anodic stability of the [Li(glyme)₁]-[TFSI], in which the molar ratio between the LiTFSI and glyme is 1:1, could be broadened to ~ 5 V vs. Li⁺/Li. The authors speculated that the enhancement of the oxidative stability is due to the donation of long pairs of ether oxygen atoms to the Li⁺ ions, leading to the reduction of the HOMO energy level of

glyme molecules. Thanks to the high anodic stability on the cathode side and the good compatibility to the Li metal anode, the Li||LCO cells with [Li(G3)₁][TFSI] and [Li(G4)₁][TFSI] can deliver a reversible capacity of 100 and 85 mA h g⁻¹ even after 200 cycles, respectively, while the cells in the dilute ether electrolytes can only ensure 10 cycles.

Resorting to LiDFOB, which is generally regarded as one of the best electrolyte additives because of its capability to form an insoluble and compact interface layer on the electrode surfaces,^{505–508} Jiao and co-workers⁴⁷³ designed a dual-salt (LiDFOB and LiTFSI) concentrated ether-based electrolytes. Compared to the NMC111 cycled in 3 M LiTFSI DME and 4 M LiDFOB DME electrolytes, the CEI on the NMC111 cathode cycled in 4 M dual-salt DME are much thinner, compact (Fig. 14a–d) and enriched with C–O, B–O, B–F and LiF species,⁴⁷³ which empowers the effective protection on the NMC cathodes, and prohibits the continuous electrolyte oxidation in the prolonged cycles. Therefore, the Li||NMC111 cell delivers a much better electrochemical performance, achieving a high capacity retention of $> 90\%$ after 300 cycles and 79% after 500 cycles even to a high cut-off voltage of 4.3 V.⁴⁷³ The Bi-salt concept in the concentrated ether electrolyte was also applicable for the combination of other salts, such as

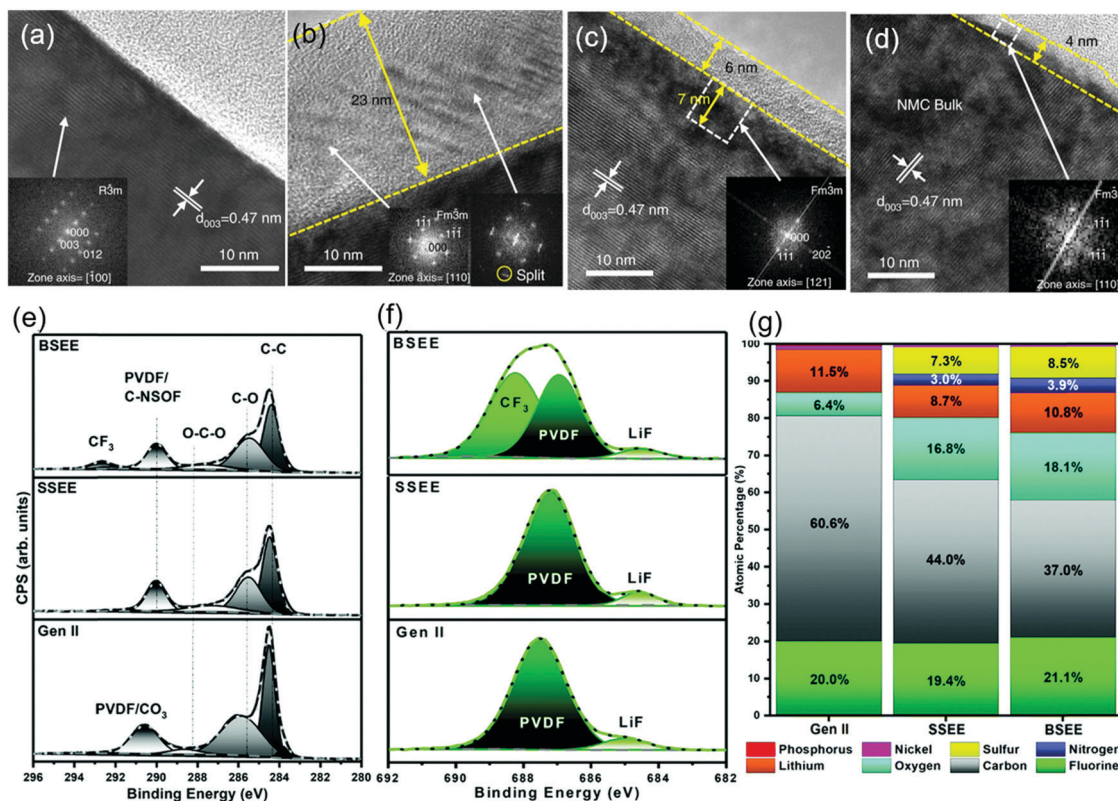


Fig. 14 TEM analysis of the CEI layers for the pristine and cycled NMC111 in concentrated ether electrolyte: the pristine NMC111 cathode (a); NMC111 cycled for 50 cycles in 3 M LiTFSI DME (b), in 4 M LiDFOB DME (c); in 4 M dual-salt (2 M LiTFSI + 2 M LiDFOB) DME (d). Insets are the fast Fourier transform (FFT) patterns of selected regions. XPS results of NMC622 cycled for 200 cycles in carbonate and concentrated ether electrolytes (BSEE, SSEE and Gen II are 4.6 m LiFSI + 2.3 m LiTFSI DME, 4.6 m LiFSI, 1.0 m LiPF₆ EC/EMC (3:7), respectively): (e) carbon 1s, (f) fluorine 1s, and (g) total elemental percentage. (a–c) Reprinted with permission from ref. 473 Copyright 2018 Springer Nature. (e–g) Reprinted with permission from ref. 472 Copyright 2019. The Royal Society of Chemistry.

LiTFSI/LiFSI,^{472,509–511} LiFSI/LiDFOB,⁵¹² LiFSI/LiTFSI,⁵¹³ and LiFSI/LiPO₂F₂.⁵¹⁴ Xu *et al.*⁴⁷² blended a 4.6 m LiFSI + 2.3 m LiTFSI DME electrolyte and realized the high reversibility of the aggressive Ni-rich NMC cathodes. Both FSI- and TFSI-anions contribute to the formation of the CEI layers with lower concentration of carbon-based moieties from the oxidized DME (Fig. 14e–g). The anodic stability of the LiTFSI/LiFSI dual-salt DME electrolyte is even better than that of the commercialized carbonate electrolyte, presenting an anodic stability of ~5.0 V (Fig. 15a). The high anodic stability (Fig. 15a) and the high compatibility to the Li metal (Fig. 15b) of the LiTFSI/LiFSI dual-salt DME electrolyte actualize an exceptional electrochemical performance of Li||NMC622 even at the high cut-off voltage of 4.4 V vs. Li⁺/Li (Fig. 15c and d).

4.3. Other organic solvent-in-salt electrolytes

Nitrile-based electrolytes are well known for their fast dynamic behavior and good oxidation resistance at high voltage. However, because of the high reactivity of the nitriles between the Li metal and the poor SEI formation capability, as the solo solvent, nitriles cannot be directly utilized in conventional LIBs.⁵¹⁵ Yet, one exception does exist if the salt concentration is highly increased, in which the unique solvation structure

with high content CIPs and AGGs could induce the formation of anion-derived SEI layers on the anodes.^{237,250} Seo and co-workers^{394–396} systematically investigated the solvation structure of acetonitrile with different concentrated Li salts including LiClO₄, LiBF₄, LiNO₃, LiTFSI, LiAsF₆, and LiPF₆. Yamada *et al.*⁵¹⁶ unveiled that as the LiTFSI concentration was increased to >4 M, enhanced reductive stability of the acetonitrile (AN) electrolyte was achieved, which renders a highly reversible Li⁺ intercalation into the graphite anode. The intercalation kinetics is even faster than that in the commercial carbonate electrolytes (Fig. 16a and b), although the ion conductivity is decimated and the viscosity is dramatically increased.

Mixtures of dinitriles (succinonitrile, glutaronitrile, and adiponitrile) and LiTFSI were systematically investigated by Ugata and co-workers,⁴⁴¹ including liquid structures, transport properties and electrochemical properties. Considerable formation of CIPs and AGGs was detected in the concentrated nitriles, in which Li⁺ dynamically exchanged coordination with nitrile and TFSI⁻, resulting in an increase in the ratio of the self-diffusing coefficients of Li⁺ and TFSI⁻. Therefore, the Li⁺ transference number in these salt-in-nitrile electrolytes could be as high as 0.74.⁴⁴¹ Adopting AIMD methods to a LiTFSI/AN

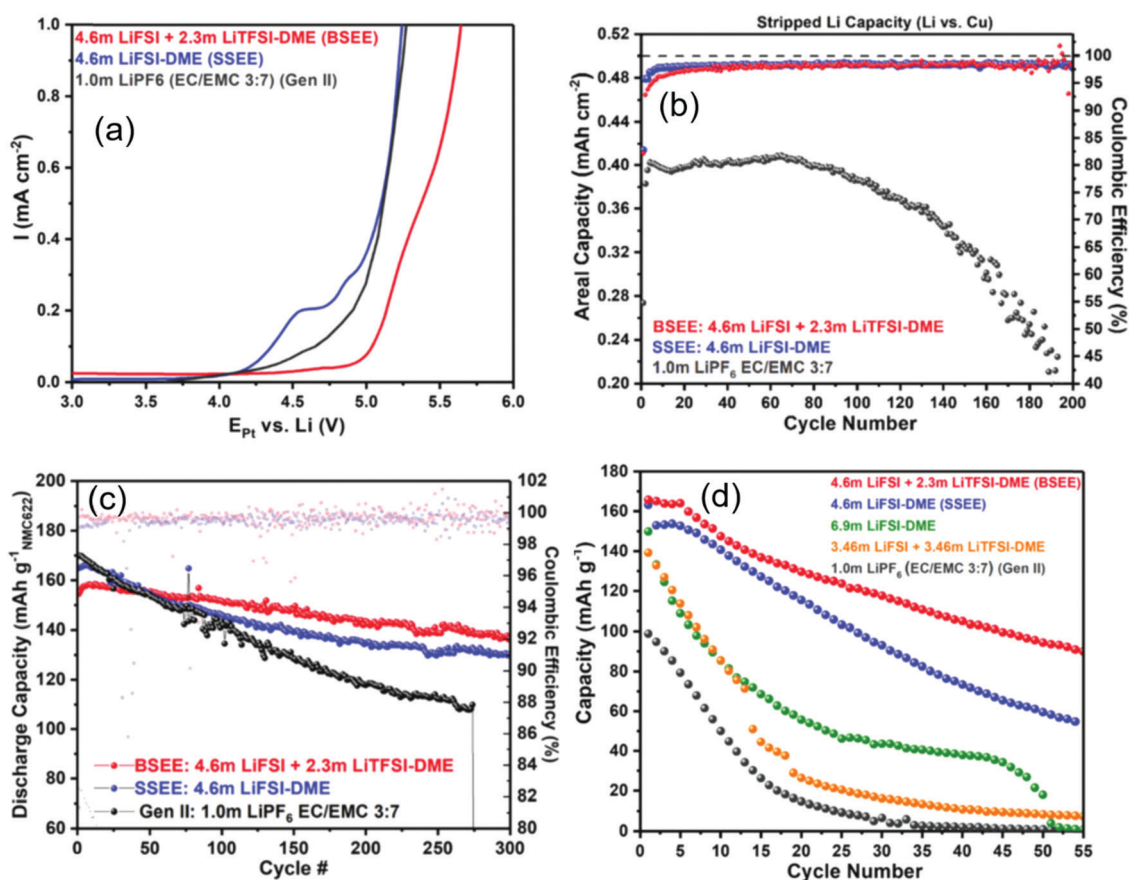


Fig. 15 Electrochemical performance for various cell configurations in different electrolytes. (a) Oxidation stability test measured via linear sweep voltammograms using a Pt vs. Li metal cell; (b) coulombic efficiency of Li plating/stripping in different electrolytes; (c) cycling performance of Li||NMC622 cells in different electrolytes; (d) cycling performance of Cu||NMC622 anode free cells in different electrolytes. Reprinted with permission from ref. 472 Copyright 2019. The Royal Society of Chemistry.

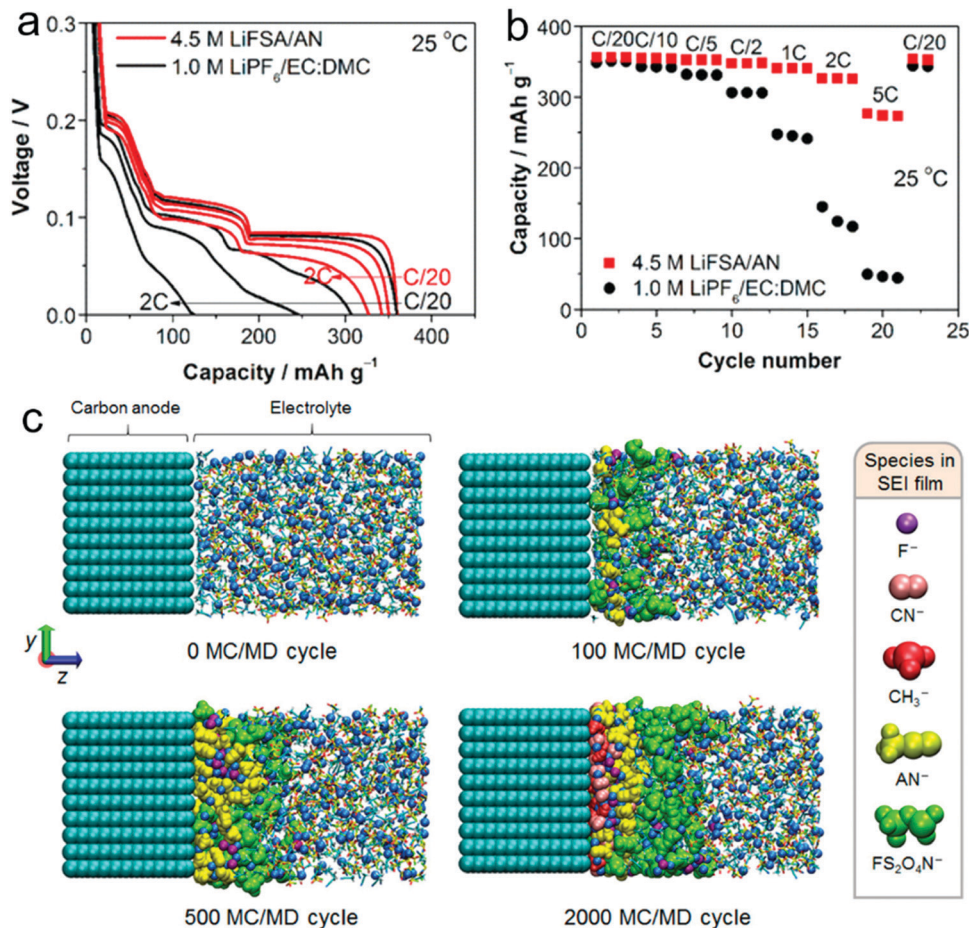


Fig. 16 Graphite anode performance in concentrated AN and conventional EC electrolytes. (a and b) Li ion intercalation voltage curves and the corresponding rate performance of the natural graphite with concentrated 4.5 M LiFSI/AN and conventional 1.0 M LiPF₆/EC-DMC electrolytes. (c) Snapshots of SEI formation processes on the graphite in a 5 M LiFSI/AN electrolyte (blue: Li⁺; white: hydrogen; red: oxygen; yellow: sulfur; cyan: carbon; green: fluorine). (a and b) Reprinted with permission from ref. 516 Copyright 2014 American Chemical Society. (c) Reprinted with permission from ref. 424 Copyright 2018 American Chemical Society.

electrolyte, Sodeyama *et al.*⁴¹³ demonstrated that TFSI⁻ anions would preferentially accept the electron in the highly concentrated electrolyte and meanwhile hinder the reductive decomposition of AN, resulting in the improved electrochemical stability on the anode surface. This surface reaction mechanism was recently echoed by Takenaka and co-workers,⁴²⁴ who presented a detailed simulation in atomistic reactions using the Red Moon method for the concentrated LiFSI/AN electrolyte. Fig. 16c shows the four typical snapshots of SEI formation processes on the graphite in a 5 M LiFSI/AN electrolyte. The FS₂O₄N⁻ anions (green) will be generated apart from the electrode surface during the reduction of FSI⁻ anions at the beginning. Instantaneously, the AN⁻ anions (yellow) without further decomposition are continually formed (500 MC/MD cycle), which will transfer the electrons to the FSI⁻ anions and enhance the formation of the Li salt-based SEI film. These simulations are in good agreement with the experimental observations.^{491,516} Quite recently, Cui and co-workers⁴⁸⁶ designed a dual-anion deep eutectic solution (D-DES) electrolyte using LiTFSI and LiDFOB as salts and pure SN as the

solvent, and realized a high reversibility of the Li||LCO cell for 500 cycles with an extremely high cutoff voltage of 4.7 V. Meanwhile, the flammability of the electrolyte is fundamentally suppressed. All of these features represent a great step forward for the next-generation Li batteries in terms of energy density and safety.

Different from the ligand structure of the nitrile, in which Li⁺ coordinated with the terminal nitrile groups, the sulfonyl group with two O atoms tends to coordinate with two different neighboring Li ions, and meanwhile the surrounding anions form ionic clusters with Li⁺ ions.^{442,517} Xu and Meng *et al.*^{448,472} make full use of the features of the concentrated electrolyte and the high anodic stability of the SL solvents. The high concentrated LiFSI salt can form an effective and stable SEI layer from the FSI⁻ anion decomposition, suppressing the solvent co-intercalation into the graphite interlayers, while the SL solvent and the salt simultaneously address the interfacial stability of the LNMO cathode. As all SL molecules are coordinated with Li⁺ ions, the oxidation potential for the LiFSI-SL complexes significantly increases from 4.65 V (Fig. 17a and b)

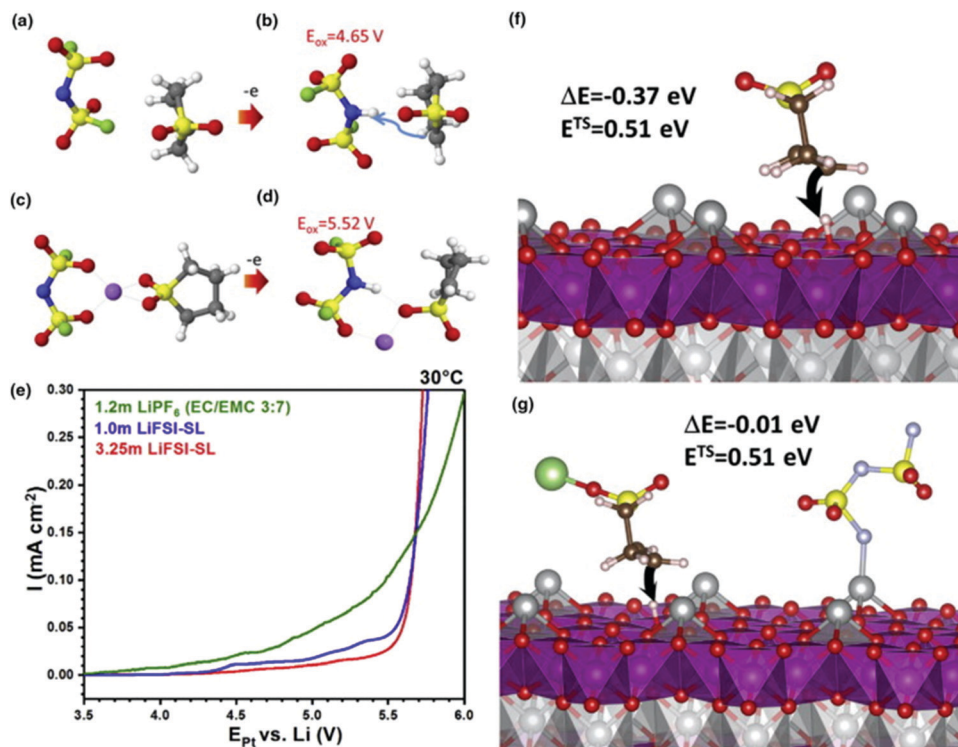


Fig. 17 (a–d) Oxidation potential (E_{ox}) (vs. Li/Li⁺) from G4MP2 QC calculations with clusters surrounded by SMD(SL) implicit solvent model. (e) LSV tests for the three electrolytes. H-Transfer reaction from SL (f) and Li–SL separated from FSI (g) to the Ni_{0.5}Mn_{1.5}O₄ cathode surface from PBE+U DFT calculations. ΔE and E^{TS} are the H-transfer reaction energy and barrier, respectively. Reprinted with permission from ref. 448 Copyright 2018 Elsevier.

to 5.52 V (Fig. 17c and d). This characteristic was confirmed by LSV tests (Fig. 17e), which show that the concentrated LiFSI-SL electrolyte exhibits the highest anodic stability for over 5.5 V among all of the tested electrolytes. DFT calculations demonstrate that the SL deprotonation reaction energy for the SL-Li⁺ complex is sufficiently close to zero (-0.01 eV, Fig. 17g), much lower than the reaction energy for the uncomplexed SL molecules (-0.37 eV, Fig. 17f), revealing the reasons for the extremely low oxidation current for the concentrated LiFSI-SL electrolytes. Moreover, in the concentrated SL electrolyte, Li⁺ ions exchange ligands dynamically, *id est*, hop from one coordination site to another,⁵¹⁷ which suppresses the concentration polarization in Li batteries and leads to improved rate capability compared to the diluted electrolytes.⁵¹⁸ A high capacity retention of 70% was retained after 1000 cycles for this 5 V high-voltage graphite||LNMO full cell in the SL-in-salt electrolyte, while the conventional carbonate electrolyte can only support less than 180 cycles.¹²⁷ Similar electrochemical performance enhancement and mechanism on “localized high-concentrated SL electrolyte” were also reported by Ren *et al.*⁴⁸² recently in Li metal batteries.

The phosphates are promising electrolyte solvents because of high anodic stability and the non-flammable features, which have been utilized as the flame-retardant additives or the co-solvents.^{519–526} Yet, the poor electrolyte/electrode interfacial contact and electrolyte instability restrict their large-scale applications.^{519,522,527} Resorting to the high concentration concept, Yamada *et al.*⁴⁸⁷ and Cao *et al.*²⁸⁶ realized the stable and compact passivation layers on the electrodes, respectively,

which allows stable charge/discharge cycling of both anodes and aggressive cathodes. The concentrated LiFSI triethyl phosphate (TEP) electrolyte possesses a wide voltage window of 0–5.5 V *via* CV test on a Pt microelectrode, and more importantly is compatible to most of the commercial electrodes, including Li metal and graphitic anodes,²⁸⁶ and Ni-rich NMC and LCO cathodes.⁴⁸⁸ The commercial LCO electrode delivers a reversible capacity of 135 mA h g⁻¹, high Coulombic efficiency of 99.7%, and an impressive capacity retention of 88% after 350 cycles in the 1:2 LiFSI-TEP + FEC-LiBOB electrolyte (Fig. 18a and b). With the high loading of 12.46 mg cm⁻² graphite and 29.4 mg cm⁻² LCO, the 18650 cell presented a favorable cycling performance (Fig. 18c and d) and good rate performance (Fig. 18e), although the ion conductivity of the 1:2 LiFSI-TEP + FEC-LiBOB electrolyte is only 1/10 of the commercial electrolyte.²⁸⁶ The cells with the 1:2 LiFSI-TEP passed all the harsh safety tests, including nail penetration tests (Fig. 18f). Following these thrilling results, Zhang *et al.*,^{479,490} Yamada *et al.*⁵²⁸ and Dong *et al.*⁴⁸⁸ further optimized these phosphate-in-salt electrolytes by introducing the fluorinated ethers and FEC into the electrolytes, and realized a highly reversible Li metal cell for over 2000 cycles.⁴⁸⁸

4.4. Water-in-salt electrolyte

In 1994, Dahn and co-workers^{529,530} first reported a kind of rechargeable aqueous Li battery with LiMn₂O₄ and VO₂(B) as electrodes, and 5 M LiNO₃ aqueous solution as the electrolyte, which were fundamentally safe and cost-effective with a

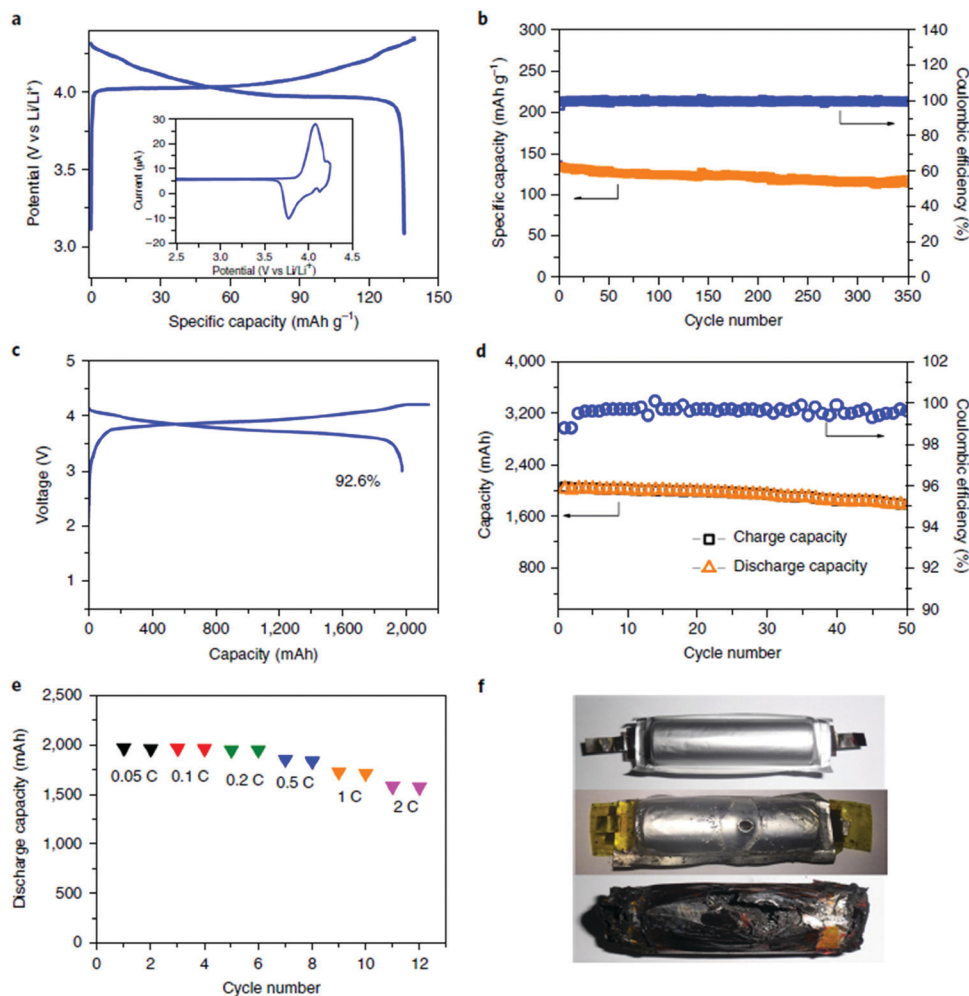


Fig. 18 Electrochemical performance for the LCO cathode and 18650 cells in the electrolyte 1 : 2 LiFSI–TEP + FEC–LiBOB. (a) The initial charge/discharge profiles for LCO. The inset is the cyclic voltammogram with a scanning rate of 0.1 mV s^{-1} . (b) Cycling performance of the LCO at a specific current of 20 mA g^{-1} . (c) The first charge/discharge profile of the 18650 cell. (d) Cycling performance at a rate of $1/20\text{C}$ ($1\text{C} = 2000 \text{ mA}$). (e) Rate performance of the 18650 cell. A constant voltage step is performed at 4.2 V with a cut-off current of 40 mA . (f) Nail penetration test for the 18650 cells using 1 : 2 LiFSI–TEP + FEC–LiBOB electrolyte (middle) and commercial electrolyte (1 M LiPF₆ EC/DEC/EMC (1 : 1 : 1 by volume)) (bottom). The top cell is the blank cell before the nail test. Reprinted with permission from ref. 286 Copyright 2018 Springer Nature.

compatible energy density with lead-acid batteries. However, the narrow electrochemical stability window of the aqueous electrolyte (1.23 V), defined by the “Pourbaix limits” of the aqueous electrolytes, critically restricted the working potentials and the selections of the anode and cathodes for the aqueous LIBs.^{531–533} Only the materials whose working potentials positioned in the window of aqueous electrolytes can be utilized as the electrodes. Therefore, aqueous LIBs are generally recognized as low energy density systems even though with intrinsic safety features.⁵³²

Things have been changing since 2015, when Suo *et al.*⁴²⁵ ground-breakingly expanded the electrochemical stability window of an aqueous electrolyte to $>3.0 \text{ V}$ by reducing the water activity and *in situ* generating the protective interphases on the anodes in the highly concentrated LiTFSI aqueous electrolyte. The SEI, composed of LiF-rich inorganic species, was realized for the first time in aqueous media thanks to the

reduction of the highly concentrated organic salts and low solubility of LiF.^{425,534–537} These *in situ* formed inorganic-rich SEI layers and hydrophobic anion absorption on cathodes fundamentally broadened the working potential windows of the aqueous electrolytes, which could cover the working potentials of most electrode materials (Fig. 19) and therefore theoretically boosted the energy density of the aqueous battery to the level of the non-aqueous counterparts unprecedentedly.^{538–541}

A 2.0 V Li ion battery was demonstrated with Mo₆S₈ as an anode and LiMn₂O₄ as a cathode in the water-in-salt electrolyte (Fig. 20a), which cycled up to 1000 times with nearly 100% Coulombic efficiency even at a low charge/discharge rate of 0.15C .⁴²⁵ Further increasing the salt concentration by the bi-salt concept induces easier formation of the SEI layer on the anodes and stabilizes the aqueous electrolyte to a greater extent,^{535,544} therefore a TiO₂ anode can be adopted in aqueous media and the actual energy density can be further increased to

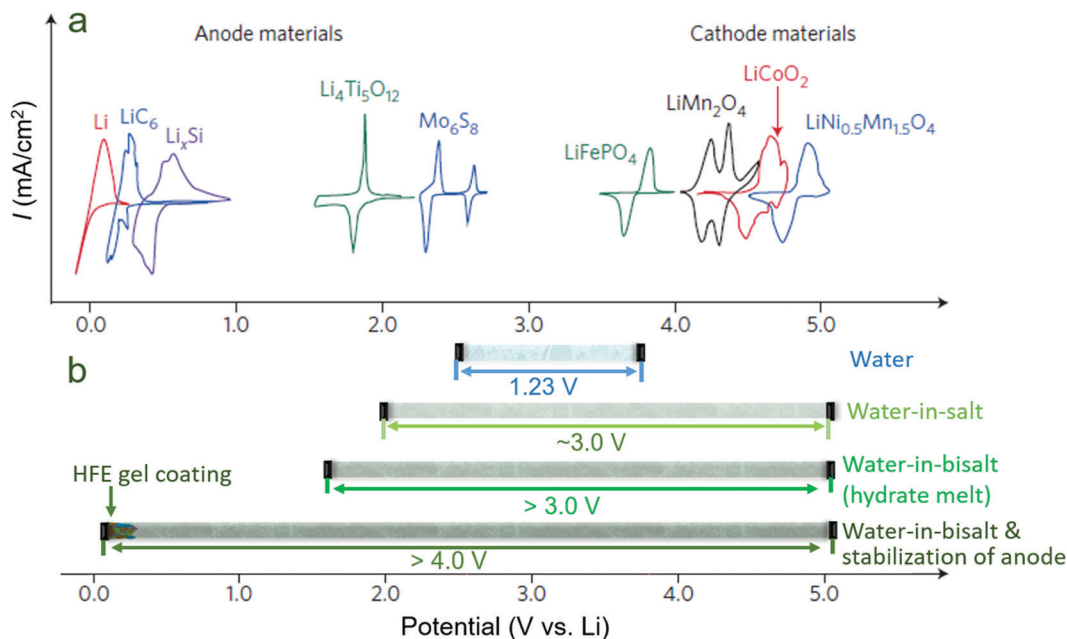


Fig. 19 Electrochemical stability window of the different aqueous electrolytes and redox potentials of cathode and anode materials. (a) The redox potentials of major anodes and cathodes used in the commercial LIBs. (b) Working voltage windows for different aqueous electrolytes. (a) Reprinted with permission from Macmillan Publisher Ltd: [Nat. Energy] from ref. 542 Copyright 2016. The working voltage windows for different aqueous electrolytes in Fig. 19b are compiled based on ref. 425, 535, 538, 542 and 543.

over 100 W h kg⁻¹.⁵³⁵ Almost simultaneously, Yamada *et al.*^{540,543} blended a eutectic hydrate melt as a high-voltage aqueous electrolyte by optimizing the mixing ratio of two organic Li salts (LiTFSI and LiBETI;⁵⁴³ LiTFSI and LiPTFSI⁵⁴⁰), which shows a voltage window larger than 3.1 V and could support a highly reversible 3.0 V LTO||LNMO full cell (Fig. 20b). However, the partial reversibility of the LNMO cathode and poor Coulombic efficiency during cycling suggest that the H₂/O₂ evolution competes with the Li⁺ de-intercalation of the anode/cathode during charging.⁵⁴³ Shortly afterwards, Wang *et al.*⁵⁴⁵ hybridized the aqueous and non-aqueous solvent-in-salt electrolytes, which inherits the non-flammability characteristics from water-in-salt electrolyte and better electrochemical stability from a carbonate-in-salt electrolyte. The as-prepared hybridized electrolyte demonstrates an apparent electrochemical window up to 4.1 V, supporting an LTO||LNMO cell to deliver an energy density of 165 W h kg⁻¹ for over 1000 cycles.⁵⁴⁵ Following these breakthroughs, Yang *et al.*⁵³⁸ passivated the commercial anodes such as graphite and Li metal with the LiTFSI-HFE gel, and realized reversible 4.0 V Li batteries in the aqueous system (Fig. 20c). The pre-coated LiTFSI-HFE gel, which is hydrophobic and completely immiscible with a water-in-salt electrolyte,⁵³⁸ could sufficiently block the remaining parasitic-reactions between the low-voltage anodes with the water-in-salt electrolytes and bridge the large potential gap between the anodic limit of the water-in-salt electrolyte and the working potentials of the commercial graphite and Li metal anodes. Compared to the traditional aqueous LIBs, the batteries using water-in-salt electrolytes could possess a double or even triple energy density (Fig. 20d).⁵⁴⁶⁻⁵⁴⁹

The water-in-salt electrolyte can be regarded as the ultimate form of the concentrated electrolyte, with a similar voltage-window

widening mechanism to the non-aqueous electrolytes. The key difference is that the SEI layers in the aqueous system only originate from the decomposition of anions and side reactions of dissolved O₂/CO₂ impurities, while the solvents also considerably contribute to the formation of SEI in the non-aqueous solvent-in-salt electrolytes.⁵⁵⁰ Similar potential widening phenomena were also detected in the Na,⁵⁵¹⁻⁵⁶² K,⁵⁶³⁻⁵⁶⁷ Mg,⁵⁶⁸ Zn⁵⁶⁹⁻⁵⁷⁷ and Al aqueous systems.⁵⁷⁸⁻⁵⁸⁰ One significant difference between the Li and Na/K aqueous electrolyte is that the cations could critically influence the stability of the anions in the aqueous solutions. Therefore, some salts that cannot be utilized in the Li aqueous medium could be utilized in the Na or K systems. For example, LiFSI is not stable in the aqueous system due to the hydrolysis of FSI⁻, yet NaFSI and KFSI can be adopted in their aqueous systems.^{566,581,582} Because of the weaker lattice energy and the higher solubility of the NaFSI, 35 m NaFSI water-in-salt electrolyte possesses an even wider voltage window than the 21 m LiTFSI electrolyte.⁵⁸² Jiang *et al.*⁵⁶⁴ built a highly reversible aqueous K ion battery with an Fe-substituted Mn-rich Prussian blue (K_xFe_yMn_{1-y}[Fe(CN)₆]_w·zH₂O) as a cathode and PTCDI (3,4,9,10-perylenetetracarboxylic diimide) as an anode in the water-in-salt electrolyte, which exhibits an unprecedentedly electrochemical performance with a high energy density of ~80 W h kg⁻¹ and a high capacity retention of 90% over 10 000 cycles thanks to the wide voltage window (~3 V) and dissolution-inhibiting feature of the 22 M KCF₃SO₃ water-in-salt electrolyte.

Although water-in-salt electrolytes were originally developed for the high-voltage aqueous batteries, these electrolytes can be virtually utilized in the double-layer capacitors and pseudo-capacitors,

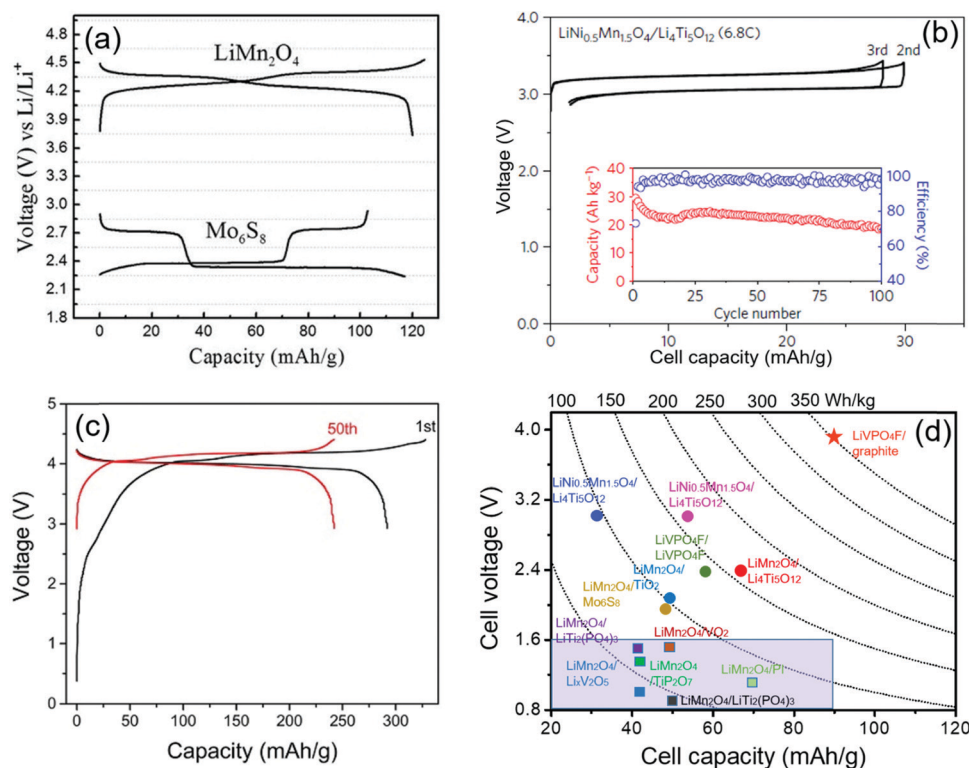


Fig. 20 Electrochemical performances of aqueous Li batteries. (a) The charge/discharge profiles of the LiMn_2O_4 and Mo_6S_8 electrodes in a 21 m LiTFSI electrolyte at a constant current of 0.2C. (b) Charge–discharge profiles of a 3.1 V LTO||LNMO full cell in the $\text{Li}(\text{TFSI})_{0.7}(\text{BETI})_{0.3}\cdot 2\text{H}_2\text{O}$ hydrate-melt electrolytes at a current of 6.8C (1.0 A g^{-1} for LNMO). (c) Charge/discharge profiles of graphite||LiVPO₄F at a current of 0.3C in a LiTFSI–HFE–gel–water–in–salt electrolyte, in which the anode was passivated by the LiTFSI–gel electrolyte. The capacity is based on anode mass. (d) The energy densities of various Li ion batteries in different aqueous electrolytes calculated based on the total weight of the cathode and anode materials. The conventional aqueous electrolyte, as represented by the light blue area, can only support a battery with a voltage of less than 1.5 V. In contrast, the water-in-salt electrolyte could enable a highly reversible battery with a voltage of as high as 3.1 V. If the anodes are passivated by the gel electrolytes, such as LiTFSI–HFE gel, the cell voltage and energy density are even comparable to the commercial non-aqueous batteries, which is shown as a five-pointed star. (a) Reprinted with permission from ref. 425 Copyright 2015, American Association for the Advancement of Science. (b) Reprinted with permission from ref. 543 Copyright 2016 Springer Nature. (c) Reprinted with permission from ref. 538 Copyright 2018 Elsevier. The data in Fig. 20d are from ref. 425, 529, 535, 536, 538, 543 and 546–549.

enhancing the working voltage and Coulombic efficiency.^{583–588} As compared to the traditional aqueous systems with a working potential window generally less than 1.6 V,^{589–591} the supercapacitors using the water-in-salt electrolytes could provide an extra potential stability of $>0.6 \text{ V}$ on catalytic electrode surfaces,^{583,586–588,592–598} which is highly favorable because the energy outputs of capacitors are proportional to the square of the operating voltages.³

As presented above, the water-in-salt electrolytes critically widens the operating window and thereby prompts the energy density of the aqueous batteries, which represent significant benefits in both fundamental science and the practical battery applications. The voltage window widening origin could be tentatively divided into three parts. (i) The high interaction between the salts and the water, which disturbs the hydrogen bonding between water, eliminates the free water molecules and thereby reduces the water activity in the electrolyte. (ii) Hydrophobic anion (TFSI[−], OTf[−] etc.) absorption on the cathode, which suppresses the water contacting to the cathode, and extends the anodic limit. (iii) *In situ* formed SEI derived

from the anion decomposition, which could block the electron transport between the electrode and electrolyte, further curbing the side reactions between the electrode and the water molecules. The first part of voltage widening could be calculated based on the Nernst equation and is the thermodynamic factor. In the concentrated electrolytes, water activity is not unity. According to the Nernst equation, the thermodynamic stability limits of the aqueous electrolytes, *i.e.* the theoretical potentials of the hydrogen evolution reaction (E_{HER}) and oxygen evolution reaction (E_{OER}), can be determined by the following equations:⁵⁹⁹

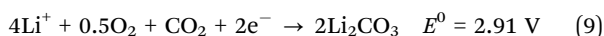
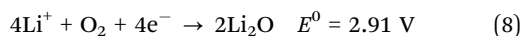
$$E_{\text{HER}} = E_{\text{H}_2/\text{H}_2\text{O}}^0 - 2.303 \frac{RT}{F} \text{pH} - \frac{RT}{2F} \ln K \quad (6)$$

$$E_{\text{OER}} = E_{\text{H}_2\text{O}/\text{O}_2}^0 - 2.303 \frac{RT}{F} \text{pH} - \frac{RT}{4F} \ln(a_{\text{H}_2\text{O}})^2 \quad (7)$$

in which, $E_{\text{H}_2/\text{H}_2\text{O}}^0$ and $E_{\text{H}_2\text{O}/\text{O}_2}^0$ are the standard potentials of the hydrogen evolution reaction (HER) and oxygen evolution reaction (OER), respectively. $a_{\text{H}_2\text{O}}$ is defined as the water

activity, F is the Faraday constant, T is the Kelvin temperature, K is the equilibrium constant of water ionization ($\text{H}_2\text{O} \rightleftharpoons \text{H}^+ + \text{OH}^-$), and R is the gas constant. As the water concentration reduces (the salt concentration increases), the water activity will be reduced, leading to a rise of the OER reaction potential according to eqn (7).⁵⁹⁹ It should be emphasized that the impact of water concentration (salt concentration) on the HER and OER potentials is asymmetrical. This conclusion was ideally echoed by Pan *et al.*⁶⁰⁰ recently, who demonstrated that the E_{OER} of highly concentrated LiNO_3 aqueous electrolyte is highly increased, while the E_{HER} is not (Fig. 21a). All of the concentrated electrolytes regardless of the salts types could result in some extending of the working voltage window, and this part, *id est*, the thermodynamic potential window, can be calculated based on eqn (6) and (7).

The organic–inorganic SEI film on the surface of graphite promises the highly reversible Li^+ intercalation/deintercalation chemistry in the graphite host at 0.1 V vs. Li^+/Li , even though the thermodynamic reduction threshold of a commercial carbonate electrolyte is as high as >1.0 V.^{113,117,601} Similar to the non-aqueous electrolyte SEI theory, the cathodic potential widening on the anode is mainly due to the SEI layers derived from the decomposition of anions in the water-in-salt electrolyte, which kinetically stabilizes the electrolytes at potential far beyond their thermodynamic stability limit. Therefore, this widening window part can be regarded as a kinetics factor and highly related to the Li salt type (Fig. 21b and c). The better the SEI formation capability, the wider the voltage widening effect that can be achieved. In a 21 m LiTFSI electrolyte, the ratio of the water molecules to Li^+ was dramatically reduced to only ~ 2.5 , which means that the electrostatic field from the Li ions cannot be neutralized by water molecules. Therefore, TFSI anions would enter into the Li ion primary solvation sheath (Fig. 21d). Multiple Li ion coordination by the TFSI^- anions stabilizes the transferred electron during reduction, leading to an SEI formation dominated by the TFSI^- reduction.⁴²⁵ XPS, soft-X-ray absorption spectra (sXAS), TOF-SIMS and EDX characterization reveals that apart from the LiF species (Fig. 21e), Li_2O and Li_2CO_3 also exist in the aqueous SEI (Fig. 21f, g, and h),⁵⁵⁰ implying that besides the reduction of anion complexes, the reduction of the CO_2 or O_2 dissolved in the electrolyte should also participate in the formation process of the SEI layer, which provides the formation source for both LiO_2 and Li_2CO_3 .⁵⁵⁰



The super-concentration of the LiTFSI in a water-in-salt electrolyte renders it possible for the *in situ* formed Li_2O and Li_2CO_3 to deposit on the anode surface without hydrolysis or dissolution.^{550,602}

Recently, Dubouis and co-workers^{603,604} proposed a different SEI formation mechanism on the anode in a water-in-salt electrolyte based on on-line electrochemical mass spectrometry (OLEMS) and operando XRD. The authors believed that water

molecules are first reduced at the anode surface, and meanwhile LiOH is *in situ* precipitated on the surface of the anode. These formed solid LiOH or the OH^- ions in the solution react with the TFSI^- anions through a nucleophilic reaction, leading to the formation of a fluorinated SEI layer (Fig. 21i). Both of the investigations from Dubouis *et al.*⁶⁰³ and Suo *et al.*⁵⁵⁰ validated the highly rich LiF species with considerable oxides in the SEI layers. The difference is in the SEI reaction mechanisms. Suo *et al.*⁵⁵⁰ believed that the SEI is generated during the electrochemical process, while Dubouis *et al.*⁶⁰³ reckoned that the SEI is derived from chemical reactions between the TFSI^- anions with the *in situ* formed LiOH intermediate, which is also formed by the electrochemical reduction of water.

The significant advances in the water-in-salt electrolyte have prompted the energy density of aqueous batteries to approach the level of commercial non-aqueous LIBs. However, one issue still needs to be carefully conquered, *i.e.*, hydrogen and oxygen evolution occurs in parallel with the Li^+ intercalation/deintercalation at the anodes and cathodes if the reaction potentials of the anodes and cathodes position at the verge of the stability window of the water-in-salt electrolyte,⁶⁰⁵ thereby hampering the commercialization of the aqueous batteries.⁶⁰⁶ That is the pivotal reason why the cycling CE reaches only approximately $\sim 99\%$ and overdosed cathodes are utilized when paring high-voltage full cells.^{534–536} These issues could be partially resolved by applying the engineering approaches to deactivate the current collectors,^{543,607} optimize cell designs⁶⁰⁸ and adding non-flammable organic solvents to effectively make full use of the active electrode materials and meanwhile suppress the parasitic reactions.

The concentrated electrolytes have been astonishingly successful, largely due to the anion derived LiF-rich SEI. The large anion size in LiTFSI and LiFSI salts reduces the Coulombic forces between the Li^+ and anions, and ensures the good solubility in the solvents. Meanwhile, at high concentrations, these anions could interact with the Li^+ and therefore dictate the interphasial processes, which effectively passivate the electrodes. Owing to the thinner and dense LiF-rich SEI layer derived from the FSI anion, LiFSI can effectively suppress Li dendrites and accommodate a large volume change of high capacity anodes and cathodes.

5. Ionic-liquid-based electrolytes

From the physical-chemistry point of view, ionic liquids (ILs) can be regarded as special salts that are in the liquid state at room temperatures or near room temperatures because of the weak electrostatic interactions between the anions and the cations.^{609–613} The main advantages of ILs as the components of electrolytes are the potentially expanded electrochemical windows, improved safety features, high thermal stability, and low volatility.^{614–617} Therefore, ILs dissolved with Li-ion salts were proposed as a viable alternative to commercial carbonate electrolytes.^{618,619} However, several issues hinder the industrial commercialization, such as high price, high

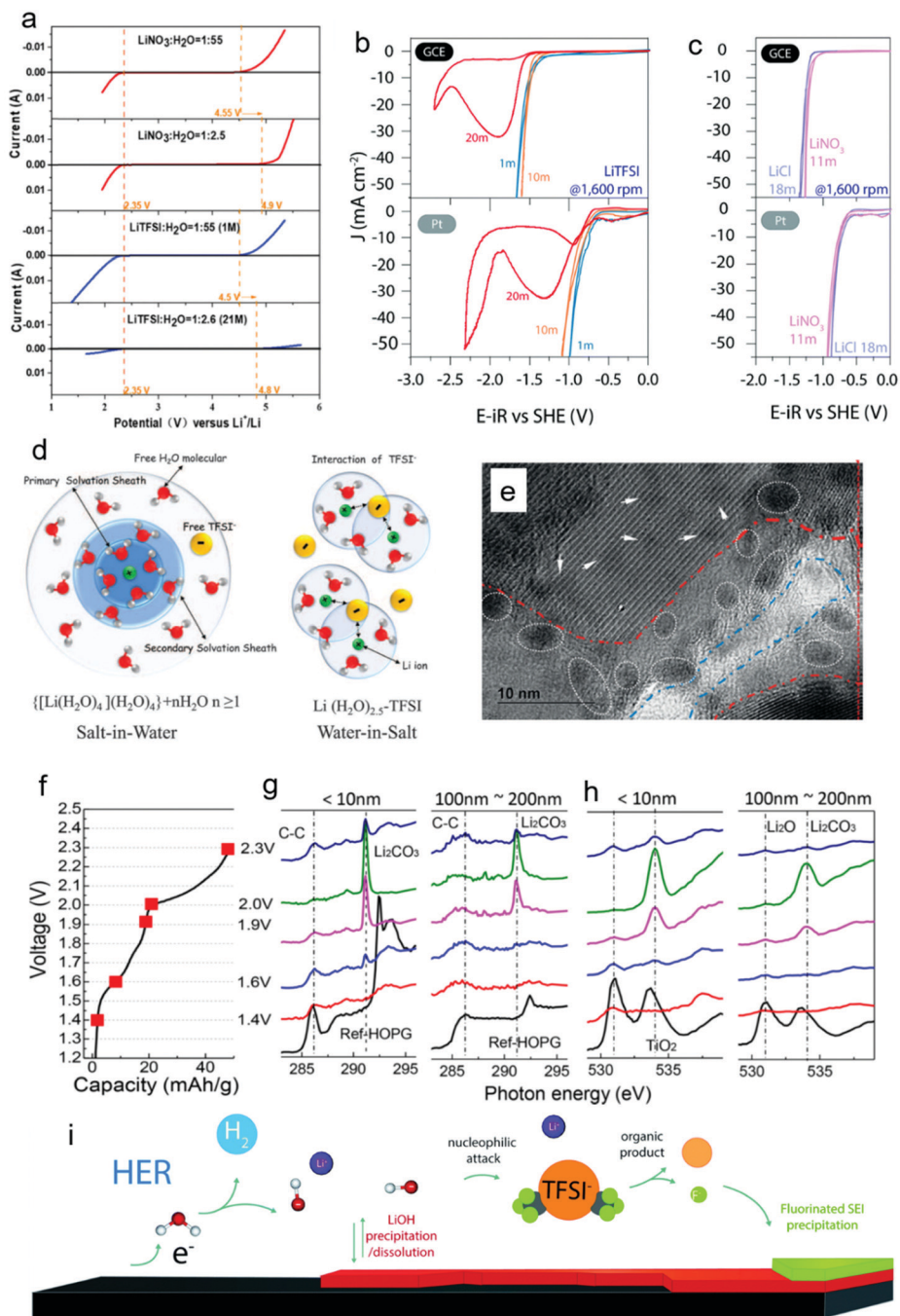


Fig. 21 Electrochemical window of aqueous electrolytes and the SEI analysis. (a) LSV tests on concentrated LiNO_3 , diluted LiNO_3 , concentrated LiTFSI and diluted LiTFSI aqueous electrolytes. The scanning rate is 0.1 mV s^{-1} , working electrode is Pt. (b) Cyclic voltammetry tests on glassy carbon (top) and Pt (bottom) disk electrodes rotated at 1600 rpm and scanning rate of 100 mV s^{-1} in different concentrations (1 m, 10 m, and 20 m) LiTFSI aqueous electrolytes. (c) Cyclic voltammetry tests on glassy carbon (top) and Pt (bottom) disk electrodes rotated at 1600 rpm and scanning rate of 100 mV s^{-1} in different salt saturated aqueous electrolytes (LiNO_3 , $\sim 11 \text{ m}$, pink; LiCl , $\sim 18 \text{ m}$, purple); (d) schematic illustration of the Li^+ solvation structure in the diluted and water-in-salt electrolytes. (e) HRTEM images of the C- TiO_2 anode cycled in a water-in-bisalt electrolyte at 0.5C. (f) The charge profile of $\text{Mo}_6\text{S}_8 \parallel \text{LiMn}_2\text{O}_4$ full cell; (g) C K-edge soft-X-ray absorption spectra (sXAS) at different voltages (1.4, 1.6, 1.9, 2.0 and 2.3 V) with highly oriented pyrolytic graphite (HOPG) as the reference; (h) O K-edge sXAS spectra at different voltages (1.4, 1.6, 1.9, 2.0 and 2.3 V) with TiO_2 as the reference; (i) schematic illustration of the SEI formation mechanism proposed by Dubouis and co-workers.⁶⁰³ (a) Reprinted with permission from ref. 600 Copyright 2018 Elsevier. (b, c and i) Reprinted with permission from ref. 603 Copyright 2018 The Royal Society of Chemistry. (d) Reprinted with permission from 425 Copyright 2015, American Association for the Advancement of Science. (e) Reprinted with permission from ref. 535 Copyright 2016 John Wiley & Sons, Inc. (f–h) Reprinted with permission from ref. 550 Copyright 2018 American Chemical Society.

viscosity and poor electrode compatibility.⁶¹⁵ Among ILs, TFSI⁻ and FSI⁻ anion based ILs are most widely investigated due to the electron-delocalized structure of the sulfonyl imide anions. Compared to TFSI⁻, FSI⁻-based ILs are less viscous and can dissolve salts with a higher concentration due to the smaller size of F than CF₃ group.^{620,621} Moreover, FSI-based ILs exhibit a better compatibility with graphite anodes because of the better SEI formation capability.⁶²²

Depending on the cation groups, ILs utilized in the electrolytes can mainly be categorized into imidazolium, tetraalkylammonium, phosphonium, sulfonium, and piperidinium-based ILs. The imidazolium-based ILs were the first ILs utilized in the electrolytes because of the high conductivity and low viscosity.⁶²³⁻⁶²⁵ However, the imidazolium-based ILs not only have poor cathodic stability due to the active acidic hydrogen groups in the imidazolium cations but also poor anodic stability, which strictly restricts their working voltage windows.⁶²⁶⁻⁶²⁸ The tetraalkylammonium-based ILs such as trimethylpropylammonium (TMPA⁺),⁶²⁹ *N*-methyl-*N*-propylpyrrolidinium (Py₁₃⁺),⁶³⁰ *N*-methyl-*N*-butylpyrrolidinium (Py₁₄⁺),⁶³¹⁻⁶³³ *N*-methyl-*N*-propylpiperidinium (PP₁₃⁺)⁶²⁹ coupled with TFSI⁻ anion exhibit a much wider electrochemical window, and suffice to support high voltage batteries.^{634,635} Yet, the high viscosity and the low

ionic conductivity critically restricted the high rate capability. Matsumoto *et al.*⁶²⁸ synthesized a series of tetraalkylammonium-based IL with small cations and TFSI⁻ anions, promoting the ion conductivity of ILs to >4 mS cm⁻¹ at 25 °C. Tsunashima and co-workers⁶³⁶⁻⁶³⁹ first introduced the phosphonium-based ILs as Li-ion electrolytes. Compared to tetraalkylammonium-based ILs, the phosphonium-based ILs possess a lower viscosity,^{639,640} a better thermal stability,⁶⁴¹ and a widened potential window (Fig. 22a), which could support high-voltage batteries.^{639,640,642} The higher anodic stability of phosphonium-based ILs was also verified by Ong *et al.*⁶⁴³ (Fig. 22b) and Pandian *et al.*⁶⁴⁴ using quantum computational methods involving the M06-L functional with a triple-zeta basis and the dichloroethane as solvent in the SMD solvent model.

Aurbach *et al.*^{645,646} examined a series of ILs 1-hexyl-3-methyl imidazolium (HMITFSI), 1-(2-methoxyethyl)-3-methyl imidazolium (MEMITFSI), *N*-ethyl-*N,N*-dimethyl-2-methoxyethylammonium (EDMETFSI), 1-methyl-1-butylpyrrolidinium (BMPTFSI), and 1-methyl-1-propylpiperidinium (MPPpTFSI) solutions with LiTFSI as Li ion salts, and compared them with an EC-based carbonate electrolyte. Among these ILs, the derivatives of piperidinium and pyrrolidinium possess an electrochemical window >5.5 V, and meanwhile are compatible with

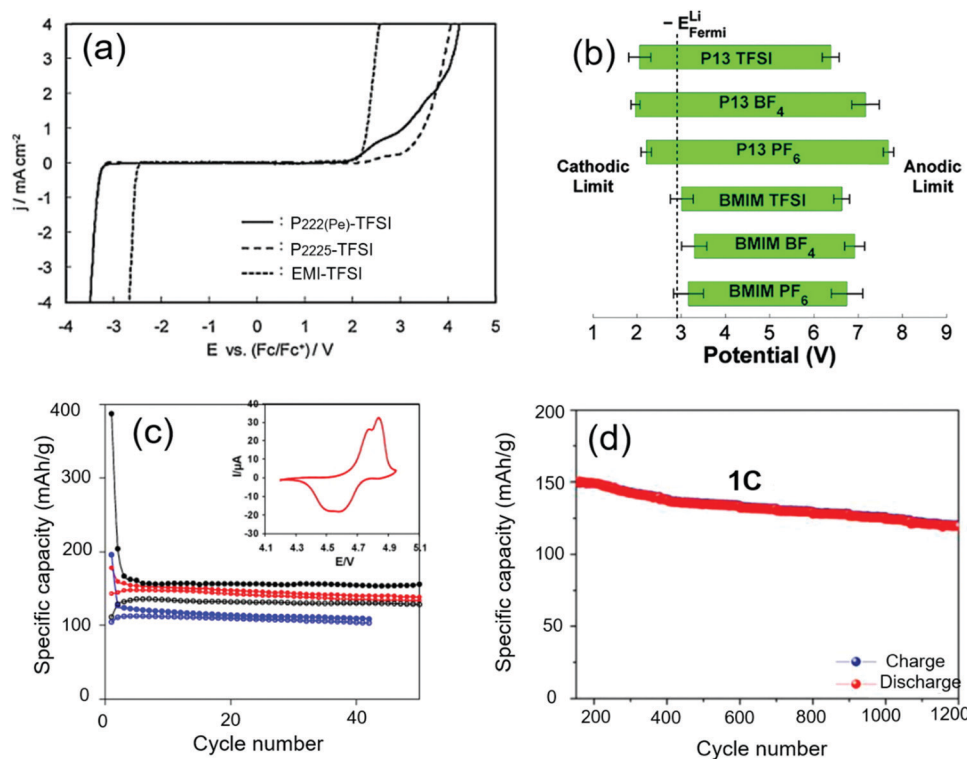


Fig. 22 (a) Electrochemical stability of EMI-TFSI (1-ethyl-3-methylimidazolium-TFSI), P2225-TFSI (triethyl-*n*-pentylphosphonium-TFSI) and P222(Pe)-TFSI (triethyl(4-pentenyl)phosphonium-TFSI) tested on a glassy carbon electrode. The linear sweep rate is 5 mV s⁻¹. (b) Calculated electrochemical stability windows for different ILs using MD + DFT, in which the Fermi level of Li metal is also compiled. (c) Cycling performance of Li||LNMO cell in different electrolytes: black curves 1.5 M LiPF₆ EC/EMC 1 : 2; blue curves 0.5 M LiTFSI BMPTFSI; red curves 0.5 M LiTFSI MPPpTFSI. Inset of figure a is the CV curve of LNMO in 0.5 M LiTFSI MPPpTFSI with a scanning rate of 20 μV s⁻¹. (d) Cycling performance of the Li||Li_{1.2}Mn_{0.56}Ni_{0.16}Co_{0.08}O₂ cell in 0.3 M LiTFSI [EC/DMC + PYR₁₃TFSI + FEC] (45 : 45 : 10) electrolyte. (a) Reprinted with permission from ref. 639 Copyright 2011 Elsevier. (b) Reprinted with permission from ref. 643 Copyright 2011 American Chemical Society. (c) Reprinted with permission from ref. 645 Copyright 2009 Elsevier. (d) Reprinted with permission from ref. 657 Copyright 2019 Elsevier.

Li metal anodes. At the anode surfaces, the SEI layers derived from the TFSI⁻ anion decomposition can passivate Li metal and graphite anodes. Therefore, a highly reversible 5 V cell of Li||LNMO is achieved based on BMPTFSI and MPPpTFSI. As shown in Fig. 22c, in the extremely low charge/discharge current density of C/16, the Li||LNMO cell in the BMPTFSI and MPPpTFSI could maintain a much higher CE with lower irreversible capacity, demonstrating a much lower parasitic oxidation reaction on high voltage cathode in these IL electrolytes than in the commercial carbonate electrolyte.

Attempts were made to improve the Li ion conductivity and lower the viscosity of the IL electrolytes based on the reported ILs, so that high-rate batteries can be realized. One of the most effective methods is mixing different ILs, therefore synergetic effects could be achieved from these ILs.^{647–650} Fox *et al.*⁶³⁰ systematically characterized the binary IL mixtures of PY_xTFSI ($x = 1, 2, 3, 4, 5$) and found that to blend an IL-mixture electrolyte with high conductivity, the melting transition (T_m) between the two ILs should be not too large, the crystal structures should be different, and the sizes of the cations in the two ILs should vary significantly. Apart from the mixture of different ILs, mixtures of the IL and carbonates,^{651–661} IL and SLs,^{368,662} IL and PEO,^{663–665} IL and PVDF–HFP⁶⁶⁵ were also intensively investigated. The IL and carbonate/SL/PEO/PVDF–HFP cocktails inherit the benefits of the IL and carbonate/SL/PEO/PVDF–HFP electrolytes, resulting in: (1) high ion conductivity,^{651,653,656} (2) enhanced electrochemical stability window,^{651,654,659,663–665} (3) ameliorated compatibility of the electrolyte and the graphite anodes,^{653,655,658,660} and (4) improved safety with reduction of the self-extinguish time.^{651,653,661} An impressive electrochemical performance with over 1200 cycles at 45 °C was achieved for the Li||Li_{1.2}Mn_{0.56}Ni_{0.16}Co_{0.08}O₂ cell (Fig. 22d) using 0.3 M LiTFSI in [EC/DMC + PYR₁₃TFSI + FEC] (45 : 45 : 10) as an electrolyte demonstrated by Gerbaldi and co-workers,⁶⁵⁷ representing a milestone for the high-voltage Li-rich NMC cells. To further improve the compatibility of the IL with the electrodes, using the additives is another economic method,^{368,656,666–668} which can further enhance the electrochemical performance of the high-voltage batteries.

Forsyth and co-workers^{669–672} demonstrated that as the Li salt concentration increases, both the Li ion transference number and the electrochemical stability enhance although the viscosity soars and conductivity decimates in the system. Adopting these concentrated IL electrolytes, a much higher cycling efficiency, lower impedance and better rate performance can be achieved for the high-voltage batteries, which are quite similar to the concentrated ether or carbonate electrolytes.^{122,433} Yet, the underlying solvation structure and the interactions between the anions and Li⁺ differ significantly.^{673,674} As the Li⁺ concentration increases in ILs, the interactions between the anion and Li⁺ become weaker and demonstrate a shift toward monodentate coordination,^{673–675} which is more significant for [TFSI]-type ILs (Fig. 23a and b), indicating a higher viscosity for concentrated [TFSI]-type ILs. These structure changes are verified by the MD snapshots (Fig. 23c and d).

Bidentate-coordinated Li⁺ ions in the low concentration ILs become monodentate-coordinated as the concentration increases, although the clusters are always composed of one Li⁺ cation and three FSI⁻ anions.

Different from the cells that cycled in the conventional carbonate electrolyte, which suffered from continuous capacity decay due to the substantially concomitant growth of R_{ct} and R_{SEI} during cycling,⁶⁷⁷ the Li||NMC811 cell displayed higher capacity retention in IL electrolytes (Fig. 23e). Higher LiFSI concentration suppresses the corrosion reactions, and promotes the capacity and energy retention by forming a robust and conductive SEI/CEI layer.⁶⁷⁶ These features in the concentrated ILs are further confirmed by Heist *et al.*,⁶⁷⁶ Zhou *et al.*,⁶⁷⁸ and Zhang *et al.*,⁶⁷⁹ respectively, who showed that the cycling performance of the cells was critically enhanced in the concentrated LiFSI-IL electrolytes. Quite recently, Dai and co-workers⁶⁸⁰ introduced NaTFSI into the LiFSI–1-ethyl-3-methylimidazolium bis(fluorosulfonyl)imide ([EMIm]FSI) system as the additive, and made up a concentrated electrolyte of 5 M LiFSI + 0.16 M NaTFSI [EMIm]FSI. A capacity retention of ~87% was achieved for the Li||LCO cell after 900 cycles at 1C, superior to the cells using 1 M LiFSI–[EMIm]FSI or 5 M LiFSI–[EMIm]FSI. Although the electrochemical stability window is expanded, however, due to the poor intrinsic anodic stability of the imidazolium-based IL, the anodic stability limit of 5 M LiFSI + 0.16 M NaTFSI [EMIm]FSI only locates at ~4.6 V vs. Li⁺/Li, and the cycling Coulombic efficiency LCO is merely about 99.3% at a current of 0.25C. Beyond all doubt, the concept of combining high concentration and the additive is one of most promising directions to maximize the electrochemical stability of the ILs.

Apart from the above mentioned ILs, novel ILs based on new cations and anions were also developed recently, such as the FTFSI anion,⁶⁸¹ H[FPFSI] anion,⁶⁸² and FPSI anion,⁶⁸³ aiming to further lower the viscosity, improve the conductivity and widen the working voltage windows. One kind of special IL electrolytes that should be mentioned is the solvate ionic liquid,^{461,462,684–686} which can also be classified as an important subset of highly “concentrated electrolytes” or “solvent-in-salt” electrolytes. For some certain highly concentrated electrolytes with equimolar mixtures of glymes and Li salts (LiTFSI, LiFSI, LiBETI, LiClO₄ *etc.*), all the Li ions theoretically complex with all the glyme molecules, forming [Li(glyme)₁]⁺, in which only independent [Li(glyme)₁]⁺ and counter anions (TFSI⁻, FSI⁻, BETI⁻, ClO₄⁻ *etc.*) exist with few free-solvent molecules, forming the essence of the ILs.⁶⁸⁷ Watanabe and co-workers⁴⁶¹ raised strict criteria for this kind of solvate IL: (1) ions and solvent molecules should be in a certain stoichiometric ratio, since all of the cations coordinate with all solvent molecules; (2) only complex cations and counter anions exist in the absolute absence of any neutral molecules; (3) the physicochemical properties critically vary with that of pure solvent and salts under using conditions; (4) low melting point; (5) low vapor pressure. Because of the complexation of the glyme molecules with Li ions, and the high concentration of the anions, these glyme-based solvate ILs can withstand

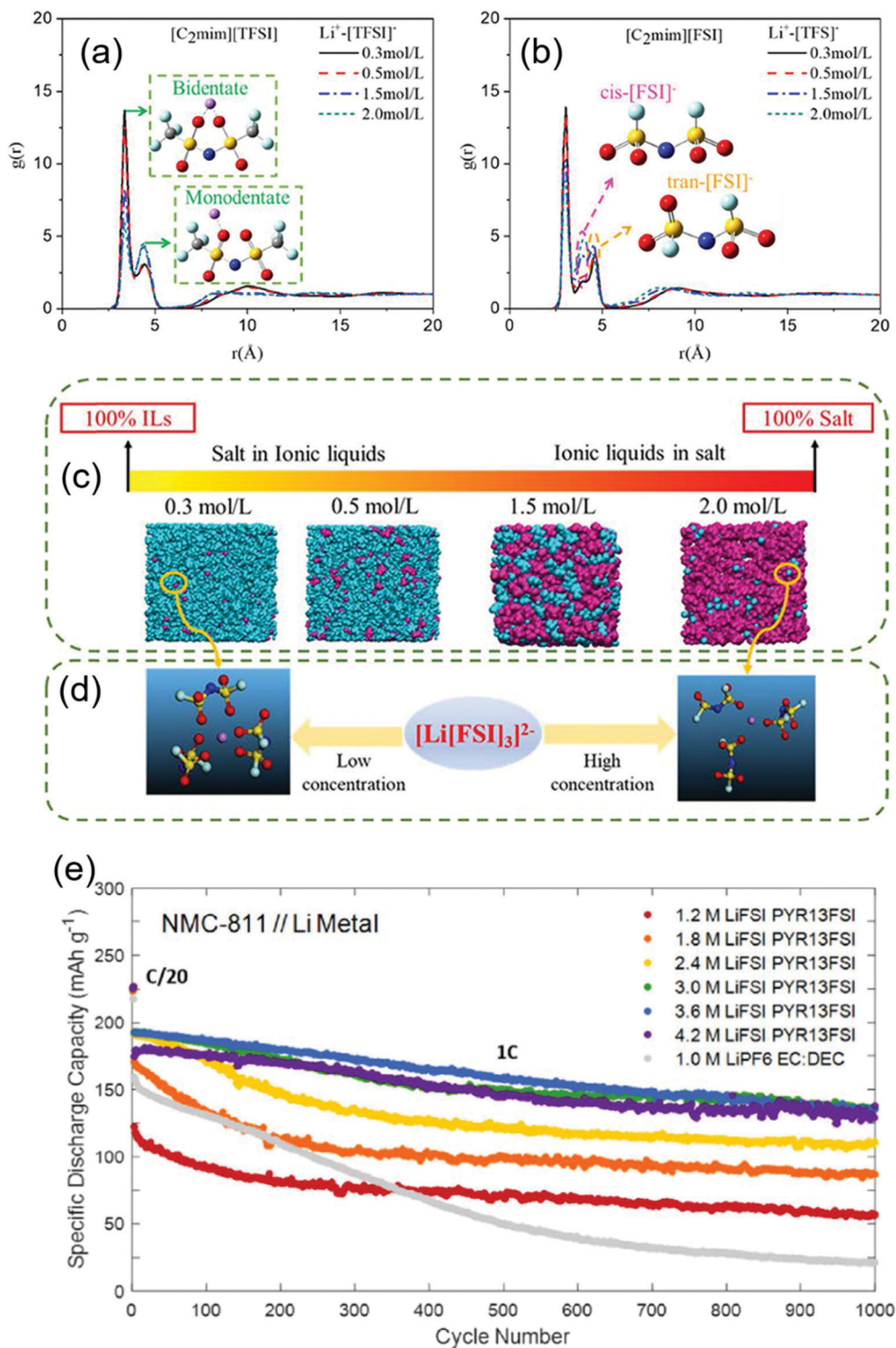


Fig. 23 Radical distribution function of [C₂mim][TFSI]-LiTFSI (a) and [C₂mim][FSI]-LiTFSI (b) for different LiTFSI concentrations at 298 K. (c) Snapshots of [C₂mim][FSI]-LiTFSI electrolyte from MD simulations (Pink denotes LiTFSI, blue represents ILs). (d) Randomly captured [Li[FSI]₃]²⁻ configurations in 0.3 M and 2.0 M [C₂mim][FSI]-LiTFSI electrolyte, respectively. (e) Cycling performance of the Li||NMC811 cell in conventional 1.0 M LiPF₆ EC/DEC electrolyte and different concentrated PYR13FSI ILs. (a-d) Reprinted with permission from ref. 673 Copyright 2020 Frontiers. (e) Reprinted with permission from ref. 676 Copyright 2019 IOP Publishing, Ltd.

high oxidation at the cathodes and therefore can be utilized as electrolytes in batteries with 4 V cathodes such as LCO,^{459,688,689} while the conventional glyme-based electrolytes cannot.

6. Additives in electrolytes

Since the advent of the LIBs in the 1990s, the non-aqueous carbonate electrolytes monopolized the Li electrolytes for almost 30 years with the skeleton composition of LiPF_6 as the salt and EC, DMC, EMC, DEC *etc.* as solvents.³ To cater for the aggressive cathodes with higher voltage, assorted additives have been developed for the commercial electrolytes to stabilize the key interfacial chemistries for desired electrochemical performance,⁶⁹⁰ although the detailed underlying mechanism remains unclear in most cases.⁶⁹¹ Considering the promoting effect on the electrochemical performance and the low cost of these additives, it is believed that the prevailed carbonate electrolytes with diversified additives will dominate the electrolyte infrastructures in the foreseeable future. These electrolyte additives could be divided into several categories according to their functions, such as SEI/CEI forming improver, overcharge protectant, salt stabilizer, fire-retardant agent *etc.*^{692,693} Several good reviews and progress reports have been devoted to these essential ingredients of the electrolytes.^{692,694–700} To differ from these literatures, in this part, we mainly focus on the additives that could enhance the electrochemical performance on high-voltage battery chemistries, and significant parts will be dictated to the recent advances on the underlying mechanisms and the understandings on the interphases of electrode/electrolyte. It should be mentioned that some solvents that were demonstrated in the EC-free electrolyte section can also function as effective additives. Herein, we utilize the threshold of 10% as the demarcation, below which it is defined as an additive.

In electrochemical devices, all the reactions should take place on the triple-phase interface; therefore, the stability of the interface dictates the stability of the devices. The higher voltage pursuing in the higher energy Li batteries have surpassed the anodic limits of the commercial carbonate electrolytes, therefore forming a protective CEI layer that blocks the electron transport and meanwhile allowing Li^+ access, seems one of the most effective strategies. Hence, the use of SEI/CEI-forming additives is one of the most effective and economical methods for improving the electrochemical performance of the LIBs.⁶⁹² In this section, all of the electrolytes discussed are 1 M LiPF_6 in EC-based carbonate electrolytes, unless stated otherwise.

Unsaturated carbonate derivatives

In this additive family, the best known one is vinylene carbonate (VC),^{131,701–703} which was patented by Sanyo Electric,⁷⁰⁴ SAFT,⁷⁰⁵ Sony,⁷⁰⁶ and Valence Technology corporation⁷⁰⁷ in the 1990s. Over 20 years, VC has been a prototype and indispensable additive in the battery electrolyte industry. In the functionality, VC undergo polymerization at both the anode^{703,708–710} and cathode surfaces,^{708,709,711–715} creating protective poly(VC) layers. Using ultra-high precision coulometry (UHPC) and storage experiments at elevated temperatures, Dahn *et al.*^{712,716–719} unveiled that in the full cell VC improves the CE of the cell and decreases self-discharge mainly by

slowing the electrolyte oxidation at the cathode surface, although VC is mainly consumed at the anode side.⁷²⁰

The radical polymerization mechanism was first proposed by Winter *et al.*⁷²¹ on the decomposition of vinylene compounds including VC and isocyanates (Fig. 24a). The reactivity of the vinylene compounds is highly related to the groups linked to the double bonds. Electron-withdrawing groups ($-\text{X}$), such as nitrile groups, make the $\text{C}=\text{C}$ group more electrophilic and thus prompt the reduction reaction (SEI formation). Meanwhile, the electron-pushing groups ($-\text{Y}$) enhance the nucleophilic feature to the vinyl-group and therefore promote the oxidation (CEI formation). This reaction mechanism was well supported by Quatani and co-workers,^{708,722} who demonstrated that VC as an additive contributes to SEI/CEI layers independently *via* a radical polymerization mechanism without cross-talk reactions using XPS analysis and theoretical calculations. The talent-designed and inter-comparable cell configurations, as shown in Fig. 24b, clearly demonstrate that VC is polymerized by oxidation on cathodes or by reduction on anodes. Poly(VC) was detected on the LiCoO_2 but not on the delithiated LiFePO_4 even though both cathodes were charged to the same potential, indicating that the polymerization is not only related to the potential but also highly relevant to the surface status of delithiated cathodes. This phenomenon ideally explains the varied effects of VC for different cathodes.⁷¹⁸ *In situ* total-reflection fluorescence X-ray absorption spectroscopy demonstrated that the Co ion reduction at the LCO surface occurring upon immersing in the conventional carbonate electrolytes can be effectively curbed in the presence of the VC additive, thanks to the formation of a protective VC-derived CEI layer.⁷¹¹ The detailed protecting mechanism for the high voltage cathodes *via* polymerization of VC is illustrated in Fig. 24c and d. The lower electrochemical potential of electron (ϕ) in the LCO cathode leads to the reduction of the Co^{3+} to Co^{2+} and associated EC oxidation in the conventional carbonate electrolytes (Fig. 24c), which brings about the degradation of the LCO surface and high resistance.^{203,723} In contrast, a stable poly(VC) layer is formed in the VC-added electrolyte on the LCO surface because of the preferential adsorption of VC on the cathode surface,^{708,711,722} which physically blocks the electron transport between the high voltage cathode and the electrolyte, and thereby suppresses redox reactions between TM cations and the electrolyte solvents (Fig. 24d). Quite recently, Laruelle *et al.*⁷²⁴ synthesized poly(VC) using two different methods, confirming the radical polymerization mechanism. The poly(VC) as a novel solid polymer electrolyte displays stable electrochemical window >4.5 V, and favorable ionic conductivity of 9.8×10^{-5} S cm^{-1} at 50 °C, which could support high voltage Li||LCO cells with decent rate capability.⁷²⁵ Thanks to the good film formation capability, VC is also extensively utilized in the novel electrolyte systems, such as sulfone-based electrolytes,^{344,353,367} ionic liquid electrolytes^{726–728} to shield the side reactions between the electrodes and the electrolytes.

Vinyl ethylene carbonate (VEC) was first proposed as a good film forming additive for the graphite anodes,⁷²⁹ which could create a similar SEI as VC on the edges of the graphite.

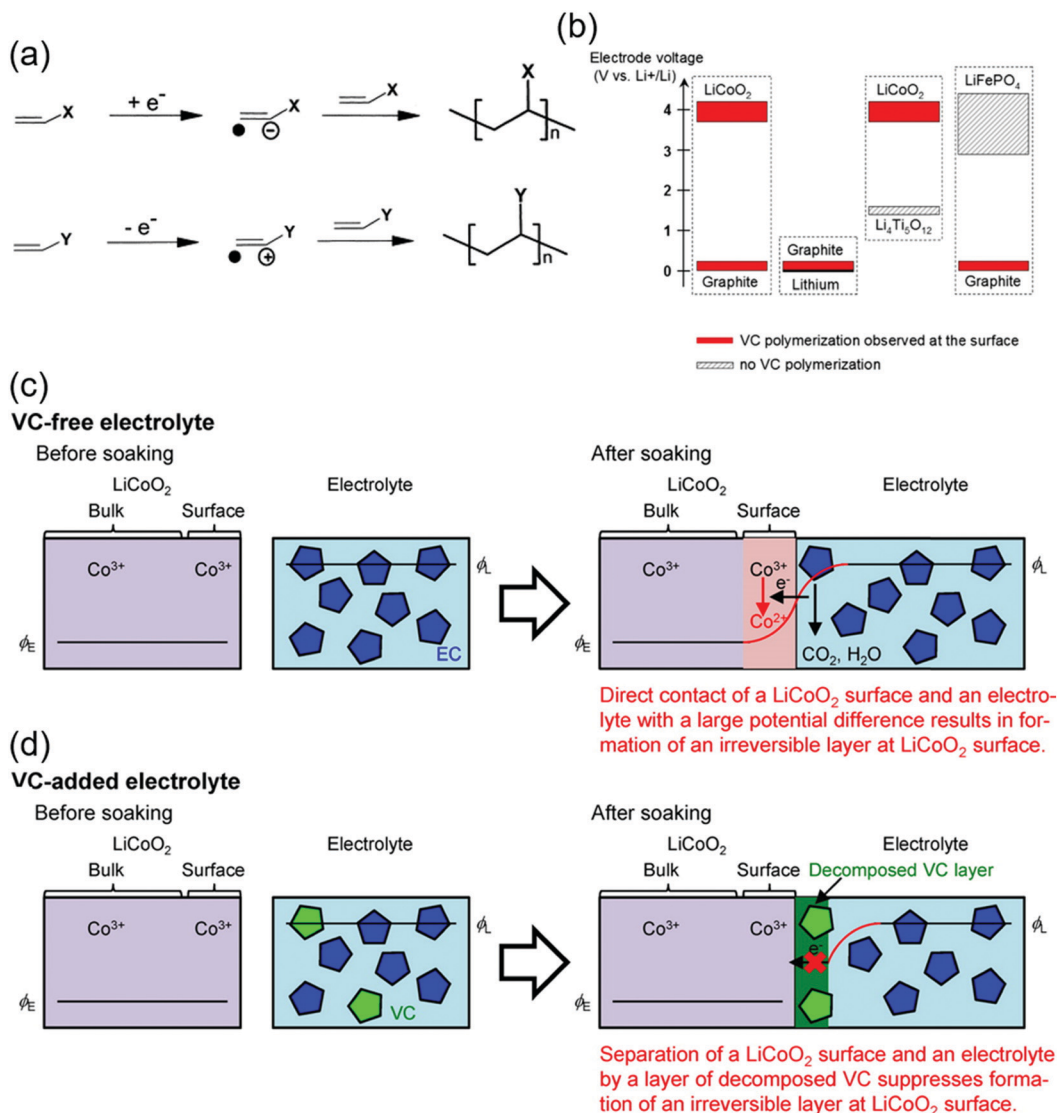


Fig. 24 (a) Polymerization of the vinylene monomers *via* reduction or oxidation reaction mechanisms. X denotes the electron-withdrawing group, while Y denotes the electron-pushing group. (b) Summary of the detected VC degradations in different cell systems as a function of the voltage and electrode nature. Schematic illustration of the interphasial reactions at an LCO/electrolyte for (c) VC-free and (d) VC-added electrolytes. ϕ_E and ϕ_L are electrochemical potentials of the electron in the cathode and electrolyte, respectively. VC and EC molecules are represented by green and blue pentagons, respectively. (a) Reprinted with permission from Ref.721 Copyright 2003 Elsevier. (b) Reprinted with permission from Ref.722 Copyright 2009 IOP Publishing, Ltd. (c and d) Reprinted with permission from ref. 711 Copyright 2015 American Chemical Society.

Dahn and co-workers⁷³⁰ quantitatively compared the effects of VC and VEC with different concentrations in graphite||LCO pouch cells between 4.2 V and 2.8 V using high precision Coulometry and EIS analysis. VC yields a positive effect on the electrochemical improvement with a better CE, lower side reactions and enhanced capacity retention. In contrast, VEC exerts little effects on the cathodes if the concentration is lower than 4% at this normal working voltage range. Recently, Nan *et al.*⁷³¹ tested the VEC additive in the graphite||NMC442 cell with a higher cutoff voltage of 4.5 V. Compared to the solvents of EC and EMC, VEC shows an evident oxidation potential at 4.4 V and generates an effective CEI film on the high-voltage cathodes,⁷³¹ favoring the cells with a high working voltage of 4.5 V. With 2.0 wt% VEC additive in electrolyte, the capacity

retention of graphite||NMC442 at 3.0–4.5 V is increased from 62.5% to 74.5% after 300 cycles. Yang and co-workers⁷³² tested the electrochemical performance of VEC additives on Li||LiNi_{0.8}Co_{0.2}O₂ cell with a cutoff voltage of 4.3 V *vs.* Li⁺/Li at different temperatures. Surprisingly, significant improvement was achieved on the cycling performance at elevated temperatures such as 50 °C, while little improvement was detected at room temperature. The relatively higher film forming potential and slower kinetics for the VEC than VC lead to these evident differences on the electrochemical performances, rendering VEC additive only functions under harsher working conditions.⁷³³

Apart from the VC and VEC, other additives containing unsaturated C–C bonds also function *via* similar mechanisms,

such as vinylene trithiocarbonate (VTTC),⁷³⁴ 2-furonitrile (2-cyanofuran),⁷³⁵ acrylic acid nitrile (AAN),⁷²¹ allyl ethyl carbonate (AEC),⁷³⁶ allyl methyl carbonate (AMC),⁷³⁷ vinyl acetate (VA),⁷³⁷ divinyl adipate (ADV),⁷³⁷ 3,3,4,4,5,5-hexafluorocyclopent-1-ene (HFCp),⁷³⁴ triallyl cyanurate (TAC),⁷³⁸ triallyl isocyanurate (TAIC),⁷³⁸ and allylboronic acid pinacol ester (ABAPE),⁷³⁹ in which the unsaturated C–C bonds serve as good building blocks for protective SEI/CEI layers on the electrodes. The only untoward effect of VC and VC derivatives that needs to be pointed out is that high concentration in the electrolyte usually increases the resistance during cycling, and therefore these additives are generally limited to less than 2%,^{740,741} and in most cases combined with other additives to reduce the cell resistance.^{720,742–744}

Fluorine-containing additive

Because of the high electron-withdrawing tendency of the F-groups, F-rich species could intrinsically withstand the oxidation. Therefore, lots of fluorinated solvents are developed with the hope to replace the conventional carbonate solvents, as demonstrated in the previous section. As of today, the cost of these fluorinated solvents is much higher than the non-fluorinated counterpart. Therefore, using the fluorinated species as the additives to improve the oxidation-resistance of the electrolytes seems a more practical and economic method for the LIB industry. These fluorine-containing compounds can

form more robust SEI/CEI films that are composed of fluorinated species/polymers, blocking the possible side reactions between the electrolyte skeleton solvents with the oxidized cathode surface.

Among these fluorine-containing additives, the best-known are FEC and LiPO_2F_2 , which have been widely utilized as the commercial electrolyte additive. These two additives pose a good effect not only on the anodes of graphite,^{307,745–747} Li metal,^{7,31,748} and Si-based alloys,^{749–753} but also on the high-voltage cathodes thanks to the good film-forming capability.^{747,752–769} Different from the slow CEI formation reactions in the EC-based electrolytes, FEC participates in the formation of the protective CEI films on high-voltage cathodes with a much faster pace, in which the *in situ* formed PEO-like polymer and inorganic species exert a much better protective effect on the high voltage cathode than the polycarbonate species from the oxidation of the EC-based electrolytes,⁷⁶⁵ and also possess a better effect than VC or ES-derived CEI layers.¹⁴⁹ Compared to the VC additive, the LiPO_2F_2 additive possesses an even better electrochemical performance in the graphite||NMC532 pouch cell.⁷⁶² It is believed that the LiPO_2F_2 additive facilitates a more compact and thinner CEI layer on the cathodes with higher amounts of fluorophosphates,^{761,762,764,770} which endow a much better electrochemical performance under harsh working conditions^{761,771,772} (Fig. 25a and b). To further improve the electrochemical performance of the cells, Dahn

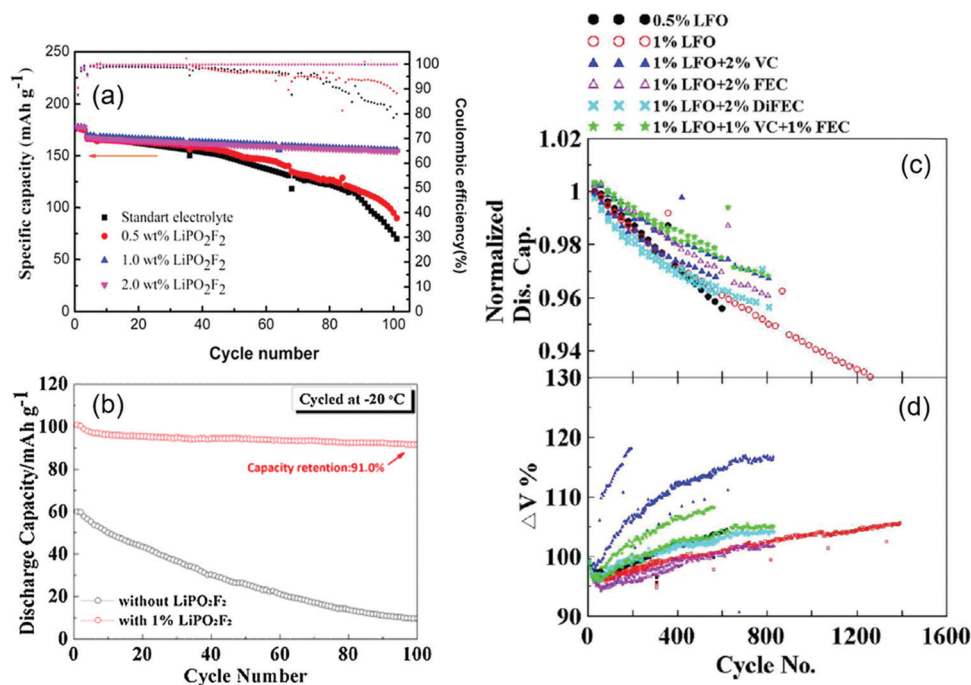


Fig. 25 Cycling performance of NMC cells in different electrolytes. (a) The reversible capacity vs. cycling number of the Li||LiNi_{0.5}Mn_{0.25}Co_{0.25}O₂ cell in an electrolyte with different LiPO₂F₂ additives at 55 °C; (b) cycling performance of the graphite||NMC532 cell in an electrolyte with and without LiPO₂F₂ additives at -20 °C. The standard electrolyte in (a and b) is 1 M LiClO₄ in EC/EMC (3 : 7) and 1 M LiPF₆ in EC/EMC/PC (4 : 7 : 1), respectively. (c) Normalized discharge capacity vs. cycling number of the graphite||NMC532 pouch cells in different electrolytes; (d) normalized cell polarization vs. cycling number of the graphite||NMC532 pouch cells in different electrolytes. LFO in figure legend is LiPO₂F₂. (a) Reprinted with permission from ref. 761 Copyright 2018 Elsevier. (b) Reprinted with permission from ref. 771 Copyright 2016 Elsevier. (c and d) Reprinted with permission from ref. 770 Copyright 2018 The Electrochemical Society.

and co-workers⁷⁷⁰ screened different additive combinations. The integration of LiPO_2F_2 with other commonly utilized additives (such as FEC, VC and DFEC) critically enhances the cycling stability, suppresses the cell impedance growth, and decreases the side reactions, in which electrolytes with 1% LiPO_2F_2 + 2%FEC (or DFEC) and 1% LiPO_2F_2 + 1%FEC + 1%VC seem best for the graphite||NMC532 with an operation voltage of 4.3 V. After 800 cycles, the cells using the electrolyte with 1% LiPO_2F_2 + 1%FEC + 1%VC can still deliver a reversible capacity of 97% with limited polarization increase (Fig. 25c and d). This synergetic effect from the LiPO_2F_2 -VC combination and LiPO_2F_2 -FEC combination on the electrochemical performance of the cell were also confirmed by Kim *et al.*⁷⁷³ and Zheng *et al.*,⁷⁷⁴ respectively. It is believed that the VC/FEC could reinforce the mechanical properties of the LiPO_2F_2 -derived interphases.

Aurbach *et al.*³¹ reported that both the aggressive LiNiO_2 cathode and Li metal anode were stabilized in the 1 M LiPF_6 FEC/DMC (1 : 4, vol) electrolyte because of the highly passivated CEI/SEI from the FEC decomposition. The cell with high LiNiO_2 loading of 4 mA h cm^{-2} , high cutoff voltage of 4.3 V, and low electrolyte volume (33 $\mu\text{L cm}^{-2}$) can be cycled for more than 700 cycles with excellent capacity retention (Fig. 26a and b), representing the best electrochemical performance ever reported for a LiNiO_2 cell. Similar effects of FEC additive were also reported in Ni-rich Li||NMC cells.⁷⁷⁵⁻⁷⁷⁷ Adding DFEC into the above FEC electrolyte can prevent the fast consumption of FEC during cycling, therefore further improving the electrochemical performance of the Li||NMC811 cells and cutting down the electrolyte dosage to an extremely low level of 14 $\mu\text{L cm}^{-2}$ (0.7 $\mu\text{L mg}_{\text{NMC811}}^{-1}$).⁷⁷⁶

Based on a similar mechanism, substantial efforts were devoted to exploring novel effective fluorine-containing additives and significant progress was achieved.^{326,778-781} Song and co-workers³²⁶ stabilized the NMC532 cathode by introducing 5 wt% FEMC into conventional EC carbonate electrolyte, realized a significantly improved cycling performance with a high reversible capacity of 205 mA h g^{-1} (Fig. 26c and d). After 50 cycles, the Li||NMC532 can still deliver a capacity retention of > 84% despite a high cutoff voltage of 4.6 V (Fig. 26e). Under these harsh working conditions, the electrolyte with FEMC exhibits much higher reversible CEs than that of the electrolyte without FEMC (Fig. 26f). FEMC additive in the electrolyte acts as the F-source, promoting the formation of CF-containing species and fluoride species (NiF_2 , MnF_2 , CoF_2 and LiF) as shown in Fig. 27, which could effectively passivate the surface of the high voltage cathode, attenuate the cathode and electrolyte interactions, and suppress the transition metal dissolutions. Quantitative analyses through XPS peak deconvolution demonstrated that more than 56% of the surface Ni exists as the state of the NiF_2 in an FEMC added electrolyte, while the NiF_2 is only about 15% for the conventional EC carbonate electrolyte.³²⁶ Choi *et al.*⁷⁷⁸ reported a dual function additive of ethyl 4,4,4-trifluorobutyrate (ETFB), which could passivate the graphite anode and stabilize the Ni-rich $\text{LiNi}_{0.7}\text{Co}_{0.15}\text{Mn}_{0.15}\text{O}_2$ cathode simultaneously. Therefore, a high capacity retention of

84.8% associated with high cycling CE of > 99.8% after 300 cycles was achieved for the graphite||NMC full cell with the high loading of a 25.6 mg cm^{-2} NMC cathode in the electrolyte containing 1% ETFB. Xia *et al.*⁷⁸² compared the effects of four fluorinated carbonates including FEC, DFEC, bis(2,2,2-trifluoroethyl)-carbonate and 2,2,3,4,4,4-hexafluorobutyl methyl carbonate as electrolyte additives on the electrochemical performance of graphite||NMC442 pouch cell. Among these four additives, DFEC exhibits a compromised electrochemical performance with a high capacity retention and moderate gas generation.

The fluorination of the methyl group in PC molecules highly changes the electrochemical behavior of the solvent, which not only passivates the graphite anode, but also significantly enhances the anti-oxidation performance on the delithiated cathode.^{779,780} Utilizing trifluoro-propylene carbonate (TFPC) as the co-solvent for the PC electrolyte, Zheng *et al.*⁷⁸⁰ realized a high reversible 5 V graphite||LNMO full cell in a wide working temperature range. However, detrimental effects were reported by Su *et al.*⁷⁸¹ for the TFPC additive on the Li||NMC622 cells. These contrary results might be due to the different SEI formation mechanism on the graphite and Li metal anodes. Apart from the compact CEI formed by the fluorinated additives, the fluorination of the carbonate lowers the binding energy between the Li^+ and the carbonyl group, widens the LUMO-HOMO gap, and therefore hoists the potential window of the electrolyte thermodynamically,⁷⁸³ which further prompts the high-voltage working limits of the batteries. However, using these fluorine-containing compounds as solvents or additives, special caution should be taken. High impurities such as water could induce the hydrolysis of the fluorine-containing species, resulting in the formation of the HF and deteriorating the electrochemical performance of the high voltage batteries.⁷⁸⁴

Phosphorus-containing additives

Phosphorus containing additives entered into the electrolyte arena first as a kind of good fire-retardant agent for non-aqueous electrolytes because of the good radical scavenging capability.^{519,692,785-790} However, most of the organophosphorus compounds pose a negative effect on cell performance due to their poor SEI/CEI formation capability and their persistent reactivity with electrode materials. Xu *et al.*⁵¹⁹ reported that triethyl phosphate delivers better cycling performance than trimethyl phosphate. Dahn and co-workers⁷⁹¹ investigated the impact of triphenyl phosphate additives on the NMC and NCA cathodes. The capacity retention of NCA cells with a triphenyl phosphate content of < 20% was as good as cells without triphenyl phosphate. However, with further addition of the triphenyl phosphate, the cell impedance was significantly increased.

To get a better protecting effect on the high voltage cathodes, combining fluorine functional groups and phosphate/phosphide was proposed, which could suppress the combustion of the electrolyte and meanwhile enhance the stability of the cathodes thanks to the synergetic effect of fluorine and phosphorus groups in the additives. These additives can be clarified as salt-types and solvent-types. Lithium tetrafluoro(oxalato)phosphate (LiTFOP)⁷⁹²

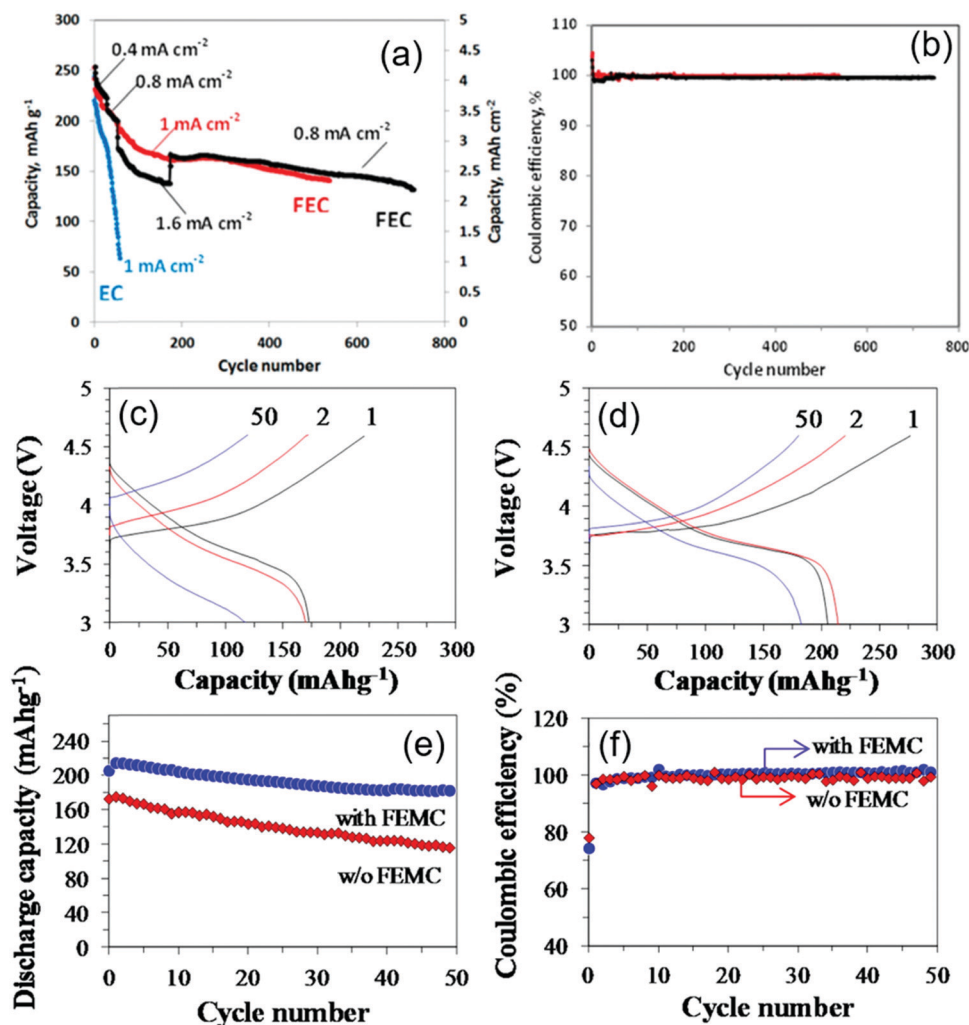


Fig. 26 Electrochemical performance of aggressive LiNiO₂ or NMC532 cathodes vs. Li metal anode in EC-based carbonate electrolyte with FEC or FEMC additives. (a) Cycling performance of Li||LiNiO₂ cell and corresponding CEs with or without FEC additive. (b) Charge/discharge profiles for Li||NMC532 cells in 1 M LiPF₆ EC/EMC (c) without and (d) with 5 wt% FEMC at 0.1C at 1st, 2nd, and 50th cycles. Reversible capacity of Li||NMC532 cells (e) and corresponding CEs (f). The cut-off voltage for Li||LiNiO₂ and Li||NMC532 is 4.3 V and 4.6 V, respectively. (a and b) Reprinted with permission from ref. 31 Copyright 2018 American Chemical Society. (c–f) Reprinted with permission from ref. 326 Copyright 2014 American Chemical Society.

and lithium difluoro(bisoxalato)phosphate (LiDFBP)^{793–796} are the representatives for the salt-type additives. For these salt-type additives, Li ions could be incorporated into the CEI formation, and therefore higher ionic conductivity can be achieved in the interfacial layers than those formed from the decomposition of electrolyte solvents or organic additives, leading to better kinetics for the cell (Fig. 28a and b).⁷⁹⁶ Eqn (10) demonstrated the possible CEI formation mechanism from the oxidation of the LiDFBP additive, which was proposed by Li *et al.*⁷⁹⁶ based on the *post mortem* analysis and the theoretical calculations. The radicals formed by DFBP⁻ oxidation release CO₂, and then polymerize with each other, generating a polymeric anion containing O, F, and P elements. In contrast to the low ion conductivity of CEI layers formed by electrolyte decomposition or the polymerization of the unsaturated solvent-type additives, the interfacial layers constructed from the salt-type additive is ionically conductive thanks to the incorporation of the Li ions with polymeric anions.

In contrast to the deterioration of the cycling performance adding the phospholanes in the reference electrolyte, grafting a fluorinated group in the phospholane can dramatically enhance the electrochemical performance of the graphite||NMC111 full cells with an improved cycling stability and higher CE (Fig. 28c and d).⁷⁹⁷ As shown in Fig. 28e, the grafted -CF₃ group effectively curbed the thickness of the CEI layers, indicating the good CEI formation capability of the -CF₃ groups in the phospholanes. *Post mortem* analysis indicates that different functional groups of the fluoro-phosphates could notably influence the morphology, composition and thickness of the *in situ* formed CEIs, in which the linear side group (such as 5F-TPrP) will promote the thickness of the CEI, while the branched group (HFIP) will result in a more compact and thinner CEI.⁷⁹⁸ Fig. 29 shows the representative phosphorous-containing bi/multifunctional additives for the Li ion electrolytes, including 3F-TPrP,⁷⁹⁹ 4F-TPrP,⁷⁹⁹ 5F-TPrP,⁷⁹⁸ HFIP,^{310,798}

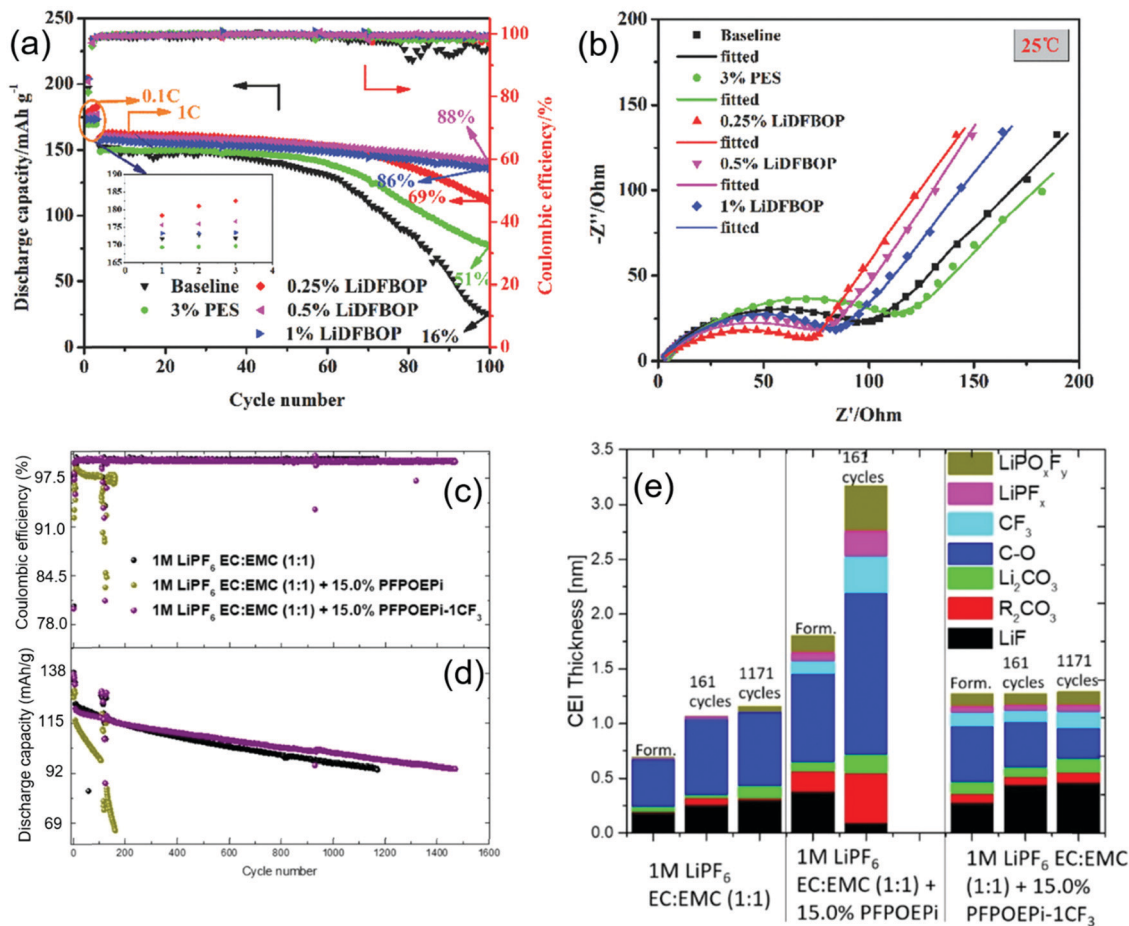


Fig. 28 (a) Cycling performance and Coulombic efficiency of Li||NMC532 in electrolyte with different additives at 3–4.5 V. (b) Electrochemical impedance spectra of NMC532 after formation cycles. The baseline electrolyte in figure a and b is 1 M LiPF₆ EC/EMC. (c) Cycling Coulombic efficiency and (d) discharge capacity for the graphite||NMC111 cells in three different electrolytes (1 M LiPF₆ EC/EMC; 1 M LiPF₆ EC/EMC + 15%PFPOEPI; 1 M LiPF₆ EC/EMC + 15%PFPOEPI–1CF₃). (e) The thickness and the compositions of the CEI after different cycles in the three electrolytes. (a and b) Reprinted with permission from ref. 796 Copyright 2018 John Wiley & Sons, Inc. (c–e) Reprinted with permission from ref. 797 Copyright 2020 John Wiley & Sons, Inc.

effectively scavenge the detrimental HF and PF₅ species. Han *et al.*⁸¹¹ screened the E_{LUMO} , E_{HOMO} , RP (reduction potentials), OP (oxidation potentials) and reactivities with HF ($-\Delta_{HF}$) for 23 possible phosphite additives, as listed in Table 5. Compared to EC and VC molecules, all of these phosphites tend to react with HF acidic species, implying the effectiveness to purify the electrolyte during cycling. Meanwhile, the PFPDPP can be oxidized at a lower voltage of 3.5 V vs. Li⁺/Li prior to the oxidation of carbonate solvents to form a compact CEI. Therefore, a capacity retention of 71% was achieved for the high-voltage Li||LNMO cells with PFPDPP additive after 300 cycles, whereas the cell in the baseline electrolyte only possesses a capacity retention of 53.4%. Some phosphorus additives containing other functional groups, such as TMPSi and TMPSa, will be discussed in the following Si-additive sections, since the Si–O functional groups appended to the coordinate P atom core of the additive play the key role in the functionality.⁸¹²

Nitrile additives

As pure solvents, nitriles have been regarded as one of the promising solvated molecules for LIBs thanks to their high

stability on the high voltage cathodes and favorable dielectric factor. We have discussed their benefits as the skeleton solvents in the novel electrolyte section. Besides this, it is believed that some nitriles can also be utilized as additives in the commercial carbonate electrolytes, stabilizing the carbonate electrolytes against oxidation at high voltages.⁴⁰⁵

A series of nitrile additives were investigated to stabilize the high voltage cathodes, including suberonitrile,³⁸⁹ tetrafluoroterephthalonitrile (TFTPN),⁸¹³ 4-(trifluoromethyl)-benzoxonitrile (4-TB),⁸¹⁴ succinonitrile (SN),^{383,405,406,815} adiponitrile,^{383,386,816–818} pimelonitrile (PN),³⁸³ fumaronitrile (FN),⁸¹⁹ 1,3,6-hexanetricarbonitrile (HTN),⁸²⁰ 1,3,5-pentanetricarbonitrile (PTN)⁸²¹ and 3,3'-(Ethylenedioxy)dipropiononitrile (EDPN)⁸²² *etc.* The molecule structures of these nitrile additives are demonstrated in Fig. 31. Besides helping to generate a conductive and robust SEI layer on the anode, nitrile groups in the additives could preferentially coordinate with high-valence transition-metal atoms on the delithiated cathodes (Fig. 32a), which reduces parasitic reactions between the delithiated cathode surface and electrolyte.^{386,389} Therefore, the Li||LiNi_{0.73}Co_{0.1}Mn_{0.15}Al_{0.02}O₂ cell delivered an unprecedented cycling capacity retention of

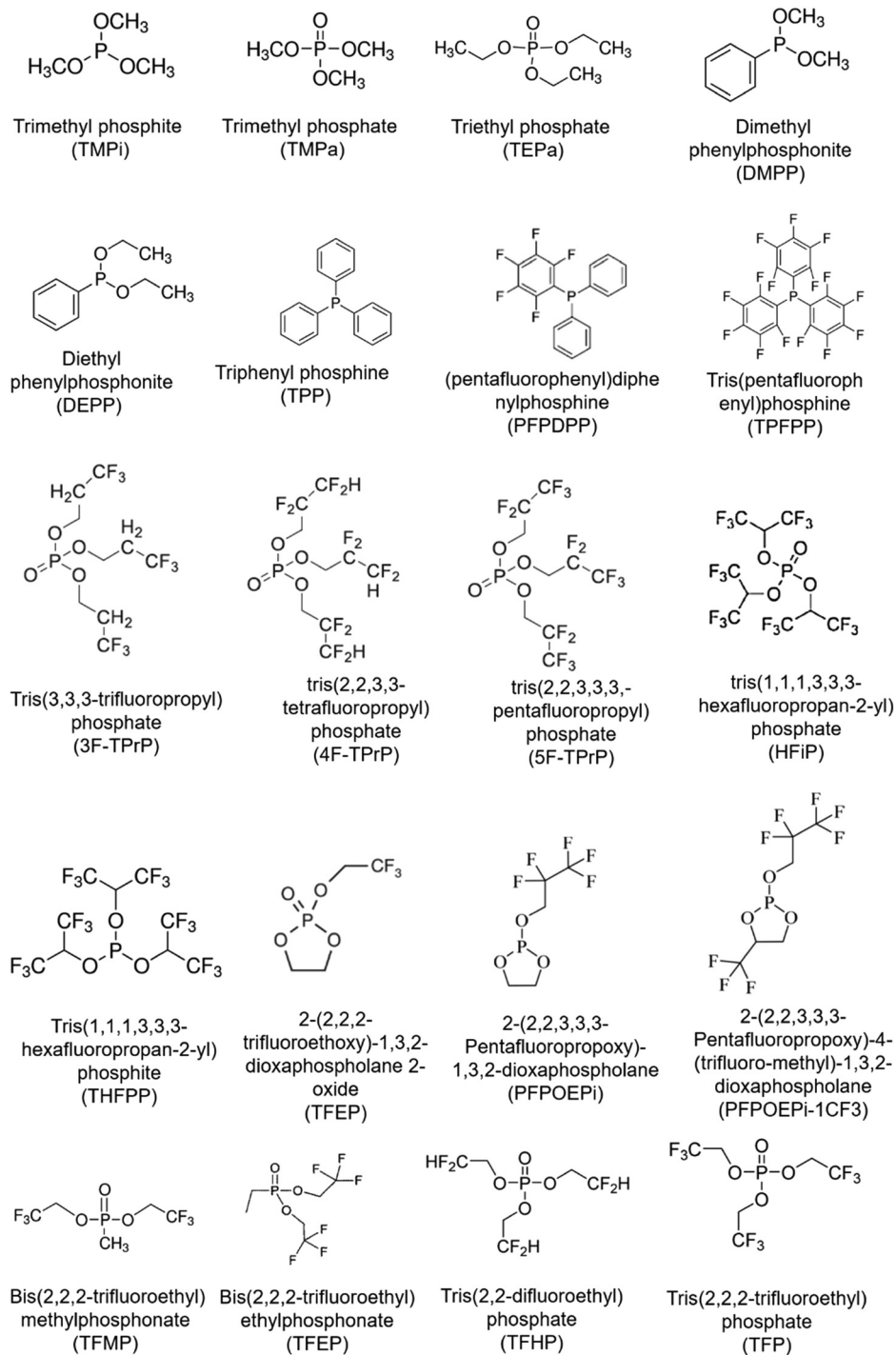


Fig. 29 Representative P-containing additives for the Li ion batteries.

>75% for over 800 cycles under a high areal loading of 1.8 mA h cm^{-2} in the electrolyte of $0.8 \text{ M LiTFSI} + 0.2 \text{ M LiDFOB} + 0.05 \text{ M LiPF}_6$ FEC/EMC (baseline electrolyte) with only 1% adiponitrile additive (Fig. 32b).

Apart from the coordination mechanism, it is believed that some nitriles can be oxidized prior to the conventional carbonate solvents and form a protective interphase layer on the cathodes, effectively enhancing the electrochemical performance of the

aggressive high-voltage cathodes. Liu *et al.*⁸¹³ proposed TFTP as a nitrile additive for LIBs, which improves the cycling stability of the graphite||LCO full cell up to 4.4 V. A high capacity retention of $\sim 91\%$ can be achieved for the graphite||LCO full cell in the electrolyte with only 0.5% TFTP for 300 cycles compared to less than 80% capacity retention for the baseline electrolyte. Wang and co-workers⁸²⁰ adopted HTN additive into the more aggressive Li-rich cathode systems, and found that HTN not only improves

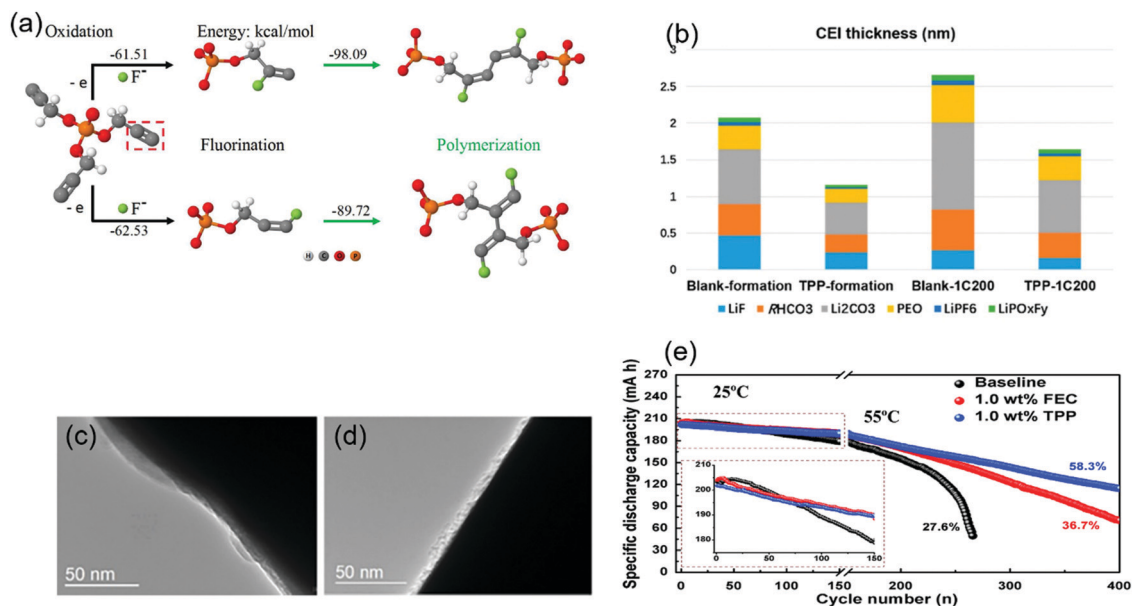


Fig. 30 Electrochemical performance and the CEI formation mechanism for the TPP additive. (a) Possible oxidation mechanism for the TPP forming the CEI layers; (b) calculated CEI thickness formed in the two electrolytes (blank electrolyte, 1 M LiPF₆ EC/DEC 3 : 7; TPP electrolyte, 1 M LiPF₆ EC/DEC + 1wt% TPP) from the XPS analysis; TEM results of the CEI layers for the two electrolyte systems: (c) blank electrolyte, (d) TPP electrolyte. (e) Cycling comparison of the graphite||NMC532 pouch cell in three different electrolytes: baseline electrolyte (1 M LiPF₆ EC/EMC 3 : 7). (a and e) Reprinted with permission from ref. 805 Copyright 2019 Elsevier. (b–d) Reprinted with permission from ref. 806 Copyright 2020 American Chemical Society.

Table 5 Calculated E_{LUMO} , E_{HOMO} , RP (reduction potentials), OP (oxidation potentials) and reactivities with HF ($-\Delta_{\text{HF}}$) for 23 phosphite additives.⁸¹¹ For comparison, the data for EC and VC are also compiled

Additives	E_{LUMO} (eV)	E_{HOMO} (eV)	RP (V vs. Li/Li ⁺)	OP (V vs. Li/Li ⁺)	$-\Delta_{\text{HF}}$ (kcal mol ⁻¹)
Triethyl phosphite	0.73	-6.51	-0.14	4.63	6.73
Triphenyl phosphite	-0.75	-6.66	0.50	5.04	3.42
Trimethyl phosphite	0.635	-6.60	-0.52	4.72	5.35
Triisopropyl phosphite	0.71	-6.43	-0.59	4.56	8.34
Tributyl phosphite	0.44	-6.54	-0.03	4.57	4.39
Diethyl trimethylsilyl phosphite	0.70	-6.62	-0.25	4.53	13.17
Tris(nonylphenyl)phosphite	-0.59	-6.51	0.03	4.80	8.38
Bis(2,2,2-trifluoroethyl)phosphite	-0.50	-7.85	0.55	5.58	4.89
Tris(trimethylsilyl)phosphite (TMSPi)	0.70	-6.52	-1.03	4.29	10.41
Triisodecyl phosphite	0.57	-6.59	0.05	4.47	8.09
Tris(<i>tert</i> -butyldimethylsilyl)phosphite	0.69	-6.34	-0.02	4.17	16.27
Diisodecylphenyl phosphite	-0.49	-6.54	-0.26	4.69	5.02
Dimethyl trimethylsilyl phosphite	0.60	-6.56	-0.10	4.50	13.89
Tris(1,1,1,3,3,3-hexafluoro-2-propyl)phosphite	-1.46	-8.61	1.33	6.36	5.43
Tris(2,4-di- <i>tert</i> -butylphenyl)phosphite	-0.63	-6.10	0.21	4.49	13.35
Tris(2-chloroethyl)phosphite	-0.01	-7.14	1.56	4.91	1.78
Benzyl diethyl phosphite	-0.34	-6.64	-0.36	4.59	6.70
Tris(2-ethylhexyl)phosphite	0.55	-6.58	-0.32	4.62	2.61
Phenyl-[(<i>R</i>)-1,1-spirobiindane-7,7-diyl]-phosphite	-0.59	-6.46	-0.06	4.96	7.84
2,2-Dimethyltrimethylene phenyl phosphite	-0.53	-6.53	0.53	4.86	7.06
4-Chlorophenyl diethyl phosphite	-0.77	-6.39	-0.07	4.85	6.98
Trioctadecyl phosphite	0.50	-6.60	-0.93	4.66	6.04
Trilauryl phosphite	0.60	-6.59	-0.62	4.30	8.69
Ethylene carbonate (EC)	0.60	-8.25	-0.32	6.92	—
Vinylene carbonate (VC)	-0.36	-7.23	-0.12	5.46	—

the oxidation potential of the electrolyte, but also suppresses the voltage degradation of the Li-rich cathode (Fig. 32 c and d). The peak intensity of the C–H and C–C significantly decreases and meanwhile the peaks belonging to PVDF are almost undetectable in the HTN-containing electrolyte (Fig. 32e), suggesting a more uniform and compact CEI film formed on the cathode surface,

which should be due to the lower HOMO orbital energy of nitriles than those of the carbonates.^{814,823,824}

Boron-containing additives

Because of the electron deficiency in the B center atoms, most of the B-containing additives could complex with the anions

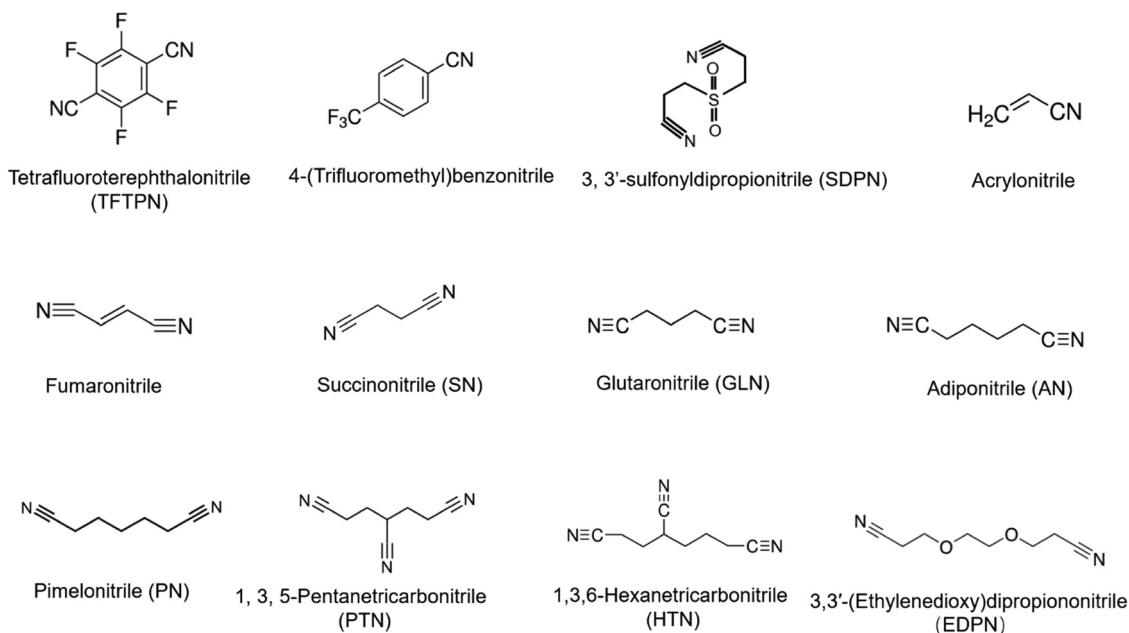


Fig. 31 Representative nitrile-based additives for the Li ion batteries.

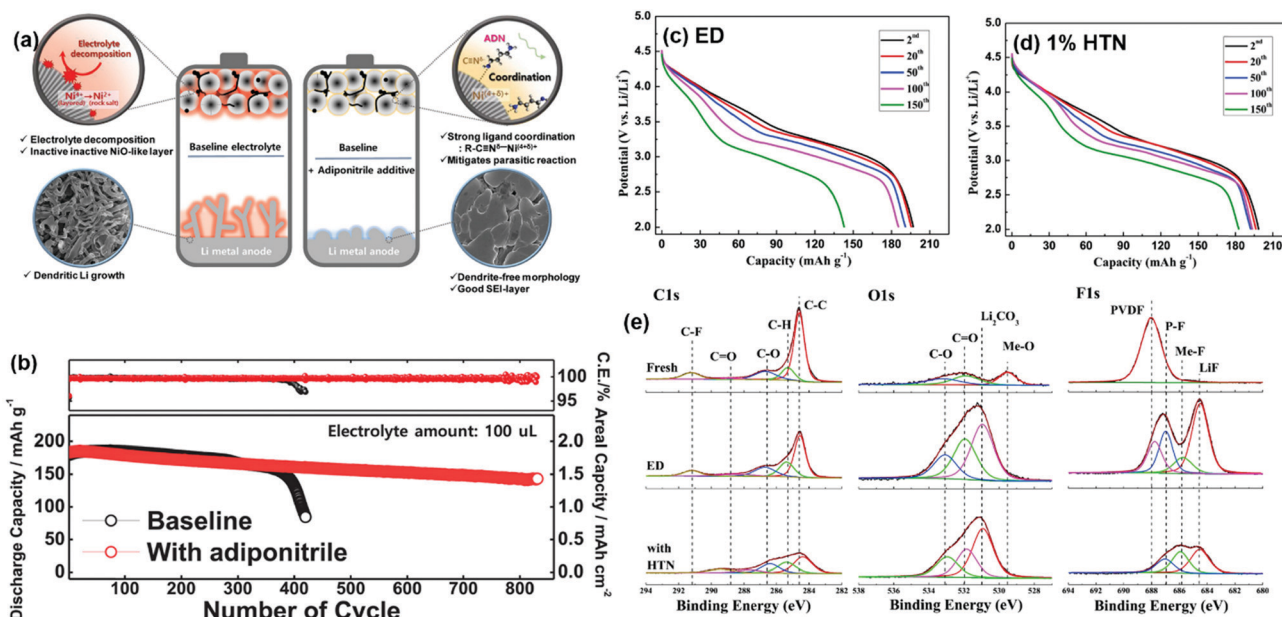


Fig. 32 Effect of nitriles on the electrochemical performance of NMC aggressive cells. (a) Schematic illustration of the effect of the adiponitrile as a bi-functional additive on the Ni-rich NMC cathode and Li metal anode; (b) comparison of the electrochemical performance of the Li||LiNi_{0.73}Co_{0.1}-Mn_{0.15}Al_{0.02}O₂ battery with/without adiponitrile additive. The baseline electrolyte in figure a and b is 0.8 M LiTFSI + 0.2 M LiDFOB + 0.05 M LiPF₆ FEC/EMC. Selected discharge profiles of the Li_{1.2}Ni_{0.13}Co_{0.13}Mn_{0.54}O₂ in standard electrolyte (ED, 1 M LiPF₆ EC/DMC with 1 : 2 vol. ratio) (c) and 1% HTN-containing electrolyte (d). (e) XPS spectra for the fresh and cycled Li_{1.2}Ni_{0.13}Co_{0.13}Mn_{0.54}O₂ in ED and 1% HTN-containing electrolyte. (a and b) Reprinted with permission from ref. 386 Copyright 2019 John Wiley & Sons, Inc. (c–e) Reprinted with permission from ref. 820 Copyright 2017 Elsevier.

and stabilize the carbonate electrolytes.^{825,826} In these boron-containing additives, lithium tetrafluoroborate (LiBF₄),⁸²⁷ lithium bis(oxalate)borate (LiBOB)^{828–830} and lithium difluoro(oxalate)borate (LiDFOB)^{831,832} were initially explored as Li salts, and then researchers found that these salts can be decomposed preferentially on the delithiated cathode due to

their higher HOMO energies, forming a borate-rich, robust and protective interphase, which could improve the electrochemical performance of the high voltage cathodes. Therefore, these borate salts are extensively explored as the electrolyte additives.^{717,833–846} For example, Zuo *et al.*⁸²⁷ showed that by adding 1.0–2.0 wt% LiBF₄ into a conventional carbonate

electrolyte, the electrochemical performance of a graphite||NMC532 pouch cell was critically improved with a higher capacity retention and lower interfacial impedance. The BF_3 decomposed from LiBF_4 can participate in the CEI formation on the NMC cathode operated at high potential, and meanwhile BF_3 as a typical Lewis-acid functions as an anion receptor to help dissolve the LiF . This promising effect derived from the BF_4^- anions was confirmed by Xing *et al.*⁸⁴⁷ in the Li||NMC811 cell, in which the improved interfacial stability of NMC instead of the Li metal anode results in the enhanced cycling performance. Choi *et al.*⁸⁴³ demonstrated that even 1% LiDFOB drastically enhances the cycling stability and rate capability of Li-rich graphite||NMC cell. The LiDFOB-containing electrolyte increased the capacity retention of graphite|| $\text{Li}_{1.17}\text{Ni}_{0.17}\text{Mn}_{0.5}\text{Co}_{0.17}\text{O}_2$ from 45.8% in a baseline electrolyte to over 82.7% within 100 cycles at 0.5C and 25 °C. Recently, Sun and co-workers^{848–851} synthesized a series of fluorinated lithium bis(malonato) borate salts and adopted them as electrolyte

additives for a 5.0 V LNMO cathode. These additives effectively improve the initial CE, and meanwhile critically enhance the cycling stability of the LNMO. It is believed that the *in situ* formed inorganic-rich SEI and B-containing CEI effectively blocked the side reactions between the electrodes and the electrolyte, suppressed the TM dissolution, and inhibited the micro-cracks.^{810,843,852–857} Besides these boron-containing salts, a type of special boron additives should be mentioned, *e.g.* TPFPB and TTFEB.⁸⁵⁸ These additives can not only form a CEI/SEI layer on the cathode/anode due to the preferentially oxidation/reduction,⁸⁵⁹ but also facilitate the Li^+ ion transport by tethering the anions in the electrolytes due to the highly electron deficient in the B-center atom.³ Fig. 33 shows the representative boron-containing additives utilized for the high-voltage cathodes.

Trimethyl borate (TMB-1), Trimethylboroxine (TMB-2) and lithium tetramethyl borate (LiTMB) have the same B–O groups and similar molecular structure, and therefore exhibit similar

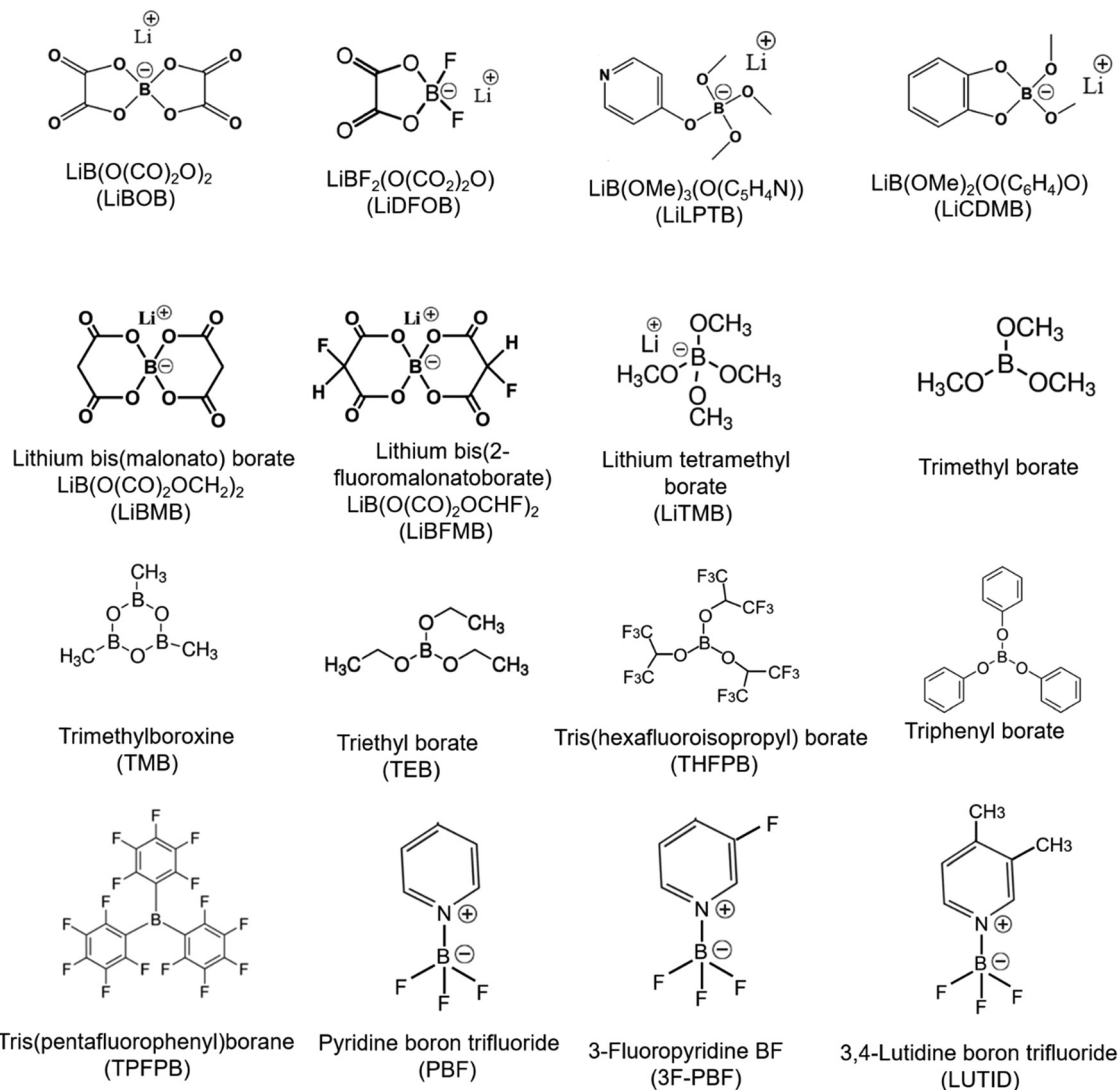


Fig. 33 Representative B-containing additives stabilizing the high-voltage cathodes for the Li ion batteries.

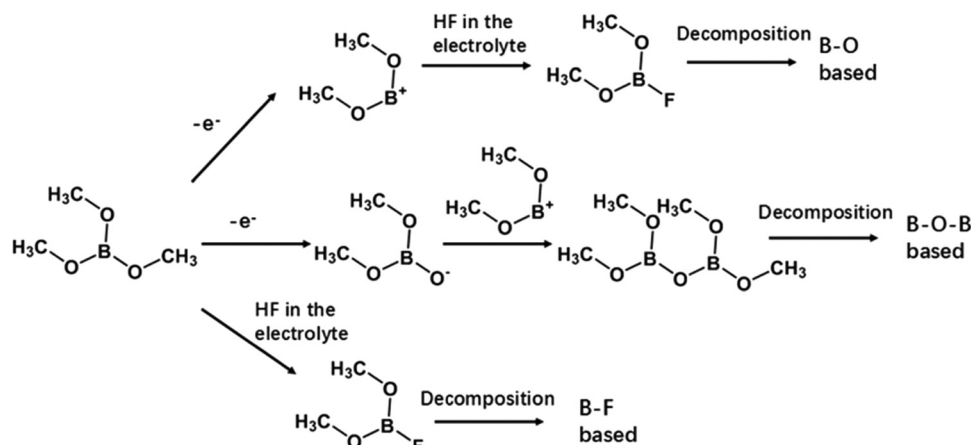


Fig. 34 Possible electrochemical reaction mechanisms for the decomposition of TMB. Reprinted with permission from ref. 863 Copyright 2019 American Chemical Society.

electrochemical performance for high-voltage cathodes, which have been evaluated in different cathode systems such as 5 V LiCoPO₄,^{754,860} LNMO,⁸⁶¹ NMC,⁸⁶² and high-voltage LCO⁸⁶³ etc. The capacity retentions of the cathodes are highly enhanced in the electrolyte containing these B-containing additives even with a higher cut-off voltage. The TMB-1, TMB-2 and LiTMB are sacrificially oxidized on the surface of the cathodes in the initial charge protocol forming a borate-based CEI layer, inhibiting the electrolyte oxidation on the catalytic surface.⁸⁶¹ Liu *et al.*⁸⁶³ proposed a possible reaction mechanism shown in Fig. 34, in which species with B-O, B-O-B, and B-F in the formed CEI layers were confirmed by the FTIR and XPS techniques.⁸⁶³

More recently, Dahn and co-workers^{864–866} developed a series of novel pyridine-boron trifluorides (PBFs) and derivatives (3-fluoropyridine BF, 2-fluoropyridine BF, 3-pyridinecarbonitrile, 3,4-lutidine boron trifluoride, 4-vinylpyridine BF, 4-trifluoromethylpyridine) as electrolyte additives for the graphite||NMC pouch cells and compared them to the well-known effective additives such as VC, triallyl phosphate (TAP), methylene methane disulfonate (MMDS), prop-1-ene sultone (PES), and tris(trimethylsilyl)-phosphite (TTSPi). Three representative molecule structures of PBFs are shown in Fig. 33 (PBF, 3F-PBF, LUTID). All of the PBFs are competitive with these well-known additives, showing excellent capacity retention (Fig. 35a and c) and maintaining low impedance even with a higher cut-off voltage (Fig. 35b, d and e). Based on these results, the authors further explored the binary additive blends. The cells with the PBF/MMDS or PBF/DTD showed significant improvements in CE with reduced impedance and good capacity retention, and even surpassed the performance of the cells with the optimized PES211 additive blend.⁸⁶⁶ However, the detailed cathode surface chemistries between the PBFs and the high voltage cathodes, and the related CEI components are not fully uncovered. On the other hand, although these binary additive blends effectively improve the electrochemical performance of the cell with higher cutoff voltage, they cannot fully cut off the electrolyte oxidation, as implied by charge end point capacity slippage.⁸⁶⁶ Beyond all doubt, these PBFs are promising

high-voltage additives and well deserve further exploration and optimizations.

Han and co-workers⁸⁶⁷ proposed three criterions for exploring novel borate-based additives for high-voltage batteries: (1) lower oxidation potential than EC solvents with low oxidation-resistance; (2) lower reduction potential than EC, which will not affect the SEI formation from the EC decomposition; (3) high F⁻ binding affinity, which could enhance the ion-pair dissociation of Li⁺ and anion and high cell performance. Based on these principles, They suggested five borate derivatives (triphenyl borate, triallyl borate, trimenthyl borate, tritoly borate and tris(1-isobutyl-3-methyl butyl)borate) as the promising CEI-forming improvers by screening 33 borate compounds for Li ion batteries *via* DFT calculations of oxidation potentials, reduction potentials and F⁻ binding affinities.⁸⁶⁷

Silicon-containing additives

The organosilicons have a number of potential advantages as electrolyte solvents or electrolyte additives, such as low flammability, low volatility, high-resistance to oxidation and environmental benignancy.^{868–873}

Silicon-based additives with Si-O and Si-N bonds not only form polymeric CEI layers on the high voltage cathodes, but also mitigate the undesirable parasitic reactions thanks to the capability of siloxane (Si-O) or silazane (Si-N) groups to scavenge HF and PF₅ detrimental species,^{811,812,874–886} which effectively protect the cathodes and CEI layers from nucleophilic attacking by these fluoride species.^{887–889} Some indispensable HF is formed by hydrolysis of the electrolyte with a trace amount of moisture contamination.^{81,890} Even though the electrolyte is highly purified, non-ignorable HF species will be generated from the reactions between the residual alkaline Li compounds such as LiOH, Li₂O or Li₂CO₃ on the layered cathode surface with the acidic LiPF₆.^{700,891–893} The amount of alkaline species increases with the increase of Ni content,²⁰⁷ leading to serious formation of HF on the Ni-rich cathodes. Moreover, as the byproducts of parasitic reactions, some acidic HF can also be formed due to the dehydrogenation reactions between the electrolyte solvents

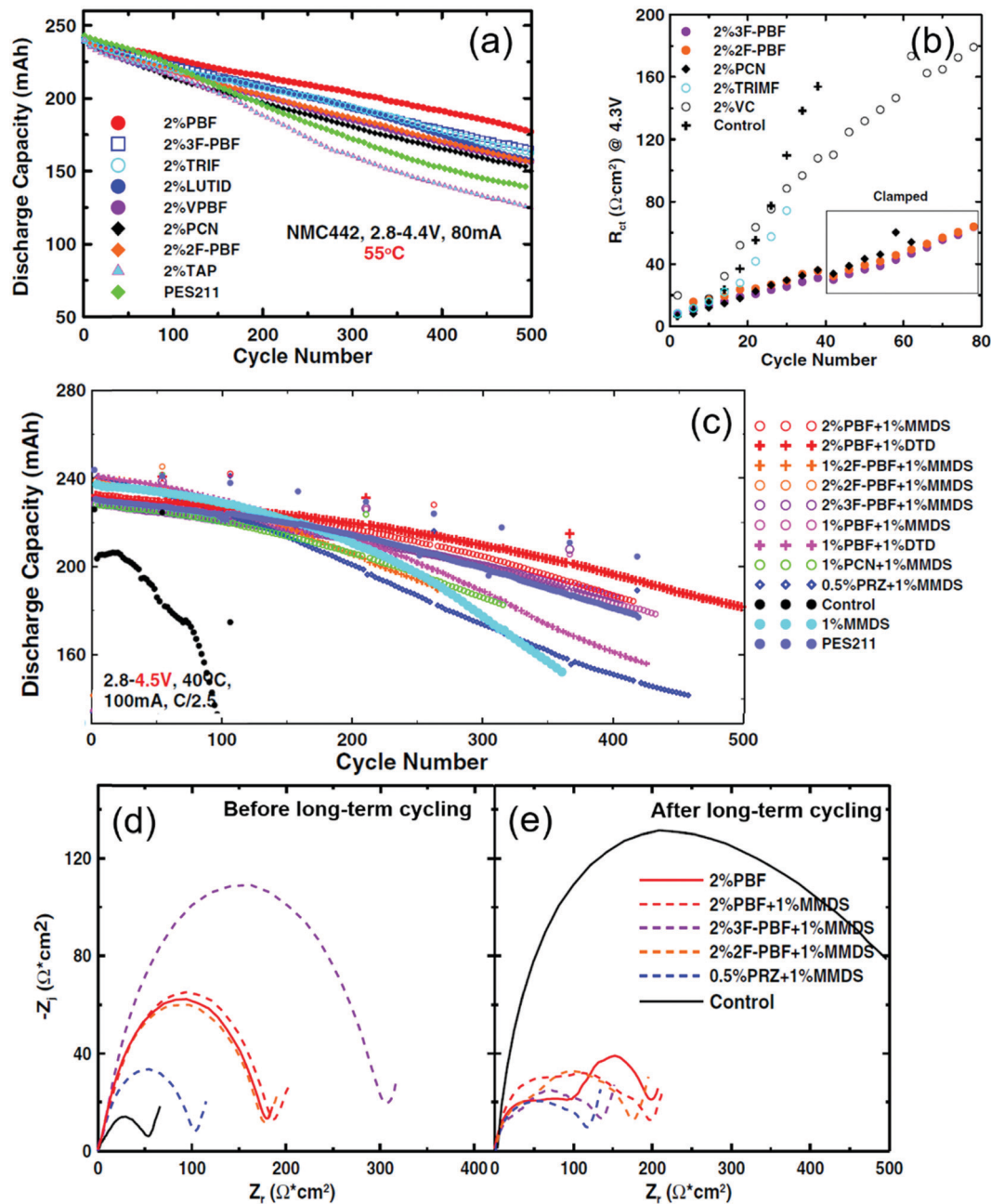


Fig. 35 Electrochemical performance of the graphite||NMC442 pouch cells with different additives. (a) Cycling stability of graphite||NMC442 with PBF-based additives and PES211, or TAP additives. (b) R_{ct} variation during cycling measured at 4.3 V for graphite||NMC442 cell in different electrolytes. (c) Cycling stability of graphite||NMC442 with different additive blends between 2.8 and 4.5 V at 40 °C. Impedance spectra of the graphite||NMC442 cell (d) before long-term cycling and (e) after long-term cycling. (a and b) Reprinted with permission from ref. 864 Copyright 2015 The Electrochemical Society. (c–e) Reprinted with permission from ref. 866 Copyright 2015 The Electrochemical Society.

and the nucleophilic TM–O radicals on delithiated cathodes at high voltage.^{193,894} These as-formed HF could destroy the SEI/CEI layers, etch the electrode materials and accelerate the dissolution of transition metals.⁸⁹⁵ Therefore, the adoption of additives that could expeditiously eliminate these acidic detrimental species seems essential for the high-energy Ni-rich batteries.

The silicon-containing additives have been applied to and critically improved the electrochemical performance of the various high-voltage cathodes, including LCO,⁸⁹⁶ NMC622,^{897–901}

NMC811,^{902–904} NCA,⁹⁰⁵ LNMO,⁸⁷⁴ Li-rich NMC,⁹⁰⁶ *etc.* Wang *et al.*⁹⁰¹ compared three different siloxane additives (octamethylcyclotetrasiloxane (D4), octamethylcyclotetrasiloxane (OMCTS) and 2,4,6,8-tetramethyl-2,4,6,8-tetravinylcyclotetrasiloxane (ViD4)) on the NMC622 cathode with a high cut-off voltage of 4.5 V, the molecular structures of which are shown in Fig. 36. Among these additives, ViD4 shows the best performance. With 0.5 wt% ViD4 in the electrolyte, Li||NMC622 exhibits a high reversible capacity of 187.2 mA h g⁻¹ and a good capacity retention of 83.6% at 1C

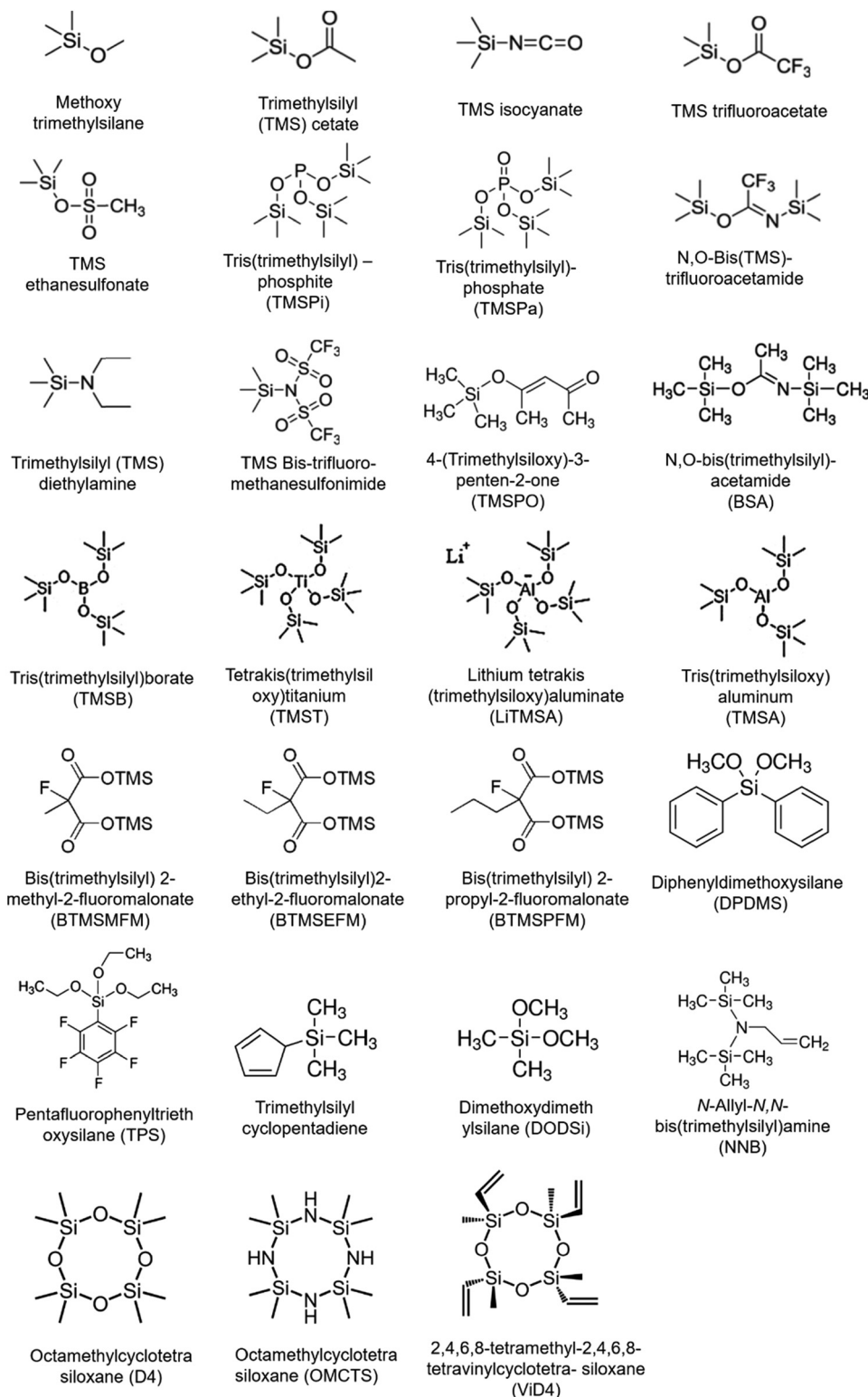


Fig. 36 Representative Si-containing additives stabilizing the high-voltage cathodes for Li ion batteries.

rate after 150 cycles, which is higher than that with D4 (81.3%), OMCTS (81.9%) and much better than the baseline carbonate electrolyte (76.1%). Detailed electrochemical characterization, DFT calculations, and surface analysis indicate that the synergistic

effects of the vinyl bond and Si-O functional group in ViD4 molecules could boost the formation of a uniform CEI layer on the high voltage cathode surface, reducing the parasitic reactions between the catalytic cathode and the electrolytes.

Among the widely investigated silyl-based additives (Fig. 36), tris(trimethylsilyl)phosphite (TMSPi)^{380,811,812,874,878,880,907–918} and tris(trimethylsilyl)phosphate (TMSPa)^{880,884,911,913–916,919–922} are the two most widely recognized, differing only in the oxidation state of the central phosphorus atoms. In 2012, Bhat and co-workers⁹²³ from Wildcat Discovery Technologies pointed out that silyl-substituted electrolyte additives such as TMSPi and

TMSPa could effectively improve the cycling performance of LIBs and are applicable to most of the prevailing cathode materials at high voltages and/or elevated temperatures. Immediately, Dahn *et al.*^{914,915} systematically compared the TMSPi and TMSPa additives on the electrochemical behaviors in the graphite||NMC111 pouch cells, and showed that both of the additives can effectively decrease the cell impedances (Fig. 37a), reduce charge end-point

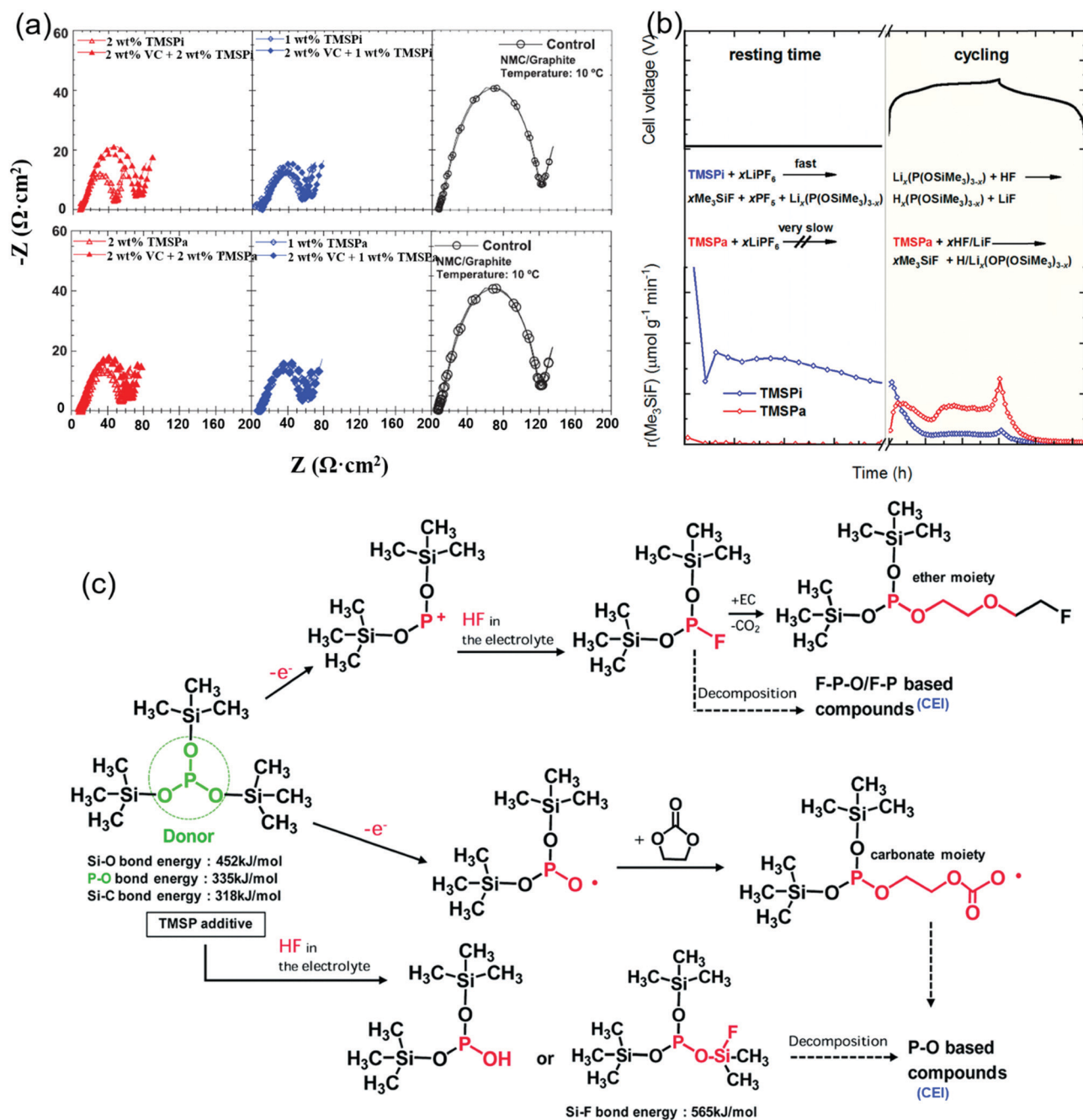


Fig. 37 (a) Impedance spectra of the graphite||NMC111 pouch cells with different additives after UHPC cycling. The control electrolyte in figure (a) is 1 M LiPF₆ EC/EMC (3 : 7). (b) The reaction mechanism for the TMSPi and TMSPa in the LiPF₆ carbonate electrolyte, resulting in varied Me₃SiF release profiles. (c) Schematic illustration of the possible reaction mechanisms of TMSPi in the conventional EC-based electrolyte. TMSPi can scavenge the HF and meanwhile contribute to the formation of the CEI on the cathodes. (a) Reprinted with permission from ref. 914 Copyright 2014 IOP Publishing, Ltd. (b) Reprinted with permission from ref. 880 Copyright 2020 American Chemical Society. (c) Reprinted with permission from ref. 874 Copyright 2014 The Royal Society of Chemistry.

capacity slippage, and improve the cycling Coulombic efficiencies, implying that these additives could form a robust and compact SEI/CEI on the electrodes and effectively restrict the parasitic reactions. Resorting to online electrochemical mass spectrometry (OEMS), Bolli *et al.*^{880,916} investigated the gases evolved during rest/cycling of graphite||NMC cells with/without TMPSi and TMPSa additives (Fig. 37b). The formation of Me₃SiF and POF₃ imply that the predominant role of both additives is to scavenge HF and PF₅ detrimental species, which safeguards the electrolytes and promises a longer cycle life for the LIBs. Although the effects to reduce the acidity of the electrolyte are similar to the TMPSi and TMPSa, yet the reaction mechanism differs. TMPSi additive reacts with PF₆⁻ immediately once they contact with each other, leading to the decomposition of additive and salts, evolution of Me₃SiF and POF₃ and formation of partially soluble Li-phosphites (Li_x(P(OSiMe₃)_{3-x})). In the following cycles, the Li-phosphite intermediates effectively scavenge the *in situ* formed HF, leading to the formation of phosphoric acid derivative and LiF. This reaction mechanism was well supported by Qi *et al.*,⁸⁷⁵ who reported that little TMPSi could be detected in the electrolyte after aging for 28 days at 20 °C.

Due to the lower oxidation potential of TMPSi than EC,^{811,907} TMPSi as the additive dominates the formation of CEI on the cathode surfaces, suppressing the electrolyte decomposition and holding-up the high-voltage cathodes from degradation effectively.^{874,907,914} Song *et al.*⁸⁷⁴ employed TMPSi as an additive for the 5 V LNMO cathode system, which not only scavenges detrimental HF from the electrolytes, but also facilitates the formation of P and F-rich CEI on the high voltage cathode, therefore highly improve the electrochemical performance of 5.0 V LNMO cathodes in both half and full cells. Based on the CEI and electrolyte composition analysis associated with the calculations, Song and co-workers⁸⁷⁴ proposed a CEI formation mechanism with TMPSi as the additive (Fig. 37c). Besides the consumption of the acidic species, the TMPSi could decompose into (Me₃SiO)₂P⁻ and Me₃SiO⁻, and subsequently these intermediates attack the surrounding EC solvent molecule, leading to the formation of the P-O and F-P-O based CEI/SEI.⁹¹⁸ Quenching the nucleophilic TM-O radicals with the P-containing CEI layers averts the dehydrogenation from the solvent molecules and in turn trims down the generation of acidic species.⁸¹² Despite its outstanding effects on the high-energy batteries, however, two concerns still exist in the large-scale utilization of the TMPSi. One is the high volatility due to its low boiling point of 78 °C, the other is the gas generation of flammable fluorotrimethylsilane in the reaction with HF.⁷⁰⁰ Grafting longer pendant groups on Si to regulate the high volatility and meanwhile to suppress the generation of flammable gas should be one of the possible solutions.

Delp and co-workers⁹²⁴ screened the electrochemical behaviors of the electrolyte solvents (EC, DMC, EMC, and FEC), salts (LiPF₆, LiBF₄, LiTFSI, LiDFOB, and LiTDI), and several intensively investigated additives (VC, PS, HFiP, and TMSPa) on the inert glassy carbon electrode and compared the results with the theoretical calculations. QC calculations indicate that the solvation capability to Li⁺ is in the following order TMSPa > EC >

DMC > VC > FEC > PS » HFiP, which means that TMSPa will replace EC in the Li⁺ solvation shell and dramatically change the CEI/SEI formation mechanisms. Different from the EC molecule, TMSPa will not transfer the hydrogen atoms to the cathode surface at high voltage. Instead, it transfers a proton to neighbor TMSPa molecules or intramolecularly upon oxidation, leading to a protective CEI layer formation without inducing acidity of the cathode surface, which could explain the reason why the electrolyte with TMSPa additive exhibits a lower impedance, suppresses the transition metal dissolution, and maintains a high capacity retention than other electrolytes.^{922,924} Recently, Luo and co-workers⁹²⁵ coupled NMC811 with the limited Li metal anode in the lean TMPSa-added electrolyte, realized a high specific energy density battery of 373 W h kg⁻¹ (Fig. 38) with an N/P ratio of 2.3 and areal capacity of 4.5 mA h cm⁻², representing a milestone towards the possible commercialization of high energy Li metal batteries. The uniform and robust Si- and P-rich CEI layers derived from the decomposition of TMSPa reinforced the cathode structure integrity and inhibited the side reactions between the catalytic NMC811 and the electrolyte (Fig. 38e and f), while rough CEI, high transition metal dissolution, and structure cracks are detected in NMC811 after cycling in a baseline electrolyte (Fig. 38c and d).

Both the tris(trimethylsilyl) borate (TMSB)^{883,926-932} and lithium tetra(trimethylsilyl) borate (LiTMSB)⁹³³ contain Si-O-B bifunctional groups, which not only eliminate the adverse acidic species in the electrolyte, but also facilitate the formation of the B-containing protective CEI layers on the high-voltage cathodes. These features are quite similar to the TMPSi and TMSPa additives. As an electron-deficient boron compound, TMSB can easily complex with anions, which improves the thermal stability of the LiPF₆ salts and enhances the electrochemical performance of the LIBs at increased temperatures. Liu *et al.*⁹²⁷ demonstrated that the cycling stability of the LiMn₂O₄ was greatly improved when the 0.5 wt% TMSB was added into the conventional carbonate electrolyte. The capacity retention of the graphite||NMC532 cell was critically enhanced from 28.5% in the conventional carbonate electrolyte to over 92.3% in the electrolyte with TMSB after 150 cycles with a high cut-off working voltage of 4.4 V.⁸⁸³ Highly electrochemical performance improvement was also detected in the 4.8 V Li-rich NMC,^{885,928} 5 V LNMO^{929,930,934} and 5 V LiCoPO₄ cathode⁹³⁵ with the addition of the TMSB in the carbonate electrolytes. After 200 cycles with a cutoff voltage of 4.8 V, the capacity retention of Li[Li_{0.2}Mn_{0.54}Ni_{0.13}Co_{0.13}]O₂ in 0.5% TMSB-containing electrolyte reaches 73.3%, while this value is less than 20% for the conventional carbonate electrolyte. Birrozzi and co-workers⁸⁸⁵ tested a series of electrolyte additives on the Li-rich cathode, including PS, bis(trimethyl)malonate (BTM), diethyl(trimethylsilyl)amine (DTA), FEC, glutaric anhydride (GA), LiBOB, LiDFOB, methylphenyl carbonate (MPC), pentafluorostyrene (PFS), succinic anhydride (SA), TMB, TMSB, TMSP, and VC. Among these additives, TMSB and PS exert the most promoting effect on the capacity retention and the Coulombic efficiency. It is believed that the thinner CEI film derived from TMSB and the combination of TMSB with PF₆⁻ and F⁻ in the

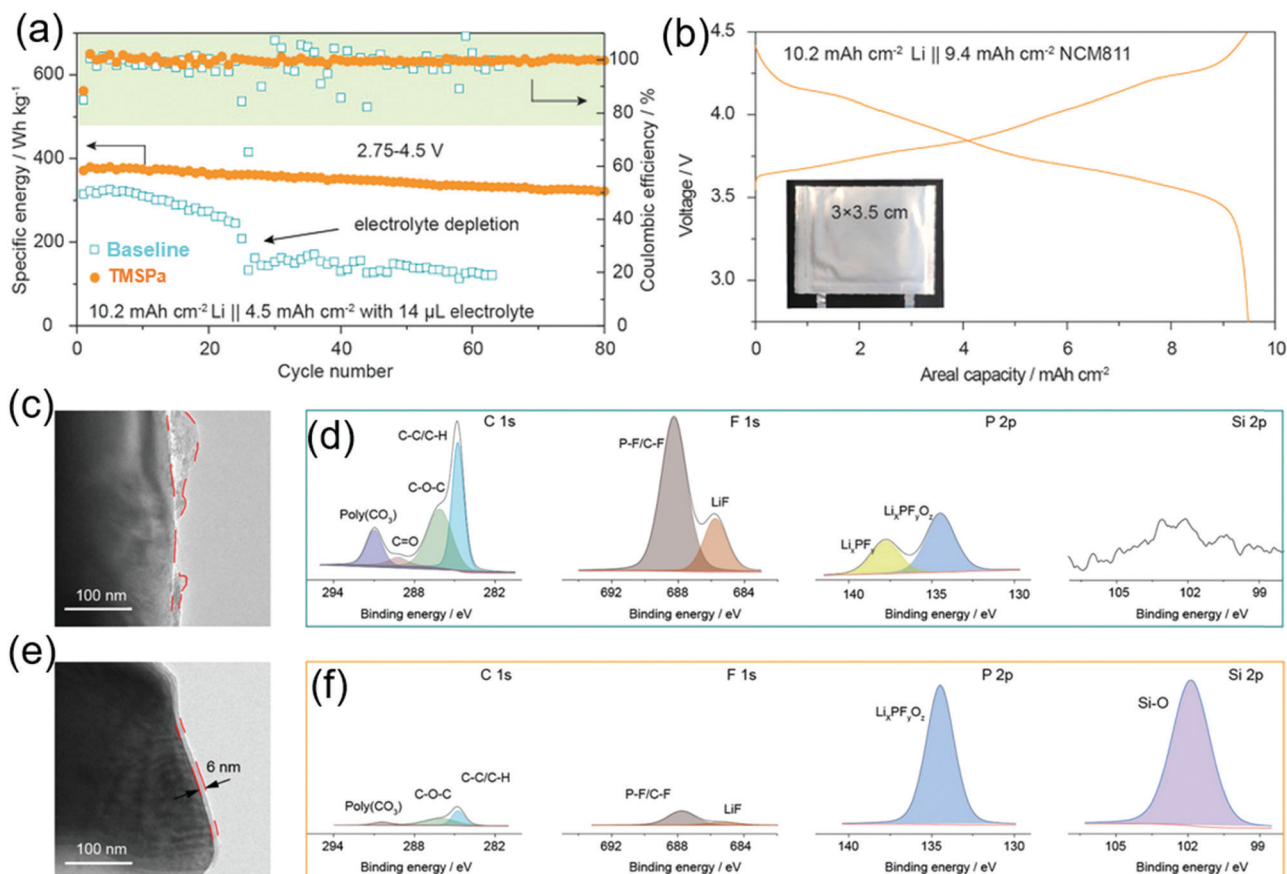


Fig. 38 Electrochemical performance of Li||NMC811 cells and the CEI characterization on the cycled NMC811 cathodes. (a) Cycling performance of the Li||NMC811 cell in a baseline electrolyte (1 M LiPF₆ EC/DEC) with and without TMSPa additive. (b) Charge/discharge profile of the Li||NMC811 pouch cell using TMSPa containing electrolyte. (c) TEM image and (d) XPS spectra of the cycled NMC811 in baseline electrolyte; (e) TEM image and (f) XPS spectra of the cycled NMC811 in electrolyte containing TMSPa additive. Reprinted with permission from ref. 925 Copyright 2020 John Wiley & Sons, Inc.

electrolyte lead to the lower interfacial impedance, prevent the possible dissolution of the metals from the cathode materials, and defend the detrimental decomposition of EC solvents.^{883,885,928–930}

Novel silane-based additives are being intensively explored. Quite recently, Chen *et al.*⁸⁹⁷ and Deng *et al.*⁹⁰⁰ developed 3-isocyanatopropyltriethoxysilane (IPTS) and diphenyldimethoxysilane (DPDMS) for the Ni-rich cathodes, respectively. After adding mere 0.5% IPTS into the carbonate base electrolyte, both of the cycling and rate performances of Li||NMC622 half-cell were significantly improved, achieving 75.1% capacity retention after 150 cycles. Adding 1 wt% DPDMS boosts the capacity retention of Li||NMC622 to 93.3% after 200 cycles at 55 °C. The IPTS and DPDMS additives suppresses the decomposition of the electrolyte, effectively reduces the transition metal dissolution and facilitates the formation of a uniform and compact CEI film on the cathode. Li *et al.*⁹³⁶ and Yang *et al.*⁸⁸² proposed *N*-allyl-*N,N*-Bis(trimethylsilyl)amine (NNB) and *N,O*-bis(trimethylsilyl)acetamide (BSA) for NCA and NMC811 aggressive cathodes, significantly prompted the cycling stability of high-energy cells.

Sulfur-containing additives

Among the sulfur-containing additives, ethylene sulfate (or 1,3,2-dioxathiolane-2,2-dioxide, DTD), 1,3-propane sultone (PS),

prop-1-ene-1,3 sultone (PES) and ethylene sulfite (ES) are representative ones,^{937–948} which have been extensively utilized in commercialized electrolytes. These additives with the SO₂/SO₃/SO₄-groups can assist to form a compact SEI layer on the graphite anodes, reduce the parasitic reactions, suppress the gas evolution and therefore further improve the initial and cycling CE of the electrolytes.^{942,943,949–952} Some of these sulfur-containing additives can also be adopted as the cathode-film additives,^{149,885,951–955} in which the sulfur is beneficial for the Li ion conductivity in the CEI layer.^{938,955–958} The representative sulfur-containing additives effective to improve the anodic stability of the electrolytes are compiled in Fig. 39.

Sulfur-containing additives can be dated back to over 25 years ago. Besenhard *et al.*^{277,287} and Ein-Eli *et al.*⁸⁸⁵ revealed that some inorganic species, such as polysulfides and SO₂,^{296,959} could be utilized as additives to modify the SEI layers of the graphite and Li metal anodes. In 1999, Winter *et al.*^{960,961} successfully realized the Li intercalation into graphite anodes using PC electrolyte plus ES or PS as the film-forming additive, triggering the hot research on the sulfur-containing additives. Four years later, Ogawa and co-workers⁹⁶² from TDK Corporation patented a series of cyclic sulfates and sultones as additives for LIBs. Sano *et al.*⁹⁴² unveiled that the cyclic sulfates DTD and its

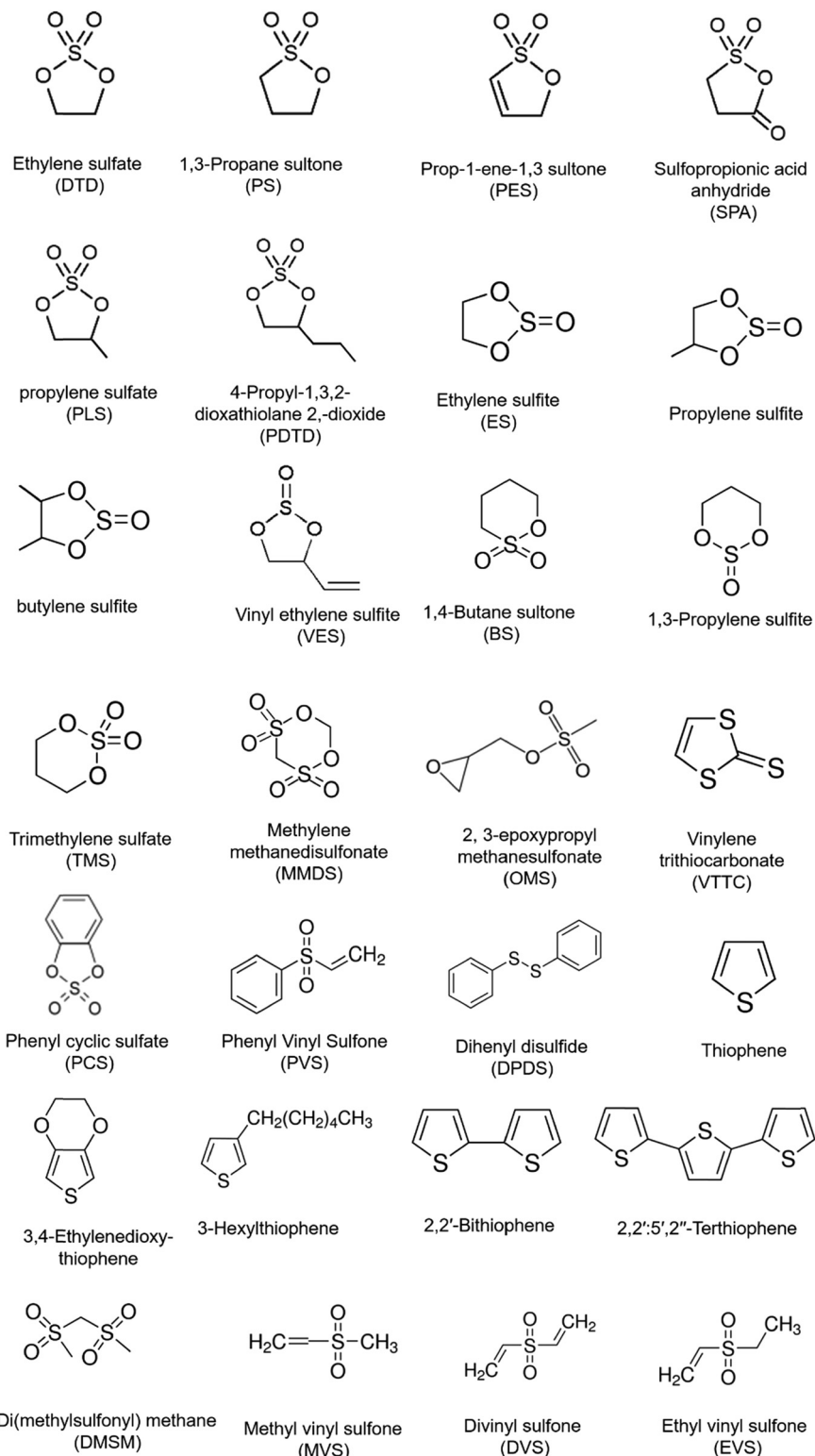


Fig. 39 Representative S-containing additives for high voltage Li batteries.

derivatives such as methyl-DTD (propylene sulfate), and ethyl-DTD (4-ethyl-1,3,2-dioxathiolane-2,2-dioxide), decomposed and formed a compact SEI layer at higher voltage than that of carbonate solvents, therefore sufficiently blocking the possible

solvent co-intercalation, and enabled the PC electrolyte for graphite anodes. Surprisingly, DTD not only enhances the SEI layers on the anodes, but also effectively modifies the cathode surfaces, which is counter-intuitive if considering the decomposition

potentials based on the CV tests^{942,950} and the HOMO/LUMO calculations.⁹⁴² This phenomenon arouses strong suspicion that the compact and thin CEI layers on the cathode in the sulfate-containing electrolyte are from the anode sides by cross-talking.^{951,963}

Dahn and co-workers^{957,958,964,965} systematically compared the cyclic sulfate additives (DTD, TMS, PLS, PS, MMDS, *etc.*) on the electrochemical performance of the graphite||NMC pouch cells. Among these additives, DTD, TMS and MMDS effectively decrease the cell impedance, improve Coulombic efficiency, and reduce the voltage drop during storage, while the PLS, even though with only an additional methyl group to DTD, is less effective, indicating that the branch groups seriously affect the electrochemical behaviors of these additives. Compared to DTD and TMS, another merit of MMDS is that when coupling with VC additive critically decimates the volume of generated gas during the formation step.⁹⁵⁷

Because of the impressive impact of DTD on both electrodes of the high energy LIBs, novel electrolyte additives with a similar structure to DTD are being explored. 4-Propyl-[1,3,2]dioxathiolane-2,2-dioxide (PDTD),^{953,954} and dihydro-1,3,2-dioxathio-[1,3,2]dioxathiole-2,2,5,5-tetraoxide (D-DTD)⁹⁵² are the representatives, both of which can form a thin and compact SEI/CEI layer on electrodes (Fig. 40a–d) with higher ionic conductivity compared to the well-known DTD additive, therefore exhibiting improved electrochemical performance

(Fig. 40e and f). The pouch cell with D-DTD delivers a superior capacity retention of >77% in the voltage range of 2.75–4.4 V at 45 °C, which is much higher than those of the cells with baseline (2.2%) or DTD-containing (14.7%) electrolytes (Fig. 40f). Moreover, the PDTD can complex with the Co ions dissolved in the electrolyte (Fig. 40g), exhibiting a much larger binding energy (1986.66 kJ mol⁻¹) than EC-Co³⁺ (1582.85 kJ mol⁻¹) and EMC-Co³⁺ (1623.37 kJ mol⁻¹), which effectively mitigates the Co³⁺ reduction on the anode.

A significant feature that needs to be mentioned for these sulfites, sulfates and sultones is the good coupling to the VC additive, which can provide much better performance than either additive independently.^{943,964,966} For example, the graphite||NMC cell with 1–2% ES + 2% VC shows similar performance in the UHPC test to the cell containing 2% VC but virtually quenches the gas generation during formation and cycling. More importantly, the combination of VC and ES reduces the cell impedance by over 50% after cycling, and dramatically enhances the rate performance and low temperature behaviors.⁹⁶⁶ Compared to 2% VC alone, the combination of MMDS with 2% VC critically enhances the charge end-point capacity slippage rate and Coulombic efficiency, lowers the cycling charge transfer resistance, and significantly mitigates the voltage decay during storage.⁹⁶⁵ The *in situ* formed Li sulfonates such as RSO₃Li and Li₂SO₃ improve the Li⁺ conductivity of the interphases,^{941,967} and therefore sufficiently offset

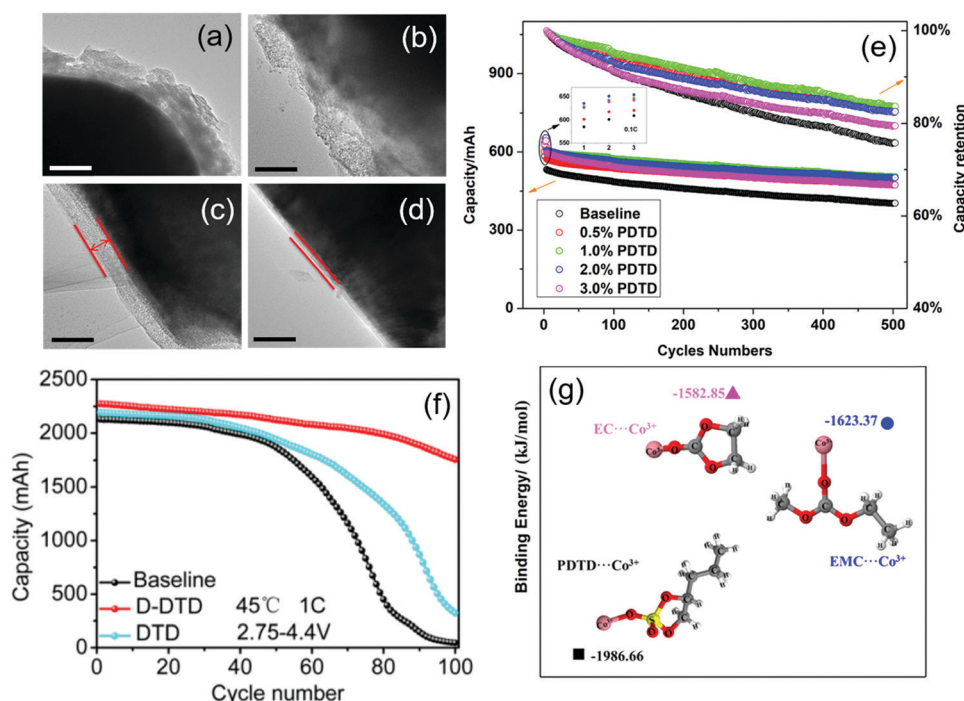


Fig. 40 TEM images of the NMC622 in (a) baseline electrolyte 1 M LiPF₆ EC/EMC (1 : 2, by weight) and (b) PDTD containing electrolyte, and graphite in baseline (c) and PDTD containing (d) electrolyte after undergoing 500 cycles. The scale bar in figure a–d is 100 nm. (e) Cycling performance of the graphite||NMC532 cells in different electrolytes at room temperature. (f) Cycling performance of the graphite||NMC532 cells in baseline, D-DTD and DTD containing electrolytes at 45 °C in the working voltage range of 2.75–4.4 V. (g) Optimized complex structures and the binding energy between Co³⁺ and EC, EMC, or PDTD molecules. (a–e) Reprinted with permission from ref. 954 Copyright 2018 American Chemical Society. (f) Reprinted with permission from ref. 952 Copyright 2020 Elsevier. (g) Reprinted with permission from ref. 953 Copyright 2018 American Chemical Society.

the low conductivity of the VC dominated SEI/CEI layers. The superposition of the electrochemical performance from additive combinations is a promising direction for further stabilizing the interphases and is now being implemented in the battery industry.

In 2014, Wagner and co-workers⁹⁶⁸ reported that the vinyl sulfones could be utilized as an impressive SEI-formation enabler in the PC electrolytes, which highly improved the reversibility of the Li||graphite half cells and graphite||NMC full cells with only 2–5% addition. Yim *et al.*⁹⁶⁹ investigated the reaction mechanism of divinyl sulfone (DVS) additive on the CEI stability of the Ni-rich cathodes. The vinyl groups in the DVS can form a cross-linked CEI layer on the cathode surface, while the sulfone groups consist of the main components of the CEI film, critically enhancing the CEI stability of the Ni-rich cathode. The cell with NCM721 as a cathode controlled with 2% DVS as electrolyte additive possesses a remarkably improved cycling performance with ~92% capacity retention at a high temperature of 60 °C after 100 cycles. In contrast, the cell in the baseline electrolyte provides only ~71% remaining capacity compared to its first cycle. Almost at the same time, Li *et al.*⁹⁷⁰ developed a novel sulfone additive of phenyl vinyl sulfone (PVS), in which the C=C bond promises preferential oxidizability, the aromatic ring guarantees the good chemical stability of the *in situ* formed CEI film,^{971,972} and the sulfur prompts the ionic conductivity. These synergetic features from three functional groups translate into a highly effective promotion of the electrochemical performance for the high voltage cathodes (Fig. 41). Testing as the electrolyte additive with only 1 wt% in a 1 M LiPF₆ EC/EMC/DEC electrolyte, LR-NMC delivers a reversible capacity of 166 mA h g⁻¹ with a capacity retention of 80% after 240 cycles (Fig. 41a), representing one of the most effective electrolyte additives for the Li-rich cathodes. It is believed that the *in situ* formed uniform CEI layers on the LR-NMC cathodes (Fig. 41b, c and d) suppress the continuous electrolyte oxidation and inhibit the transition metal dissolution.

Besides these sulfone or sulfate additives, thiophene derivatives and phenyl disulfide were also proposed as good high-voltage electrolyte additives.^{973–982} At high-voltage, the thiophene derivatives tend to be polymerized on the cathode surface prior to the oxidation of the electrolyte solvents, which can suppress the side reactions between the electrolytes and the catalytic cathode surface and improve the cycling performance of the cathodes. Using the spin coating method, Chae *et al.*⁹⁸⁰ prepared poly(3-alkylthiophene) (P3HT)-modified NMC811 and tested the electrochemical performance. After the 50th cycle, the capacity retention was improved from 84% to >91% after coating with P3HT. The XPS results demonstrated that after coating P3HT, the electrolyte decomposition on the NMC811 was considerably suppressed with the critically lower peak intensity of P and F species.

To maximize the electrochemical performances, any changes in the cell components call for specified additive recipes to be catered to. The DTD additive has been extensively utilized to enhance the electrochemical performance in

graphite||NMC cells, while it seems less effective in graphite||LCO pouch cells.⁹⁸³ TMS and DTD additives increase the impedance of graphite||LCO cells during cycling, but they decrease the impedance in graphite||NMC cells.⁹⁸³ Even for the same cells, different additive combinations should be tactically designed if working conditions and/or charge-discharge protocols vary.⁹⁸⁴

The best additive should possess the following characteristics: (i) it should decompose before the carbonate skeleton components to passivate the electrodes; (ii) it should suppress the gas generation; (iii) the derived SEI/CEI should be thin and compact with low resistance; (iv) the derived SEI/CEI should sustain the higher voltage and the larger volume change of the electrodes. However, up to now, no solo additive could meet all of these harsh requirements. Therefore, recipes of diversified additives are becoming the mainstream to satisfy the high-voltage aggressive conditions and requirements.⁹⁸⁵ Even in a single additive, different functional groups are generally contained,^{888,969} which induces different radicals, species, and ingredients for the interphases. For example, as demonstrated in TMSPI additive, P,Si-containing species, and P,F-rich species will be generated during the oxidation process on the delithiated cathodes, resulting in the compact CEI formation.⁸⁹⁹ To evaluate the effectiveness of the additive combinations for the high-energy pouch cells, Dahn and co-workers⁹¹¹ screened over 110 additive sets and introduced a “Figure of Merit” parameter, including the Coulombic efficiency, charge endpoint capacity slippage and voltage drop during storage, electrochemical impedance, gas evolution, *etc.* Based on the “Figure of Merit”, they developed a series of additive blends for different cell systems, for example, 2% VC + 1% DTD and 2% FEC + 1% DTD for the single crystal artificial graphite||NMC532 cells,⁹⁸⁴ 2% VC + 0.3% TMOBX for graphite||LCO cells,⁹⁸⁶ and 2% PES + 1% TTSPi + 1% MMDS (PES211) for high-voltage graphite||NMC pouch cells.^{333,987,988} Cui *et al.*⁹⁸⁹ also confirmed the effectiveness of 1% TMSPI + 1% PCS for 5.0 V graphite||LNMO cells. These diversified additive recipes constitute the best additives for the targeted high-energy battery systems.

7. Electrolyte design principles and perspective

Since the EC-based electrolyte commercialization in the 1990s, LIBs have dominated the energy storage for portable electronics for almost 30 years and for EVs for 10 years thanks to the ideal coupling of the EC-based electrolyte and graphite anodes. In the forthcoming years, the global LIBs market is expected to grow from USD 90 billion in 2020 to over USD 150 billion by 2025 with a high compound annual growth rate (CAGR) of >10%. This review systematically highlighted several promising opportunities offered by the high voltage electrolyte chemistries to further boost up energy densities for next generation batteries. Breakthroughs in chemistries have been achieved to tackle the relatively narrow voltage window of the conventional EC-based electrolytes, such as EC-free electrolytes, solvent-in-salt electrolytes, and electrolytes with multifunctional additives. These high

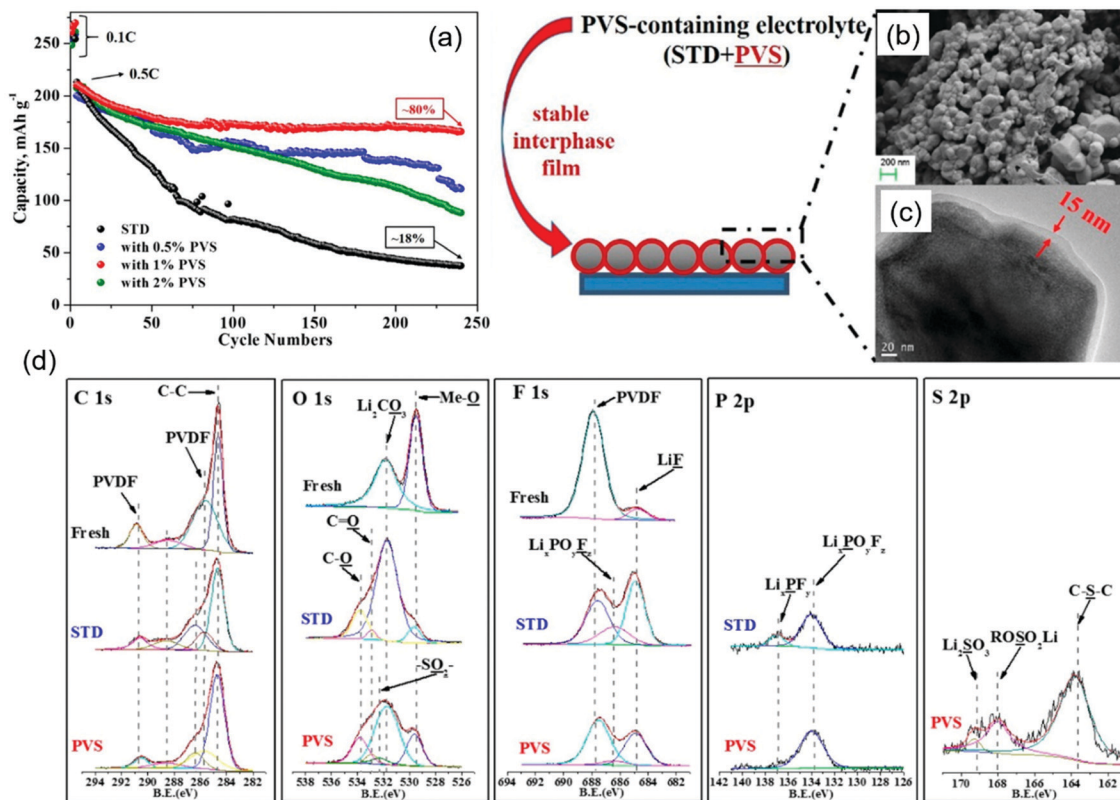


Fig. 41 (a) Cycling performance of the $\text{Li}_{1.2}\text{Mn}_{0.54}\text{Ni}_{0.13}\text{Co}_{0.13}\text{O}_2$ cathode in 1 M LiPF_6 EC/EMC/DEC electrolyte (STD) with different contents of PVS additives. SEM (b) and TEM (c) images of the cathode cycled in 1 M LiPF_6 EC/EMC/DEC containing 1% PVS additive. (d) XPS spectra of the fresh $\text{Li}_{1.2}\text{Mn}_{0.54}\text{Ni}_{0.13}\text{Co}_{0.13}\text{O}_2$, $\text{Li}_{1.2}\text{Mn}_{0.54}\text{Ni}_{0.13}\text{Co}_{0.13}\text{O}_2$ cycled in 1 M LiPF_6 EC/EMC/DEC electrolyte (STD) and in 1 M LiPF_6 EC/EMC/DEC electrolyte containing 1% PVS additive. Reprinted with permission from ref. 970 Copyright 2016 American Chemical Society.

voltage electrolytes with special design and multiple functionalities have successfully proven their great potential in expanding the working potential range for Li batteries, and therefore would critically increase the energy density and energy quality.

To achieve high-energy density, high-energy cathodes (NMC811, Li-rich NMC, *etc.*) and high capacity anodes (Li metal, Si anode, *etc.*) with large volume change are entering into the arena of Li batteries, which is different from conventional electrodes (LCO, graphite) with less volume changes. EC-based electrolytes enable the micro-sized graphite anodes to form an organic-inorganic composite SEI due to the simultaneous reduction of LiPF_6 and EC-based carbonate solvents at ~ 0.8 V vs. Li/Li^+ , which strongly bonds graphite anodes and is strong enough to accommodate 12% volume change of graphite during lithiation/delithiation without breaking. Meanwhile, the EC-based electrolytes could support a 4.3 V cathode with small volume changes, which ensures commercial LIBs a high CE of $>99.9\%$ and cycle life of >1000 . Si and Li metal anodes have more than 10 times higher capacity than state-of-the-art graphite anodes with a volume change of $>300\%$ and essential infinity, respectively. The Si microparticle (SiMP) anode can only survive for <20 cycles in EC-based electrolytes, because the *in situ* formed organic-inorganic SEI and SiMPs cannot sustain such a high volume change and will crack during lithiation/delithiation cycles (Fig. 42a). Li metal anodes

also decay fast with a low cycling CE of only $<90\%$ in EC-based electrolytes. To reduce the deformation of the SEI layer, the SEI layer should have a low affinity to the Si/Li anodes, so that the lithiated Si or the deposited Li can slip at the interface during volume change without damaging the SEI (Fig. 42b). Among the known components in SEI, LiF possesses the highest interfacial energy against Li_xSi or Li metal, suggesting that Li_xSi or Li metal can slip easily without damaging the LiF SEI shell as the volume changes. In addition, the wide bandgap and high electronic blocking effect of LiF (Fig. 42c) significantly reduces the thickness of the LiF-rich SEI (Fig. 42d and e). Moreover, the high shear modulus of LiF creates a robust shell that can suppress the anode pulverization. Since LiF has a wide electrochemical stability window of 6.5 V, the LiF-rich CEI with thickness of ~ 5 nm could effectively protect the high energy cathodes (Fig. 42f and g).^{281,319} As discussed earlier, a LiF-rich SEI/CEI can be formed in solvent-in-salt electrolytes, localized concentrated electrolytes, fluorinated electrolytes *etc.* By using a highly stable solvent, LiF-rich SEI or CEI can also be obtained due to the suppression of the solvent reduction.²⁵⁰ Therefore, besides basic functions, novel electrolytes designed for high voltage and high energy batteries should follow these two critical principles: (1) the *in situ* formed SEI should have a highest interfacial energy to high capacity anodes, which can minimize the SEI damage during lithiation/delithiation cycles;

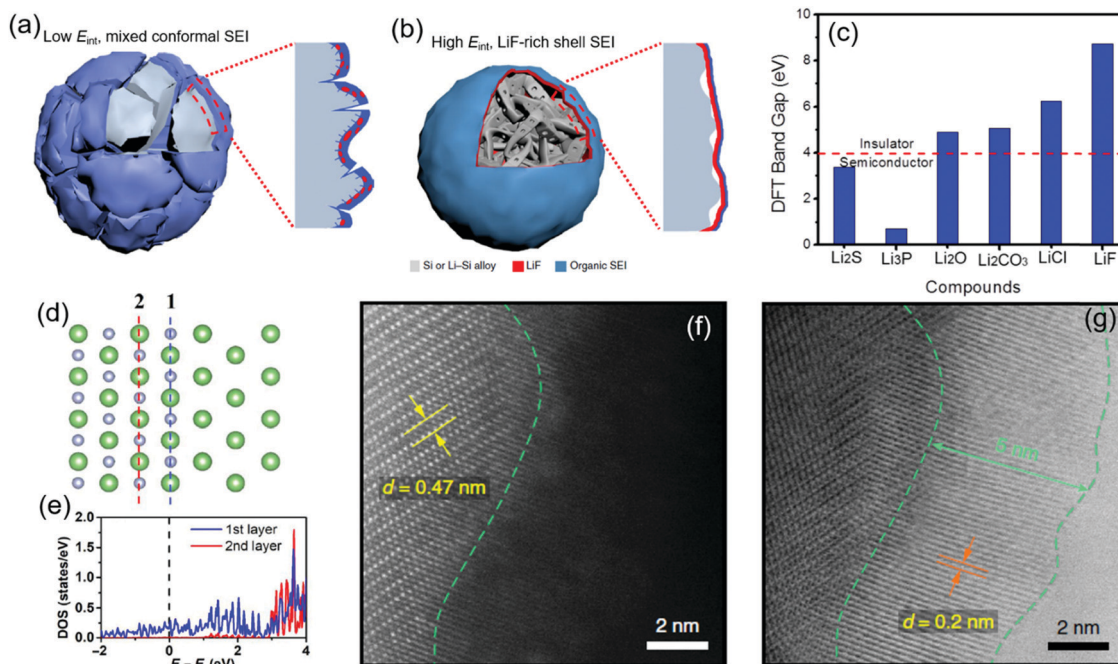


Fig. 42 Schematic illustration of the cycled alloy anode with an organic–inorganic non-uniform SEI layer with low interfacial energy (E_{int}) (a) and an inorganic, uniform SEI layer with high interfacial energy (b). (c) Comparison of the bandgaps for inorganic components in SEI layers. Li/LiF interfaces (d) and its corresponding density of state (DOS) by atomic layer with the Fermi level at 0 eV (e). HAADF-STEM (f) and ABF-STEM (g) images for the NMC811 cycled in 1 M LiFSI DME/TFEO (1.2 : 3 by mole). (a and b) Reprinted with permission from ref. 250 Copyright 2020 Springer Nature. (c–e) Reprinted with permission from ref. 276 Copyright 2018, American Association for the Advancement of Science. (f and g) Reprinted with permission from ref. 319 Copyright 2019 Springer Nature.

(2) the *in situ* formed SEI/CEI should have a lowest electronic conductivity, which can minimize the side reactions between the electrolyte and electrodes.

Besides the high electrochemical performance, the cost of electrolyte systems should be comparable to the commercial electrolyte systems. For the higher voltage LIBs, the carbonate electrolyte with diversified additive recipes can achieve a balanced cost and the electrochemical enhancement, therefore, would dominate the LIB electrolyte market in the near future. The carbonate skeleton with VC + DTD,⁹⁸⁴ FEC + DTD,⁹⁸⁴ LiPO₂F₂ + FEC,⁷⁷⁰ PES + MMDS + TTSPi⁹¹² additive combinations are promising for the graphite||NMC cells. While the fluorinated electrolytes, concentrated non-aqueous electrolytes and localized high-concentrated electrolytes may be first commercialized in the high-energy Li metal batteries. The profitable academic exploration for the novel electrolyte components stimulated the flourishing electrolyte industry. For example, in the past five years, the market supply of LiFSI salt has increased from less than 500 t per a to over 10 000 t per a, and meanwhile the price has been decimated.

Despite these exciting progresses in the high-voltage electrolytes, some scientific and engineering challenges remain in some systems in the perspective of physical and chemical nature, compatibility, and balances, which should be the critical topics for future research:

(1) Up to now, the high voltage electrolyte blends are far from meeting the requirements of “smart” feature or “precise”

design. Almost all of the electrolyte blends or additive blends were explored by trial and error. During these trials, features of anodes and cathodes have to be considered, such as the surface state of the electrodes, compositions and phases of the electrodes, cut-off voltage, *etc.* Any advances of the anodes and cathodes would incur novel electrolytes to maximize the electrochemical performance. Therefore, the development of electrolytes always lags behind the development of electrodes and has been the bottleneck for the next-generation high-energy Li batteries. To shorten the development period of the suitable electrolytes, big databases or AI⁹⁹⁰ might be one of the possible solutions.

(2) *Post-mortem*, *in situ* and *operando* analysis are needed to probe the interfacial reactions between the electrolytes and the electrodes and couple the electrochemical performance on half-cells and on full-cells. Besides, models with powerful predictive capability on the interactions between the electrolytes and electrodes should be developed, which would deepen the understanding of interphases and the electrochemistries, and guide the exploration of new electrolytes.

(3) Some environmental and safety issues should be considered in the development of next generation electrolytes. For example, PS as an effective additive for the high-voltage electrolyte has been listed as a very high concern substance for authorization due to the high carcinogenic properties since 2015 by REACH.

(4) With the significant advances of highly conductive solid state electrolytes (SSEs) in recent years, the development of

high-voltage liquid or polymer electrolytes will be facing competition from the SSEs. Considering the fact that none electrolytes are thermodynamically stable to the Li metal anodes, all of the SSEs and liquid/polymer electrolytes face the interface issues in the battery. Only electrolytes with *in situ* formed passivation layers that could be self-healed can promise the superior electrochemical performance.

(5) As the EV advances, the battery electrolytes must satisfy four requirements: high voltage, 5C fast charging, wide operation temperature range of $-30\text{ }^{\circ}\text{C}$ to $+60\text{ }^{\circ}\text{C}$ and less-flammability. Since higher energy is stored in the limited battery space, safety issues are becoming more prominent. Therefore, novel electrolytes in the EV batteries should be with improved safety, wider working temperature and voltage range and better rate capability.

With astonishing advances of cutting-edge characterization techniques, novel theoretical calculation tools, and impressive novel electrolyte systems, we believe that, all of the as-mentioned issues could be resolved eventually. The combination of the significant improvement of the electrochemical performance for the high-voltage electrolytes and the urgent cost-driven development of the Li batteries could turn these promising electrolytes into viable next-generation high-energy Li batteries.

Abbreviations

EC	Ethylene carbonate
PC	Propylene carbonate
DMC	Dimethyl carbonate
DEC	Diethyl carbonate
EMC	Ethyl methyl carbonate
FEC	Fluoroethylene carbonate
DFEC	(4 <i>R</i> ,5 <i>S</i>)-4,5-Difluoro-1,3-dioxolan-2-one
VC	Vinylene carbonate
VEC	Vinyl ethylene carbonate
MEC	Methylene-ethylene carbonate
FEMC	3,3,3-Fluoroethylmethyl carbonate
BC	Butylene carbonate
CC	Catechol carbonate
PES	Prop-1-ene-1,3-sultone
SA	Succinic anhydride
PPF	Pyridine phosphorus pentafluoride
CEI	Cathode electrolyte interphase
SEI	Solid electrolyte interphase
LCO	LiCoO ₂
NMC	Lithium nickel manganese cobalt oxide (LiNi _x Mn _y Co _{1-x-y} O ₂)
NCA	LiNi _{0.8} Co _{0.15} Al _{0.05} O ₂
LNMO	LiNi _{0.5} Mn _{1.5} O ₄
LCMO	LiCoMnO ₄
LFP	LiFePO ₄
LCPO	LiCoPO ₄
LNPO	LiNiPO ₄
LCPOF	Li ₂ CoPO ₄ F
LSV	Linear-sweep voltammetry

LUMO	Lowest unoccupied molecular orbital
HOMO	Highest occupied molecular orbital
DME	1,2-Dimethoxyethane
DOL	1,3-Dioxolane
THF	Tetrahydrofuran
BTFE	Bis(2,2,2-trifluoroethyl)ether
HFPMP	1,1,1,3,3,3-Hexafluoroisopropyl methyl ether
PEO	Polyethylene oxides
TEGDME	Tetraethylene glycol dimethyl ether
LiDFOB	Lithium difluoro(oxalato)borate
LiTFOP	Lithium tetrafluoro(oxalato)phosphate
LiDFBP	Lithium difluoro(bisoxalato)phosphate
TMB-1	Trimethyl borate
TMB-2	Trimethylboroxine
LiTMB	Lithium tetramethyl borate
TTSPi	Tris-(trimethyl-silyl)-phosphite
PBF	Pyridine-boron trifluoride
BTM	Bis(trimethyl)malonate
IPTS	3-Isocyanatopropyltriethoxysilane
DPDMS	Diphenyldimethoxysilane
DTD	Ethylene sulfate or 1,3,2-dioxathiolane-2,2-dioxide
PDTD	4-Propyl-[1,3,2]dioxathiolane-2,2-dioxide
D-DTD	Dihydro-1,3,2-dioxathiole-[1,3,2]dioxathiole-2,2,5,5-tetraoxide
PVS	Phenyl vinyl sulfone
DVS	Divinyl sulfone
P3HT	Poly(3-alkylthiophene)
PTCDI	3,4,9,10-Perylenetetracarboxylic diimide
PTSI	<i>p</i> -Toluenesulfonyl isocyanate
VTTC	Vinylene trithiocarbonate
AAN	Acrylic acid nitrile
AEC	Allyl ethyl carbonate
AMC	Allyl methyl carbonate
VA	Vinyl acetate
ADV	Divinyl adipate
HFCp	3,3,4,4,5,5-Hexafluorocyclopent-1-ene
TAC	Triallyl cyanurate
TAIC	Triallyl isocyanurate
ABAPE	Allylboronic acid pinacol ester
FEMC	Methyl (2,2,2-trifluoroethyl) carbonate
ETFB	Ethyl 4,4,4-trifluorobutyrate
TFPC	Trifluoro-propylene carbonate
HFIP	Tris(hexafluoro-iso-propyl)phosphate
TPP	Tripropargyl phosphate
TPFPP	Tris(pentafluorophenyl)phosphine
DEPP	Diethyl phenylphosphonite
TFTPN	Tetrafluoroterephthalonitrile
4-TB	4-(Trifluoromethyl)-benzonitrile
SN	Succinonitrile
PN	Pimelonitrile
FN	Fumaronitrile
HTN	1,3,6-Hexanetricarbonitrile
PTN	1,3,5-Pentanetricarbonitrile
EDPN	3,3'-(Ethylenedioxy)dipropiononitrile
OMCTS	Octamethylcyclotetrasiloxane

ViD4	2,4,6,8-Tetramethyl-2,4,6,8-tetravinylcyclotetra-siloxane
SL	Sulfone
EMES	Ethyl methoxyethyl sulfone
EMS	Ethylmethyl sulfone
TMS	Tetramethylene sulfone
EA	Ethyl acetate
SN	Succinonitrile
ES	Ethylene sulfite
PS	1,3-Propane sultone
PES	Prop-1-ene-1,3-sultone
MMDS	Methylene methanedisulfonate
DTD	1,3,2-Dioxathiolane-2,2-dioxide
TMSPi	Tris(trimethylsilyl)phosphite
TMSPa	Tris(trimethylsilyl)phosphate
HFIP	Tris(hexafluoroisopropyl)phosphate
TMSB	Tris(trimethylsilyl) borate
PTSI	<i>p</i> -Toluenesulfonyl isocyanate.
CE	Coulombic efficiency
OCV	Open circuit voltage
CDs	Contact dimers
CIPs	Contact ion pairs
AGGs	Aggregates clusters
DFT	Density functional theory
MD	Molecule dynamic
QC	Quantum chemistry
HER	Hydrogen evolution reaction
OER	Oxygen evolution reaction
TOF-SIMS	Time-of-flight secondary ion mass spectrometry
sXAS	Soft-X-ray absorption spectra
OEMS	Online electrochemical mass spectrometry
AIMD	<i>Ab initio</i> molecular dynamics
B3LYP	Becke, 3-parameter, Lee–Yang–Parr
PBE	Perdew–Burke–Ernzerhof
MP2	Moller–Plesset perturbation theory to the second order
SMD	Solvation model based on density
PCM	Polarizable continuum model
IPCM	Isodensity polarizable continuum model
LSV	Linear sweep voltammetry
CE	Coulombic efficiency
CHPC	Ultra-high precision coulometry
SERS	Surface-enhanced Raman spectroscopy
CAGR	Compound annual growth rate
REACH	Registration, evaluation and authorization of chemicals

Conflicts of interest

There are no conflicts to declare.

Acknowledgements

This work was supported by the National Natural Science Foundation of China (22072134), the Natural Science

Foundation of Zhejiang Province (LZ21B030002), the Fundamental Research Funds for the Zhejiang Provincial Universities (2021XZZX010), the Fundamental Research Funds for the Central Universities (2021FZZX001-09), and “Hundred Talents Program” of Zhejiang University.

References

- 1 A. Yoshino, *Angew. Chem., Int. Ed.*, 2012, **51**, 5798–5800.
- 2 V. Etacheri, R. Marom, R. Elazari, G. Salitra and D. Aurbach, *Energy Environ. Sci.*, 2011, **4**, 3243–3262.
- 3 K. Xu, *Chem. Rev.*, 2014, **114**, 11503–11618.
- 4 M. Moshkovich, M. Cojocar, H. E. Gottlieb and D. Aurbach, *J. Electroanal. Chem.*, 2001, **497**, 84–96.
- 5 K. Kanamura, *J. Power Sources*, 1999, **81–82**, 123–129.
- 6 X. Mu, H. Pan, P. He and H. Zhou, *Adv. Mater.*, 2020, **32**, 1903790.
- 7 X.-Q. Zhang, X.-B. Cheng, X. Chen, C. Yan and Q. Zhang, *Adv. Funct. Mater.*, 2017, **27**, 1605989.
- 8 J. B. Goodenough and Y. Kim, *J. Power Sources*, 2011, **196**, 6688–6694.
- 9 T. Placke, R. Kloepsch, S. Dühnen and M. Winter, *J. Solid State Electrochem.*, 2017, **21**, 1939–1964.
- 10 J.-L. Shi, D.-D. Xiao, M. Ge, X. Yu, Y. Chu, X. Huang, X.-D. Zhang, Y.-X. Yin, X.-Q. Yang, Y.-G. Guo, L. Gu and L.-J. Wan, *Adv. Mater.*, 2018, **30**, 1705575.
- 11 J. Zheng, S. Myeong, W. Cho, P. Yan, J. Xiao, C. Wang, J. Cho and J.-G. Zhang, *Adv. Energy Mater.*, 2017, **7**, 1601284.
- 12 G. Assat and J.-M. Tarascon, *Nat. Energy*, 2018, **3**, 373–386.
- 13 W. Li, B. Song and A. Manthiram, *Chem. Soc. Rev.*, 2017, **46**, 3006–3059.
- 14 J. Kim, H. Lee, H. Cha, M. Yoon, M. Park and J. Cho, *Adv. Energy Mater.*, 2018, **8**, 1702028.
- 15 Z. Lu, D. D. MacNeil and J. R. Dahn, *Electrochem. Solid-State Lett.*, 2001, **4**, A191–A194.
- 16 Z. Lu and J. R. Dahn, *J. Electrochem. Soc.*, 2002, **149**, A815–A822.
- 17 J.-S. Kim, C. S. Johnson, J. T. Vaughey, M. M. Thackeray, S. A. Hackney, W. Yoon and C. P. Grey, *Chem. Mater.*, 2004, **16**, 1996–2006.
- 18 E. Hu, X. Yu, R. Lin, X. Bi, J. Lu, S. Bak, K.-W. Nam, H. L. Xin, C. Jaye, D. A. Fischer, K. Amine and X.-Q. Yang, *Nat. Energy*, 2018, **3**, 690–698.
- 19 M. M. Thackeray, S.-H. Kang, C. S. Johnson, J. T. Vaughey, R. Benedek and S. A. Hackney, *J. Mater. Chem.*, 2007, **17**, 3112–3125.
- 20 N. Yabuuchi, K. Yoshii, S.-T. Myung, I. Nakai and S. Komaba, *J. Am. Chem. Soc.*, 2011, **133**, 4404–4419.
- 21 P. Rozier and J. M. Tarascon, *J. Electrochem. Soc.*, 2015, **162**, A2490–A2499.
- 22 P. K. Nayak, E. M. Erickson, F. Schipper, T. R. Penki, N. Munichandraiah, P. Adelhelm, H. Sclar, F. Amalraj, B. Markovsky and D. Aurbach, *Adv. Energy Mater.*, 2018, **8**, 1702397.

- 23 J.-H. Kim, N. P. W. Pieczonka and L. Yang, *Chem. Phys. Chem.*, 2014, **15**, 1940–1954.
- 24 W. Li, E. M. Erickson and A. Manthiram, *Nat. Energy*, 2020, **5**, 26–34.
- 25 M. Hu, X. Pang and Z. Zhou, *J. Power Sources*, 2013, **237**, 229–242.
- 26 B. Xu, D. Qian, Z. Wang and Y. S. Meng, *Mater. Sci. Eng., R*, 2012, **73**, 51–65.
- 27 A. Manthiram, J. C. Knight, S.-T. Myung, S.-M. Oh and Y.-K. Sun, *Adv. Energy Mater.*, 2016, **6**, 1501010.
- 28 M. S. Whittingham, *Chem. Rev.*, 2014, **114**, 11414–11443.
- 29 A. Kraysberg and Y. Ein-Eli, *Adv. Energy Mater.*, 2012, **2**, 922–939.
- 30 S.-T. Myung, F. Maglia, K.-J. Park, C. S. Yoon, P. Lamp, S.-J. Kim and Y.-K. Sun, *ACS Energy Lett.*, 2017, **2**, 196–223.
- 31 E. Markevich, G. Salitra, Y. Talyosef, U.-H. Kim, H.-H. Ryu, Y.-K. Sun and D. Aurbach, *ACS Appl. Energy Mater.*, 2018, **1**, 2600–2607.
- 32 D. Aurbach, K. Gamolsky, B. Markovsky, G. Salitra, Y. Gofer, U. Heider, R. Oesten and M. Schmidt, *J. Electrochem. Soc.*, 2000, **147**, 1322–1331.
- 33 D. Aurbach, *J. Power Sources*, 2000, **89**, 206–218.
- 34 F. Schipper, E. M. Erickson, C. Erk, J.-Y. Shin, F. F. Chesneau and D. Aurbach, *J. Electrochem. Soc.*, 2016, **164**, A6220–A6228.
- 35 M. He, C.-C. Su, Z. Feng, L. Zeng, T. Wu, M. J. Bedzyk, P. Fenter, Y. Wang and Z. Zhang, *Adv. Energy Mater.*, 2017, **7**, 1700109.
- 36 X. Xu, S. Deng, H. Wang, J. Liu and H. Yan, *Nano-Micro Lett.*, 2017, **9**, 22.
- 37 R. Santhanam and B. Rambabu, *J. Power Sources*, 2010, **195**, 5442–5451.
- 38 K. Amine, H. Tukamoto, H. Yasuda and Y. Fujita, *J. Power Sources*, 1997, **68**, 604–608.
- 39 Q. Zhong, A. Bonakdarpour, M. Zhang, Y. Gao and J. R. Dahn, *J. Electrochem. Soc.*, 1997, **144**, 205–213.
- 40 T. Ohzuku, S. Takeda and M. Iwanaga, *J. Power Sources*, 1999, **81–82**, 90–94.
- 41 J. H. Kim, S. T. Myung, C. S. Yoon, S. G. Kang and Y. K. Sun, *Chem. Mater.*, 2004, **16**, 906–914.
- 42 G. T. K. Fey, W. Li and J. R. Dahn, *J. Electrochem. Soc.*, 1994, **141**, 2279–2282.
- 43 G. T.-k. Fey and W.-b. Perng, *Mater. Chem. Phys.*, 1997, **47**, 279–282.
- 44 S. Chitra, P. Kalyani, B. Yebka, T. Mohan, E. Haro-Poniatowski, R. Gangadharan and C. Julien, *Mater. Chem. Phys.*, 2000, **65**, 32–37.
- 45 K. Amine, H. Yasuda and M. Yamachi, *Electrochem. Solid-State Lett.*, 2000, **3**, 178–179.
- 46 J. Wolfenstine and J. Allen, *J. Power Sources*, 2004, **136**, 150–153.
- 47 F. Wang, J. Yang, Y. NuLi and J. Wang, *J. Power Sources*, 2010, **195**, 6884–6887.
- 48 R. Sharabi, E. Markevich, V. Borgel, G. Salitra, D. Aurbach, G. Semrau, M. A. Schmidt, N. Schall and C. Stinner, *Electrochem. Commun.*, 2011, **13**, 800–802.
- 49 D. Di Lecce, J. Manzi, F. M. Vitucci, A. De Bonis, S. Panero and S. Brutti, *Electrochim. Acta*, 2015, **185**, 17–27.
- 50 N. N. Bramnik, K. Nikolowski, C. Baehtz, K. G. Bramnik and H. Ehrenberg, *Chem. Mater.*, 2007, **19**, 908–915.
- 51 N. N. Bramnik, K. G. Bramnik, T. Buhrmester, C. Baehtz, H. Ehrenberg and H. Fuess, *J. Solid State Electrochem.*, 2004, **8**, 558–564.
- 52 J. M. Lloris, C. Pérez Vicente and J. L. Tirado, *Electrochem. Solid-State Lett.*, 2002, **5**, A234.
- 53 S. Okada, S. Sawa, M. Egashira, J.-i. Yamaki, M. Tabuchi, H. Kageyama, T. Konishi and A. Yoshino, *J. Power Sources*, 2001, **97–98**, 430–432.
- 54 P. Deniard, A. M. Dulac, X. Rocquefelte, V. Grigorova, O. Lebacqz, A. Pasturel and S. Jobic, *J. Phys. Chem. Solids*, 2004, **65**, 229–233.
- 55 F. Zhou, M. Cococcioni, K. Kang and G. Ceder, *Electrochem. Commun.*, 2004, **6**, 1144–1148.
- 56 J. Wolfenstine and J. Allen, *J. Power Sources*, 2005, **142**, 389–390.
- 57 T. Muraliganth and A. Manthiram, *J. Phys. Chem. C*, 2010, **114**, 15530–15540.
- 58 A. Mauger, C. M. Julien, M. Armand, J. B. Goodenough and K. Zaghib, *Curr. Opin. Electrochem.*, 2017, **6**, 63–69.
- 59 H. Kawai, M. Nagata, H. Tukamoto and A. R. Westa, *Electrochem. Solid-State Lett.*, 1998, **1**, 212–214.
- 60 C. Dräger, F. Sigel, S. Indris, D. Mikhailova, L. Pfaffmann, M. Knapp and H. Ehrenberg, *J. Power Sources*, 2017, **371**, 55–64.
- 61 A. Windmüller, C. A. Bridges, C.-L. Tsai, S. Lobe, C. Dellen, G. M. Veith, M. Finsterbusch, S. Uhlenbruck and O. Guillon, *ACS Appl. Energy Mater.*, 2018, **1**, 715–724.
- 62 L. Chen, X. Fan, E. Hu, X. Ji, J. Chen, S. Hou, T. Deng, J. Li, D. Su, X. Yang and C. Wang, *Chem*, 2019, **5**, 896–912.
- 63 S. Okada, M. Ueno, Y. Uebou and J.-i. Yamaki, *J. Power Sources*, 2005, **146**, 565–569.
- 64 N. R. Khasanova, A. N. Gavrilov, E. V. Antipov, K. G. Bramnik and H. Hübner, *J. Power Sources*, 2011, **196**, 355–360.
- 65 D. Wang, J. Xiao, W. Xu, Z. Nie, C. Wang, G. Graff and J.-G. Zhang, *J. Power Sources*, 2011, **196**, 2241–2245.
- 66 X. Wu, Z. Gong, S. Tan and Y. Yang, *J. Power Sources*, 2012, **220**, 122–129.
- 67 S. S. Fedotov, A. A. Kabanov, N. A. Kabanova, V. A. Blatov, A. Zhugayevych, A. M. Abakumov, N. R. Khasanova and E. V. Antipov, *J. Phys. Chem. C*, 2017, **121**, 3194–3202.
- 68 J.-T. Hu and J.-G. Zhang, *Chin. J. Struct. Chem.*, 2019, **38**, 2005–2008.
- 69 S. S. Zhang, *Energy Storage Mater.*, 2020, **24**, 247–254.
- 70 R. Hausbrand, G. Cherkashinin, H. Ehrenberg, M. Gröting, K. Albe, C. Hess and W. Jaegermann, *Mater. Sci. Eng., B*, 2015, **192**, 3–25.
- 71 A. Tornheim, S. Sharifi-Asl, J. C. Garcia, J. Bareño, H. Iddir, R. Shahbazian-Yassar and Z. Zhang, *Nano Energy*, 2019, **55**, 216–225.
- 72 J. Li, H. Liu, J. Xia, A. R. Cameron, M. Nie, G. A. Botton and J. R. Dahn, *J. Electrochem. Soc.*, 2017, **164**, A655–A665.

- 73 F. Lin, I. M. Markus, D. Nordlund, T.-C. Weng, M. D. Asta, H. L. Xin and M. M. Doeff, *Nat. Commun.*, 2014, **5**, 3529.
- 74 M. Gu, I. Belharouak, J. Zheng, H. Wu, J. Xiao, A. Genc, K. Amine, S. Thevuthasan, D. R. Baer, J.-G. Zhang, N. D. Browning, J. Liu and C. Wang, *ACS Nano*, 2013, **7**, 760–767.
- 75 Y. Ruan, X. Song, Y. Fu, C. Song and V. Battaglia, *J. Power Sources*, 2018, **400**, 539–548.
- 76 G. G. Amatucci, J. M. Tarascon and L. C. Klein, *Solid State Ionics*, 1996, **83**, 167–173.
- 77 C. Zhan, T. Wu, J. Lu and K. Amine, *Energy Environ. Sci.*, 2018, **11**, 243–257.
- 78 Y. Zhao, H. Pan, J. Wang, R. Chen, F. Luo, X. Yu and H. Li, *Chin. Phys. B*, 2020, **29**, 088201.
- 79 C. Zhan, J. Lu, A. Jeremy Kropf, T. Wu, A. N. Jansen, Y.-K. Sun, X. Qiu and K. Amine, *Nat. Commun.*, 2013, **4**, 2437.
- 80 K. Leung, *Chem. Mater.*, 2017, **29**, 2550–2562.
- 81 N. P. W. Pieczonka, Z. Liu, P. Lu, K. L. Olson, J. Moote, B. R. Powell and J.-H. Kim, *J. Phys. Chem. C*, 2013, **117**, 15947–15957.
- 82 H. R. Morin, D. G. Graczyk, Y. Tsai, S. Lopykinski, H. Iddir, J. C. Garcia, N. Dietz Rago, S. Trask, L. Flores, S.-B. Son, Z. Zhang, N. M. Johnson and I. Bloom, *ACS Appl. Energy Mater.*, 2020, **3**, 2565–2575.
- 83 Y. Han, S. Heng, Y. Wang, Q. Qu and H. Zheng, *ACS Energy Lett.*, 2020, 2421–2433, DOI: 10.1021/acsenergylett.0c01032.
- 84 M. Evertz, F. Horsthemke, J. Kasnatscheew, M. Börner, M. Winter and S. Nowak, *J. Power Sources*, 2016, **329**, 364–371.
- 85 H. Zheng, Q. Sun, G. Liu, X. Song and V. S. Battaglia, *J. Power Sources*, 2012, **207**, 134–140.
- 86 H. Y. Asl and A. Manthiram, *Science*, 2020, **369**, 140–141.
- 87 P. Yan, J. Zheng, M. Gu, J. Xiao, J.-G. Zhang and C.-M. Wang, *Nat. Commun.*, 2017, **8**, 14101.
- 88 R. Tatara, P. Karayaylali, Y. Yu, Y. Zhang, L. Giordano, F. Maglia, R. Jung, J. P. Schmidt, I. Lund and Y. Shao-Horn, *J. Electrochem. Soc.*, 2019, **166**, A5090–A5098.
- 89 J. Cabana, B. J. Kwon and L. Hu, *Acc. Chem. Res.*, 2018, **51**, 299–308.
- 90 G. Alva, C. Kim, T. Yi, J. B. Cook, L. Xu, G. M. Nolis and J. Cabana, *J. Phys. Chem. C*, 2014, **118**, 10596–10605.
- 91 S. Liu, J. Su, J. Zhao, X. Chen, C. Zhang, T. Huang, J. Wu and A. Yu, *J. Power Sources*, 2018, **393**, 92–98.
- 92 M. Gauthier, T. J. Carney, A. Grimaud, L. Giordano, N. Pour, H.-H. Chang, D. P. Fenning, S. F. Lux, O. Paschos, C. Bauer, F. Maglia, S. Lupart, P. Lamp and Y. Shao-Horn, *J. Phys. Chem. Lett.*, 2015, **6**, 4653–4672.
- 93 D. Tang, Y. Sun, Z. Yang, L. Ben, L. Gu and X. Huang, *Chem. Mater.*, 2014, **26**, 3535–3543.
- 94 W. Li, *J. Electrochem. Soc.*, 2020, **167**, 090514.
- 95 M. Hirayama, H. Ido, K. Kim, W. Cho, K. Tamura, J. i. Mizuki and R. Kanno, *J. Am. Chem. Soc.*, 2010, **132**, 15268–15276.
- 96 I. A. Shkrob, A. J. Kropf, T. W. Marin, Y. Li, O. G. Poluektov, J. Niklas and D. P. Abraham, *J. Phys. Chem. C*, 2014, **118**, 24335–24348.
- 97 D. R. Vissers, Z. Chen, Y. Shao, M. Engelhard, U. Das, P. Redfern, L. A. Curtiss, B. Pan, J. Liu and K. Amine, *ACS Appl. Mater. Interfaces*, 2016, **8**, 14244–14251.
- 98 J. Betz, J.-P. Brinkmann, R. Nölle, C. Lürenbaum, M. Kolek, M. C. Stan, M. Winter and T. Placke, *Adv. Energy Mater.*, 2019, **9**, 1900574.
- 99 B. Markovsky, A. Rodkin, G. Salitra, Y. Talyosef, D. Aurbach and H. J. Kim, *J. Electrochem. Soc.*, 2004, **151**, A1068.
- 100 A. Tornheim, R. Sahore, M. He, J. R. Croy and Z. Zhang, *J. Electrochem. Soc.*, 2018, **165**, A3360–A3368.
- 101 J. Li, L. E. Downie, L. Ma, W. Qiu and J. R. Dahn, *J. Electrochem. Soc.*, 2015, **162**, A1401–A1408.
- 102 L. Xing, O. Borodin, G. D. Smith and W. Li, *J. Phys. Chem. A*, 2011, **115**, 13896–13905.
- 103 O. Borodin and T. R. Jow, *ECS Trans.*, 2011, **33**, 77–84.
- 104 M. Ue, M. Takeda, M. Takehara and S. Mori, *J. Electrochem. Soc.*, 1997, **144**, 2684–2688.
- 105 X.-B. Cheng, R. Zhang, C.-Z. Zhao and Q. Zhang, *Chem. Rev.*, 2017, **117**, 10403–10473.
- 106 J.-G. Zhang, W. Xu, J. Xiao, X. Cao and J. Liu, *Chem. Rev.*, 2020, **120**, 13312–13348.
- 107 H. Yang, J. Li, Z. Sun, R. Fang, D.-W. Wang, K. He, H.-M. Cheng and F. Li, *Energy Storage Mater.*, 2020, **30**, 113–129.
- 108 Y. Jie, X. Ren, R. Cao, W. Cai and S. Jiao, *Adv. Funct. Mater.*, 2020, **30**, 1910777.
- 109 S. Chen, K. Wen, J. Fan, Y. Bando and D. Golberg, *J. Mater. Chem. A*, 2018, **6**, 11631–11663.
- 110 A. Banerjee, X. Wang, C. Fang, E. A. Wu and Y. S. Meng, *Chem. Rev.*, 2020, **120**, 6878–6933.
- 111 D. Zhou, D. Shanmukaraj, A. Tkacheva, M. Armand and G. Wang, *Chem*, 2019, **5**, 2326–2352.
- 112 M. Li, C. Wang, Z. Chen, K. Xu and J. Lu, *Chem. Rev.*, 2020, **120**, 6783–6819.
- 113 R. Fong, U. von Sacken and J. R. Dahn, *J. Electrochem. Soc.*, 1990, **137**, 2009–2013.
- 114 J. M. Tarascon and D. Guyomard, *Solid State Ionics*, 1994, **69**, 293–305.
- 115 D. Guyomard and J. M. Tarascon, *J. Electrochem. Soc.*, 1993, **140**, 3071–3081.
- 116 J. Henschel, F. Horsthemke, Y. P. Stenzel, M. Evertz, S. Girod, C. Lürenbaum, K. Kösters, S. Wiemers-Meyer, M. Winter and S. Nowak, *J. Power Sources*, 2020, **447**, 227370.
- 117 K. Xu, *Chem. Rev.*, 2004, **104**, 4303–4418.
- 118 J. Xia, R. Petibon, D. Xiong, L. Ma and J. R. Dahn, *J. Power Sources*, 2016, **328**, 124–135.
- 119 L. Ma, S. L. Glazier, R. Petibon, J. Xia, J. M. Peters, Q. Liu, J. Allen, R. N. C. Doig and J. R. Dahn, *J. Electrochem. Soc.*, 2017, **164**, A5008–A5018.
- 120 L. Yang, B. Ravdel and B. L. Lucht, *Electrochem. Solid-State Lett.*, 2010, **13**, A95–A97.
- 121 L. Xia, B. Tang, L. Yao, K. Wang, A. Cheris, Y. Pan, S. Lee, Y. Xia, G. Z. Chen and Z. Liu, *ChemistrySelect*, 2017, **2**, 7353–7361.
- 122 X. Fan, L. Chen, X. Ji, T. Deng, S. Hou, J. Chen, J. Zheng, F. Wang, J. Jiang, K. Xu and C. Wang, *Chem*, 2018, **4**, 174–185.

- 123 X. Fan, L. Chen, O. Borodin, X. Ji, J. Chen, S. Hou, T. Deng, J. Zheng, C. Yang, S.-C. Liou, K. Amine, K. Xu and C. Wang, *Nat. Nanotechnol.*, 2018, **13**, 715–722.
- 124 W. Li, A. Dolocan, J. Li, Q. Xie and A. Manthiram, *Adv. Energy Mater.*, 2019, **9**, 1901152.
- 125 R. Petibon, J. Xia, L. Ma, M. K. G. Bauer, K. J. Nelson and J. R. Dahn, *J. Electrochem. Soc.*, 2016, **163**, A2571–A2578.
- 126 Q. Q. Liu, D. J. Xiong, R. Petibon, C. Y. Du and J. R. Dahn, *J. Electrochem. Soc.*, 2016, **163**, A3010–A3015.
- 127 E. R. Logan, E. M. Tonita, K. L. Gering, L. Ma, M. K. G. Bauer, J. Li, L. Y. Beaulieu and J. R. Dahn, *J. Electrochem. Soc.*, 2018, **165**, A705–A716.
- 128 J. L. Tebbe, T. F. Fuerst and C. B. Musgrave, *ACS Appl. Mater. Interfaces*, 2016, **8**, 26664–26674.
- 129 L. Yu, H. Liu, Y. Wang, N. Kuwata, M. Osawa, J. Kawamura and S. Ye, *Angew. Chem., Int. Ed.*, 2013, **52**, 5753–5756.
- 130 N. Kumar, K. Leung and D. J. Siegel, *J. Electrochem. Soc.*, 2014, **161**, E3059–E3065.
- 131 D. Aurbach, B. Markovsky, A. Rodkin, E. Levi, Y. S. Cohen, H. J. Kim and M. Schmidt, *Electrochim. Acta*, 2002, **47**, 4291–4306.
- 132 L. Xing and O. Borodin, *Phys. Chem. Chem. Phys.*, 2012, **14**, 12838–12843.
- 133 M. Metzger, C. Marino, J. Sicklinger, D. Haering and H. A. Gasteiger, *J. Electrochem. Soc.*, 2015, **162**, A1123–A1134.
- 134 K. Leung, *J. Phys. Chem. C*, 2012, **116**, 9852–9861.
- 135 S. Xu, G. Luo, R. Jacobs, S. Fang, M. K. Mahanthappa, R. J. Hamers and D. Morgan, *ACS Appl. Mater. Interfaces*, 2017, **9**, 20545–20553.
- 136 Y. Zhang, Y. Katayama, R. Tatara, L. Giordano, Y. Yu, D. Fraggedakis, J. G. Sun, F. Maglia, R. Jung, M. Z. Bazant and Y. Shao-Horn, *Energy Environ. Sci.*, 2020, **13**, 183–199.
- 137 R. Sahore, D. C. O'Hanlon, A. Tornheim, C.-W. Lee, J. C. Garcia, H. Iddir, M. Balasubramanian and I. Bloom, *J. Electrochem. Soc.*, 2020, **167**, 020513.
- 138 M. Gauthier, P. Karayaylali, L. Giordano, S. Feng, S. F. Lux, F. Maglia, P. Lamp and Y. Shao-Horn, *J. Electrochem. Soc.*, 2018, **165**, A1377–A1387.
- 139 A. T. S. Freiberg, M. K. Roos, J. Wandt, R. de Vivie-Riedle and H. A. Gasteiger, *J. Phys. Chem. A*, 2018, **122**, 8828–8839.
- 140 M. G. S. R. Thomas, P. G. Bruce and J. B. Goodenough, *J. Electrochem. Soc.*, 1985, **132**, 1521–1528.
- 141 K. Kanamura, S. Toriyama, S. Shiraiishi, M. Ohashi and Z.-i. Takehara, *J. Electroanal. Chem.*, 1996, **419**, 77–84.
- 142 D. Aurbach, B. Markovsky, G. Salitra, E. Markevich, Y. Talyossef, M. Koltypin, L. Nazar, B. Ellis and D. Kovacheva, *J. Power Sources*, 2007, **165**, 491–499.
- 143 D. Aurbach, M. D. Levi, E. Levi, H. Teller, B. Markovsky, G. Salitra, U. Heider and L. Heider, *J. Electrochem. Soc.*, 1998, **145**, 3024–3034.
- 144 D. Aurbach, B. Markovsky, M. D. Levi, E. Levi, A. Schechter, M. Moshkovich and Y. Cohen, *J. Power Sources*, 1999, **81–82**, 95–111.
- 145 E. Levi, M. D. Levi, G. Salitra, D. Aurbach, R. Oesten, U. Heider and L. Heider, *Solid State Ionics*, 1999, **126**, 97–108.
- 146 K. Edstrom, T. Gustafsson and J. O. Thomas, *Electrochim. Acta*, 2004, **50**, 397–403.
- 147 F. Buchner, M. Fingerle, J. Kim, T. Spath, R. Hausbrand and R. J. Behm, *Adv. Mater. Interfaces*, 2019, **6**, 11.
- 148 K. Edström, T. Gustafsson and J. O. Thomas, *Electrochim. Acta*, 2004, **50**, 397–403.
- 149 Y. Qian, P. Niehoff, M. Börner, M. Grütze, X. Mönnighoff, P. Behrends, S. Nowak, M. Winter and F. M. Schappacher, *J. Power Sources*, 2016, **329**, 31–40.
- 150 W. Lu, J. Zhang, J. Xu, X. Wu and L. Chen, *ACS Appl. Mater. Interfaces*, 2017, **9**, 19313–19318.
- 151 J. Li, W. Li, Y. You and A. Manthiram, *Adv. Energy Mater.*, 2018, **8**, 1801957.
- 152 S. Malmgren, K. Ciosek, M. Hahlin, T. Gustafsson, M. Gorgoi, H. Rensmo and K. Edstrom, *Electrochim. Acta*, 2013, **97**, 23–32.
- 153 R. Dedryvère, D. Foix, S. Franger, S. Patoux, L. Daniel and D. Gonbeau, *J. Phys. Chem. C*, 2010, **114**, 10999–11008.
- 154 S. Malmgren, K. Ciosek, M. Hahlin, T. Gustafsson, M. Gorgoi, H. Rensmo and K. Edström, *Electrochim. Acta*, 2013, **97**, 23–32.
- 155 M. Balasubramanian, H. S. Lee, X. Sun, X. Q. Yang, A. R. Moodenbaugh, J. McBreen, D. A. Fischer and Z. Fu, *Electrochem. Solid-State Lett.*, 2002, **5**, A22–A25.
- 156 J. Lei, L. Li, R. Kostecki, R. Muller and F. McLarnon, *J. Electrochem. Soc.*, 2005, **152**, A774–A777.
- 157 N.-S. Choi, J.-G. Han, S.-Y. Ha, I. Park and C.-K. Back, *RSC Adv.*, 2015, **5**, 2732–2748.
- 158 J. F. Browning, L. Baggetto, K. L. Jungjohann, Y. Wang, W. E. Tenhaeff, J. K. Keum, D. L. Wood and G. M. Veith, *ACS Appl. Mater. Interfaces*, 2014, **6**, 18569–18576.
- 159 G. Cherkashinin, M. Motzko, N. Schulz, T. Späth and W. Jaegermann, *Chem. Mater.*, 2015, **27**, 2875–2887.
- 160 D. Ensling, G. Cherkashinin, S. Schmid, S. Bhuvanewari, A. Thissen and W. Jaegermann, *Chem. Mater.*, 2014, **26**, 3948–3956.
- 161 F. Single, B. Horstmann and A. Latz, *Phys. Chem. Chem. Phys.*, 2016, **18**, 17810–17814.
- 162 M. Lu, H. Cheng and Y. Yang, *Electrochim. Acta*, 2008, **53**, 3539–3546.
- 163 V. Eshkenazi, E. Peled, L. Burstein and D. Golodnitsky, *Solid State Ionics*, 2004, **170**, 83–91.
- 164 N. Liu, H. Li, Z. Wang, X. Huang and L. Chen, *Electrochem. Solid-State Lett.*, 2006, **9**, A328.
- 165 K. Hayashi, Y. Nemoto, S.-i. Tobishima and J.-i. Yamaki, *Electrochim. Acta*, 1999, **44**, 2337–2344.
- 166 M. Egashira, H. Takahashi, S. Okada and J.-i. Yamaki, *J. Power Sources*, 2001, **92**, 267–271.
- 167 K. Xu, S. P. Ding and T. R. Jow, *J. Electrochem. Soc.*, 1999, **146**, 4172–4178.
- 168 F. Ossola, G. Pistoia, R. Seeber and P. Ugo, *Electrochim. Acta*, 1988, **33**, 47–50.
- 169 K. Leung, *J. Phys. Chem. C*, 2013, **117**, 1539–1547.
- 170 P. Tundo, L. Rossi and A. Loris, *J. Org. Chem.*, 2005, **70**, 2219–2224.

- 171 S. K. Martha, B. Markovsky, J. Grinblat, Y. Gofer, O. Haik, E. Zinigrad, D. Aurbach, T. Drezen, D. Wang, G. Deghenghi and I. Exnar, *J. Electrochem. Soc.*, 2009, **156**, A541–A552.
- 172 S. K. Martha, J. Grinblat, O. Haik, E. Zinigrad, T. Drezen, J. H. Miners, I. Exnar, A. Kay, B. Markovsky and D. Aurbach, *Angew. Chem., Int. Ed.*, 2009, **48**, 8559–8563.
- 173 S.-M. Oh, S.-W. Oh, C.-S. Yoon, B. Scrosati, K. Amine and Y.-K. Sun, *Adv. Funct. Mater.*, 2010, **20**, 3260–3265.
- 174 J.-Y. Luo, H.-M. Xiong and Y.-Y. Xia, *J. Phys. Chem. C*, 2008, **112**, 12051–12057.
- 175 H. B. Lin, Y. M. Zhang, J. N. Hu, Y. T. Wang, L. D. Xing, M. Q. Xu, X. P. Li and W. S. Li, *J. Power Sources*, 2014, **257**, 37–44.
- 176 J. Geder, H. E. Hoster, A. Jossen, J. Garche and D. Y. W. Yu, *J. Power Sources*, 2014, **257**, 286–292.
- 177 J. Li, A. R. Cameron, H. Li, S. Glazier, D. Xiong, M. Chatzidakis, J. Allen, G. A. Botton and J. R. Dahn, *J. Electrochem. Soc.*, 2017, **164**, A1534–A1544.
- 178 H. Li, J. Li, X. Ma and J. R. Dahn, *J. Electrochem. Soc.*, 2018, **165**, A1038–A1045.
- 179 G. Qian, Y. Zhang, L. Li, R. Zhang, J. Xu, Z. Cheng, S. Xie, H. Wang, Q. Rao, Y. He, Y. Shen, L. Chen, M. Tang and Z.-F. Ma, *Energy Storage Mater.*, 2020, **27**, 140–149.
- 180 J. E. Harlow, X. Ma, J. Li, E. Logan, Y. Liu, N. Zhang, L. Ma, S. L. Glazier, M. M. E. Cormier, M. Genovese, S. Buteau, A. Cameron, J. E. Stark and J. R. Dahn, *J. Electrochem. Soc.*, 2019, **166**, A3031–A3044.
- 181 Y. Liu, J. Harlow and J. Dahn, *J. Electrochem. Soc.*, 2020, **167**, 020512.
- 182 E. Markevich, G. Salitra, Y. Talyosef, U.-H. Kim, H.-H. Ryu, Y.-K. Sun and D. Aurbach, *ACS Appl. Energy Mater.*, 2018, **1**, 2600–2607.
- 183 T. Deng, X. Fan, L. Cao, J. Chen, S. Hou, X. Ji, L. Chen, S. Li, X. Zhou, E. Hu, D. Su, X.-Q. Yang and C. Wang, *Joule*, 2019, **3**, 2550–2564.
- 184 J. Fan and P. S. Fedkiw, *J. Power Sources*, 1998, **72**, 165–173.
- 185 J. B. Goodenough and Y. Kim, *Chem. Mater.*, 2009, **22**, 587–603.
- 186 P. Peljo and H. H. Girault, *Energy Environ. Sci.*, 2018, **11**, 2306–2309.
- 187 M. Ue, A. Murakami and S. Nakamura, *J. Electrochem. Soc.*, 2002, **149**, A1572–A1577.
- 188 V. R. Koch, L. A. Dominey, C. Nanjundiah and M. J. Ondrechen, *J. Electrochem. Soc.*, 1996, **143**, 798–803.
- 189 R. L. Wang, L. M. Moshurchak, W. M. Lamanna, M. Bulinski and J. R. Dahn, *J. Electrochem. Soc.*, 2008, **155**, A66–A73.
- 190 P. Johansson and P. Jacobsson, *J. Power Sources*, 2006, **153**, 336–344.
- 191 B. C. Melot and J. M. Tarascon, *Acc. Chem. Res.*, 2013, **46**, 1226–1238.
- 192 T. A. Barnes, J. W. Kaminski, O. Borodin and T. F. Miller, *J. Phys. Chem. C*, 2015, **119**, 3865–3880.
- 193 B. Oleg, O. Marco, E. S. Carrie, W. L. Kenneth and K. Jaroslaw, *Nanotechnology*, 2015, **26**, 354003.
- 194 X. Zhang, J. K. Pugh and P. N. Ross, *J. Electrochem. Soc.*, 2001, **148**, E183–E188.
- 195 O. Borodin, X. Ren, J. Vatamanu, A. von Wald Cresce, J. Knap and K. Xu, *Acc. Chem. Res.*, 2017, **50**, 2886–2894.
- 196 O. Borodin, W. Behl and T. R. Jow, *J. Phys. Chem. C*, 2013, **117**, 8661–8682.
- 197 L. Giordano, P. Karayaylali, Y. Yu, Y. Katayama, F. Maglia, S. Lux and Y. Shao-Horn, *J. Phys. Chem. Lett.*, 2017, **8**, 3881–3887.
- 198 Y.-H. Liu, S. Takeda, I. Kaneko, H. Yoshitake, T. Mukai, M. Yanagida, Y. Saito and T. Sakai, *J. Phys. Chem. C*, 2018, **122**, 5864–5870.
- 199 Y. Yu, P. Karayaylali, Y. Katayama, L. Giordano, M. Gauthier, F. Maglia, R. Jung, I. Lund and Y. Shao-Horn, *J. Phys. Chem. C*, 2018, **122**, 27368–27382.
- 200 N. Dupre, M. Cuisinier and D. Guyomard, *Interface Mag.*, 2011, **20**, 61–67.
- 201 A. M. Andersson, D. P. Abraham, R. Haasch, S. MacLaren, J. Liu and K. Amine, *J. Electrochem. Soc.*, 2002, **149**, A1358–A1369.
- 202 Y.-C. Lu, A. N. Mansour, N. Yabuuchi and Y. Shao-Horn, *Chem. Mater.*, 2009, **21**, 4408–4424.
- 203 D. Takamatsu, Y. Koyama, Y. Orikasa, S. Mori, T. Nakatsutsumi, T. Hirano, H. Tanida, H. Arai, Y. Uchimoto and Z. Ogumi, *Angew. Chem., Int. Ed.*, 2012, **51**, 11597–11601.
- 204 R. Dedryvère, H. Martinez, S. Leroy, D. Lemordant, F. Bonhomme, P. Biensan and D. Gonbeau, *J. Power Sources*, 2007, **174**, 462–468.
- 205 M. A. Teshager, S. D. Lin, B.-J. Hwang, F.-M. Wang, S. Hy and A. M. Haregewoin, *ChemElectroChem*, 2016, **3**, 337–345.
- 206 Y.-K. Sun, S.-T. Myung, B.-C. Park, J. Prakash, I. Belharouak and K. Amine, *Nat. Mater.*, 2009, **8**, 320–324.
- 207 H.-J. Noh, S. Youn, C. S. Yoon and Y.-K. Sun, *J. Power Sources*, 2013, **233**, 121–130.
- 208 L. Ma, M. Nie, J. Xia and J. R. Dahn, *J. Power Sources*, 2016, **327**, 145–150.
- 209 D. P. Abraham, R. D. Twisten, M. Balasubramanian, J. Kropf, D. Fischer, J. McBreen, I. Petrov and K. Amine, *J. Electrochem. Soc.*, 2003, **150**, A1450–A1456.
- 210 H. Liu, M. Bugnet, M. Z. Tessaro, K. J. Harris, M. J. R. Dunham, M. Jiang, G. R. Goward and G. A. Botton, *Phys. Chem. Chem. Phys.*, 2016, **18**, 29064–29075.
- 211 R. Jung, M. Metzger, F. Maglia, C. Stinner and H. A. Gasteiger, *J. Electrochem. Soc.*, 2017, **164**, A1361–A1377.
- 212 R. Jung, M. Metzger, F. Maglia, C. Stinner and H. A. Gasteiger, *J. Phys. Chem. Lett.*, 2017, **8**, 4820–4825.
- 213 F. La Mantia, F. Rosciano, N. Tran and P. Novák, *J. Appl. Electrochem.*, 2008, **38**, 893–896.
- 214 D. J. Xiong, L. D. Ellis, J. Li, H. Li, T. Hynes, J. P. Allen, J. Xia, D. S. Hall, I. G. Hill and J. R. Dahn, *J. Electrochem. Soc.*, 2017, **164**, A3025–A3037.
- 215 S.-i. Tobishima and T. Okada, *Electrochim. Acta*, 1985, **30**, 1715–1722.
- 216 J.-C. Lee and M. H. Litt, *Macromolecules*, 2000, **33**, 1618–1627.
- 217 S. E. Sloop, J. B. Kerr and K. Kinoshita, *J. Power Sources*, 2003, **119–121**, 330–337.

- 218 J.-G. Lee, B. Kim, J. Cho, Y.-W. Kim and B. Park, *J. Electrochem. Soc.*, 2004, **151**, A801–A805.
- 219 S.-T. Myung, K. Izumi, S. Komaba, Y.-K. Sun, H. Yashiro and N. Kumagai, *Chem. Mater.*, 2005, **17**, 3695–3704.
- 220 Y. J. Kim, J. Cho, T.-J. Kim and B. Park, *J. Electrochem. Soc.*, 2003, **150**, A1723–A1725.
- 221 Y.-K. Sun, S.-W. Cho, S.-W. Lee, C. S. Yoon and K. Amine, *J. Electrochem. Soc.*, 2007, **154**, A168–A172.
- 222 J. M. Zheng, Z. R. Zhang, X. B. Wu, Z. X. Dong, Z. Zhu and Y. Yang, *J. Electrochem. Soc.*, 2008, **155**, A775–A782.
- 223 Y.-K. Sun, C. S. Yoon, S.-T. Myung, I. Belharouak and K. Amine, *J. Electrochem. Soc.*, 2009, **156**, A1005–A1010.
- 224 Y.-S. Park, K.-H. Choi, H.-K. Park and S.-M. Lee, *J. Electrochem. Soc.*, 2010, **157**, A850–A853.
- 225 H.-M. Cheng, F.-M. Wang, J. P. Chu, R. Santhanam, J. Rick and S.-C. Lo, *J. Phys. Chem. C*, 2012, **116**, 7629–7637.
- 226 B. Han, T. Paulauskas, B. Key, C. Peebles, J. S. Park, R. F. Klie, J. T. Vaughey and F. Dogan, *ACS Appl. Mater. Interfaces*, 2017, **9**, 14769–14778.
- 227 A. M. Wise, C. Ban, J. N. Weker, S. Misra, A. S. Cavanagh, Z. Wu, Z. Li, M. S. Whittingham, K. Xu, S. M. George and M. F. Toney, *Chem. Mater.*, 2015, **27**, 6146–6154.
- 228 D. S. Hall, R. Gauthier, A. Eldesoky, V. S. Murray and J. R. Dahn, *ACS Appl. Mater. Interfaces*, 2019, **11**, 14095–14100.
- 229 Y. Su, S. Cui, Z. Zhuo, W. Yang, X. Wang and F. Pan, *ACS Appl. Mater. Interfaces*, 2015, **7**, 25105–25112.
- 230 J. Cho, T.-G. Kim, C. Kim, J.-G. Lee, Y.-W. Kim and B. Park, *J. Power Sources*, 2005, **146**, 58–64.
- 231 X. Zhang, I. Belharouak, L. Li, Y. Lei, J. W. Elam, A. Nie, X. Chen, R. S. Yassar and R. L. Axelbaum, *Adv. Energy Mater.*, 2013, **3**, 1299–1307.
- 232 J. Zheng, M. Gu, J. Xiao, B. J. Polzin, P. Yan, X. Chen, C. Wang and J.-G. Zhang, *Chem. Mater.*, 2014, **26**, 6320–6327.
- 233 M. R. Laskar, D. H. K. Jackson, S. Xu, R. J. Hamers, D. Morgan and T. F. Kuech, *ACS Appl. Mater. Interfaces*, 2017, **9**, 11231–11239.
- 234 H. Yu, Y. Gao and X. Liang, *J. Electrochem. Soc.*, 2019, **166**, A2021–A2027.
- 235 L. David, K. Dahlberg, D. Mohanty, R. E. Ruther, A. Huq, M. Chi, S. J. An, C. Mao, D. M. King, L. Stevenson and D. L. Wood, *ACS Appl. Energy Mater.*, 2019, **2**, 1308–1313.
- 236 Y. Yamada and A. Yamada, *J. Electrochem. Soc.*, 2015, **162**, A2406–A2423.
- 237 J. Wang, Y. Yamada, K. Sodeyama, C. H. Chiang, Y. Tateyama and A. Yamada, *Nat. Commun.*, 2016, **7**, 12032.
- 238 R. Petibon, C. P. Aiken, L. Ma, D. Xiong and J. R. Dahn, *Electrochim. Acta*, 2015, **154**, 287–293.
- 239 S. Phadke and M. Anouti, *Electrochim. Acta*, 2017, **223**, 31–38.
- 240 R. Tatara, Y. Yu, P. Karayaylali, A. K. Chan, Y. Zhang, R. Jung, F. Maglia, L. Giordano and Y. Shao-Horn, *ACS Appl. Mater. Interfaces*, 2019, **11**, 34973–34988.
- 241 I. A. Shkrob, Y. Zhu, T. W. Marin and D. Abraham, *J. Phys. Chem. C*, 2013, **117**, 19255–19269.
- 242 L. Yang, B. Ravdel and B. L. Lucht, *Electrochem. Solid-State Lett.*, 2010, **13**, A95.
- 243 M. Aykol, S. Kirklin and C. Wolverton, *Adv. Energy Mater.*, 2014, **4**, 1400690.
- 244 C. Lu, H. Wu, Y. Zhang, H. Liu, B. Chen, N. Wu and S. Wang, *J. Power Sources*, 2014, **267**, 682–691.
- 245 K. J. Rosina, M. Jiang, D. Zeng, E. Salager, A. S. Best and C. P. Grey, *J. Mater. Chem.*, 2012, **22**, 20602–20610.
- 246 X. Liu, T. Huang and A. Yu, *Electrochim. Acta*, 2015, **163**, 82–92.
- 247 M. Metzger, J. Sicklinger, D. Haering, C. Kavakli, C. Stinner, C. Marino and H. A. Gasteiger, *J. Electrochem. Soc.*, 2015, **162**, A1227–A1235.
- 248 D. Chen, M. A. Mahmoud, J.-H. Wang, G. H. Waller, B. Zhao, C. Qu, M. A. El-Sayed and M. Liu, *Nano Lett.*, 2019, **19**, 2037–2043.
- 249 S. Liu, L. Wang, C. Zhang, B. Chu, C. Wang, T. Huang and A. Yu, *J. Power Sources*, 2019, **438**, 226979.
- 250 J. Chen, X. Fan, Q. Li, H. Yang, M. R. Khoshi, Y. Xu, S. Hwang, L. Chen, X. Ji, C. Yang, H. He, C. Wang, E. Garfunkel, D. Su, O. Borodin and C. Wang, *Nat. Energy*, 2020, **5**, 386–397.
- 251 S. Fang, D. Jackson, M. L. Dreibelbis, T. F. Kuech and R. J. Hamers, *J. Power Sources*, 2018, **373**, 184–192.
- 252 L. Benitez, D. Cristancho, J. M. Seminario, J. M. Martinez de la Hoz and P. B. Balbuena, *Electrochim. Acta*, 2014, **140**, 250–257.
- 253 A. Wang, S. Kadam, H. Li, S. Shi and Y. Qi, *npj Comput. Mater.*, 2018, **4**, 15.
- 254 A. Marzouk, V. Ponce, L. Benitez, F. A. Soto, K. Hankins, J. M. Seminario, P. B. Balbuena and F. El-Mellouhi, *J. Phys. Chem. C*, 2018, **122**, 25858–25868.
- 255 Y. Takanashi, Y. Orikasa, M. Mogi, M. Oishi, H. Murayama, K. Sato, H. Yamashige, D. Takamatsu, T. Fujimoto, H. Tanida, H. Arai, T. Ohta, E. Matsubara, Y. Uchimoto and Z. Ogumi, *J. Power Sources*, 2011, **196**, 10679–10685.
- 256 L. M. Z. De Juan, I. V. B. Maggay, M. T. Nguyen, W.-R. Liu and T. Yonezawa, *ACS Appl. Nano Mater.*, 2018, **1**, 3509–3519.
- 257 L. Chen, X. Fan, X. Ji, J. Chen, S. Hou and C. Wang, *Joule*, 2019, **3**, 732–744.
- 258 W. Huang, H. Wang, D. T. Boyle, Y. Li and Y. Cui, *ACS Energy Lett.*, 2020, **5**, 1128–1135.
- 259 M. J. Zachman, Z. Tu, S. Choudhury, L. A. Archer and L. F. Kourkoutis, *Nature*, 2018, **560**, 345–349.
- 260 L. Baggetto, D. Mohanty, R. A. Meisner, C. A. Bridges, C. Daniel, D. L. Wood III, N. J. Dudney and G. M. Veith, *RSC Adv.*, 2014, **4**, 23364–23371.
- 261 S. Jurng, Z. L. Brown, J. Kim and B. L. Lucht, *Energy Environ. Sci.*, 2018, **11**, 2600–2608.
- 262 D. E. Galvez-Aranda and J. M. Seminario, *J. Electrochem. Soc.*, 2018, **165**, A717–A730.
- 263 M. He, R. Guo, G. M. Hobold, H. Gao and B. M. Gallant, *Proc. Natl. Acad. Sci. U. S. A.*, 2020, **117**, 73–79.
- 264 H. Yildirim, A. Kinaci, M. K. Y. Chan and J. P. Greeley, *ACS Appl. Mater. Interfaces*, 2015, **7**, 18985–18996.

- 265 C. Li and J. Maier, *Solid State Ionics*, 2012, **225**, 408–411.
- 266 Q. Zhang, J. Pan, P. Lu, Z. Liu, M. W. Verbrugge, B. W. Sheldon, Y.-T. Cheng, Y. Qi and X. Xiao, *Nano Lett.*, 2016, **16**, 2011–2016.
- 267 A. Ramasubramanian, V. Yurkiv, T. Foroozan, M. Ragone, R. Shahbazian-Yassar and F. Mashayek, *J. Phys. Chem. C*, 2019, **123**, 10237–10245.
- 268 S. Breuer, V. Pregartner, S. Lunghammer and H. M. R. Wilkening, *J. Phys. Chem. C*, 2019, **123**, 5222–5230.
- 269 J. Zheng, G. Ji, X. Fan, J. Chen, Q. Li, H. Wang, Y. Yang, K. C. DeMella, S. R. Raghavan and C. Wang, *Adv. Energy Mater.*, 2019, **9**, 1803774.
- 270 C. Cui, C. Yang, N. Eidson, J. Chen, F. Han, L. Chen, C. Luo, P.-F. Wang, X. Fan and C. Wang, *Adv. Mater.*, 2020, **32**, 1906427.
- 271 Y. Lu, Z. Tu and L. A. Archer, *Nat. Mater.*, 2014, **13**, 961–969.
- 272 N. von Aspern, G.-V. Rösenthaller, M. Winter and I. Cekic-Laskovic, *Angew. Chem., Int. Ed.*, 2019, **58**, 15978–16000.
- 273 S. Choudhury and L. A. Archer, *Adv. Electron. Mater.*, 2016, **2**, 1500246.
- 274 T. Li, X.-Q. Zhang, P. Shi and Q. Zhang, *Joule*, 2019, **3**, 2647–2661.
- 275 L. Suo, W. Xue, M. Gobet, S. G. Greenbaum, C. Wang, Y. Chen, W. Yang, Y. Li and J. Li, *Proc. Natl. Acad. Sci. U. S. A.*, 2018, **115**, 1156–1161.
- 276 X. Fan, X. Ji, F. Han, J. Yue, J. Chen, L. Chen, T. Deng, J. Jiang and C. Wang, *Sci. Adv.*, 2018, **4**, eaau9245.
- 277 X. Fan, Y. Zhu, C. Luo, L. Suo, Y. Lin, T. Gao, K. Xu and C. Wang, *ACS Nano*, 2016, **10**, 5567–5577.
- 278 X. Fan, Y. Zhu, C. Luo, T. Gao, L. Suo, S.-C. Liou, K. Xu and C. Wang, *J. Power Sources*, 2016, **307**, 435–442.
- 279 J. Zheng, P. Yan, J. Zhang, M. H. Engelhard, Z. Zhu, B. J. Polzin, S. Trask, J. Xiao, C. Wang and J. Zhang, *Nano Res.*, 2017, **10**, 4221–4231.
- 280 Y.-X. Lin, Z. Liu, K. Leung, L.-Q. Chen, P. Lu and Y. Qi, *J. Power Sources*, 2016, **309**, 221–230.
- 281 C. Wang, Y. S. Meng and K. Xu, *J. Electrochem. Soc.*, 2018, **166**, A5184–A5186.
- 282 Y. Li, B. Xu, H. Xu, H. Duan, X. Lü, S. Xin, W. Zhou, L. Xue, G. Fu, A. Manthiram and J. B. Goodenough, *Angew. Chem., Int. Ed.*, 2017, **56**, 753–756.
- 283 X. Ding, Y.-X. Li, F. Chen, X.-D. He, A. Yasmin, Q. Hu, Z.-Y. Wen and C.-H. Chen, *J. Mater. Chem. A*, 2019, **7**, 11513–11519.
- 284 C. Cui, X. Fan, X. Zhou, J. Chen, Q. Wang, L. Ma, C. Yang, E. Hu, X.-Q. Yang and C. Wang, *J. Am. Chem. Soc.*, 2020, **142**, 8918–8927.
- 285 N. Ehteshami, L. Ibing, L. Stolz, M. Winter and E. Paillard, *J. Power Sources*, 2020, **451**, 227804.
- 286 Z. Zeng, V. Murugesan, K. S. Han, X. Jiang, Y. Cao, L. Xiao, X. Ai, H. Yang, J.-G. Zhang, M. L. Sushko and J. Liu, *Nat. Energy*, 2018, **3**, 674–681.
- 287 J. O. Besenhard, M. W. Wagner, M. Winter, A. D. Jannakoudakis, P. D. Jannakoudakis and E. Theodoridou, *J. Power Sources*, 1993, **44**, 413–420.
- 288 D. Aurbach, Y. Ein-Eli, O. Chusid, Y. Carmeli, M. Babai and H. Yamin, *J. Electrochem. Soc.*, 2019, **141**, 603–611.
- 289 A. J. Gmitter, I. Plitz and G. G. Amatucci, *J. Electrochem. Soc.*, 2012, **159**, A370–A379.
- 290 R. Petibon, J. Harlow, D. B. Le and J. R. Dahn, *Electrochim. Acta*, 2015, **154**, 227–234.
- 291 S. L. Glazier, R. Petibon, J. Xia and J. R. Dahn, *J. Electrochem. Soc.*, 2017, **164**, A567–A573.
- 292 J. Xia, Q. Liu, A. Hebert, T. Hynes, R. Petibon and J. R. Dahn, *J. Electrochem. Soc.*, 2017, **164**, A1268–A1273.
- 293 D. J. Xiong, T. Hynes and J. R. Dahn, *J. Electrochem. Soc.*, 2017, **164**, A2089–A2100.
- 294 D. J. Xiong, M. Bauer, L. D. Ellis, T. Hynes, S. Hyatt, D. S. Hall and J. R. Dahn, *J. Electrochem. Soc.*, 2018, **165**, A126–A131.
- 295 J. Xia, S. L. Glazier, R. Petibon and J. R. Dahn, *J. Electrochem. Soc.*, 2017, **164**, A1239–A1250.
- 296 J. O. Besenhard, M. Winter, J. Yang and W. Biberacher, *J. Power Sources*, 1995, **54**, 228–231.
- 297 S. Klein, S. van Wickeren, S. Röser, P. Bärmann, K. Borzutzki, B. Heidrich, M. Börner, M. Winter, T. Placke and J. Kasnatscheew, *Adv. Energy Mater.*, 2021, **11**, 2003738.
- 298 G. Nagasubramanian and C. J. Orendorff, *J. Power Sources*, 2011, **196**, 8604–8609.
- 299 K. C. Möller, T. Hodal, W. K. Appel, M. Winter and J. O. Besenhard, *J. Power Sources*, 2001, **97–98**, 595–597.
- 300 T. Achiha, T. Nakajima, Y. Ohzawa, M. Koh, A. Yamauchi, M. Kagawa and H. Aoyama, *J. Electrochem. Soc.*, 2009, **156**, A483–A488.
- 301 T. Achiha, T. Nakajima, Y. Ohzawa, M. Koh, A. Yamauchi, M. Kagawa and H. Aoyama, *J. Electrochem. Soc.*, 2010, **157**, A707–A712.
- 302 N. Nanbu, K. Takimoto, M. Takehara, M. Ue and Y. Sasaki, *Electrochem. Commun.*, 2008, **10**, 783–786.
- 303 J. Arai, *J. Electrochem. Soc.*, 2003, **150**, A219–A228.
- 304 J.-I. Yamaki, I. Yamazaki, M. Egashira and S. Okada, *J. Power Sources*, 2001, **102**, 288–293.
- 305 K. Sato, I. Yamazaki, S. Okada and J.-i. Yamaki, *Solid State Ionics*, 2002, **148**, 463–466.
- 306 N.-S. Choi, K. H. Yew, K. Y. Lee, M. Sung, H. Kim and S.-S. Kim, *J. Power Sources*, 2006, **161**, 1254–1259.
- 307 R. McMillan, H. Sleg, Z. X. Shu and W. Wang, *J. Power Sources*, 1999, **81–82**, 20–26.
- 308 R. Mogi, M. Inaba, S.-K. Jeong, Y. Iriyama, T. Abe and Z. Ogumi, *J. Electrochem. Soc.*, 2002, **149**, A1578–A1583.
- 309 X. J. Wang, H. S. Lee, H. Li, X. Q. Yang and X. J. Huang, *Electrochem. Commun.*, 2010, **12**, 386–389.
- 310 A. von Cresce and K. Xu, *J. Electrochem. Soc.*, 2011, **158**, A337–A342.
- 311 J. Arai, *J. Appl. Electrochem.*, 2002, **32**, 1071–1079.
- 312 J. Arai, *J. Power Sources*, 2003, **119–121**, 388–392.
- 313 K. Naoi, E. Iwama, N. Ogihara, Y. Nakamura, H. Segawa and Y. Ino, *J. Electrochem. Soc.*, 2009, **156**, A272–A276.
- 314 K. Naoi, E. Iwama, Y. Honda and F. Shimodate, *J. Electrochem. Soc.*, 2010, **157**, A190–A195.

- 315 X. Fan, X. Ji, L. Chen, J. Chen, T. Deng, F. Han, J. Yue, N. Piao, R. Wang, X. Zhou, X. Xiao, L. Chen and C. Wang, *Nat. Energy*, 2019, **4**, 882–890.
- 316 T. Doi, Y. Shimizu, M. Hashinokuchi and M. Inaba, *J. Electrochem. Soc.*, 2017, **164**, A6412–A6416.
- 317 S. Chen, J. Zheng, D. Mei, K. S. Han, M. H. Engelhard, W. Zhao, W. Xu, J. Liu and J.-G. Zhang, *Adv. Mater.*, 2018, **30**, 1706102.
- 318 J. Zheng, S. Chen, W. Zhao, J. Song, M. H. Engelhard and J.-G. Zhang, *ACS Energy Lett.*, 2018, **3**, 315–321.
- 319 X. Cao, X. Ren, L. Zou, M. H. Engelhard, W. Huang, H. Wang, B. E. Matthews, H. Lee, C. Niu, B. W. Arey, Y. Cui, C. Wang, J. Xiao, J. Liu, W. Xu and J.-G. Zhang, *Nat. Energy*, 2019, **4**, 796–805.
- 320 G. Ma, L. Wang, X. He, J. Zhang, H. Chen, W. Xu and Y. Ding, *ACS Appl. Energy Mater.*, 2018, **1**, 5446–5452.
- 321 T. Doi, R. Matsumoto, Z. Cao, M. Haruta, M. Hashinokuchi and M. Inaba, *Sustainable Energy Fuels*, 2018, **2**, 1197–1205.
- 322 Z. Zhang, L. Hu, H. Wu, W. Weng, M. Koh, P. C. Redfern, L. A. Curtiss and K. Amine, *Energy Environ. Sci.*, 2013, **6**, 1806–1810.
- 323 L. Hu, Z. Zhang and K. Amine, *Electrochem. Commun.*, 2013, **35**, 76–79.
- 324 L. Hu, Z. Xue, K. Amine and Z. Zhang, *J. Electrochem. Soc.*, 2014, **161**, A1777–A1781.
- 325 M. Takehara, N. Tsukimori, N. Nanbu, M. Ue and Y. Sasaki, *Electrochemistry*, 2003, **71**, 1201–1204.
- 326 Y.-M. Lee, K.-M. Nam, E.-H. Hwang, Y.-G. Kwon, D.-H. Kang, S.-S. Kim and S.-W. Song, *J. Phys. Chem. C*, 2014, **118**, 10631–10639.
- 327 S. Lin and J. Zhao, *ACS Appl. Mater. Interfaces*, 2020, **12**, 8316–8323.
- 328 Q. Yi, Y. Lu, X. Sun, H. Zhang, H. Yu and C. Sun, *ACS Appl. Mater. Interfaces*, 2019, **11**, 46965–46972.
- 329 X. Zheng, Z. Gu, X. Liu, Z. Wang, J. Wen, X. Wu, W. Luo and Y. Huang, *Energy Environ. Sci.*, 2020, **13**, 1788–1798.
- 330 S. Komaba, T. Ishikawa, N. Yabuuchi, W. Murata, A. Ito and Y. Ohsawa, *ACS Appl. Mater. Interfaces*, 2011, **3**, 4165–4168.
- 331 J. Xia, M. Nie, J. C. Burns, A. Xiao, W. M. Lamanna and J. R. Dahn, *J. Power Sources*, 2016, **307**, 340–350.
- 332 J. Xia, R. Petibon, A. Xiao, W. M. Lamanna and J. R. Dahn, *J. Power Sources*, 2016, **330**, 175–185.
- 333 L. Ma, J. Xia and J. R. Dahn, *J. Electrochem. Soc.*, 2014, **161**, A2250–A2254.
- 334 J. Xia, L. Madec, L. Ma, L. D. Ellis, W. Qiu, K. J. Nelson, Z. Lu and J. R. Dahn, *J. Power Sources*, 2015, **295**, 203–211.
- 335 M. C. Smart, B. V. Ratnakumar, V. S. Ryan-Mowrey, S. Surampudi, G. K. S. Prakash, J. Hu and I. Cheung, *J. Power Sources*, 2003, **119–121**, 359–367.
- 336 C. V. Amanchukwu, Z. Yu, X. Kong, J. Qin, Y. Cui and Z. Bao, *J. Am. Chem. Soc.*, 2020, **142**, 7393–7403.
- 337 K. Deng, Q. Zeng, D. Wang, Z. Liu, Z. Qiu, Y. Zhang, M. Xiao and Y. Meng, *J. Mater. Chem. A*, 2020, **8**, 1557–1577.
- 338 T. Zhang and E. Paillard, *Front. Chem. Sci. Eng.*, 2018, **12**, 577–591.
- 339 S. Tan, Y. J. Ji, Z. R. Zhang and Y. Yang, *Chem. Phys. Chem.*, 2014, **15**, 1956–1969.
- 340 K. Xu and C. A. Angell, *J. Electrochem. Soc.*, 1998, **145**, L70–L72.
- 341 K. Xu and C. A. Angell, *J. Electrochem. Soc.*, 2002, **149**, A920–A926.
- 342 X.-G. Sun and C. Austen Angell, *Solid State Ionics*, 2004, **175**, 257–260.
- 343 X.-G. Sun and C. A. Angell, *Electrochem. Commun.*, 2005, **7**, 261–266.
- 344 X. Sun and C. A. Angell, *Electrochem. Commun.*, 2009, **11**, 1418–1421.
- 345 L. Xue, K. Ueno, S.-Y. Lee and C. A. Angell, *J. Power Sources*, 2014, **262**, 123–128.
- 346 J. A. Seel and J. R. Dahn, *J. Electrochem. Soc.*, 2000, **147**, 892–898.
- 347 A. Abouimrane, I. Belharouak and K. Amine, *Electrochem. Commun.*, 2009, **11**, 1073–1076.
- 348 C. Li, Y. Zhao, H. Zhang, J. Liu, J. Jing, X. Cui and S. Li, *Electrochim. Acta*, 2013, **104**, 134–139.
- 349 L. Xue, S.-Y. Lee, Z. Zhao and C. A. Angell, *J. Power Sources*, 2015, **295**, 190–196.
- 350 R. T. Carlin, H. C. De Long, J. Fuller and P. C. Trulove, *J. Electrochem. Soc.*, 1994, **141**, L73–L76.
- 351 M.-C. Lin, M. Gong, B. Lu, Y. Wu, D.-Y. Wang, M. Guan, M. Angell, C. Chen, J. Yang, B.-J. Hwang and H. Dai, *Nature*, 2015, **520**, 324–328.
- 352 J. A. Read, A. V. Cresce, M. H. Ervin and K. Xu, *Energy Environ. Sci.*, 2014, **7**, 617–620.
- 353 X. Zhang, Y. Tang, F. Zhang and C.-S. Lee, *Adv. Energy Mater.*, 2016, **6**, 1502588.
- 354 M. Wang and Y. Tang, *Adv. Energy Mater.*, 2018, **8**, 1703320.
- 355 S. Rothermel, P. Meister, G. Schmuelling, O. Fromm, H.-W. Meyer, S. Nowak, M. Winter and T. Placke, *Energy Environ. Sci.*, 2014, **7**, 3412–3423.
- 356 Y. Wu, M. Gong, M.-C. Lin, C. Yuan, M. Angell, L. Huang, D.-Y. Wang, X. Zhang, J. Yang, B.-J. Hwang and H. Dai, *Adv. Mater.*, 2016, **28**, 9218–9222.
- 357 Q. Zhang, J.-J. Chen, X.-Y. Wang, C. Yang, M.-S. Zheng and Q.-F. Dong, *Phys. Chem. Chem. Phys.*, 2015, **17**, 10353–10357.
- 358 Z. Lu and J. R. Dahn, *J. Electrochem. Soc.*, 2001, **148**, A710.
- 359 N. Shao, X.-G. Sun, S. Dai and D.-e. Jiang, *J. Phys. Chem. B*, 2011, **115**, 12120–12125.
- 360 N. Shao, X.-G. Sun, S. Dai and D.-e. Jiang, *J. Phys. Chem. B*, 2012, **116**, 3235–3238.
- 361 L. Xing, W. Tu, J. Vatamanu, Q. Liu, W. Huang, Y. Wang, H. Zhou, R. Zeng and W. Li, *Electrochim. Acta*, 2014, **133**, 117–122.
- 362 Y. Wang, L. Xing, W. Li and D. Bedrov, *J. Phys. Chem. Lett.*, 2013, **4**, 3992–3999.
- 363 L. Xing, J. Vatamanu, O. Borodin, G. D. Smith and D. Bedrov, *J. Phys. Chem. C*, 2012, **116**, 23871–23881.
- 364 O. Borodin, W. Behl and T. R. Jow, *J. Phys. Chem. C*, 2013, **117**, 8661–8682.
- 365 C.-C. Su, M. He, P. C. Redfern, L. A. Curtiss, I. A. Shkrob and Z. Zhang, *Energy Environ. Sci.*, 2017, **10**, 900–904.

- 366 B. Flamme, M. Haddad, P. Phansavath, V. Ratovelomanana-Vidal and A. Chagnes, *ChemElectroChem*, 2018, **5**, 2279–2287.
- 367 J. Xia and J. R. Dahn, *J. Power Sources*, 2016, **324**, 704–711.
- 368 A. Hofmann, M. Schulz, S. Indris, R. Heinzmann and T. Hanemann, *Electrochim. Acta*, 2014, **147**, 704–711.
- 369 L. Mao, B. Li, X. Cui, Y. Zhao, X. Xu, X. Shi, S. Li and F. Li, *Electrochim. Acta*, 2012, **79**, 197–201.
- 370 Y. Watanabe, S.-i. Kinoshita, S. Wada, K. Hoshino, H. Morimoto and S.-i. Tobishima, *J. Power Sources*, 2008, **179**, 770–779.
- 371 F. Wu, J. Xiang, L. Li, J. Chen, G. Tan and R. Chen, *J. Power Sources*, 2012, **202**, 322–331.
- 372 T. Zhang, W. Porcher and E. Paillard, *J. Power Sources*, 2018, **395**, 212–220.
- 373 H. Zhou, Z. Yang, D. Xiao, K. Xiao and J. Li, *J. Mater. Sci.: Mater. Electron.*, 2018, **29**, 6648–6659.
- 374 G. Kumar, T. R. Kartha and B. S. Mallik, *J. Phys. Chem. C*, 2018, **122**, 26315–26325.
- 375 S. Li, B. Li, X. Xu, X. Shi, Y. Zhao, L. Mao and X. Cui, *J. Power Sources*, 2012, **209**, 295–300.
- 376 E. Björklund, M. Göttliger, K. Edström, R. Younesi and D. Brandell, *Batteries Supercaps*, 2020, **3**, 201–207.
- 377 J. Demeaux, E. De Vito, M. Le Digabel, H. Galiano, B. Claude-Montigny and D. Lemordant, *Phys. Chem. Chem. Phys.*, 2014, **16**, 5201–5212.
- 378 T. Zhang, I. de Meatza, X. Qi and E. Paillard, *J. Power Sources*, 2017, **356**, 97–102.
- 379 J. Xia, J. Self, L. Ma and J. R. Dahn, *J. Electrochem. Soc.*, 2015, **162**, A1424–A1431.
- 380 D. Lu, G. Xu, Z. Hu, Z. Cui, X. Wang, J. Li, L. Huang, X. Du, Y. Wang, J. Ma, X. Lu, H.-J. Lin, C.-T. Chen, A. A. Nugroho, L. H. Tjeng and G. Cui, *Small Methods*, 2019, **3**, 1900546.
- 381 Y. Abu-Lebdeh and I. Davidson, *J. Power Sources*, 2009, **189**, 576–579.
- 382 Y. Abu-Lebdeh and I. Davidson, *J. Electrochem. Soc.*, 2009, **156**, A60.
- 383 G.-Y. Kim and J. R. Dahn, *J. Electrochem. Soc.*, 2015, **162**, A437–A447.
- 384 Y.-S. Kim, T.-H. Kim, H. Lee and H.-K. Song, *Energy Environ. Sci.*, 2011, **4**, 4038–4045.
- 385 Y.-S. Kim, H. Lee and H.-K. Song, *ACS Appl. Mater. Interfaces*, 2014, **6**, 8913–8920.
- 386 S. H. Lee, J.-Y. Hwang, S.-J. Park, G.-T. Park and Y.-K. Sun, *Adv. Funct. Mater.*, 2019, **29**, 1902496.
- 387 Q. Zhang, K. Liu, F. Ding, W. Li, X. Liu and J. Zhang, *ACS Appl. Mater. Interfaces*, 2017, **9**, 29820–29828.
- 388 Q. Zhang, K. Liu, F. Ding, W. Li, X. Liu and J. Zhang, *Electrochim. Acta*, 2019, **298**, 818–826.
- 389 Y. Ji, Z. Zhang, M. Gao, Y. Li, M. J. McDonald and Y. Yang, *J. Electrochem. Soc.*, 2015, **162**, A774–A780.
- 390 M. Ue, K. Ida and S. Mori, *J. Electrochem. Soc.*, 1994, **141**, 2989–2996.
- 391 A. Brandt, P. Isken, A. Lex-Balducci and A. Balducci, *J. Power Sources*, 2012, **204**, 213–219.
- 392 O. Hanna, S. Luski and D. Aurbach, *J. Electrochem. Soc.*, 2016, **164**, A231–A236.
- 393 A. Narayanan Kirshnamoorthy, K. Oldiges, M. Winter, A. Heuer, I. Cekic-Laskovic, C. Holm and J. Smiatek, *Phys. Chem. Chem. Phys.*, 2018, **20**, 25701–25715.
- 394 D. M. Seo, O. Borodin, S.-D. Han, Q. Ly, P. D. Boyle and W. A. Henderson, *J. Electrochem. Soc.*, 2012, **159**, A553–A565.
- 395 D. M. Seo, O. Borodin, S.-D. Han, P. D. Boyle and W. A. Henderson, *J. Electrochem. Soc.*, 2012, **159**, A1489–A1500.
- 396 D. M. Seo, O. Borodin, D. Balogh, M. O'Connell, Q. Ly, S.-D. Han, S. Passerini and W. A. Henderson, *J. Electrochem. Soc.*, 2013, **160**, A1061–A1070.
- 397 M. Nagahama, N. Hasegawa and S. Okada, *J. Electrochem. Soc.*, 2010, **157**, A748–A752.
- 398 H. Duncan, N. Salem and Y. Abu-Lebdeh, *J. Electrochem. Soc.*, 2013, **160**, A838–A848.
- 399 D. Yaakov, Y. Gofer, D. Aurbach and I. C. Halalay, *J. Electrochem. Soc.*, 2010, **157**, A1383–A1391.
- 400 D. Farhat, F. Ghamouss, J. Maibach, K. Edström and D. Lemordant, *Chem. Phys. Chem.*, 2017, **18**, 1333–1344.
- 401 D. Farhat, D. Lemordant, J. Jacquemin and F. Ghamouss, *J. Electrochem. Soc.*, 2019, **166**, A3487–A3495.
- 402 I. Cekic-Laskovic, N. von Aspern, L. Imholt, S. Kaymaksiz, K. Oldiges, B. R. Rad and M. Winter, *Top. Curr. Chem.*, 2017, **375**, 37.
- 403 N. Ehteshami, A. Eguia-Barrio, I. de Meatza, W. Porcher and E. Paillard, *J. Power Sources*, 2018, **397**, 52–58.
- 404 N. Ehteshami and E. Paillard, *ECS Trans.*, 2017, **77**, 11–20.
- 405 H. Zhi, L. Xing, X. Zheng, K. Xu and W. Li, *J. Phys. Chem. Lett.*, 2017, **8**, 6048–6052.
- 406 S. Han, Y. Liu, H. Zhang, C. Fan, W. Fan, L. Yu and X. Du, *Surf. Interface Anal.*, 2020, **52**, 364–373.
- 407 W. R. McKinnon, *J. Electrochem. Soc.*, 1985, **132**, 364.
- 408 F. Li, T. Zhang, Y. Yamada, A. Yamada and H. Zhou, *Adv. Energy Mater.*, 2013, **3**, 532–538.
- 409 K. Ueno, J.-W. Park, A. Yamazaki, T. Mandai, N. Tachikawa, K. Dokko and M. Watanabe, *J. Phys. Chem. C*, 2013, **117**, 20509–20516.
- 410 D. W. McOwen, D. M. Seo, O. Borodin, J. Vatamanu, P. D. Boyle and W. A. Henderson, *Energy Environ. Sci.*, 2014, **7**, 416–426.
- 411 J. J. Hu, G. K. Long, S. Liu, G. R. Li and X. P. Gao, *Chem. Commun.*, 2014, **50**, 14647–14650.
- 412 Y. Yamada, K. Usui, C. H. Chiang, K. Kikuchi, K. Furukawa and A. Yamada, *ACS Appl. Mater. Interfaces*, 2014, **6**, 10892–10899.
- 413 K. Sodeyama, Y. Yamada, K. Aikawa, A. Yamada and Y. Tateyama, *J. Phys. Chem. C*, 2014, **118**, 14091–14097.
- 414 S.-i. Okuoka, Y. Ogasawara, Y. Suga, M. Hibino, T. Kudo, H. Ono, K. Yonehara, Y. Sumida, Y. Yamada, A. Yamada, M. Oshima, E. Tochigi, N. Shibata, Y. Ikuhara and N. Mizuno, *Sci. Rep.*, 2014, **4**, 5684.
- 415 J. Qian, W. A. Henderson, W. Xu, P. Bhattacharya, M. Engelhard, O. Borodin and J.-G. Zhang, *Nat. Commun.*, 2015, **6**, 6362.
- 416 J. Qian, B. D. Adams, J. Zheng, W. Xu, W. A. Henderson, J. Wang, M. E. Bowden, S. Xu, J. Hu and J.-G. Zhang, *Adv. Funct. Mater.*, 2016, **26**, 7094–7102.

- 417 S. Miyoshi, H. Nagano, T. Fukuda, T. Kurihara, M. Watanabe, S. Ida and T. Ishihara, *J. Electrochem. Soc.*, 2016, **163**, A1206–A1213.
- 418 K. Kimura, M. Yajima and Y. Tominaga, *Electrochem. Commun.*, 2016, **66**, 46–48.
- 419 B. Liu, W. Xu, P. Yan, X. Sun, M. E. Bowden, J. Read, J. Qian, D. Mei, C.-M. Wang and J.-G. Zhang, *Adv. Funct. Mater.*, 2016, **26**, 605–613.
- 420 Y. Pan, G. Wang and B. L. Lucht, *Electrochim. Acta*, 2016, **217**, 269–273.
- 421 T. Doi, R. Masuhara, M. Hashinokuchi, Y. Shimizu and M. Inaba, *Electrochim. Acta*, 2016, **209**, 219–224.
- 422 M. He, K. C. Lau, X. Ren, N. Xiao, W. D. McCulloch, L. A. Curtiss and Y. Wu, *Angew. Chem., Int. Ed.*, 2016, **55**, 15310–15314.
- 423 Y. Yamada and A. Yamada, *Chem. Lett.*, 2017, **46**, 1056–1064.
- 424 N. Takenaka, T. Fujie, A. Bouibes, Y. Yamada, A. Yamada and M. Nagaoka, *J. Phys. Chem. C*, 2018, **122**, 2564–2571.
- 425 L. Suo, O. Borodin, T. Gao, M. Olguin, J. Ho, X. Fan, C. Luo, C. Wang and K. Xu, *Science*, 2015, **350**, 938–943.
- 426 Y. Zhu, X. Fan, L. Suo, C. Luo, T. Gao and C. Wang, *ACS Nano*, 2016, **10**, 1529–1538.
- 427 J. Zheng, X. Fan, G. Ji, H. Wang, S. Hou, K. C. DeMella, S. R. Raghavan, J. Wang, K. Xu and C. Wang, *Nano Energy*, 2018, **50**, 431–440.
- 428 Y. Ding, J. Yun, H. Liu, Z. Wan, M. Shen, L. Zhang, Q. Qu and H. Zheng, *Pure Appl. Chem.*, 2014, **86**, 585.
- 429 B. Ravikumar, M. Mynam and B. Rai, *J. Phys. Chem. C*, 2018, **122**, 8173–8181.
- 430 S.-K. Jeong, M. Inaba, Y. Iriyama, T. Abe and Z. Ogumi, *Electrochem. Solid-State Lett.*, 2003, **6**, A13–A15.
- 431 Y. Yamada, Y. Takazawa, K. Miyazaki and T. Abe, *J. Phys. Chem. C*, 2010, **114**, 11680–11685.
- 432 Y. Yamada, Y. Koyama, T. Abe and Z. Ogumi, *J. Phys. Chem. C*, 2009, **113**, 8948–8953.
- 433 Y. Yamada, M. Yaegashi, T. Abe and A. Yamada, *Chem. Commun.*, 2013, **49**, 11194–11196.
- 434 M. Nie, D. P. Abraham, D. M. Seo, Y. Chen, A. Bose and B. L. Lucht, *J. Phys. Chem. C*, 2013, **117**, 25381–25389.
- 435 Y. Maeyoshi, D. Ding, M. Kubota, H. Ueda, K. Abe, K. Kanamura and H. Abe, *ACS Appl. Mater. Interfaces*, 2019, **11**, 25833–25843.
- 436 T. Doi, Y. Shimizu, M. Hashinokuchi and M. Inaba, *J. Electrochem. Soc.*, 2016, **163**, A2211–A2215.
- 437 Y. Yamada, J. Wang, S. Ko, E. Watanabe and A. Yamada, *Nat. Energy*, 2019, **4**, 269–280.
- 438 M. Takeuchi, N. Matubayasi, Y. Kameda, B. Minofar, S.-i. Ishiguro and Y. Umabayashi, *J. Phys. Chem. B*, 2012, **116**, 6476–6487.
- 439 H. Tsunekawa, A. Narumi, M. Sano, A. Hiwara, M. Fujita and H. Yokoyama, *J. Phys. Chem. B*, 2003, **107**, 10962–10966.
- 440 C.-H. Yim, J. Tam, H. Soboleski and Y. Abu-Lebdeh, *J. Electrochem. Soc.*, 2017, **164**, A1002–A1011.
- 441 Y. Ugata, R. Tatara, K. Ueno, K. Dokko and M. Watanabe, *J. Chem. Phys.*, 2020, **152**, 104502.
- 442 A. Nakanishi, K. Ueno, D. Watanabe, Y. Ugata, Y. Matsumae, J. Liu, M. L. Thomas, K. Dokko and M. Watanabe, *J. Phys. Chem. C*, 2019, **123**, 14229–14238.
- 443 S. Hwang, D.-H. Kim, J. H. Shin, J. E. Jang, K. H. Ahn, C. Lee and H. Lee, *J. Phys. Chem. C*, 2018, **122**, 19438–19446.
- 444 I. Popov, R. L. Sacci, N. C. Sanders, R. A. Matsumoto, M. W. Thompson, N. C. Osti, T. Kobayashi, M. Tyagi, E. Mamontov, M. Pruski, P. T. Cummings and A. P. Sokolov, *J. Phys. Chem. C*, 2020, **124**, 8457–8466.
- 445 J. Self, K. D. Fong and K. A. Persson, *ACS Energy Lett.*, 2019, **4**, 2843–2849.
- 446 J. Zheng, J. A. Lochala, A. Kwok, Z. D. Deng and J. Xiao, *Adv. Sci.*, 2017, **4**, 1700032.
- 447 P. Shi, H. Zheng, X. Liang, Y. Sun, S. Cheng, C. Chen and H. Xiang, *Chem. Commun.*, 2018, **54**, 4453–4456.
- 448 J. Alvarado, M. A. Schroeder, M. Zhang, O. Borodin, E. Gobrogge, M. Olguin, M. S. Ding, M. Gobet, S. Greenbaum, Y. S. Meng and K. Xu, *Mater. Today*, 2018, **21**, 341–353.
- 449 T. Doi, M. Hashinokuchi and M. Inaba, *Curr. Opin. Electrochem.*, 2018, **9**, 49–55.
- 450 A. von Wald Cresce, O. Borodin and K. Xu, *J. Phys. Chem. C*, 2012, **116**, 26111–26117.
- 451 O. Borodin and D. Bedrov, *J. Phys. Chem. C*, 2014, **118**, 18362–18371.
- 452 K. Xu and A. von Wald Cresce, *J. Mater. Res.*, 2012, **27**, 2327–2341.
- 453 K. Takada, Y. Yamada, E. Watanabe, J. Wang, K. Sodeyama, Y. Tateyama, K. Hirata, T. Kawase and A. Yamada, *ACS Appl. Mater. Interfaces*, 2017, **9**, 33802–33809.
- 454 A. Bouibes, N. Takenaka, S. Saha and M. Nagaoka, *J. Phys. Chem. Lett.*, 2019, **10**, 5949–5955.
- 455 T. Shiga, C.-a. Okuda, Y. Kato and H. Kondo, *J. Phys. Chem. C*, 2018, **122**, 9738–9745.
- 456 K. Matsumoto, K. Inoue, K. Nakahara, R. Yuge, T. Noguchi and K. Utsugi, *J. Power Sources*, 2013, **231**, 234–238.
- 457 L. Suo, Y.-S. Hu, H. Li, M. Armand and L. Chen, *Nat. Commun.*, 2013, **4**, 1481.
- 458 T. Takashi, Y. Kazuki, H. Takeshi, T. Mizuho, N. Megumi, K. Yuichi, T. Naoki, D. Kaoru and W. Masayoshi, *Chem. Lett.*, 2010, **39**, 753–755.
- 459 K. Yoshida, M. Nakamura, Y. Kazue, N. Tachikawa, S. Tsuzuki, S. Seki, K. Dokko and M. Watanabe, *J. Am. Chem. Soc.*, 2011, **133**, 13121–13129.
- 460 K. Ueno, K. Yoshida, M. Tsuchiya, N. Tachikawa, K. Dokko and M. Watanabe, *J. Phys. Chem. B*, 2012, **116**, 11323–11331.
- 461 T. Mandai, K. Yoshida, K. Ueno, K. Dokko and M. Watanabe, *Phys. Chem. Chem. Phys.*, 2014, **16**, 8761–8772.
- 462 K. Ueno, R. Tatara, S. Tsuzuki, S. Saito, H. Doi, K. Yoshida, T. Mandai, M. Matsugami, Y. Umabayashi, K. Dokko and M. Watanabe, *Phys. Chem. Chem. Phys.*, 2015, **17**, 8248–8257.
- 463 Z. Cao, M. Hashinokuchi, T. Doi and M. Inaba, *J. Electrochem. Soc.*, 2019, **166**, A82–A88.
- 464 D. Y. Wang, J. C. Burns and J. R. Dahn, *J. Electrochem. Soc.*, 2014, **161**, A1278–A1283.

- 465 W. Liu, J. Li, W. Li, H. Xu, C. Zhang and X. Qiu, *Nat. Commun.*, 2020, **11**, 3629.
- 466 Q. Liu, H. Xu, F. Wu, D. Mu, L. Shi, L. Wang, J. Bi and B. Wu, *ACS Appl. Energy Mater.*, 2019, **2**, 8878–8884.
- 467 W. Wang, J. Zhang, Q. Yang, S. Wang, W. Wang and B. Li, *ACS Appl. Mater. Interfaces*, 2020, **12**, 22901–22909.
- 468 S. Ko, Y. Yamada and A. Yamada, *Batteries Supercaps*, 2020, **3**, 910–916.
- 469 Z. Cao, M. Haruta, T. Doi and M. Inaba, *J. Electrochem. Soc.*, 2019, **166**, A4005–A4013.
- 470 X. Ren, L. Zou, S. Jiao, D. Mei, M. H. Engelhard, Q. Li, H. Lee, C. Niu, B. D. Adams, C. Wang, J. Liu, J.-G. Zhang and W. Xu, *ACS Energy Lett.*, 2019, **4**, 896–902.
- 471 Y. Leng, S. Ge, R. S. Longchamps, X.-G. Yang, T. Liu and C.-Y. Wang, *J. Electrochem. Soc.*, 2020, **167**, 110543.
- 472 J. Alvarado, M. A. Schroeder, T. P. Pollard, X. Wang, J. Z. Lee, M. Zhang, T. Wynn, M. Ding, O. Borodin, Y. S. Meng and K. Xu, *Energy Environ. Sci.*, 2019, **12**, 780–794.
- 473 S. Jiao, X. Ren, R. Cao, M. H. Engelhard, Y. Liu, D. Hu, D. Mei, J. Zheng, W. Zhao, Q. Li, N. Liu, B. D. Adams, C. Ma, J. Liu, J.-G. Zhang and W. Xu, *Nat. Energy*, 2018, **3**, 739–746.
- 474 H. Wu, Y. Xu, X. Ren, B. Liu, M. H. Engelhard, M. S. Ding, P. Z. El-Khoury, L. Zhang, Q. Li, K. Xu, C. Wang, J.-G. Zhang and W. Xu, *Adv. Energy Mater.*, 2019, **9**, 1902108.
- 475 J. Fu, X. Ji, J. Chen, L. Chen, X. Fan, D. Mu and C. Wang, *Angew. Chem., Int. Ed.*, 2020, **59**, 22194–22201.
- 476 X. Ren, L. Zou, X. Cao, M. H. Engelhard, W. Liu, S. D. Burton, H. Lee, C. Niu, B. E. Matthews, Z. Zhu, C. Wang, B. W. Arey, J. Xiao, J. Liu, J.-G. Zhang and W. Xu, *Joule*, 2019, **3**, 1662–1676.
- 477 Y. Lee, T. K. Lee, S. Kim, J. Lee, Y. Ahn, K. Kim, H. Ma, G. Park, S.-M. Lee, S. K. Kwak and N.-S. Choi, *Nano Energy*, 2020, **67**, 104309.
- 478 S. Lin, H. Hua, Z. Li and J. Zhao, *ACS Appl. Mater. Interfaces*, 2020, **12**, 33710–33718.
- 479 S. Chen, J. Zheng, L. Yu, X. Ren, M. H. Engelhard, C. Niu, H. Lee, W. Xu, J. Xiao, J. Liu and J.-G. Zhang, *Joule*, 2018, **2**, 1548–1558.
- 480 X. Zhang, L. Zou, Y. Xu, X. Cao, M. H. Engelhard, B. E. Matthews, L. Zhong, H. Wu, H. Jia, X. Ren, P. Gao, Z. Chen, Y. Qin, C. Kompella, B. W. Arey, J. Li, D. Wang, C. Wang, J.-G. Zhang and W. Xu, *Adv. Energy Mater.*, 2020, **10**, 2000368.
- 481 X. Zhang, H. Jia, Y. Xu, L. Zou, M. H. Engelhard, B. E. Matthews, C. Wang, J.-G. Zhang and W. Xu, *J. Power Sources Adv.*, 2020, **5**, 100024.
- 482 X. Ren, S. Chen, H. Lee, D. Mei, M. H. Engelhard, S. D. Burton, W. Zhao, J. Zheng, Q. Li, M. S. Ding, M. Schroeder, J. Alvarado, K. Xu, Y. S. Meng, J. Liu, J.-G. Zhang and W. Xu, *Chem*, 2018, **4**, 1877–1892.
- 483 D.-J. Yoo, S. Yang, K. J. Kim and J. W. Choi, *Angew. Chem., Int. Ed.*, 2020, **59**, 14869–14876.
- 484 W. Dai, N. Dong, Y. Xia, S. Chen, H. Luo, Y. Liu and Z. Liu, *Electrochim. Acta*, 2019, **320**, 134633.
- 485 N. Piao, X. Ji, H. Xu, X. Fan, L. Chen, S. Liu, M. N. Garaga, S. G. Greenbaum, L. Wang, C. Wang and X. He, *Adv. Energy Mater.*, 2020, **10**, 1903568.
- 486 Z. Hu, F. Xian, Z. Guo, C. Lu, X. Du, X. Cheng, S. Zhang, S. Dong, G. Cui and L. Chen, *Chem. Mater.*, 2020, **32**, 3405–3413.
- 487 J. Wang, Y. Yamada, K. Sodeyama, E. Watanabe, K. Takada, Y. Tateyama and A. Yamada, *Nat. Energy*, 2018, **3**, 22–29.
- 488 Y. Dong, N. Zhang, C. Li, Y. Zhang, M. Jia, Y. Wang, Y. Zhao, L. Jiao, F. Cheng and J. Xu, *ACS Appl. Energy Mater.*, 2019, **2**, 2708–2716.
- 489 H. Jia, L. Zou, P. Gao, X. Cao, W. Zhao, Y. He, M. H. Engelhard, S. D. Burton, H. Wang, X. Ren, Q. Li, R. Yi, X. Zhang, C. Wang, Z. Xu, X. Li, J.-G. Zhang and W. Xu, *Adv. Energy Mater.*, 2019, **9**, 1900784.
- 490 X. Cao, Y. Xu, L. Zhang, M. H. Engelhard, L. Zhong, X. Ren, H. Jia, B. Liu, C. Niu, B. E. Matthews, H. Wu, B. W. Arey, C. Wang, J.-G. Zhang and W. Xu, *ACS Energy Lett.*, 2019, **4**, 2529–2534.
- 491 Z. Peng, X. Cao, P. Gao, H. Jia, X. Ren, S. Roy, Z. Li, Y. Zhu, W. Xie, D. Liu, Q. Li, D. Wang, W. Xu and J.-G. Zhang, *Adv. Funct. Mater.*, 2020, **30**, 2001285.
- 492 E. Krämer, T. Schedlbauer, B. Hoffmann, L. Terborg, S. Nowak, H. J. Gores, S. Passerini and M. Winter, *J. Electrochem. Soc.*, 2013, **160**, A356–A360.
- 493 M. Dahbi, F. Ghamouss, F. Tran-Van, D. Lemordant and M. Anouti, *J. Power Sources*, 2011, **196**, 9743–9750.
- 494 K. Park, S. Yu, C. Lee and H. Lee, *J. Power Sources*, 2015, **296**, 197–203.
- 495 R. Petibon, L. Madec, D. W. Abarbanel and J. R. Dahn, *J. Power Sources*, 2015, **300**, 419–429.
- 496 W. Xu, J. Wang, F. Ding, X. Chen, E. Nasybulin, Y. Zhang and J.-G. Zhang, *Energy Environ. Sci.*, 2014, **7**, 513–537.
- 497 S. Saito, H. Watanabe, K. Ueno, T. Mandai, S. Seki, S. Tsuzuki, Y. Kameda, K. Dokko, M. Watanabe and Y. Umabayashi, *J. Phys. Chem. B*, 2016, **120**, 3378–3387.
- 498 X. Dong, Y. Lin, P. Li, Y. Ma, J. Huang, D. Bin, Y. Wang, Y. Qi and Y. Xia, *Angew. Chem.*, 2019, **131**, 5679–5683.
- 499 J. Scheers, S. Fantini and P. Johansson, *J. Power Sources*, 2014, **255**, 204–218.
- 500 M. Balaish, A. Kraytsberg and Y. Ein-Eli, *Phys. Chem. Chem. Phys.*, 2014, **16**, 2801–2822.
- 501 K. Yoshida, M. Tsuchiya, N. Tachikawa, K. Dokko and M. Watanabe, *J. Phys. Chem. C*, 2011, **115**, 18384–18394.
- 502 C. Zhang, K. Ueno, A. Yamazaki, K. Yoshida, H. Moon, T. Mandai, Y. Umabayashi, K. Dokko and M. Watanabe, *J. Phys. Chem. B*, 2014, **118**, 5144–5153.
- 503 C. Zhang, A. Yamazaki, J. Murai, J.-W. Park, T. Mandai, K. Ueno, K. Dokko and M. Watanabe, *J. Phys. Chem. C*, 2014, **118**, 17362–17373.
- 504 T. M. Pappenfus, W. A. Henderson, B. B. Owens, K. R. Mann and W. H. Smyrl, *J. Electrochem. Soc.*, 2004, **151**, A209–A215.
- 505 M. Xu, L. Zhou, L. Hao, L. Xing, W. Li and B. L. Lucht, *J. Power Sources*, 2011, **196**, 6794–6801.
- 506 S. Zugmann, D. Moosbauer, M. Amereller, C. Schreiner, F. Wudy, R. Schmitz, R. Schmitz, P. Isken, C. Dippel,

- R. Müller, M. Kunze, A. Lex-Balducci, M. Winter and H. J. Gores, *J. Power Sources*, 2011, **196**, 1417–1424.
- 507 J. Liu, Z. Chen, S. Busking, I. Belharouak and K. Amine, *J. Power Sources*, 2007, **174**, 852–855.
- 508 Y. Zhu, Y. Li and D. P. Abraham, *J. Electrochem. Soc.*, 2014, **161**, A1580–A1585.
- 509 T. T. Beyene, H. K. Bezabh, M. A. Weret, T. M. Hagos, C.-J. Huang, C.-H. Wang, W.-N. Su, H. Dai and B.-J. Hwang, *J. Electrochem. Soc.*, 2019, **166**, A1501–A1509.
- 510 P. Liu, Q. Ma, Z. Fang, J. Ma, Y.-S. Hu, Z.-B. Zhou, H. Li, X.-J. Huang and L.-Q. Chen, *Chin. Phys. B*, 2016, **25**, 078203.
- 511 F. Qiu, X. Li, H. Deng, D. Wang, X. Mu, P. He and H. Zhou, *Adv. Energy Mater.*, 2019, **9**, 1803372.
- 512 X. Liu, C. Shen, N. Gao, Q. Hou, F. Song, X. Tian, Y. He, J. Huang, Z. Fang and K. Xie, *Electrochim. Acta*, 2018, **289**, 422–427.
- 513 Q. Ma, Z. Fang, P. Liu, J. Ma, X. Qi, W. Feng, J. Nie, Y.-S. Hu, H. Li, X. Huang, L. Chen and Z. Zhou, *ChemElectroChem*, 2016, **3**, 531–536.
- 514 N. Dong, G. Yang, H. Luo, H. Xu, Y. Xia and Z. Liu, *J. Power Sources*, 2018, **400**, 449–456.
- 515 Q. Wang, S. M. Zakeeruddin, I. Exnar and M. Grätzel, *J. Electrochem. Soc.*, 2004, **151**, A1598–A1603.
- 516 Y. Yamada, K. Furukawa, K. Sodeyama, K. Kikuchi, M. Yaegashi, Y. Tateyama and A. Yamada, *J. Am. Chem. Soc.*, 2014, **136**, 5039–5046.
- 517 K. Dokko, D. Watanabe, Y. Ugata, M. L. Thomas, S. Tsuzuki, W. Shinoda, K. Hashimoto, K. Ueno, Y. Umabayashi and M. Watanabe, *J. Phys. Chem. B*, 2018, **122**, 10736–10745.
- 518 N. Zhang, N. Zaker, H. Li, A. Liu, J. Inglis, L. Jing, J. Li, Y. Li, G. A. Botton and J. R. Dahn, *Chem. Mater.*, 2019, **31**, 10150–10160.
- 519 K. Xu, M. S. Ding, S. Zhang, J. L. Allen and T. R. Jow, *J. Electrochem. Soc.*, 2002, **149**, A622–A626.
- 520 K. Xu, S. Zhang, J. L. Allen and T. R. Jow, *J. Electrochem. Soc.*, 2002, **149**, A1079–A1082.
- 521 C. W. Lee, R. Venkatachalapathy and J. Prakash, *Electrochem. Solid-State Lett.*, 2000, **3**, 63–65.
- 522 X. Wang, E. Yasukawa and S. Kasuya, *J. Electrochem. Soc.*, 2001, **148**, A1058–A1065.
- 523 X. L. Yao, S. Xie, C. H. Chen, Q. S. Wang, J. H. Sun, Y. L. Li and S. X. Lu, *J. Power Sources*, 2005, **144**, 170–175.
- 524 Y. E. Hyung, D. R. Vissers and K. Amine, *J. Power Sources*, 2003, **119–121**, 383–387.
- 525 J. Hu, Z. Jin, H. Zhong, H. Zhan, Y. Zhou and Z. Li, *J. Power Sources*, 2012, **197**, 297–300.
- 526 H. F. Xiang, H. Y. Xu, Z. Z. Wang and C. H. Chen, *J. Power Sources*, 2007, **173**, 562–564.
- 527 J. Kalthoff, G. G. Eshetu, D. Bresser and S. Passerini, *ChemSusChem*, 2015, **8**, 2154–2175.
- 528 K. Takada, Y. Yamada and A. Yamada, *ACS Appl. Mater. Interfaces*, 2019, **11**, 35770–35776.
- 529 W. Li, J. R. Dahn and D. S. Wainwright, *Science*, 1994, **264**, 1115–1118.
- 530 W. Li, W. R. McKinnon and J. R. Dahn, *J. Electrochem. Soc.*, 1994, **141**, 2310–2316.
- 531 Y. Wang, J. Yi and Y. Xia, *Adv. Energy Mater.*, 2012, **2**, 830–840.
- 532 H. Kim, J. Hong, K.-Y. Park, H. Kim, S.-W. Kim and K. Kang, *Chem. Rev.*, 2014, **114**, 11788–11827.
- 533 R. Ruffo, C. Wessells, R. A. Huggins and Y. Cui, *Electrochem. Commun.*, 2009, **11**, 247–249.
- 534 L. Suo, F. Han, X. Fan, H. Liu, K. Xu and C. Wang, *J. Mater. Chem. A*, 2016, **4**, 6639–6644.
- 535 L. Suo, O. Borodin, W. Sun, X. Fan, C. Yang, F. Wang, T. Gao, Z. Ma, M. Schroeder, A. von Cresce, S. M. Russell, M. Armand, A. Angell, K. Xu and C. Wang, *Angew. Chem., Int. Ed.*, 2016, **55**, 7136–7141.
- 536 F. Wang, Y. Lin, L. Suo, X. Fan, T. Gao, C. Yang, F. Han, Y. Qi, K. Xu and C. Wang, *Energy Environ. Sci.*, 2016, **9**, 3666–3673.
- 537 K. Xu, *Natl. Sci. Rev.*, 2016, **4**, 19–20.
- 538 C. Yang, J. Chen, T. Qing, X. Fan, W. Sun, A. von Cresce, M. S. Ding, O. Borodin, J. Vatamanu, M. A. Schroeder, N. Eidson, C. Wang and K. Xu, *Joule*, 2017, **1**, 122–132.
- 539 C. Yang, L. Suo, O. Borodin, F. Wang, W. Sun, T. Gao, X. Fan, S. Hou, Z. Ma, K. Amine, K. Xu and C. Wang, *Proc. Natl. Acad. Sci. U. S. A.*, 2017, **114**, 6197–6202.
- 540 S. Ko, Y. Yamada, K. Miyazaki, T. Shimada, E. Watanabe, Y. Tateyama, T. Kamiya, T. Honda, J. Akikusa and A. Yamada, *Electrochem. Commun.*, 2019, **104**, 106488.
- 541 J. Zhang, C. Cui, P.-F. Wang, Q. Li, L. Chen, F. Han, T. Jin, S. Liu, H. Choudhary, S. R. Raghavan, N. Eidson, A. von Cresce, L. Ma, J. Uddin, D. Addison, C. Yang and C. Wang, *Energy Environ. Sci.*, 2020, **13**, 2878–2887.
- 542 K. Xu and C. Wang, *Nat. Energy*, 2016, **1**, 16161.
- 543 Y. Yamada, K. Usui, K. Sodeyama, S. Ko, Y. Tateyama and A. Yamada, *Nat. Energy*, 2016, **1**, 16129.
- 544 J. Forero-Saboya, E. Hosseini-Bab-Anari, M. E. Abdelhamid, K. Moth-Poulsen and P. Johansson, *J. Phys. Chem. Lett.*, 2019, **10**, 4942–4946.
- 545 F. Wang, O. Borodin, M. S. Ding, M. Gobet, J. Vatamanu, X. Fan, T. Gao, N. Eidson, Y. Liang, W. Sun, S. Greenbaum, K. Xu and C. Wang, *Joule*, 2018, **2**, 927–937.
- 546 C. Yang, X. Ji, X. Fan, T. Gao, L. Suo, F. Wang, W. Sun, J. Chen, L. Chen, F. Han, L. Miao, K. Xu, K. Gerasopoulos and C. Wang, *Adv. Mater.*, 2017, **29**, 1701972.
- 547 X. He, B. Yan, X. Zhang, Z. Liu, D. Bresser, J. Wang, R. Wang, X. Cao, Y. Su, H. Jia, C. P. Grey, H. Frielinghaus, D. G. Truhlar, M. Winter, J. Li and E. Paillard, *Nat. Commun.*, 2018, **9**, 5320.
- 548 H. Wang, K. Huang, Y. Zeng, S. Yang and L. Chen, *Electrochim. Acta*, 2007, **52**, 3280–3285.
- 549 H. Wang, Y. Zeng, K. Huang, S. Liu and L. Chen, *Electrochim. Acta*, 2007, **52**, 5102–5107.
- 550 L. Suo, D. Oh, Y. Lin, Z. Zhuo, O. Borodin, T. Gao, F. Wang, A. Kushima, Z. Wang, H.-C. Kim, Y. Qi, W. Yang, F. Pan, J. Li, K. Xu and C. Wang, *J. Am. Chem. Soc.*, 2017, **139**, 18670–18680.
- 551 L. Suo, O. Borodin, Y. Wang, X. Rong, W. Sun, X. Fan, S. Xu, M. A. Schroeder, A. V. Cresce, F. Wang, C. Yang, Y.-S. Hu, K. Xu and C. Wang, *Adv. Energy Mater.*, 2017, **7**, 1701189.

- 552 H. Zhang, S. Jeong, B. Qin, D. Vieira Carvalho, D. Buchholz and S. Passerini, *ChemSusChem*, 2018, **11**, 1382–1389.
- 553 J. Han, H. Zhang, A. Varzi and S. Passerini, *ChemSusChem*, 2018, **11**, 3704–3707.
- 554 L. Jiang, L. Liu, J. Yue, Q. Zhang, A. Zhou, O. Borodin, L. Suo, H. Li, L. Chen, K. Xu and Y.-S. Hu, *Adv. Mater.*, 2020, **32**, 1904427.
- 555 S. Wheeler, I. Capone, S. Day, C. Tang and M. Pasta, *Chem. Mater.*, 2019, **31**, 2619–2626.
- 556 J. Yue, L. Lin, L. Jiang, Q. Zhang, Y. Tong, L. Suo, Y.-s. Hu, H. Li, X. Huang and L. Chen, *Adv. Energy Mater.*, 2020, **10**, 2000665.
- 557 J. Han, M. Zarrabeitia, A. Mariani, Z. Jusys, M. Hekmatfar, H. Zhang, D. Geiger, U. Kaiser, R. J. Behm, A. Varzi and S. Passerini, *Nano Energy*, 2020, **77**, 105176.
- 558 R.-S. Kühnel, D. Reber and C. Battaglia, *ACS Energy Lett.*, 2017, **2**, 2005–2006.
- 559 M. H. Lee, S. J. Kim, D. Chang, J. Kim, S. Moon, K. Oh, K.-Y. Park, W. M. Seong, H. Park, G. Kwon, B. Lee and K. Kang, *Mater. Today*, 2019, **29**, 26–36.
- 560 W. Li, K. Wang, M. Zhou, H. Zhan, S. Cheng and K. Jiang, *ACS Appl. Mater. Interfaces*, 2018, **10**, 22059–22066.
- 561 K. Nakamoto, R. Sakamoto, Y. Sawada, M. Ito and S. Okada, *Small Methods*, 2019, **3**, 1800220.
- 562 D. Luo, P. Lei, Y. Huang, G. Tian and X. Xiang, *J. Electroanal. Chem.*, 2019, **838**, 66–72.
- 563 D. P. Leonard, Z. Wei, G. Chen, F. Du and X. Ji, *ACS Energy Lett.*, 2018, **3**, 373–374.
- 564 L. Jiang, Y. Lu, C. Zhao, L. Liu, J. Zhang, Q. Zhang, X. Shen, J. Zhao, X. Yu, H. Li, X. Huang, L. Chen and Y.-S. Hu, *Nat. Energy*, 2019, **4**, 495–503.
- 565 J. Han, A. Mariani, H. Zhang, M. Zarrabeitia, X. Gao, D. V. Carvalho, A. Varzi and S. Passerini, *Energy Storage Mater.*, 2020, **30**, 196–205.
- 566 H. Chen, Z. Zhang, Z. Wei, G. Chen, X. Yang, C. Wang and F. Du, *Sustainable Energy Fuels*, 2020, **4**, 128–131.
- 567 Q. Zheng, S. Miura, K. Miyazaki, S. Ko, E. Watanabe, M. Okoshi, C.-P. Chou, Y. Nishimura, H. Nakai, T. Kamiya, T. Honda, J. Akikusa, Y. Yamada and A. Yamada, *Angew. Chem., Int. Ed.*, 2019, **58**, 14202–14207.
- 568 F. Wang, X. Fan, T. Gao, W. Sun, Z. Ma, C. Yang, F. Han, K. Xu and C. Wang, *ACS Cent. Sci.*, 2017, **3**, 1121–1128.
- 569 F. Wang, O. Borodin, T. Gao, X. Fan, W. Sun, F. Han, A. Faraone, J. A. Dura, K. Xu and C. Wang, *Nat. Mater.*, 2018, **17**, 543–549.
- 570 F. Wang, E. Hu, W. Sun, T. Gao, X. Ji, X. Fan, F. Han, X.-Q. Yang, K. Xu and C. Wang, *Energy Environ. Sci.*, 2018, **11**, 3168–3175.
- 571 P. Hu, M. Yan, T. Zhu, X. Wang, X. Wei, J. Li, L. Zhou, Z. Li, L. Chen and L. Mai, *ACS Appl. Mater. Interfaces*, 2017, **9**, 42717–42722.
- 572 J. Zhao, Y. Li, X. Peng, S. Dong, J. Ma, G. Cui and L. Chen, *Electrochem. Commun.*, 2016, **69**, 6–10.
- 573 F. Wan, Y. Zhang, L. Zhang, D. Liu, C. Wang, L. Song, Z. Niu and J. Chen, *Angew. Chem., Int. Ed.*, 2019, **58**, 7062–7067.
- 574 L. Zhang, I. A. Rodríguez-Pérez, H. Jiang, C. Zhang, D. P. Leonard, Q. Guo, W. Wang, S. Han, L. Wang and X. Ji, *Adv. Funct. Mater.*, 2019, **29**, 1902653.
- 575 X. Wu, Y. Xu, C. Zhang, D. P. Leonard, A. Markir, J. Lu and X. Ji, *J. Am. Chem. Soc.*, 2019, **141**, 6338–6344.
- 576 H. Qiu, X. Du, J. Zhao, Y. Wang, J. Ju, Z. Chen, Z. Hu, D. Yan, X. Zhou and G. Cui, *Nat. Commun.*, 2019, **10**, 5374.
- 577 C.-Y. Chen, K. Matsumoto, K. Kubota, R. Hagiwara and Q. Xu, *Adv. Energy Mater.*, 2019, **9**, 1900196.
- 578 W. Pan, Y. Wang, Y. Zhang, H. Y. H. Kwok, M. Wu, X. Zhao and D. Y. C. Leung, *J. Mater. Chem. A*, 2019, **7**, 17420–17425.
- 579 A. Zhou, L. Jiang, J. Yue, Y. Tong, Q. Zhang, Z. Lin, B. Liu, C. Wu, L. Suo, Y.-S. Hu, H. Li and L. Chen, *ACS Appl. Mater. Interfaces*, 2019, **11**, 41356–41362.
- 580 Z. Hu, Y. Guo, H. Jin, H. Ji and L.-J. Wan, *Chem. Commun.*, 2020, **56**, 2023–2026.
- 581 D. Reber, R. Figi, R.-S. Kühnel and C. Battaglia, *Electrochim. Acta*, 2019, **321**, 134644.
- 582 R.-S. Kühnel, D. Reber and C. Battaglia, *ACS Energy Lett.*, 2017, 2005–2006, DOI: 10.1021/acsenergylett.7b00623.
- 583 P. Lannelongue, R. Bouchal, E. Mourad, C. Bodin, M. Olarte, S. le Vot, F. Favier and O. Fontaine, *J. Electrochem. Soc.*, 2018, **165**, A657–A663.
- 584 X. Bu, L. Su, Q. Dou, S. Lei and X. Yan, *J. Mater. Chem. A*, 2019, **7**, 7541–7547.
- 585 Q. Dou, S. Lei, D.-W. Wang, Q. Zhang, D. Xiao, H. Guo, A. Wang, H. Yang, Y. Li, S. Shi and X. Yan, *Energy Environ. Sci.*, 2018, **11**, 3212–3219.
- 586 Q. Liu, J. Zhou, C. Song, X. Li, Z. Wang, J. Yang, J. Cheng, H. Li and B. Wang, *Energy Storage Mater.*, 2020, **24**, 495–503.
- 587 L. Dai, O. Arcelus, L. Sun, H. Wang, J. Carrasco, H. Zhang, W. Zhang and J. Tang, *J. Mater. Chem. A*, 2019, **7**, 24800–24806.
- 588 M. Ma, Z. Shi, Y. Li, Y. Yang, Y. Zhang, Y. Wu, H. Zhao and E. Xie, *J. Mater. Chem. A*, 2020, **8**, 4827–4835.
- 589 V. L. Martins and R. M. Torresi, *Curr. Opin. Electrochem.*, 2020, **21**, 62–68.
- 590 Z. Liu, Y. Huang, Y. Huang, Q. Yang, X. Li, Z. Huang and C. Zhi, *Chem. Soc. Rev.*, 2020, **49**, 180–232.
- 591 M. Toupin, T. Brousse and D. Bélanger, *Chem. Mater.*, 2004, **16**, 3184–3190.
- 592 M. Zhang, S. Makino, D. Mochizuki and W. Sugimoto, *J. Power Sources*, 2018, **396**, 498–505.
- 593 Y. Zhang, P. Nie, C. Xu, G. Xu, B. Ding, H. Dou and X. Zhang, *Electrochim. Acta*, 2018, **268**, 512–519.
- 594 A. Tatlisu, Z. Huang and R. Chen, *ChemSusChem*, 2018, **11**, 3899–3904.
- 595 X. Bu, Y. Zhang, L. Su, Q. Dou, Y. Xue and X. Lu, *Ionics*, 2019, **25**, 6007–6015.
- 596 T. Qin, Z. Xu, Z. Wang, S. Peng and D. He, *J. Mater. Chem. A*, 2019, **7**, 26011–26019.
- 597 W. Deng, X. Wang, C. Liu, C. Li, J. Chen, N. Zhu, R. Li and M. Xue, *Energy Storage Mater.*, 2019, **20**, 373–379.
- 598 J. Qin, S. Wang, F. Zhou, P. Das, S. Zheng, C. Sun, X. Bao and Z.-S. Wu, *Energy Storage Mater.*, 2019, **18**, 397–404.

- 599 Y. Yokoyama, T. Fukutsuka, K. Miyazaki and T. Abe, *J. Electrochem. Soc.*, 2018, **165**, A3299–A3303.
- 600 J. Zheng, G. Tan, P. Shan, T. Liu, J. Hu, Y. Feng, L. Yang, M. Zhang, Z. Chen, Y. Lin, J. Lu, J. C. Neuefeind, Y. Ren, K. Amine, L.-W. Wang, K. Xu and F. Pan, *Chem*, 2018, **4**, 2872–2882.
- 601 R. Imhof and P. Novák, *J. Electrochem. Soc.*, 1998, **145**, 1081–1087.
- 602 S. Ko, Y. Yamada and A. Yamada, *ACS Appl. Mater. Interfaces*, 2019, **11**, 45554–45560.
- 603 N. Dubouis, P. Lemaire, B. Mirvaux, E. Salager, M. Deschamps and A. Grimaud, *Energy Environ. Sci.*, 2018, **11**, 3491–3499.
- 604 N. Dubouis, A. Serva, E. Salager, M. Deschamps, M. Salanne and A. Grimaud, *J. Phys. Chem. Lett.*, 2018, **9**, 6683–6688.
- 605 L. Droguet, A. Grimaud, O. Fontaine and J.-M. Tarascon, *Adv. Energy Mater.*, 2020, **10**, 2002440.
- 606 R.-S. Kühnel, D. Reber and C. Battaglia, *J. Electrochem. Soc.*, 2020, **167**, 070544.
- 607 N. Takenaka, T. Inagaki, T. Shimada, Y. Yamada, M. Nagaoka and A. Yamada, *J. Chem. Phys.*, 2020, **152**, 124706.
- 608 J.-Y. Luo, W.-J. Cui, P. He and Y.-Y. Xia, *Nat. Chem.*, 2010, **2**, 760–765.
- 609 G. A. Giffin, *J. Mater. Chem. A*, 2016, **4**, 13378–13389.
- 610 M. Galiński, A. Lewandowski and I. Stepniak, *Electrochim. Acta*, 2006, **51**, 5567–5580.
- 611 J. P. Hallett and T. Welton, *Chem. Rev.*, 2011, **111**, 3508–3576.
- 612 M. V. Fedorov and A. A. Kornyshev, *Chem. Rev.*, 2014, **114**, 2978–3036.
- 613 A. Eftekhari, Y. Liu and P. Chen, *J. Power Sources*, 2016, **334**, 221–239.
- 614 M. Armand, F. Endres, D. R. MacFarlane, H. Ohno and B. Scrosati, *Nat. Mater.*, 2009, **8**, 621–629.
- 615 A. Lewandowski and A. Świdorska-Mocek, *J. Power Sources*, 2009, **194**, 601–609.
- 616 S. Wilken, S. Xiong, J. Scheers, P. Jacobsson and P. Johansson, *J. Power Sources*, 2015, **275**, 935–942.
- 617 M. C. Buzzeo, R. G. Evans and R. G. Compton, *Chem. Phys. Chem.*, 2004, **5**, 1106–1120.
- 618 R. S. Kühnel, N. Böckenfeld, S. Passerini, M. Winter and A. Balducci, *Electrochim. Acta*, 2011, **56**, 4092–4099.
- 619 Q. Yang, Z. Zhang, X.-G. Sun, Y.-S. Hu, H. Xing and S. Dai, *Chem. Soc. Rev.*, 2018, **47**, 2020–2064.
- 620 H. Matsumoto, H. Sakaebe, K. Tatsumi, M. Kikuta, E. Ishiko and M. Kono, *J. Power Sources*, 2006, **160**, 1308–1313.
- 621 Q. Zhou, W. A. Henderson, G. B. Appetecchi, M. Montanino and S. Passerini, *J. Phys. Chem. B*, 2008, **112**, 13577–13580.
- 622 A. Guerfi, S. Duchesne, Y. Kobayashi, A. Vijh and K. Zaghib, *J. Power Sources*, 2008, **175**, 866–873.
- 623 H. Nakagawa, S. Izuchi, K. Kuwana, T. Nukuda and Y. Aihara, *J. Electrochem. Soc.*, 2003, **150**, A695.
- 624 B. Garcia, S. Lavallée, G. Perron, C. Michot and M. Armand, *Electrochim. Acta*, 2004, **49**, 4583–4588.
- 625 J.-K. Kim, A. Matic, J.-H. Ahn and P. Jacobsson, *J. Power Sources*, 2010, **195**, 7639–7643.
- 626 K. Dong, S. Zhang, D. Wang and X. Yao, *J. Phys. Chem. A*, 2006, **110**, 9775–9782.
- 627 Z.-B. Zhou, H. Matsumoto and K. Tatsumi, *Chem. – Eur. J.*, 2004, **10**, 6581–6591.
- 628 M. Hajime, Y. Masahiro, T. Kazumi, N. Masakatsu, K. Yukiko and M. Yoshinori, *Chem. Lett.*, 2000, 922–923.
- 629 H. Sakaebe and H. Matsumoto, *Electrochem. Commun.*, 2003, **5**, 594–598.
- 630 E. T. Fox, J. E. F. Weaver and W. A. Henderson, *J. Phys. Chem. C*, 2012, **116**, 5270–5274.
- 631 J. H. Shin, P. Basak, J. B. Kerr and E. J. Cairns, *Electrochim. Acta*, 2008, **54**, 410–414.
- 632 Q. Zhou, P. D. Boyle, L. Malpezzi, A. Mele, J.-H. Shin, S. Passerini and W. A. Henderson, *Chem. Mater.*, 2011, **23**, 4331–4337.
- 633 J. Zheng, D. Zhu, Y. Yang and Y. Fung, *Electrochim. Acta*, 2012, **59**, 14–22.
- 634 H. Sakaebe, H. Matsumoto and K. Tatsumi, *J. Power Sources*, 2005, **146**, 693–697.
- 635 H. Sakaebe, H. Matsumoto and K. Tatsumi, *Electrochim. Acta*, 2007, **53**, 1048–1054.
- 636 K. Tsunashima and M. Sugiya, *Electrochem. Commun.*, 2007, **9**, 2353–2358.
- 637 T. Katsuhiko, Y. Fumihiko and S. Masashi, *Chem. Lett.*, 2008, **37**, 314–315.
- 638 K. Tsunashima, A. Kawabata, M. Matsumiya, S. Kodama, R. Enomoto, M. Sugiya and Y. Kunugi, *Electrochem. Commun.*, 2011, **13**, 178–181.
- 639 K. Tsunashima, Y. Ono and M. Sugiya, *Electrochim. Acta*, 2011, **56**, 4351–4355.
- 640 K. J. Fraser and D. R. MacFarlane, *Aust. J. Chem.*, 2009, **62**, 309–321.
- 641 A. I. Bhatt, I. May, V. A. Volkovich, M. E. Hetherington, B. Lewin, R. C. Thied and N. Ertok, *J. Chem. Soc., Dalton Trans.*, 2002, 4532–4534, DOI: 10.1039/B208968H.
- 642 W. Weng, Z. Zhang, J. Lu and K. Amine, *Chem. Commun.*, 2011, **47**, 11969–11971.
- 643 S. P. Ong, O. Andreussi, Y. Wu, N. Marzari and G. Ceder, *Chem. Mater.*, 2011, **23**, 2979–2986.
- 644 S. Pandian, S. G. Raju, K. S. Hariharan, S. M. Kolake, D.-H. Park and M.-J. Lee, *J. Power Sources*, 2015, **286**, 204–209.
- 645 V. Borgel, E. Markevich, D. Aurbach, G. Semrau and M. Schmidt, *J. Power Sources*, 2009, **189**, 331–336.
- 646 E. Markevich, V. Baranchugov and D. Aurbach, *Electrochem. Commun.*, 2006, **8**, 1331–1334.
- 647 J. J. Fillion and J. F. Brennecke, *J. Chem. Eng. Data*, 2017, **62**, 1884–1901.
- 648 S. Omar, J. Lemus, E. Ruiz, V. R. Ferro, J. Ortega and J. Palomar, *J. Phys. Chem. B*, 2014, **118**, 2442–2450.
- 649 E. Karpierz, L. Niedzicki, T. Trzeciak, M. Zawadzki, M. Dranka, J. Zachara, G. Z. Żukowska, A. Bitner-Michalska and W. Wieczorek, *Sci. Rep.*, 2016, **6**, 35587.
- 650 M. Montanino, M. Moreno, F. Alessandrini, G. B. Appetecchi, S. Passerini, Q. Zhou and W. A. Henderson, *Electrochim. Acta*, 2012, **60**, 163–169.

- 651 L. Lombardo, S. Brutti, M. A. Navarra, S. Panero and P. Reale, *J. Power Sources*, 2013, **227**, 8–14.
- 652 M. A. Navarra, J. Manzi, L. Lombardo, S. Panero and B. Scrosati, *ChemSusChem*, 2011, **4**, 125–130.
- 653 I. Quinzeni, S. Ferrari, E. Quartarone, C. Tomasi, M. Fagnoni and P. Mustarelli, *J. Power Sources*, 2013, **237**, 204–209.
- 654 C. Arbizzani, G. Gabrielli and M. Mastragostino, *J. Power Sources*, 2011, **196**, 4801–4805.
- 655 A. Balducci, S. S. Jeong, G. T. Kim, S. Passerini, M. Winter, M. Schmuck, G. B. Appetecchi, R. Marcilla, D. Mecerreyes, V. Barsukov, V. Khomenko, I. Cantero, I. De Meazza, M. Holzapfel and N. Tran, *J. Power Sources*, 2011, **196**, 9719–9730.
- 656 N. Plylahan, M. Kerner, D.-H. Lim, A. Matic and P. Johansson, *Electrochim. Acta*, 2016, **216**, 24–34.
- 657 J. R. Nair, F. Colò, A. Kazzazi, M. Moreno, D. Bresser, R. Lin, F. Bella, G. Meligrana, S. Fantini, E. Simonetti, G. B. Appetecchi, S. Passerini and C. Gerbaldi, *J. Power Sources*, 2019, **412**, 398–407.
- 658 X. Gao, Y. Ding, Q. Qu, G. Liu, V. S. Battaglia and H. Zheng, *Electrochim. Acta*, 2018, **260**, 640–647.
- 659 C. Ma, D. Wang, Y. Yang, Q. Wu, Z. Chen, C. Zhu, Y. Gao and C. Li, *J. Electrochem. Soc.*, 2019, **166**, A3441–A3447.
- 660 X. Gao, G. Zhu, Q. Qu, G. Liu, V. S. Battaglia and H. Zheng, *J. Electrochem. Soc.*, 2018, **165**, A3844–A3853.
- 661 S. Zhang, J. Li, N. Jiang, X. Li, S. Pasupath, Y. Fang, Q. Liu and D. Dang, *Chem. – Asian J.*, 2019, **14**, 2810–2814.
- 662 J. Xiang, F. Wu, R. Chen, L. Li and H. Yu, *J. Power Sources*, 2013, **233**, 115–120.
- 663 J.-H. Shin, W. A. Henderson and S. Passerini, *Electrochem. Solid-State Lett.*, 2005, **8**, A125.
- 664 J. R. Nair, L. Porcarelli, F. Bella and C. Gerbaldi, *ACS Appl. Mater. Interfaces*, 2015, **7**, 12961–12971.
- 665 G. Yang, Y. Song, Q. Wang, L. Zhang and L. Deng, *Mater. Des.*, 2020, **190**, 108563.
- 666 F. Wu, Q. Zhu, R. Chen, N. Chen, Y. Chen and L. Li, *Nano Energy*, 2015, **13**, 546–553.
- 667 L. Dong, F. Liang, D. Wang, C. Zhu, J. Liu, D. Gui and C. Li, *Electrochim. Acta*, 2018, **270**, 426–433.
- 668 F. Liang, J. Yu, D. wang, L. Dong, C. Ma, J. Chen, B. Yang, C. Zhu, Y. Gao and C. Li, *Electrochim. Acta*, 2019, **307**, 83–91.
- 669 M. Forsyth, G. M. A. Girard, A. Basile, M. Hilder, D. R. MacFarlane, F. Chen and P. C. Howlett, *Electrochim. Acta*, 2016, **220**, 609–617.
- 670 G. M. A. Girard, M. Hilder, H. Zhu, D. Nucciarone, K. Whitbread, S. Zavorine, M. Moser, M. Forsyth, D. R. MacFarlane and P. C. Howlett, *Phys. Chem. Chem. Phys.*, 2015, **17**, 8706–8713.
- 671 H. Yoon, P. C. Howlett, A. S. Best, M. Forsyth and D. R. MacFarlane, *J. Electrochem. Soc.*, 2013, **160**, A1629–A1637.
- 672 F. Chen, R. Kerr and M. Forsyth, *J. Chem. Phys.*, 2018, **148**, 193813.
- 673 J. Tong, S. Wu, N. von Solms, X. Liang, F. Huo, Q. Zhou, H. He and S. Zhang, *Front. Chem.*, 2020, **7**, 945.
- 674 M. Forsyth, L. Porcarelli, X. Wang, N. Goujon and D. Mecerreyes, *Acc. Chem. Res.*, 2019, **52**, 686–694.
- 675 V. Lesch, Z. Li, D. Bedrov, O. Borodin and A. Heuer, *Phys. Chem. Chem. Phys.*, 2016, **18**, 382–392.
- 676 A. Heist and S.-H. Lee, *J. Electrochem. Soc.*, 2019, **166**, A1860–A1866.
- 677 A. Heist, S. Hafner and S.-H. Lee, *J. Electrochem. Soc.*, 2019, **166**, A873–A879.
- 678 C. Liu, X. Ma, F. Xu, L. Zheng, H. Zhang, W. Feng, X. Huang, M. Armand, J. Nie, H. Chen and Z. Zhou, *Electrochim. Acta*, 2014, **149**, 370–385.
- 679 Q. Liu, T. L. Dzwiniel, K. Z. Pupek and Z. Zhang, *J. Electrochem. Soc.*, 2019, **166**, A3959–A3964.
- 680 H. Sun, G. Zhu, Y. Zhu, M.-C. Lin, H. Chen, Y.-Y. Li, W. H. Hung, B. Zhou, X. Wang, Y. Bai, M. Gu, C.-L. Huang, H.-C. Tai, X. Xu, M. Angell, J.-J. Shyue and H. Dai, *Adv. Mater.*, 2020, **32**, 2001741.
- 681 M. Hajime, T. Naohiro, U. Tatsuya, T. Seiji, S. Hikari, A. Kinji and T. Kuniaki, *Chem. Lett.*, 2008, **37**, 1020–1021.
- 682 H. Hong-Bo, Z. Yi-Xuan, L. Kai, N. Jin, H. Xue-Jie, A. Michel and Z. Zhi-Bin, *Chem. Lett.*, 2010, **39**, 472–474.
- 683 K. Liu, Y.-X. Zhou, H.-B. Han, S.-S. Zhou, W.-F. Feng, J. Nie, H. Li, X.-J. Huang, M. Armand and Z.-B. Zhou, *Electrochim. Acta*, 2010, **55**, 7145–7151.
- 684 C. Austen Angell, Y. Ansari and Z. Zhao, *Faraday Discuss.*, 2012, **154**, 9–27.
- 685 T. Mandai, R. Nozawa, S. Tsuzuki, K. Yoshida, K. Ueno, K. Dokko and M. Watanabe, *J. Phys. Chem. B*, 2013, **117**, 15072–15085.
- 686 N. Arai, H. Watanabe, E. Nozaki, S. Seki, S. Tsuzuki, K. Ueno, K. Dokko, M. Watanabe, Y. Kameda and Y. Umabayashi, *J. Phys. Chem. Lett.*, 2020, **11**, 4517–4523.
- 687 D. Dong, F. Sälzer, B. Roling and D. Bedrov, *Phys. Chem. Chem. Phys.*, 2018, **20**, 29174–29183.
- 688 T. Tamura, T. Hachida, K. Yoshida, N. Tachikawa, K. Dokko and M. Watanabe, *J. Power Sources*, 2010, **195**, 6095–6100.
- 689 A. Orita, K. Kamijima, M. Yoshida, K. Dokko and M. Watanabe, *J. Power Sources*, 2011, **196**, 3874–3880.
- 690 H. Zhao, X. Yu, J. Li, B. Li, H. Shao, L. Li and Y. Deng, *J. Mater. Chem. A*, 2019, **7**, 8700–8722.
- 691 Y. Qian, S. Hu, X. Zou, Z. Deng, Y. Xu, Z. Cao, Y. Kang, Y. Deng, Q. Shi, K. Xu and Y. Deng, *Energy Storage Mater.*, 2019, **20**, 208–215.
- 692 S. S. Zhang, *J. Power Sources*, 2006, **162**, 1379–1394.
- 693 C.-G. Shi, C.-H. Shen, X.-X. Peng, C.-X. Luo, L.-F. Shen, W.-J. Sheng, J.-J. Fan, Q. Wang, S.-J. Zhang, B.-B. Xu, J.-J. Xian, Y.-M. Wei, L. Huang, J.-T. Li and S.-G. Sun, *Nano Energy*, 2019, **65**, 104084.
- 694 W. Zhao, Y. Ji, Z. Zhang, M. Lin, Z. Wu, X. Zheng, Q. Li and Y. Yang, *Curr. Opin. Electrochem.*, 2017, **6**, 84–91.
- 695 Y. Wang and W.-H. Zhong, *ChemElectroChem*, 2015, **2**, 22–36.
- 696 H. Zhang, G. G. Eshetu, X. Judez, C. Li, L. M. Rodriguez-Martínez and M. Armand, *Angew. Chem., Int. Ed.*, 2018, **57**, 15002–15027.

- 697 L. Cao, M. Skyllas-Kazacos, C. Menictas and J. Noack, *J. Energy Chem.*, 2018, **27**, 1269–1291.
- 698 A. M. Haregewoin, A. S. Wotango and B.-J. Hwang, *Energy Environ. Sci.*, 2016, **9**, 1955–1988.
- 699 J.-G. Han, K. Kim, Y. Lee and N.-S. Choi, *Adv. Mater.*, 2019, **31**, 1804822.
- 700 K. Kim, H. Ma, S. Park and N.-S. Choi, *ACS Energy Lett.*, 2020, 1537–1553, DOI: 10.1021/acscenergylett.0c00468.
- 701 D. Aurbach, K. Gamolsky, B. Markovsky, Y. Gofer, M. Schmidt and U. Heider, *Electrochim. Acta*, 2002, **47**, 1423–1439.
- 702 Y. Jin, N.-J. H. Kneusels, L. E. Marbella, E. Castillo-Martínez, P. C. M. M. Magusin, R. S. Weatherup, E. Jónsson, T. Liu, S. Paul and C. P. Grey, *J. Am. Chem. Soc.*, 2018, **140**, 9854–9867.
- 703 Y. Wang, S. Nakamura, K. Tasaki and P. B. Balbuena, *J. Am. Chem. Soc.*, 2002, **124**, 4408–4421.
- 704 M. Fujimoto, M. Takahashi and K. Nishio, *US Pat.*, 5352548, 1994.
- 705 B. Simon and J.-P. Boeue, *US Pat.*, 5626981, 1997.
- 706 Y. Naruse, S. Fujita and A. Omaru, *US Pat.*, 5714281, 1998.
- 707 J. Barker and F. Gao, *US Pat.*, 5712059, 1998.
- 708 L. El Ouatani, R. Dedryvère, C. Siret, P. Biensan, S. Reynaud, P. Iratçabal and D. Gonbeau, *J. Electrochem. Soc.*, 2009, **156**, A103.
- 709 A. L. Michan, B. S. Parimalam, M. Leskes, R. N. Kerber, T. Yoon, C. P. Grey and B. L. Lucht, *Chem. Mater.*, 2016, **28**, 8149–8159.
- 710 H. Ota, K. Shima, M. Ue and J.-i. Yamaki, *Electrochim. Acta*, 2004, **49**, 565–572.
- 711 D. Takamatsu, Y. Orikasa, S. Mori, T. Nakatsutsumi, K. Yamamoto, Y. Koyama, T. Minato, T. Hirano, H. Tanida, H. Arai, Y. Uchimoto and Z. Ogumi, *J. Phys. Chem. C*, 2015, **119**, 9791–9797.
- 712 J. C. Burns, N. N. Sinha, D. J. Coyle, G. Jain, C. M. VanElzen, W. M. Lamanna, A. Xiao, E. Scott, J. P. Gardner and J. R. Dahn, *J. Electrochem. Soc.*, 2011, **159**, A85–A90.
- 713 W. J. Lee, K. Prasanna, Y. N. Jo, K. J. Kim, H. S. Kim and C. W. Lee, *Phys. Chem. Chem. Phys.*, 2014, **16**, 17062–17071.
- 714 E.-G. Shim, T.-H. Nam, J.-G. Kim, H.-S. Kim and S.-I. Moon, *J. Power Sources*, 2007, **172**, 901–907.
- 715 J.-Y. Eom, I.-H. Jung and J.-H. Lee, *J. Power Sources*, 2011, **196**, 9810–9814.
- 716 R. Petibon, C. P. Aiken, N. N. Sinha, J. C. Burns, H. Ye, C. M. VanElzen, G. Jain, S. Trussler and J. R. Dahn, *J. Electrochem. Soc.*, 2012, **160**, A117–A124.
- 717 D. Y. Wang, N. N. Sinha, J. C. Burns, R. Petibon and J. R. Dahn, *J. Power Sources*, 2014, **270**, 68–78.
- 718 J. C. Burns, G. Jain, A. J. Smith, K. W. Eberman, E. Scott, J. P. Gardner and J. R. Dahn, *J. Electrochem. Soc.*, 2011, **158**, A255.
- 719 N. N. Sinha, A. J. Smith, J. C. Burns, G. Jain, K. W. Eberman, E. Scott, J. P. Gardner and J. R. Dahn, *J. Electrochem. Soc.*, 2011, **158**, A1194.
- 720 R. Petibon, J. Xia, J. C. Burns and J. R. Dahn, *J. Electrochem. Soc.*, 2014, **161**, A1618–A1624.
- 721 H. J. Santner, K. C. Möller, J. Ivančo, M. G. Ramsey, F. P. Netzer, S. Yamaguchi, J. O. Besenhard and M. Winter, *J. Power Sources*, 2003, **119–121**, 368–372.
- 722 L. El Ouatani, R. Dedryvère, C. Siret, P. Biensan and D. Gonbeau, *J. Electrochem. Soc.*, 2009, **156**, A468.
- 723 K. Yamamoto, T. Minato, S. Mori, D. Takamatsu, Y. Orikasa, H. Tanida, K. Nakanishi, H. Murayama, T. Masese, T. Mori, H. Arai, Y. Koyama, Z. Ogumi and Y. Uchimoto, *J. Phys. Chem. C*, 2014, **118**, 9538–9543.
- 724 S. Grugeon, P. Jankowski, D. Cailieu, C. Forestier, L. Sannier, M. Armand, P. Johansson and S. Laruelle, *J. Power Sources*, 2019, **427**, 77–84.
- 725 J. Chai, Z. Liu, J. Ma, J. Wang, X. Liu, H. Liu, J. Zhang, G. Cui and L. Chen, *Adv. Sci.*, 2017, **4**, 1600377.
- 726 E. Bolimowska, F. Castiglione, J. Devemy, H. Rouault, A. Mele, A. A. H. Pádua and C. C. Santini, *J. Phys. Chem. B*, 2018, **122**, 8560–8569.
- 727 J. E. Morales-Ugarte, E. Bolimowska, H. Rouault, J. Santos-Peña, C. C. Santini and A. Benayad, *J. Phys. Chem. C*, 2018, **122**, 18223–18230.
- 728 E. Bolimowska, J. E. Morales-Ugarte, H. Rouault, J. Santos-Peña, C. Santini and A. Benayad, *J. Phys. Chem. C*, 2017, **121**, 16166–16173.
- 729 Y. Hu, W. Kong, H. Li, X. Huang and L. Chen, *Electrochem. Commun.*, 2004, **6**, 126–131.
- 730 R. Petibon, E. C. Henry, J. C. Burns, N. N. Sinha and J. R. Dahn, *J. Electrochem. Soc.*, 2013, **161**, A66–A74.
- 731 X. Zuo, J. Wu, M. Zhao, C. Wang, J. Liu and J. Nan, *Ionics*, 2016, **22**, 201–208.
- 732 J. Li, W. Yao, Y. S. Meng and Y. Yang, *J. Phys. Chem. C*, 2008, **112**, 12550–12556.
- 733 S. Y. Lee and Y. J. Park, *ACS Omega*, 2020, **5**, 3579–3587.
- 734 G. H. Lane, A. S. Best, D. R. MacFarlane, M. Forsyth and A. F. Hollenkamp, *Electrochim. Acta*, 2010, **55**, 2210–2215.
- 735 C. Korepp, H. J. Santner, T. Fujii, M. Ue, J. O. Besenhard, K. C. Möller and M. Winter, *J. Power Sources*, 2006, **158**, 578–582.
- 736 J.-T. Lee, Y.-W. Lin and Y.-S. Jan, *J. Power Sources*, 2004, **132**, 244–248.
- 737 K. Abe, H. Yoshitake, T. Kitakura, T. Hattori, H. Wang and M. Yoshio, *Electrochim. Acta*, 2004, **49**, 4613–4622.
- 738 Y.-H. Cho, K. Kim, S. Ahn and H. K. Liu, *J. Power Sources*, 2011, **196**, 1483–1487.
- 739 Z. Luo, H. Zhang, L. Yu, D. Huang and J. Shen, *J. Electroanal. Chem.*, 2019, **833**, 520–526.
- 740 Y. Qian, C. Schultz, P. Niehoff, T. Schwieters, S. Nowak, F. M. Schappacher and M. Winter, *J. Power Sources*, 2016, **332**, 60–71.
- 741 D. Pritzl, S. Solchenbach, M. Wetjen and H. A. Gasteiger, *J. Electrochem. Soc.*, 2017, **164**, A2625–A2635.
- 742 J. C. Burns, R. Petibon, K. J. Nelson, N. N. Sinha, A. Kassam, B. M. Way and J. R. Dahn, *J. Electrochem. Soc.*, 2013, **160**, A1668–A1674.
- 743 D. Xu, Y. Kang, J. Wang, S. Hu, Q. Shi, Z. Lu, D. He, Y. Zhao, Y. Qian, H. Lou and Y. Deng, *J. Power Sources*, 2019, **437**, 226929.

- 744 J. Oh, J. Kim, Y. M. Lee, J. Y. Kim, D. O. Shin, M. J. Lee, S. Hong, Y.-G. Lee and K. M. Kim, *Mater. Res. Bull.*, 2020, **132**, 111008.
- 745 S.-K. Jeong, M. Inaba, R. Mogi, Y. Iriyama, T. Abe and Z. Ogumi, *Langmuir*, 2001, **17**, 8281–8286.
- 746 M. Nie, J. Demeaux, B. T. Young, D. R. Heskett, Y. Chen, A. Bose, J. C. Woicik and B. L. Lucht, *J. Electrochem. Soc.*, 2015, **162**, A7008–A7014.
- 747 Q. Q. Liu, L. Ma, C. Y. Du and J. R. Dahn, *Electrochim. Acta*, 2018, **263**, 237–248.
- 748 P. Shi, L. Zhang, H. Xiang, X. Liang, Y. Sun and W. Xu, *ACS Appl. Mater. Interfaces*, 2018, **10**, 22201–22209.
- 749 V. Etacheri, O. Haik, Y. Goffer, G. A. Roberts, I. C. Stefan, R. Fasching and D. Aurbach, *Langmuir*, 2012, **28**, 965–976.
- 750 Y.-M. Lin, K. C. Klavetter, P. R. Abel, N. C. Davy, J. L. Snider, A. Heller and C. B. Mullins, *Chem. Commun.*, 2012, **48**, 7268–7270.
- 751 H. Nakai, T. Kubota, A. Kita and A. Kawashima, *J. Electrochem. Soc.*, 2011, **158**, A798.
- 752 E. Markevich, G. Salitra and D. Aurbach, *ACS Energy Lett.*, 2017, **2**, 1337–1345.
- 753 K. Fridman, R. Sharabi, R. Elazari, G. Gershinsky, E. Markevich, G. Salitra, D. Aurbach, A. Garsuch and J. Lampert, *Electrochem. Commun.*, 2013, **33**, 31–34.
- 754 R. Sharabi, E. Markevich, K. Fridman, G. Gershinsky, G. Salitra, D. Aurbach, G. Semrau, M. A. Schmidt, N. Schall and C. Bruenig, *Electrochem. Commun.*, 2013, **28**, 20–23.
- 755 Y. Chen, W. Zhao, Q. Zhang, G. Yang, J. Zheng, W. Tang, Q. Xu, C. Lai, J. Yang and C. Peng, *Adv. Funct. Mater.*, 2020, **30**, 2000396.
- 756 G. Yang, J. Shi, C. Shen, S. Wang, L. Xia, H. Hu, H. Luo, Y. Xia and Z. Liu, *RSC Adv.*, 2017, **7**, 26052–26059.
- 757 D. Zhao, S. Song, X. Ye, P. Wang, J. Wang, Y. Wei, C. Li, L. Mao, H. Zhang and S. Li, *Appl. Surf. Sci.*, 2019, **491**, 595–606.
- 758 L. Liu, S. Gu, S. Wang, X. Zhang and S. Chen, *RSC Adv.*, 2020, **10**, 1704–1710.
- 759 D. Liu, K. Qian, Y.-B. He, D. Luo, H. Li, M. Wu, F. Kang and B. Li, *Electrochim. Acta*, 2018, **269**, 378–387.
- 760 C. Wang, L. Yu, W. Fan, J. Liu, L. Ouyang, L. Yang and M. Zhu, *ACS Appl. Energy Mater.*, 2018, **1**, 2647–2656.
- 761 W. Zhao, G. Zheng, M. Lin, W. Zhao, D. Li, X. Guan, Y. Ji, G. F. Ortiz and Y. Yang, *J. Power Sources*, 2018, **380**, 149–157.
- 762 L. Ma, L. Ellis, S. L. Glazier, X. Ma, Q. Liu, J. Li and J. R. Dahn, *J. Electrochem. Soc.*, 2018, **165**, A891–A899.
- 763 B. Liu, H. Zhou, C. Yin, H. Guan and J. Li, *Electrochim. Acta*, 2019, **321**, 134690.
- 764 J.-W. Seok, J. Lee, T. Rodgers, D.-H. Ko and J.-H. Shim, *Trans. Electr. Electron. Mater.*, 2019, **20**, 548–553.
- 765 E. Markevich, G. Salitra, K. Fridman, R. Sharabi, G. Gershinsky, A. Garsuch, G. Semrau, M. A. Schmidt and D. Aurbach, *Langmuir*, 2014, **30**, 7414–7424.
- 766 J. Chen, L. Xing, X. Yang, X. Liu, T. Li and W. Li, *Electrochim. Acta*, 2018, **290**, 568–576.
- 767 L. Wang, Y. Ma, Y. Qu, X. Cheng, P. Zuo, C. Du, Y. Gao and G. Yin, *Electrochim. Acta*, 2016, **191**, 8–15.
- 768 Y. Li, F. Lian, L. Ma, C. Liu, L. Yang, X. Sun and K. Chou, *Electrochim. Acta*, 2015, **168**, 261–270.
- 769 A. Benmayza, W. Lu, V. Ramani and J. Prakash, *Electrochim. Acta*, 2014, **123**, 7–13.
- 770 L. Ma, L. Ellis, S. L. Glazier, X. Ma and J. R. Dahn, *J. Electrochem. Soc.*, 2018, **165**, A1718–A1724.
- 771 B. Yang, H. Zhang, L. Yu, W. Fan and D. Huang, *Electrochim. Acta*, 2016, **221**, 107–114.
- 772 Q. Lei, T. Yang, X. Zhao, W. Fan, W. Wang, L. Yu, S. Guo, X. Zuo, R. Zeng and J. Nan, *J. Electroanal. Chem.*, 2019, **846**, 113141.
- 773 K.-E. Kim, J. Y. Jang, I. Park, M.-H. Woo, M.-H. Jeong, W. C. Shin, M. Ue and N.-S. Choi, *Electrochem. Commun.*, 2015, **61**, 121–124.
- 774 X. Zheng, G. Fang, Y. Pan, Q. Li and M. Wu, *J. Power Sources*, 2019, **439**, 227081.
- 775 E. Markevich, G. Salitra, Y. Talyosef and D. Aurbach, *J. Electrochem. Soc.*, 2019, **166**, A2834–A2839.
- 776 E. Markevich, G. Salitra, M. Afri, Y. Talyosef and D. Aurbach, *J. Electrochem. Soc.*, 2020, **167**, 070509.
- 777 E. Markevich, G. Salitra, P. Hartmann, J. Kulisch, D. Aurbach, K.-J. Park, C. S. Yoon and Y.-K. Sun, *J. Electrochem. Soc.*, 2019, **166**, A5265–A5274.
- 778 K. Kim, Y. Kim, S. Park, H. J. Yang, S. J. Park, K. Shin, J.-J. Woo, S. Kim, S. Y. Hong and N.-S. Choi, *J. Power Sources*, 2018, **396**, 276–287.
- 779 W. Beichel, P. Klose, H. Blattmann, J. Hoecker, D. Kratzert and I. Krossing, *ChemElectroChem*, 2018, **5**, 1415–1420.
- 780 J. Yun, L. Zhang, Q. Qu, H. Liu, X. Zhang, M. Shen and H. Zheng, *Electrochim. Acta*, 2015, **167**, 151–159.
- 781 C.-C. Su, M. He, R. Amine, Z. Chen, R. Sahore, N. Dietz Rago and K. Amine, *Energy Storage Mater.*, 2019, **17**, 284–292.
- 782 J. Xia, R. Petibon, A. Xiao, W. M. Lamanna and J. R. Dahn, *J. Electrochem. Soc.*, 2016, **163**, A1637–A1645.
- 783 A. K. Kushwaha, M. R. Sahoo and S. K. Nayak, *Chemistry-Select*, 2019, **4**, 1251–1258.
- 784 H. Shin, J. Park, A. M. Sastry and W. Lu, *J. Electrochem. Soc.*, 2015, **162**, A1683–A1692.
- 785 N. D. Nam, I. J. Park and J. G. Kim, *ECS Trans.*, 2011, **33**, 7–15.
- 786 Y. M. Todorov, M. Aoki, H. Mimura, K. Fujii, N. Yoshimoto and M. Morita, *J. Power Sources*, 2016, **332**, 322–329.
- 787 R. P. Dunn, J. Kifle, F. C. Krause, C. Hwang, B. V. Ratnakumar, M. C. Smart and B. L. Lucht, *J. Electrochem. Soc.*, 2012, **159**, A2100–A2108.
- 788 K. Ciosek Högstrom, H. Lundgren, S. Wilken, T. G. Zavalis, M. Behm, K. Edstrom, P. Jacobsson, P. Johansson and G. Lindbergh, *J. Power Sources*, 2014, **256**, 430–439.
- 789 E.-G. Shim, I.-J. Park, T.-H. Nam, J.-G. Kim, H.-S. Kim and S.-I. Moon, *Met. Mater. Int.*, 2010, **16**, 587–594.
- 790 E.-G. Shim, T.-H. Nam, J.-G. Kim, H.-S. Kim and S.-I. Moon, *Electrochim. Acta*, 2009, **54**, 2276–2283.
- 791 P. Ping, Q. S. Wang, J. H. Sun, X. Xia and J. R. Dahn, *J. Electrochem. Soc.*, 2012, **159**, A1467–A1473.

- 792 Y. Qin, Z. Chen, J. Liu and K. Amine, *Electrochem. Solid-State Lett.*, 2010, **13**, A11.
- 793 J.-G. Han, I. Park, J. Cha, S. Park, S. Park, S. Myeong, W. Cho, S.-S. Kim, S. Y. Hong, J. Cho and N.-S. Choi, *ChemElectroChem*, 2017, **4**, 56–65.
- 794 D. Zhao, J. Wang, H. Lu, P. Wang, H. Liu and S. Li, *J. Power Sources*, 2020, **456**, 228006.
- 795 T. Yang, H. Zeng, W. Wang, X. Zhao, W. Fan, C. Wang, X. Zuo, R. Zeng and J. Nan, *J. Mater. Chem. A*, 2019, **7**, 8292–8301.
- 796 B. Liao, H. Li, M. Xu, L. Xing, Y. Liao, X. Ren, W. Fan, L. Yu, K. Xu and W. Li, *Adv. Energy Mater.*, 2018, **8**, 1800802.
- 797 N. von Aspern, M. Leissing, C. Wölke, D. Diddens, T. Kobayashi, M. Börner, O. Stubbmann-Kazakova, V. Kozel, G.-V. Rösenthaller, J. Smiatek, S. Nowak, M. Winter and I. Cekic-Laskovic, *ChemElectroChem*, 2020, **7**, 1499–1508.
- 798 N. von Aspern, S. Röser, B. Rezaei Rad, P. Murmann, B. Streipert, X. Mönnighoff, S. D. Tillmann, M. Shevchuk, O. Stubbmann-Kazakova, G.-V. Rösenthaller, S. Nowak, M. Winter and I. Cekic-Laskovic, *J. Fluorine Chem.*, 2017, **198**, 24–33.
- 799 P. Murmann, N. von Aspern, P. Janssen, N. Kalinovich, M. Shevchuk, G.-V. Rösenthaller, M. Winter and I. Cekic-Laskovic, *J. Electrochem. Soc.*, 2018, **165**, A1935–A1942.
- 800 Z. Zeng, X. Jiang, B. Wu, L. Xiao, X. Ai, H. Yang and Y. Cao, *Electrochim. Acta*, 2014, **129**, 300–304.
- 801 X. Zhu, X. Jiang, X. Ai, H. Yang and Y. Cao, *Electrochim. Acta*, 2015, **165**, 67–71.
- 802 M. S. Ding, K. Xu and T. R. Jow, *J. Electrochem. Soc.*, 2002, **149**, A1489.
- 803 X. Mönnighoff, P. Murmann, W. Weber, M. Winter and S. Nowak, *Electrochim. Acta*, 2017, **246**, 1042–1051.
- 804 N. von Aspern, D. Diddens, T. Kobayashi, M. Börner, O. Stubbmann-Kazakova, V. Kozel, G.-V. Rösenthaller, J. Smiatek, M. Winter and I. Cekic-Laskovic, *ACS Appl. Mater. Interfaces*, 2019, **11**, 16605–16618.
- 805 W. Zhao, B. Zheng, H. Liu, F. Ren, J. Zhu, G. Zheng, S. Chen, R. Liu, X. Yang and Y. Yang, *Nano Energy*, 2019, **63**, 103815.
- 806 Y. Qian, Y. Kang, S. Hu, Q. Shi, Q. Chen, X. Tang, Y. Xiao, H. Zhao, G. Luo, K. Xu and Y. Deng, *ACS Appl. Mater. Interfaces*, 2020, **12**, 10443–10451.
- 807 J. Xu, Y. Hu, T. Liu and X. Wu, *Nano Energy*, 2014, **5**, 67–73.
- 808 M. Xu, Y. Liu, B. Li, W. Li, X. Li and S. Hu, *Electrochem. Commun.*, 2012, **18**, 123–126.
- 809 X. Yang, J. Chen, Q. Zheng, W. Tu, L. Xing, Y. Liao, M. Xu, Q. Huang, G. Cao and W. Li, *J. Mater. Chem. A*, 2018, **6**, 16149–16163.
- 810 S. Jeong, K. C. Kim, S. R. Lee and J. Mun, *Electrochim. Acta*, 2019, **300**, 156–162.
- 811 Y.-K. Han, J. Yoo and T. Yim, *J. Mater. Chem. A*, 2015, **3**, 10900–10909.
- 812 C. Peebles, R. Sahore, J. A. Gilbert, J. C. Garcia, A. Tornheim, J. Bareño, H. Iddir, C. Liao and D. P. Abraham, *J. Electrochem. Soc.*, 2017, **164**, A1579–A1586.
- 813 Y. Liu, K. Wang, Y. Lin, Y. Zhu, W. Tu, M. Xu, X. Liu, B. Li and W. Li, *Electrochim. Acta*, 2017, **256**, 307–315.
- 814 W. Huang, L. Xing, Y. Wang, M. Xu, W. Li, F. Xie and S. Xia, *J. Power Sources*, 2014, **267**, 560–565.
- 815 N. Xu, H. Zhou, Y. Liao, G. Li, M. Xu and W. Li, *Solid State Ionics*, 2019, **341**, 115049.
- 816 S. Li, D. Zhao, P. Wang, X. Cui and F. Tang, *Electrochim. Acta*, 2016, **222**, 668–677.
- 817 X. Wang, W. Xue, K. Hu, Y. Li, Y. Li and R. Huang, *ACS Appl. Energy Mater.*, 2018, **1**, 5347–5354.
- 818 X. Wang, W. Xue, Z. Xu, Y. Li, Y. Li and R. Huang, *J. Electrochem. Soc.*, 2019, **166**, A802–A809.
- 819 X. Wang, X. Zheng, Y. Liao, Q. Huang, L. Xing, M. Xu and W. Li, *J. Power Sources*, 2017, **338**, 108–116.
- 820 L. Wang, Y. Ma, Q. Li, Z. Zhou, X. Cheng, P. Zuo, C. Du, Y. Gao and G. Yin, *J. Power Sources*, 2017, **361**, 227–236.
- 821 B. Duan, B. Hong, J. Li, Z. Qin, F. Jiang and Y. Lai, *Electrochim. Acta*, 2018, **286**, 86–91.
- 822 C. Wang, L. Yu, W. Fan, J. Liu, L. Ouyang, L. Yang and M. Zhu, *ACS Appl. Mater. Interfaces*, 2017, **9**, 9630–9639.
- 823 T. Huang, X. Zheng, Y. Pan, W. Wang, G. Fang and M. Wu, *Electrochim. Acta*, 2015, **156**, 328–335.
- 824 X. Zheng, T. Huang, Y. Pan, W. Wang, G. Fang, K. Ding and M. Wu, *J. Power Sources*, 2016, **319**, 116–123.
- 825 Z. Wang, L. Xing, J. Li, M. Xu and W. Li, *J. Power Sources*, 2016, **307**, 587–592.
- 826 L. F. Li, H. S. Lee, H. Li, X. Q. Yang, K. W. Nam, W. S. Yoon, J. McBreen and X. J. Huang, *J. Power Sources*, 2008, **184**, 517–521.
- 827 X. Zuo, C. Fan, J. Liu, X. Xiao, J. Wu and J. Nan, *J. Electrochem. Soc.*, 2013, **160**, A1199–A1204.
- 828 U. Lischka, U. Wietelmann and M. Wegner, *German Pat.*, DE19829030 C1, 1999.
- 829 W. Xu and C. A. Angell, *Electrochem. Solid-State Lett.*, 2001, **4**, E1.
- 830 K. Xu, S. Zhang, T. R. Jow, W. Xu and C. A. Angell, *Electrochem. Solid-State Lett.*, 2002, **5**, A26–A29.
- 831 S. Shui Zhang, *Electrochem. Commun.*, 2006, **8**, 1423–1428.
- 832 T. Schedlbauer, S. Krüger, R. Schmitz, R. W. Schmitz, C. Schreiner, H. J. Gores, S. Passerini and M. Winter, *Electrochim. Acta*, 2013, **92**, 102–107.
- 833 K. Xu, S. Zhang and T. R. Jow, *Electrochem. Solid-State Lett.*, 2005, **8**, A365.
- 834 M. Xu, L. Zhou, Y. Dong, Y. Chen, A. Garsuch and B. L. Lucht, *J. Electrochem. Soc.*, 2013, **160**, A2005–A2013.
- 835 Y. Dong, J. Demeaux, Y. Zhang, M. Xu, L. Zhou, A. D. MacIntosh and B. L. Lucht, *J. Electrochem. Soc.*, 2016, **164**, A128–A136.
- 836 M. Xu, L. Zhou, Y. Dong, Y. Chen, J. Demeaux, A. D. MacIntosh, A. Garsuch and B. L. Lucht, *Energy Environ. Sci.*, 2016, **9**, 1308–1319.
- 837 Y. Dong, B. T. Young, Y. Zhang, T. Yoon, D. R. Heskett, Y. Hu and B. L. Lucht, *ACS Appl. Mater. Interfaces*, 2017, **9**, 20467–20475.
- 838 N. P. W. Pieczonka, L. Yang, M. P. Balogh, B. R. Powell, K. Chemelewski, A. Manthiram, S. A. Krachkovskiy,

- G. R. Goward, M. Liu and J.-H. Kim, *J. Phys. Chem. C*, 2013, **117**, 22603–22612.
- 839 S.-Y. Ha, J.-G. Han, Y.-M. Song, M.-J. Chun, S.-I. Han, W.-C. Shin and N.-S. Choi, *Electrochim. Acta*, 2013, **104**, 170–177.
- 840 M. Xu, N. Tsiouvaras, A. Garsuch, H. A. Gasteiger and B. L. Lucht, *J. Phys. Chem. C*, 2014, **118**, 7363–7368.
- 841 Y. Zhu, Y. Li, M. Bettge and D. P. Abraham, *J. Electrochem. Soc.*, 2012, **159**, A2109–A2117.
- 842 Y. Ji, S. Li, G. Zhong, Z. Zhang, Y. Li, M. J. McDonald and Y. Yang, *J. Electrochem. Soc.*, 2015, **162**, A7015–A7023.
- 843 J. Cha, J.-G. Han, J. Hwang, J. Cho and N.-S. Choi, *J. Power Sources*, 2017, **357**, 97–106.
- 844 Q. Wu, W. Lu, M. Miranda, T. K. Honaker-Schroeder, K. Y. Lakhsassi and D. Dees, *Electrochem. Commun.*, 2012, **24**, 78–81.
- 845 Y. Zhu, Y. Li, M. Bettge and D. P. Abraham, *Electrochim. Acta*, 2013, **110**, 191–199.
- 846 Q. Zhang, K. Wang, X. Wang, Y. Zhong, M. Liu, X. Liu, K. Xu, W. Fan, L. Yu and W. Li, *ACS Appl. Mater. Interfaces*, 2019, **11**, 20854–20863.
- 847 G. Lan, H. Zhou, L. Xing, J. Chen, Z. Li, R. Guo, Y. Che and W. Li, *J. Energy Chem.*, 2019, **39**, 235–243.
- 848 Y. Li, G. M. Veith, K. L. Browning, J. Chen, D. K. Hensley, M. P. Paranthaman, S. Dai and X.-G. Sun, *Nano Energy*, 2017, **40**, 9–19.
- 849 Y. Li, S. Wan, G. M. Veith, R. R. Unocic, M. P. Paranthaman, S. Dai and X.-G. Sun, *Adv. Energy Mater.*, 2017, **7**, 1601397.
- 850 C. Liao, K. S. Han, L. Baggetto, D. A. Hillesheim, R. Custelcean, E.-S. Lee, B. Guo, Z. Bi, D.-e. Jiang, G. M. Veith, E. W. Hagaman, G. M. Brown, C. Bridges, M. P. Paranthaman, A. Manthiram, S. Dai and X.-G. Sun, *Adv. Energy Mater.*, 2014, **4**, 1301368.
- 851 X.-G. Sun, S. Wan, H. Y. Guang, Y. Fang, K. S. Reeves, M. Chi and S. Dai, *J. Mater. Chem. A*, 2017, **5**, 1233–1241.
- 852 S. J. Lee, J.-G. Han, Y. Lee, M.-H. Jeong, W. C. Shin, M. Ue and N.-S. Choi, *Electrochim. Acta*, 2014, **137**, 1–8.
- 853 Q. Dong, F. Guo, Z. Cheng, Y. Mao, R. Huang, F. Li, H. Dong, Q. Zhang, W. Li, H. Chen, Z. Luo, Y. Shen, X. Wu and L. Chen, *ACS Appl. Energy Mater.*, 2020, **3**, 695–704.
- 854 H. Gao, F. Maglia, P. Lamp, K. Amine and Z. Chen, *ACS Appl. Mater. Interfaces*, 2017, **9**, 44542–44549.
- 855 J. Mun, J. Lee, T. Hwang, J. Lee, H. Noh and W. Choi, *J. Electroanal. Chem.*, 2015, **745**, 8–13.
- 856 X. Cui, F. Tang, C. Li, Y. Zhang, P. Wang, H. Feng, J. Zhao, F. Li and S. Li, *Electrochim. Acta*, 2017, **253**, 291–301.
- 857 S. Huang, S. Wang, G. Hu, L.-Z. Cheong and C. Shen, *Appl. Surf. Sci.*, 2018, **441**, 265–271.
- 858 Y. Ma, Z. Zhou, C. Li, L. Wang, Y. Wang, X. Cheng, P. Zuo, C. Du, H. Huo, Y. Gao and G. Yin, *Energy Storage Mater.*, 2018, **11**, 197–204.
- 859 H. Yue, Y. Yang, Y. Xiao, Z. Dong, S. Cheng, Y. Yin, C. Ling, W. Yang, Y. Yu and S. Yang, *J. Mater. Chem. A*, 2019, **7**, 594–602.
- 860 A. Freiberg, M. Metzger, D. Haering, S. Bretzke, S. Puravankara, T. Nilges, C. Stinner, C. Marino and H. A. Gasteiger, *J. Electrochem. Soc.*, 2014, **161**, A2255–A2261.
- 861 M. Xu, L. Zhou, Y. Dong, U. Tottempudi, J. Demeaux, A. Garsuch and B. L. Lucht, *ECS Electrochem. Lett.*, 2015, **4**, A83–A86.
- 862 Q. Yu, Z. Chen, L. Xing, D. Chen, H. Rong, Q. Liu and W. Li, *Electrochim. Acta*, 2015, **176**, 919–925.
- 863 Q. Liu, G. Yang, S. Liu, M. Han, Z. Wang and L. Chen, *ACS Appl. Mater. Interfaces*, 2019, **11**, 17435–17443.
- 864 M. Nie, J. Xia and J. R. Dahn, *J. Electrochem. Soc.*, 2015, **162**, A1186–A1195.
- 865 M. Nie, J. Xia, L. Ma and J. R. Dahn, *J. Electrochem. Soc.*, 2015, **162**, A2066–A2074.
- 866 M. Nie, J. Xia and J. R. Dahn, *J. Electrochem. Soc.*, 2015, **162**, A1693–A1701.
- 867 Y.-K. Han, K. Lee, J. Yoo and Y. S. Huh, *Theor. Chem. Acc.*, 2014, **133**, 1562.
- 868 N. A. Rossi and R. West, *Polym. Int.*, 2009, **58**, 267–272.
- 869 K. Amine, Q. Wang, D. R. Vissers, Z. Zhang, N. A. A. Rossi and R. West, *Electrochem. Commun.*, 2006, **8**, 429–433.
- 870 H. P. Zhang, Q. Xia, B. Wang, L. C. Yang, Y. P. Wu, D. L. Sun, C. L. Gan, H. J. Luo, A. W. Bebeda and T. v. Ree, *Electrochem. Commun.*, 2009, **11**, 526–529.
- 871 L. Zhang, Z. Zhang, S. Harring, M. Straughan, R. Butorac, Z. Chen, L. Lyons, K. Amine and R. West, *J. Mater. Chem.*, 2008, **18**, 3713–3717.
- 872 X. Chen, M. Usrey, A. Peña-Hueso, R. West and R. J. Hamers, *J. Power Sources*, 2013, **241**, 311–319.
- 873 H. Lyu, Y. Li, C. J. Jafta, C. A. Bridges, H. M. Meyer, A. Borisevich, M. P. Paranthaman, S. Dai and X.-G. Sun, *J. Power Sources*, 2019, **412**, 527–535.
- 874 Y.-M. Song, J.-G. Han, S. Park, K. T. Lee and N.-S. Choi, *J. Mater. Chem. A*, 2014, **2**, 9506–9513.
- 875 X. Qi, L. Tao, H. Hahn, C. Schultz, D. R. Gallus, X. Cao, S. Nowak, S. Röser, J. Li, I. Cekic-Laskovic, B. R. Rad and M. Winter, *RSC Adv.*, 2016, **6**, 38342–38349.
- 876 D. R. Gallus, R. Wagner, S. Wiemers-Meyer, M. Winter and I. Cekic-Laskovic, *Electrochim. Acta*, 2015, **184**, 410–416.
- 877 S. L. Guillot, A. Peña-Hueso, M. L. Usrey and R. J. Hamers, *J. Electrochem. Soc.*, 2017, **164**, A1907–A1917.
- 878 Y.-M. Song, C.-K. Kim, K.-E. Kim, S. Y. Hong and N.-S. Choi, *J. Power Sources*, 2016, **302**, 22–30.
- 879 J. Vidal Laveda, J. E. Low, F. Pagani, E. Stilp, S. Dilger, V. Baran, M. Heere and C. Battaglia, *ACS Appl. Energy Mater.*, 2019, **2**, 7036–7044.
- 880 A. Guéguen, C. Bolli, M. A. Mendez and E. J. Berg, *ACS Appl. Energy Mater.*, 2020, **3**, 290–299.
- 881 L. Imholt, S. Röser, M. Börner, B. Streipert, B. R. Rad, M. Winter and I. Cekic-Laskovic, *Electrochim. Acta*, 2017, **235**, 332–339.
- 882 Y. Zheng, N. Xu, S. Chen, Y. Liao, G. Zhong, Z. Zhang and Y. Yang, *ACS Appl. Energy Mater.*, 2020, **3**, 2837–2845.
- 883 X. Zuo, C. Fan, J. Liu, X. Xiao, J. Wu and J. Nan, *J. Power Sources*, 2013, **229**, 308–312.
- 884 H. Rong, M. Xu, B. Xie, W. Huang, X. Liao, L. Xing and W. Li, *J. Power Sources*, 2015, **274**, 1155–1161.

- 885 A. Birrozzi, N. Laszczynski, M. Hekmatfar, J. von Zamory, G. A. Giffin and S. Passerini, *J. Power Sources*, 2016, **325**, 525–533.
- 886 V. Tarnopolsky, US7494746B2, 2009.
- 887 W. Tu, C. Ye, X. Yang, L. Xing, Y. Liao, X. Liu and W. Li, *J. Power Sources*, 2017, **364**, 23–32.
- 888 Y. Li, K. Wang, J. Chen, W. Zhang, X. Luo, Z. Hu, Q. Zhang, L. Xing and W. Li, *ACS Appl. Mater. Interfaces*, 2020, **12**, 28169–28178.
- 889 T. van Ree, *Curr. Opin. Electrochem.*, 2020, **21**, 22–30.
- 890 S. F. Lux, I. T. Lucas, E. Pollak, S. Passerini, M. Winter and R. Kostecki, *Electrochem. Commun.*, 2012, **14**, 47–50.
- 891 S. S. Zhang, X. Fan and C. Wang, *ChemElectroChem*, 2019, **6**, 1536–1541.
- 892 J.-H. Park, B. Choi, Y.-S. Kang, S. Y. Park, D. J. Yun, I. Park, J. H. Shim, J.-H. Park, H. N. Han and K. Park, *Energy Technol.*, 2018, **6**, 1361–1369.
- 893 X. Xiong, Z. Wang, P. Yue, H. Guo, F. Wu, J. Wang and X. Li, *J. Power Sources*, 2013, **222**, 318–325.
- 894 I. A. Shkrob and D. P. Abraham, *J. Phys. Chem. C*, 2016, **120**, 15119–15128.
- 895 O. K. Park, Y. Cho, S. Lee, H.-C. Yoo, H.-K. Song and J. Cho, *Energy Environ. Sci.*, 2011, **4**, 1621–1633.
- 896 V. V. Bhat, G. Cheng, S. Kaye, B. Li, R. Olugbile and J.-H. Yang, *US Pat.*, 8308971 B1, 2012.
- 897 S. Wang, S. Chen, W. Gao, L. Liu and S. Zhang, *J. Power Sources*, 2019, **423**, 90–97.
- 898 X. Yan, C. Chen, X. Zhu, L. Pan, X. Zhao and L. Zhang, *J. Power Sources*, 2020, **461**, 228099.
- 899 B. Deng, H. Wang, X. Li, Y. Ding, D. Sun, J. Ma, M. Chen, T. Chen, F. Gao, M. Qu and G. Peng, *Energy Technol.*, 2019, **7**, 1800981.
- 900 B. Deng, H. Wang, W. Ge, X. Li, X. Yan, T. Chen, M. Qu and G. Peng, *Electrochim. Acta*, 2017, **236**, 61–71.
- 901 H. Wang, D. Sun, X. Li, W. Ge, B. Deng, M. Qu and G. Peng, *Electrochim. Acta*, 2017, **254**, 112–122.
- 902 S. H. Jang, K. Jung and T. Yim, *Curr. Appl. Phys.*, 2018, **18**, 1345–1351.
- 903 S. H. Jang and T. Yim, *Chem. Phys. Chem.*, 2017, **18**, 3402–3406.
- 904 F. An, H. Zhao, W. Zhou, Y. Ma and P. Li, *Sci. Rep.*, 2019, **9**, 14108.
- 905 B. Liu, Q. Li, M. H. Engelhard, Y. He, X. Zhang, D. Mei, C. Wang, J.-G. Zhang and W. Xu, *ACS Appl. Mater. Interfaces*, 2019, **11**, 21496–21505.
- 906 C. Ye, W. Tu, L. Yin, Q. Zheng, C. Wang, Y. Zhong, Y. Zhang, Q. Huang, K. Xu and W. Li, *J. Mater. Chem. A*, 2018, **6**, 17642–17652.
- 907 S. Mai, M. Xu, X. Liao, J. Hu, H. Lin, L. Xing, Y. Liao, X. Li and W. Li, *Electrochim. Acta*, 2014, **147**, 565–571.
- 908 B. Koo, J. Lee, Y. Lee, J. K. Kim and N.-S. Choi, *Electrochim. Acta*, 2015, **173**, 750–756.
- 909 J.-G. Han, S. J. Lee, J. Lee, J.-S. Kim, K. T. Lee and N.-S. Choi, *ACS Appl. Mater. Interfaces*, 2015, **7**, 8319–8329.
- 910 Y. Zhu, X. Luo, M. Xu, L. Zhang, L. Yu, W. Fan and W. Li, *J. Power Sources*, 2016, **317**, 65–73.
- 911 D. Y. Wang, J. Xia, L. Ma, K. J. Nelson, J. E. Harlow, D. Xiong, L. E. Downie, R. Petibon, J. C. Burns, A. Xiao, W. M. Lamanna and J. R. Dahn, *J. Electrochem. Soc.*, 2014, **161**, A1818–A1827.
- 912 L. Ma, J. Xia and J. R. Dahn, *J. Electrochem. Soc.*, 2015, **162**, A1170–A1174.
- 913 Y.-K. Han, J. Yoo and T. Yim, *Electrochim. Acta*, 2016, **215**, 455–465.
- 914 N. N. Sinha, J. C. Burns and J. R. Dahn, *J. Electrochem. Soc.*, 2014, **161**, A1084–A1089.
- 915 D. Y. Wang and J. R. Dahn, *J. Electrochem. Soc.*, 2014, **161**, A1890–A1897.
- 916 C. Bolli, A. Guéguen, M. A. Mendez and E. J. Berg, *Chem. Mater.*, 2019, **31**, 1258–1267.
- 917 T. Yim and Y.-K. Han, *ACS Appl. Mater. Interfaces*, 2017, **9**, 32851–32858.
- 918 H. Liu, A. J. Naylor, A. S. Menon, W. R. Brant, K. Edström and R. Younesi, *Adv. Mater. Interfaces*, 2020, **7**, 2000277.
- 919 X. Liao, X. Zheng, J. Chen, Z. Huang, M. Xu, L. Xing, Y. Liao, Q. Lu, X. Li and W. Li, *Electrochim. Acta*, 2016, **212**, 352–359.
- 920 J. Zhang, J. Wang, J. Yang and Y. NuLi, *Electrochim. Acta*, 2014, **117**, 99–104.
- 921 H. Rong, M. Xu, L. Xing and W. Li, *J. Power Sources*, 2014, **261**, 148–155.
- 922 G. Yan, X. Li, Z. Wang, H. Guo and C. Wang, *J. Power Sources*, 2014, **248**, 1306–1311.
- 923 V. Bhat, G. Cheng, S. Kaye, B. Li, R. Olugbile and J. H. Yang, *US Pat.*, US2012/0315534 A1, 2012.
- 924 S. A. Delp, O. Borodin, M. Olguin, C. G. Eisner, J. L. Allen and T. R. Jow, *Electrochim. Acta*, 2016, **209**, 498–510.
- 925 Q. Ma, X. Zhang, A. Wang, Y. Xia, X. Liu and J. Luo, *Adv. Funct. Mater.*, 2020, **30**, 2002824.
- 926 Z. Cai, Y. Liu, J. Zhao, L. Li, Y. Zhang and J. Zhang, *J. Power Sources*, 2012, **202**, 341–346.
- 927 Y. Liu, L. Tan and L. Li, *J. Power Sources*, 2013, **221**, 90–96.
- 928 J. Li, L. Xing, R. Zhang, M. Chen, Z. Wang, M. Xu and W. Li, *J. Power Sources*, 2015, **285**, 360–366.
- 929 X. Liao, Q. Huang, S. Mai, X. Wang, M. Xu, L. Xing, Y. Liao and W. Li, *J. Power Sources*, 2014, **272**, 501–507.
- 930 H. Rong, M. Xu, B. Xie, X. Liao, W. Huang, L. Xing and W. Li, *Electrochim. Acta*, 2014, **147**, 31–39.
- 931 C. Yan, Y. Xu, J. Xia, C. Gong and K. Chen, *J. Energy Chem.*, 2016, **25**, 659–666.
- 932 X. Liao, P. Sun, M. Xu, L. Xing, Y. Liao, L. Zhang, L. Yu, W. Fan and W. Li, *Appl. Energy*, 2016, **175**, 505–511.
- 933 S. H. Jang, K.-J. Lee, J. Mun, Y.-K. Han and T. Yim, *J. Power Sources*, 2019, **410–411**, 15–24.
- 934 F. Chen, Y. Liao, M. Li, J. Huang, Q. Huang and W. Li, *Solid State Ionics*, 2018, **327**, 1–10.
- 935 Y. Wang, H. Ming, J. Qiu, Z. Yu, M. Li, S. Zhang and Y. Yang, *J. Electroanal. Chem.*, 2017, **802**, 8–14.
- 936 Q. Zheng, L. Xing, X. Yang, X. Li, C. Ye, K. Wang, Q. Huang and W. Li, *ACS Appl. Mater. Interfaces*, 2018, **10**, 16843–16851.
- 937 B. Li, M. Xu, T. Li, W. Li and S. Hu, *Electrochem. Commun.*, 2012, **17**, 92–95.
- 938 G. Park, H. Nakamura, Y. Lee and M. Yoshio, *J. Power Sources*, 2009, **189**, 602–606.

- 939 B. T. Yu, W. H. Qiu, F. S. Li and L. Cheng, *J. Power Sources*, 2006, **158**, 1373–1378.
- 940 G. H. Wrodnigg, *J. Electrochem. Soc.*, 1999, **146**, 470.
- 941 L. D. Xing, W. S. Li, M. Q. Xu, T. T. Li and L. Zhou, *J. Power Sources*, 2011, **196**, 7044–7047.
- 942 A. Sano and S. Maruyama, *J. Power Sources*, 2009, **192**, 714–718.
- 943 B. Zhang, M. Metzger, S. Solchenbach, M. Payne, S. Meini, H. A. Gasteiger, A. Garsuch and B. L. Lucht, *J. Phys. Chem. C*, 2015, **119**, 11337–11348.
- 944 X. Zuo, M. Xu, W. Li, D. Su and J. Liu, *Electrochem. Solid-State Lett.*, 2006, **9**, A196.
- 945 T. Hamamoto, A. Hitaka, Y. Nakada and K. Abe, *US Pat.*, 6033809A, 2000.
- 946 D. S. Hall, J. P. Allen, S. L. Glazier, L. D. Ellis, L. Ma, J. M. Peters, I. G. Hill and J. R. Dahn, *J. Electrochem. Soc.*, 2017, **164**, A3445–A3453.
- 947 Z. Ding, X. Li, T. Wei, Z. Yin and X. Li, *Electrochim. Acta*, 2016, **196**, 622–628.
- 948 P. Janssen, R. Schmitz, R. Müller, P. Isken, A. Lex-Balducci, C. Schreiner, M. Winter, I. Cekić-Lasković and R. Schmitz, *Electrochim. Acta*, 2014, **125**, 101–106.
- 949 M. Q. Xu, W. S. Li, X. X. Zuo, J. S. Liu and X. Xu, *J. Power Sources*, 2007, **174**, 705–710.
- 950 X. Li, Z. Yin, X. Li and C. Wang, *Ionics*, 2014, **20**, 795–801.
- 951 M. Hekmatfar, I. Hasa, R. Eghbal, D. V. Carvalho, A. Moretti and S. Passerini, *Adv. Mater. Interfaces*, 2020, **7**, 1901500.
- 952 T. Yang, W. Wang, S. Li, J. Lu, W. Fan, X. Zuo and J. Nan, *J. Power Sources*, 2020, **470**, 228462.
- 953 S. Wu, Y. Lin, L. Xing, G. Sun, H. Zhou, K. Xu, W. Fan, L. Yu and W. Li, *ACS Appl. Mater. Interfaces*, 2019, **11**, 17940–17951.
- 954 Y. Lin, M. Xu, S. Wu, Y. Tian, Z. Cao, L. Xing and W. Li, *ACS Appl. Mater. Interfaces*, 2018, **10**, 16400–16409.
- 955 Y. Che, X. Lin, L. Xing, X. Guan, R. Guo, G. Lan, Q. Zheng, W. Zhang and W. Li, *J. Energy Chem.*, 2021, **52**, 361–371.
- 956 M. Xu, W. Li and B. L. Lucht, *J. Power Sources*, 2009, **193**, 804–809.
- 957 J. Xia, N. N. Sinha, L. P. Chen, G. Y. Kim, D. J. Xiong and J. R. Dahn, *J. Electrochem. Soc.*, 2013, **161**, A84–A88.
- 958 J. Xia, N. N. Sinha, L. P. Chen and J. R. Dahn, *J. Electrochem. Soc.*, 2013, **161**, A264–A274.
- 959 Y. Ein-Eli, *J. Electrochem. Soc.*, 1997, **144**, 1159.
- 960 G. H. Wrodnigg, J. O. Besenhard and M. Winter, *J. Electrochem. Soc.*, 1999, **146**, 470–472.
- 961 G. H. Wrodnigg, T. M. Wrodnigg, J. O. Besenhard and M. Winter, *Electrochem. Commun.*, 1999, **1**, 148–150.
- 962 K. Ogawa, A. Sano, T. Iijima, K. Inoue and S. Maruyama, *US Pat.*, 20050186481A1, 2005.
- 963 O. C. Harris, S. E. Lee, C. Lees and M. Tang, *J. Phys.: Energy*, 2020, **2**, 032002.
- 964 L. Madec, J. Xia, R. Petibon, K. J. Nelson, J.-P. Sun, I. G. Hill and J. R. Dahn, *J. Phys. Chem. C*, 2014, **118**, 29608–29622.
- 965 J. Xia, J. E. Harlow, R. Petibon, J. C. Burns, L. P. Chen and J. R. Dahn, *J. Electrochem. Soc.*, 2014, **161**, A547–A553.
- 966 J. Xia, C. P. Aiken, L. Ma, G. Y. Kim, J. C. Burns, L. P. Chen and J. R. Dahn, *J. Electrochem. Soc.*, 2014, **161**, A1149–A1157.
- 967 R. Chen, F. Wu, L. Li, Y. Guan, X. Qiu, S. Chen, Y. Li and S. Wu, *J. Power Sources*, 2007, **172**, 395–403.
- 968 R. Wagner, S. Brox, J. Kasnatscheew, D. R. Gallus, M. Amereller, I. Cekić-Laskovic and M. Winter, *Electrochem. Commun.*, 2014, **40**, 80–83.
- 969 T. Yim, K. S. Kang, J. Mun, S. H. Lim, S.-G. Woo, K. J. Kim, M.-S. Park, W. Cho, J. H. Song, Y.-K. Han, J.-S. Yu and Y.-J. Kim, *J. Power Sources*, 2016, **302**, 431–438.
- 970 X. Zheng, X. Wang, X. Cai, L. Xing, M. Xu, Y. Liao, X. Li and W. Li, *ACS Appl. Mater. Interfaces*, 2016, **8**, 30116–30125.
- 971 K. Abe, T. Takaya, H. Yoshitake, Y. Ushigoe, M. Yoshio and H. Wang, *Electrochem. Solid-State Lett.*, 2004, **7**, A462.
- 972 K. Abe, Y. Ushigoe, H. Yoshitake and M. Yoshio, *J. Power Sources*, 2006, **153**, 328–335.
- 973 L. Xia, Y. Xia and Z. Liu, *Electrochim. Acta*, 2015, **151**, 429–436.
- 974 W. Tu, P. Xia, J. Li, L. Zeng, M. Xu, L. Xing, L. Zhang, L. Yu, W. Fan and W. Li, *Electrochim. Acta*, 2016, **208**, 251–259.
- 975 K.-S. Lee, Y.-K. Sun, J. Noh, K. S. Song and D.-W. Kim, *Electrochem. Commun.*, 2009, **11**, 1900–1903.
- 976 M. Zhao, X. Zuo, X. Ma, X. Xiao, L. Yu and J. Nan, *J. Power Sources*, 2016, **323**, 29–36.
- 977 L. Y. Xing, M. Hu, Q. Tang, J. P. Wei, X. Qin and Z. Zhou, *Electrochim. Acta*, 2012, **59**, 172–178.
- 978 Y.-S. Lee, K.-S. Lee, Y.-K. Sun, Y. M. Lee and D.-W. Kim, *J. Power Sources*, 2011, **196**, 6997–7001.
- 979 M. Hu, J. Wei, L. Xing and Z. Zhou, *J. Power Sources*, 2013, **222**, 373–378.
- 980 B.-J. Chae, J. H. Park, H. J. Song, S. H. Jang, K. Jung, Y. D. Park and T. Yim, *Electrochim. Acta*, 2018, **290**, 465–473.
- 981 A. Abouimrane, S. A. Odom, H. Tavassol, M. V. Schulmerich, H. Wu, R. Bhargava, A. A. Gewirth, J. S. Moore and K. Amine, *J. Electrochem. Soc.*, 2012, **160**, A268–A271.
- 982 X. Zuo, M. Zhao, X. Ma, X. Xiao, J. Liu and J. Nan, *Electrochim. Acta*, 2017, **245**, 705–714.
- 983 J. Xia, R. Petibon, N. N. Sinha and J. R. Dahn, *J. Electrochem. Soc.*, 2015, **162**, A2227–A2235.
- 984 J. Li, H. Li, W. Stone, S. Glazier and J. R. Dahn, *J. Electrochem. Soc.*, 2018, **165**, A626–A635.
- 985 D. Y. Wang, N. N. Sinha, R. Petibon, J. C. Burns and J. R. Dahn, *J. Power Sources*, 2014, **251**, 311–318.
- 986 J. C. Burns, N. N. Sinha, G. Jain, H. Ye, C. M. VanElzen, W. M. Lamanna, A. Xiao, E. Scott, J. Choi and J. R. Dahn, *J. Electrochem. Soc.*, 2012, **159**, A1105–A1113.
- 987 L. Ma, J. Self, M. Nie, S. Glazier, D. Y. Wang, Y.-S. Lin and J. R. Dahn, *J. Power Sources*, 2015, **299**, 130–138.
- 988 L. Madec, L. Ma, K. J. Nelson, R. Petibon, J.-P. Sun, I. G. Hill and J. R. Dahn, *J. Electrochem. Soc.*, 2016, **163**, A1001–A1009.
- 989 G. Xu, C. Pang, B. Chen, J. Ma, X. Wang, J. Chai, Q. Wang, W. An, X. Zhou, G. Cui and L. Chen, *Adv. Energy Mater.*, 2018, **8**, 1701398.
- 990 Z. Khodr, C. Mallet, J.-C. Daigle, Z. Feng, K. Amouzegar, J. Claverie and K. Zaghbi, *J. Electrochem. Soc.*, 2020, **167**, 120535.